VOL. 27 NO. 3 OCTOBER 1970
PUBLISHED MONTHLY
Completing volume 27

JOURNAL OF ELECTROANALYTICAL CHEMISTRY AND INTERFACIAL ELECTROCHEMISTRY

International Journal devoted to all Aspects of Electroanalytical Chemistry, Double Layer Studies, Electrokinetics, Colloid Stability, and Electrode Kinetics.

ELSEVIER SEQUOIA S.A.
LAUSANNE

GENERAL INFORMATION

Detailed *Suggestions and Instructions to Authors* were published in the June 1969 issue of the journal, *J. Electroanal. Chem.*, 21 (1969) 565–572. A free reprint can be obtained by application to the publisher.

Types of contributions

(a) Original research work not previously published in other periodicals (regular papers). (b) Reviews on recent developments in various fields. (c) Short communications. (d) Preliminary notes.

A Preliminary Note is a brief report of work which has progressed to the stage when it is considered that the science of chemistry would be advanced if the results were made available as soon as possible to others working on the same subject. Preliminary Notes can in general be published within 4–8 weeks of their acceptance by the editor although this implies that proofs cannot be sent to the author(s). The publisher will attend to correction of the proof but it should be remembered that errors in the manuscript will also appear in the published Note. Preliminary Notes, clearly marked as such, must be sent to Dr. R. Parsons (address given below).

Submission of papers

Papers should be sent to one of the following Editors:

Dr. R. PARSONS, Department of Chemistry, The University, Bristol BS8 1TS, England.
Dr. R. DE LEVIE, Department of Chemistry, Georgetown University, Washington, D.C. 20007, U.S.A.
Dr. R. H. OTTEWILL, Department of Chemistry, The University, Bristol BS8 1TS, England.

For rapid handling papers originating from the American continent should be sent to Dr. DE LEVIE, those of colloid interest to Dr. OTTEWILL, and all others to Dr. PARSONS.

Authors should preferably submit two copies in double-spaced typing on pages of uniform size. Legends for figures should be typed on a separate page. The figures should be in a form suitable for reproduction, drawn in Indian ink on drawing paper or tracing paper, with lettering etc. in thin pencil. The sheets of drawing or tracing paper should preferably be of the same dimensions as those on which the article is typed. Photographs should be submitted as clear black and white prints on glossy paper. Standard symbols should be used in line drawings, the following are available to the printers:

▼ ▽ ■ □ ● ◎ ▪ ◘ ⊕ ⊡ ▪ + ×

All references should be given at the end of the paper. They should be numbered and the numbers should appear in the text at the appropriate places.

A summary of 50 to 200 words should be included.

Authors are recommended to use wherever possible the "Système International d'Unités" (SI Units) approved by the Conférence Générale des Poids et Mesures in 1960. If units are used which are not SI units, authors should provide a conversion factor to SI units. Axes of graphs and headings for tables should always be given clearly with the units of the quantities concerned. It is recommended that this should be done in the form consistent with "Quantity calculus", *e.g.* time as t/min or e.m.f. as E/mV, or capacity per unit area as $C/\mathrm{F\,m^{-2}}$.

Reprints

Fifty reprints will be supplied free of charge. Additional reprints (minimum 100) can be ordered at quoted prices. They must be ordered on order forms which are sent together with the proofs.

Publication

The *Journal of Electroanalytical Chemistry and Interfacial Electrochemistry* appears monthly. In the period November 1970–December 1971, 6 volumes will appear.

Subscription price for 1971 (covering Nov. 1970–Dec. 1971): Sfr. 476.— (U.S. $112.—) incl. postage. Additional cost for copies by air mail available on request. For subscribers in the U.S.A. and Canada, 2nd class postage paid at New York, N.Y. For advertising rates apply to the publishers.

Subscriptions should be sent to:

ELSEVIER SEQUOIA S.A., P.O. Box 851, 1001 Lausanne 1, Switzerland

A New Important Encyclopaedic Work of Reference

COMPREHENSIVE CHEMICAL KINETICS

edited by C.H. BAMFORD F.R.S., and C.F.H. TIPPER

The aim of this series is to cover in a critical way the practice and theory of kinetics and the kinetics of inorganic and organic reactions in the gas and condensed phases or at interfaces.
Each chapter is written by an expert in the field so that the series as a whole will serve as a direct source of reference and information over the whole range of kinetics.
The vast amount of material scattered through the literature has never before been gathered together and presented in this accessible form.

Elsevier

P.O. BOX 211,
AMSTERDAM - THE NETHERLANDS

Volume 1. The Practice of Kinetics

1. Experimental methods for the study of slow reactions (L. Batt)
2. Experimental methods for the study of fast reactions (D.N. Hague)
3. Experimental methods for the study of heterogeneous reactions (D. Shooter)
4. The detection and estimation of intermediates (R.P. Wayne)
5. The treatment of experimental data (D. Margerison)

7 x 10″, xiii + 450 pages, 32 tables, 161 illus., 1174 lit. refs., 1969, Dfl. 95.00, £11.5.0
SBN 444-40673-5

Volume 2. The Theory of Kinetics

1. Kinetic characterization of complex reaction systems (Z.G. Szabó)
2. Chain reactions (V.N. Kondratiev)
3. Theory of the kinetics of elementary gas phase reactions (R.P. Wayne)
4. Theory of elementary reactions in solution (I.D. Clark and R.P. Wayne)
5. Theory of solid phase kinetics (L.G. Harrison)

7 x 10″, xiii + 486 pages, 13 tables, 77 illus., 794 lit. refs., 1969, Dfl. 100.00, £11.10.0
SBN 444-40674-3

Volume 3. The Formation and Decay of Excited Species

1. Effect of low energy radiation (C.S. Burton and W.A. Noyes, Jr.)
2. Effect of high energy radiation (G. Hughes)
3. The chemical production of excited states (T. Carrington and D. Garvin)
4. The transfer of energy between chemical species (A.B. Callear and J.D. Lambert)

7 x 10″, xii + 300 pages, 30 tables, 53 illus., 1969, Dfl. 70.00, £8.5.0
SBN 444-40802-9

The series as a whole will comprise about 25 volumes divided into a number of sections:

Section 1. The practice and theory of kinetics (3 volumes)
Section 2. Decomposition and isomerisation reactions (2 volumes)
Section 3. Inorganic reactions (2 volumes)
Section 4. Organic reactions (6 volumes)
Section 5. Polymerization reactions (2 volumes)
Section 6. Oxidation and combustion reactions (2 volumes)
Section 7. Selected elementary reactions (2 volumes)

Other sections are planned on heterogeneous reactions, solid state reactions, and kinetics and technological processes.

ELECTROANALYTICAL CHEMISTRY AND INTERFACIAL ELECTROCHEMISTRY
Elsevier Sequoia S.A., Lausanne – Printed in The Netherlands

OXYGEN REDUCTION AT SMOOTH PRE-REDUCED GOLD AND IRIDIUM ELECTRODES IN 85% ORTHOPHOSPHORIC ACID

A. J. APPLEBY
Institute of Gas Technology, III Centre, Chicago, Illinois, 60616 (U.S.A.)
(Received January 20th, 1970; in revised form April 14th, 1970)

INTRODUCTION

The investigation of the reduction of oxygen at gold electrodes in acid solution is of great importance because gold is the only noble metal with a completely filled *d*-band. The significance of the role of the *d*-orbital vacancies in adsorption-controlled electrochemical phenomena has been pointed out by a number of workers[1,2]. It has, for example, been shown that the coverage with adsorbed oxygen of the noble metals at their rest potentials is closely related to their *d*-band vacancies[2]. Although it is generally accepted that gold is a poor oxygen electrode catalyst in acid solution[3–6], it is thus of great theoretical interest in the study of electrocatalysis. In this paper, oxygen reduction on gold as a function of temperature in 85% orthophosphoric acid is contrasted with that on pre-reduced iridium. Although some studies on oxygen reduction on this metal have been reported[1,7,8], none of them has been conducted on unambiguously phase oxide-free electrodes.

EXPERIMENTAL

All reactions were conducted in an all-silica electrochemical cell equipped with a bubbling hydrogen reference electrode, as described in previous work[9]. The apparatus was suspended in an oil bath whose temperature could be varied between ambient and 136° C. The working electrodes consisted of 1 cm^2 foils in the case of gold, or small disks of approximately 5-mm diameter and approximately 1 mm thick in the case of iridium. The latter were cut from a rod of iridium of zone-refined (99.999% nominal purity) grade using a diamond saw, and were ground and polished with graded alumina powders to a mirror finish. Gold foils were cut from a mirror-bright 99.99% purity sheet. Electrodes were welded to gold wires* and suspended so they could be easily moved in and out of the solution by means of Teflon sliding seals. Before use they were degreased using organic solvents and were washed in concentrated hydrochloric acid, conductivity water, and the electrolyte itself. Iridium electrodes were then potentiostatted at 50 mV (HRE) for 2 h to reduce any residual oxide.

The electrolyte was prepurified by treatment with hydrogen peroxide in a

* Preliminary experiments using platinum electrodes established that a Pt–Au weld immersed in the electrolyte had no effect on open-circuit and Tafel behavior of platinum.

manner previously described[9]. Gases were supplied to the cell *via* presaturators containing orthophosphoric acid at the same concentration and temperature as the cell electrolyte. Ultra high-purity hydrogen was further purified by platinized asbestos at 400° C before being led to the cell. Ultra high-purity oxygen or oxygen–nitrogen mixtures (reproducibly mixed to the required p_{O_2} by capillary flow meters) were similarly pretreated, and were continuously bubbled through the cell at a rate of about 10 ml/min. All polarization measurements throughout this work were carried out by conventional galvanostatic methods, although linear sweep voltammetry in nitrogen-saturated solution was also used to examine the adsorption and reduction of oxidation products of water on both metals in the potential range of interest in oxygen electrode work. A Vibron electrometer (input impedence $10^{15}\Omega$) was used for potential measurements, and polarizing currents were measured using a Keithley electrometer. A large-area gold counter-electrode was used. This metal is a poor electrocatalyst for oxygen reduction so that any contamination of iridium working electrodes would have little effect on the results.

Kinetic data and open-circuit potentials given in this paper refer to 85% orthophosphoric acid saturated with oxygen initially at 1 atm pressure, unless otherwise stated. All potentials are referred to a bubbling hydrogen electrode in the same solution (HRE potentials).

RESULTS

Gold electrodes

Open-circuit potentials. Open-circuit potentials noted on gold electrodes were considerably lower than those previously noted on platinum and were much more dependent on temperature. A list of experimental values is given in Table 1. Results at 26° C are some 200 mV lower than those noted by other workers in dilute acids[5,6,10]. The values of open-circuit potentials rise slowly with time; the data in parentheses were noted after 24 h exposure to the solution.

Tafel plots. A series of Tafel plots obtained galvanostatically is shown in Fig. 1. Very little hysteresis was noted between data obtained in the descending direction followed by that for the ascending direction, even after the electrode had been standing in the solution for 24 h. On platinum, traces of non-oxidizable capillary-active impurities present in the electrolyte are adsorbed on the electrode after standing

TABLE 1

OPEN-CIRCUIT POTENTIALS ON GOLD ELECTRODES, OXYGEN-SATURATED SOLUTION

Temp./°C	*Potential/mV(HRE)*
26.0	508
52.1	568
76.1	605 (680)
95.9	667 (685)
116.0	695 (701)
136.1	715 (726)

Values in parentheses are after standing 24 h at open circuit.

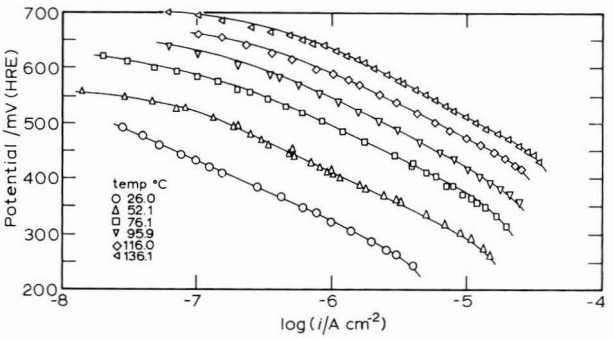

Fig. 1. Oxygen reduction on gold in purified 85% orthophosphoric acid.

for long periods at open circuit.* This results in an electrode which is initially 2 or 3 times less active on the first descending cathodic plot. Initial activity is, however, restored by pulsing to 50 mV when the impurities desorb[11]. No such effect was noted on gold. It therefore appears that the heat of adsorption of impurities is low on this metal presumably because of its filled *d*-band.

Electrodes that have been anodically pulsed into the region (1.5 V) where gold forms an oxide are initially, although only for a short period of time, much more active than electrodes in the normal state. A typical decay curve of such an electrode from the active to the normal state is shown in Fig. 2. Such effects have also been noted by Genshaw *et al.* in dilute sulfuric acid[4].

i_0 and $1/\alpha$ Values. Experimental values of i_0 and $1/\alpha$ are shown in Table 2. The values of i_0 have been obtained by extrapolation of the Tafel lines to the reversible potential at each temperature[11], and have been corrected for oxygen partial pressure effects, assuming the reaction to be first-order (see below).

TABLE 2

KINETIC RESULTS FOR GOLD (corrected for p_{O_2})

Temp./°C	i_0/Acm^{-2}	*Slope/mV decade*$^{-1}$	$1/\alpha$
26.0	1.9×10^{-15}	107	1.80
52.1	7.3×10^{-14}	115	1.79
76.1	6.8×10^{-13}	117	1.71
95.9	4.4×10^{-12}	121	1.66
116.0	1.9×10^{-11}	122	1.58
136.1	1.5×10^{-10}	124	1.53

Order of reaction of oxygen. Tafel plots for three different oxygen partial pressures at 52.1° C are shown in Fig. 3. Oxygen reduction is approximately first-order at constant potential.

Effect of impurities. To investigate the effect of traces of platinum in the solution, some experiments were conducted using a platinum, rather than gold, counter-

* The material is perhaps polyphosphate. Some development of oxide (rather than adsorbed impurites) on the electrode may account for a part of this deactivation effect.

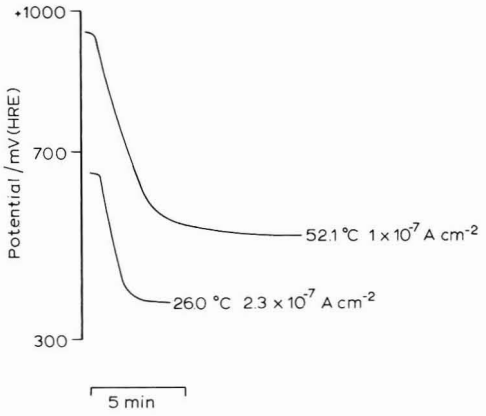

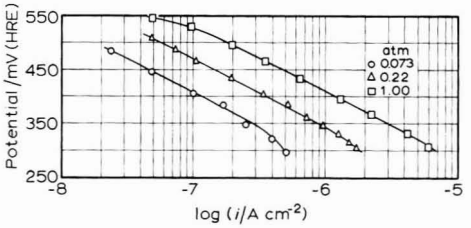

Fig. 2. Potential decay curves at constant current for activated gold electrodes.

Fig. 3. Tafel plots for oxygen reduction on gold at 52.1°C; O_2 partial pressure dependence.

electrode. At low temperatures (below 75° C), little effect was noted. At higher temperatures, gold electrodes showed progressively greater activity when a platinum counterelectrode was used. Traces of platinum dissolved from the counterelectrode during anodizing are plated onto the gold working electrode, resulting in lower polarization. A typical Tafel plot obtained on the gold electrode under these circumstances at 136° C is shown in Fig. 4. At this temperature, activity is increased by a factor of approximately 4.0 at 650 mV, with the two plots merging at lower potentials. At 96° C the corresponding increase was approximately by a factor of 1.4 at 500 mV(HRE.)

These results made it clear that great care must be taken in conducting experiments on electrocatalysis using apparatus containing platinum electrodes or support

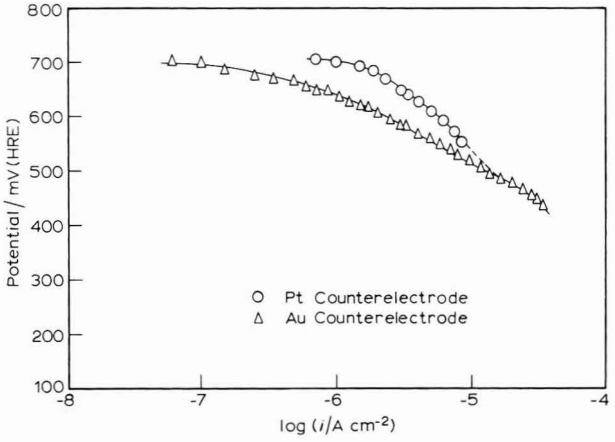

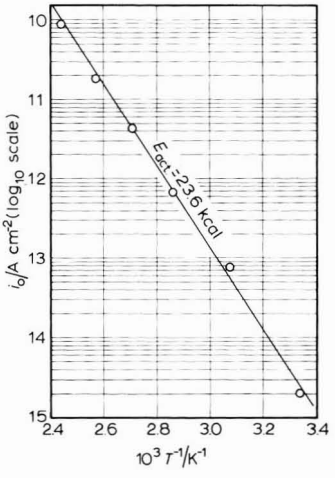

Fig. 4. Oxygen electrode on gold in 85% orthophosphoric acid at 136.1°C.

Fig. 5. Arrhenius plot of i_0 values for oxygen reduction on bright gold in 85% orthophosphoric acid.

wires, especially at high temperatures. Because of the much greater electrocatalytic activity of platinum compared with, for example, gold, the presence of only trace quantities of the former in the solution can lead to gross errors.

Activation energy for oxygen reduction on gold. An Arrhenius plot of log i_0 against $1/T$ is given in Fig. 5. The activation energy was determined to be 23.6 ± 0.8 kcal* at the reversible potential, close to the value obtained earlier for oxide-free platinum (22.9 kcal)[11].

Iridium

Open-circuit potentials. Open-circuit potentials on iridium were somewhat lower than those previously noted on platinum. Experimental values are given in Table 3. As in the case of gold, the second value at each temperature was noted after standing 24 h in the solution.

TABLE 3

OPEN-CIRCUIT POTENTIALS ON IRIDIUM ELECTRODES, OXYGEN-SATURATED SOLUTION

Temp./°C	*Potential/mV (HRE)*
21.0	902 (916)
52.1	898
76.1	927 (938)
95.9	901 (933)
116.0	928
136.1	923

Values in parentheses are after standing 24 h at open circuit.

Tafel plots. A series of Tafel plots was obtained using the technique developed for oxide-free platinum. The electrode was subjected to a series of galvanostatic pulses between open-circuit potential and 50 mV(HRE) to ensure a reproducible impurity free surface[11,12], and the electrode was then allowed to come to its final rest potential at each applied cathodic current density. Results obtained in this manner are plotted in Fig. 6.

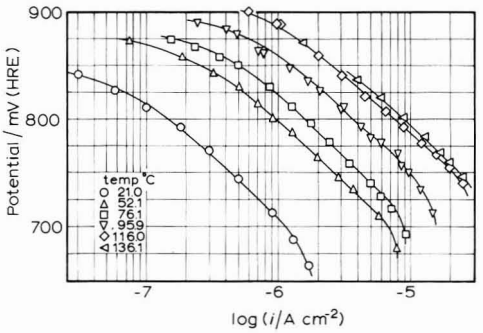

Fig. 6. Tafel plots on iridium electrodes in purified 85% orthophosphoric acid.

* 1 cal = 4.184 J.

The final potential noted for each current density slowly decayed from the maximum value at the rate of a few mV per hour due to deactivation by adsorption of impurities.

Iridium electrodes that stood overnight in the solution produced Tafel plots of lower slope and lower activity at low current density than those shown in Fig. 6. At higher current densities, Tafel plots obtained by pulsing and by stepwise polarization from high potential became coincident. The hysteresis may be attributed to electrode deactivation by adsorption of nonoxidizable capillary-active impurities present in the electrolyte.

i_0 and $1/\alpha$ Values. Experimental values of i_0 and $1/\alpha$ are shown in Table 4. Again, i_0 values are corrected for oxygen partial pressure[11]. Values of $1/\alpha$ approximate to $2RT/F$ at low temperatures, but fall to lower values as the temperature is raised.

Order of reaction for oxygen. Data for four oxygen partial pressures at 52.1° C are shown in Fig. 7. Again, a first-order relationship at constant potential applies.

Activation energy. The experimental value of i_0 at each temperature is plotted in Arrhenius form in Fig. 8. Activation energy is approximately 12.6 ± 1.0 kcal at the reversible potential. The value is substantially lower than the values obtained on gold or oxide-free platinum, although this can be accounted for to some extent by the relative temperature-independence of the Tafel slope on iridium.

TABLE 4

KINETIC RESULTS FOR IRIDIUM (corrected for p_{O_2})

Temp./°C	i_0/Acm^{-2}	*Slope/mV decade*$^{-1}$	$1/\alpha$
21.0	1.1×10^{-11}	112	1.90
52.1	1.6×10^{-10}	115	1.79
76.1	4.7×10^{-10}	118	1.73
95.9	1.4×10^{-9}	116	1.59
116.0	3.5×10^{-9}	110	1.43
136.1	$\sim 7.0 \times 10^{-9}$	~ 110	1.36

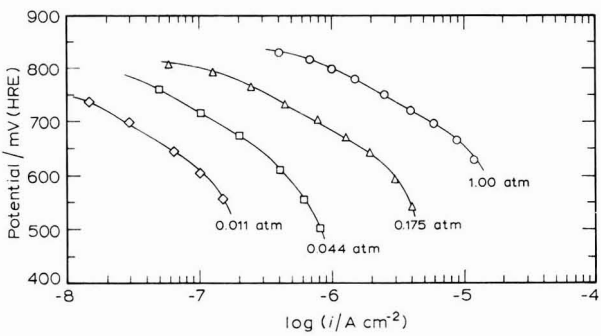

Fig. 7. Tafel plots for oxygen reduction on iridium at 52.1°C; O_2 partial pressure dependence.

DISCUSSION

It has been shown that oxygen reduction on platinum in a phase oxide-free

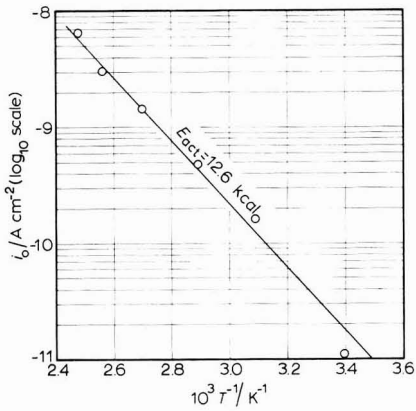

Fig. 8. Arrhenius plot of i_0 values for oxygen reduction on iridium in 85% orthophosphoric acid.

condition in acid solution has the reaction

$$S + O_2 + H^+ + e^- \rightarrow SO_2H$$

as the rate-determining step[11,13], where S is a surface adsorption site on the metal.

Formally, the reaction rate for this step can be written, at constant potential,

$$i = kF\, p_{O_2}[H^+] \exp(-\beta \Delta G/RT) \exp(-\beta FV/RT)$$

where k is a constant, ΔG is the free energy of adsorption of O_2H, and the other symbols have their usual meanings. This equation assumes a negligible free energy of adsorption for O_2 molecules[14]. In the Tafel region, $-O$ and $-OH$ radicals, derived from oxidation of water, are adsorbed on a platinum electrode in coverages that are linearly dependent on potential[13,17]. This implies that the heat of adsorption of $-O$ and $-OH$ radicals on the electrode is linearly coverage-dependent in the medium coverage range; that is, the Temkin isotherm is obeyed. If it is assumed that the heat of adsorption of $-O_2H$ varies with the total coverage[15] of oxygenated species on the electrode, and assuming ΔS to be coverage-independent[16]

$$\Delta G = \Delta H + r\theta - T\Delta S$$

where ΔH is the heat of adsorption at low coverage, and r is the change in heat of adsorption as the total coverage, θ, moves from limitingly low to limitingly high values. Hence under these conditions,

$$i \propto p_{O_2}[H^+] \exp(-\beta r\theta/RT) \exp(-\beta FV/RT)$$

It can be shown that, assuming the Temkin isotherm to apply in the coverage range $0.1 < \theta < 0.9$, where θ is the total electrode coverage of oxygenated species[11,13],

$$\log [H^+] + r\theta = FV$$

Substituting in (2), with $\beta = 1/2$

$$i \propto p_{O_2}[H^+]^{\frac{3}{2}} \exp(-FV/RT)$$

which is in agreement with the experimental Tafel slope[11,13], pH dependence[13], and O_2 reaction order on platinum[11,13].

On gold electrodes in acid solution Tafel slopes close to $2RT/F$ are observed[1,3-6]. Under Langmuir adsorption conditions, we may use the formula[18]

$$\alpha = \beta n + n_a/v$$

where α is the transfer coefficient, β is the symmetry factor of the rate-determining step, n is the number of electrons transferred in one unit rate-determining step of stoichiometric number v, and n_a is the number of electrons transferred before the rate-determining step. Oxygen reduction has been determined to be first-order in the present experiments; hence v is unity.

For the experimental value of $\alpha = \frac{1}{2}$, we have

$$\tfrac{1}{2} = \beta n + n_a$$

Simultaneous two-electron charge transfers can be excluded on activation energy grounds[1]. Hence, the probable value of n is equal to 1 or zero if a chemical rate-determining step is involved. Thus,

$$\beta + n_a = \tfrac{1}{2} \quad \text{if } n = 1$$

or

$$n_a = \tfrac{1}{2} \quad \text{if } n = 0$$

The latter condition is clearly impossible, and assuming physical values for β of 0.5 ± 0.1, n_a must be zero, with $n = 1$.

Hence, under the Langmuir conditions the rate-determining step is a primary charge transfer of the type:

$$O_2 + e^- \rightarrow O_2^-$$

Such a reaction has been suggested by Krasil'shchikov[19] and is supported by Kolthoff and Jordan's[20] pH dependence of zero.

Recent work by Gnanamuthu and Petrocelli* suggests, however, that the pH-dependence behavior of gold is quite complex[1]. These authors show that in the region of pH 0–5, the Tafel slope for oxygen reduction on gold is about $2RT/F$, and i is pH-dependent at constant potential. Above pH 5, the slope falls as pH rises, and pH-dependence is small.

On this basis, the most probable rate-determining step on gold in acid solutions is

$$S + O_2 + H^+ + e^- \rightarrow SO_2H$$

the same as that on platinum. On gold, however, the $S-O_2H$ bond is comparatively weak, so that the major reaction product after further electron transfer is hydrogen peroxide[4,5]. On platinum the higher heat of adsorption encourages O–O bond fission[11,21].

There is little doubt that on gold the coverage with adsorbed oxygen is very low in the potential range of interest. A cyclic voltammetric scan in nitrogen-saturated 85% orthophosphoric acid solution is shown in Fig. 9. It shows virtually no pseudo-capacitance in the 300–700 mV range. It is therefore improbable that adsorption conditions other than Langmuirian occur.

---

* The same authors point out that $O_2 + e^- \rightarrow O_2^-$ may have a Tafel slope greater than $2RT/F$.

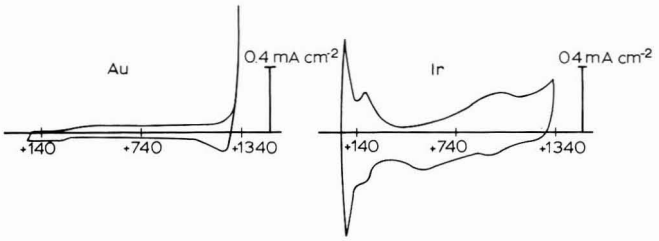

Fig. 9. Cyclic voltammetric scans at 260 mV s^{-1}, nitrogen-saturated 85% orthophosphoric acid at 95.9°C (horizontal scale = mV (HRE)).

It is interesting to note that a double Tafel slope, with a step-like transition region separating the two zones, has been observed by many workers on gold oxygen electrodes. The upper portion only occurs at low current densities, and in it oxygen is reduced directly to water. In view of the work reported here using a platinum counter-electrode, it is tempting to suggest that this portion of the curve was a result of traces of platinum in the solution derived from the purification procedure.

On iridium, similar Tafel slopes to those on gold are encountered, and again oxygen reduction is first-order. Under the Langmuirian conditions, therefore, the same rate-determining step as that on gold may be expected.* It becomes much more difficult to account for the mechanistic data on iridium if Temkin (or other coverage-dependent) adsorption conditions apply.

Dahms and Bockris[22] show a sharp potential-coverage dependence for iridium electrodes in 1 *M* sulfuric acid at 80° C, which would indicate behavior approximating Langmuirian, and Böld and Breiter[23] consider their cyclic voltammetric scans on iridium, which show quasi-reversible behavior, best explained in Langmuirian terms. Similar scans are obtained in nitrogen-saturated 85% orthophosphoric acid solution (Fig. 9). Heats of adsorption of oxygenated compounds on iridium are considerably higher than those on gold. Hence, a mechanism involving adsorbed–O_2H radicals should have a lower activation energy on iridium, which is in agreement with the experimental data obtained here. In consequence, the rate-determining step on pre-reduced iridium is in all probability the same as that on oxide-free gold and platinum for the oxygen reduction reaction in acid solutions.

ACKNOWLEDGEMENT

The author wishes to thank the sponsors of the Target Fuel Cell program and Pratt and Whitney Aircraft Division of United Aircraft Corporation for permission to publish this work, along with the members of IGT who helped in the preparation of the publication.

SUMMARY

Cathodic reduction of oxygen has been studied on bright gold and bright pre-

* No pH-dependence data are available, but it is improbable that the H^+ order is zero in strong acid solutions.

reduced iridium electrodes in purified 85% orthophosphoric acid as a function of temperature. Tafel slopes on both metals were close to $2RT/F$ at room temperature, but slopes were not significantly temperature-dependent. As was the case for platinum[11], exchange current values on gold were about 2–3 orders of magnitude lower in 85% orthophosphoric acid than in dilute acids at room temperature[3,4,13]; i_0 for gold was about 10^{-15} A cm^{-2} at 26.0° C, i_0 on iridium was higher ($\sim 10^{-11}$ at 21° C), but the high Tafel slope on this metal makes it a less effective electrocatalyst than platinum under the same potential conditions. Oxygen reduction is first-order on these metals. Activation energy at the reversible potential on gold was determined to be 23.6 ± 0.8 kcal; on iridium the value was 12.6 ± 1.0 kcal.

The suggested rate-determining step for both metals is

$$O_2 + H^+ + e^- \rightarrow -O_2H_{ads}$$

the $-O_2H$ radical being adsorbed under Langmuir conditions. The stronger affinity of iridium for adsorbed oxygenated compounds accounts for its lower activation energy.

It has been established that iridium is sensitive to traces of capillary-active impurities in solution, which result in deactivated electrodes with lower Tafel slopes. Gold is very sensitive to traces of platinum from counterelectrodes or preelectrolysis electrodes.

REFERENCES

1 D. S. GNANAMUTHU AND J. V. PETROCELLI, *J. Electrochem. Soc.*, 114 (1967) 1036.
2 M. L. B. RAO, A. DAMJANOVIC AND J. O'M. BOCKRIS, *J. Phys. Chem.*, 67 (1963) 2508.
3 A. DAMJANOVIC AND V. BRUSIĆ, *Electrochim. Acta*, 12 (1967) 1171.
4 M. A. GENSHAW, A. DAMJANOVIC AND J. O'M. BOCKRIS, *J. Electroanal. Chem.*, 15 (1967) 163.
5 G. BIANCHI, F. MAZZA AND T. MUSSINI, *Electrochim. Acta*, 11 (1966) 1509.
6 J. P. HOARE, *Electrochim. Acta*, 11 (1966) 203.
7 J. P. HOARE, *J. Electroanal. Chem.*, 18 (1968) 251.
8 A. DAMJANOVIC, A. DEY AND J. O'M. BOCKRIS, *J. Electrochem. Soc.*, 113 (1966) 739.
9 A. J. APPLEBY, *J. Electroanal. Chem.*, 24 (1970) 97.
10 J. P. HOARE, *J. Electrochem. Soc.*, 110 (1963) 245.
11 A. J. APPLEBY, *J. Electrochem. Soc.*, 117 (1970) 328.
12 S. D. JAMES, *J. Electrochem. Soc.*, 114 (1967) 1113.
13 A. DAMJANOVIC AND V. BRUSIĆ, *Electrochim. Acta*, 12 (1967) 615.
14 J. O'M. BOCKRIS AND T. EMI, private communication.
15 B. E. CONWAY AND E. GILEADI, *Trans. Faraday Soc.*, 58 (1962) 2493.
16 R. PARSONS, *Trans. Faraday Soc.*, 54 (1958) 1053.
17 H. WROBLOWA, M. L. B. RAO, A. DAMJANOVIC AND J. O'M. BOCKRIS, *J. Electroanal. Chem.*, 15 (1967) 139.
18 A. DAMJANOVIC, A. DEY AND J. O'M. BOCKRIS, *Electrochim. Acta*, 11 (1966) 791.
19 A. I. KRASIL'SHCHIKOV, *Soviet Electrochemistry*, Vol. II, Plenum Publishing Corp., New York, 1961.
20 I. M. KOLTHOFF AND J. JORDAN, *J. Am. Chem. Soc.*, 74 (1952) 4801.
21 A. DAMJANOVIC, M. A. GENSHAW AND J. O'M. BOCKRIS, *J. Electrochem. Soc.*, 114 (1967) 466.
22 H. DAHMS AND J. O'M. BOCKRIS, *J. Electrochem. Soc.*, 111 (1964) 728.
23 W. BÖLD AND M. BREITER, *Electrochim. Acta*, 5 (1961) 169.

ELECTROANALYTICAL CHEMISTRY AND INTERFACIAL ELECTROCHEMISTRY
Elsevier Sequoia S.A., Lausanne – Printed in The Netherlands

OXYGEN REDUCTION STUDIES AT SMOOTH PRE-REDUCED RUTHENIUM AND RHODIUM ELECTRODES IN 85% ORTHOPHOSPHORIC ACID

A. J. APPLEBY
Institute of Gas Technology, Chicago, Illinois (U.S.A.)
(Received January 20th, 1970; in revised form April 11th, 1970)

INTRODUCTION

Rhodium electrodes that have been previously oxidized and then subjected to reducing conditions are reported by Hoare[1] to have Tafel slopes for oxygen reduction varying between 85 and 303 mV/decade in dilute sulfuric acid at room temperature. Under similar conditions, Gnanamuthu and Petrocelli[2] report a slope of 120 mV/decade, with 80 mV for ruthenium. A paper by Damjanovic *et al.*[3] gives a Tafel plot on pre-reduced rhodium electrode in dilute perchloric acid at room temperature in which the slope appears to be about 50 mV/decade, similar to that on platinum electrodes with the same surface preparation. Apart from Gnanamuthu and Petrocelli's[2] work, no V–log i data for oxygen reduction on ruthenium electrodes in acid solution have been reported. In this paper, ruthenium and rhodium oxygen electrodes in the pre-reduced (phase-oxide-free) condition are studied in 85% orthophosphoric acid as a function of temperature.

EXPERIMENTAL

All experiments were conducted in the all-silica cell used in previous work. Experimental conditions, supply and purification of gases, and details of the galvanostatic circuit used in polarization measurements have been previously published[4]. Electrodes were in the form of small disks of rhodium and ruthenium of zone-refined (99.999% nominal) purity, cut from 5-mm diameter rods using a diamond saw. They were welded to gold wires and were ground and polished to a mirror finish using graded alumina powders. Following this treatment, electrodes were degreased with organic solvents and washed in concentrated HCl, conductivity water, and the electrolyte itself before use. They were then potentiostatted in the cell at a potential of 50 mV (HRE) for 2 h to reduce any residual oxides before measurements were taken. Towards the end of this period the electrolyte was saturated with oxygen by bubbling.

The electrolyte (85% orthophosphoric acid) was prepared by treatment with hydrogen peroxide as in previous experiments[4]. No preelectrolysis was used to avoid the possibility of contamination of the electrolyte with platinum. For the same reason, a gold counterelectrode was used in the electrochemical circuit, as in previous work[5].

Polarization measurements on the electrodes were all made galvanostatically.

Cyclic voltammetry, using a Wenking potentiostat driven by a triangular sweep generator, was used in nitrogen-saturated solution to study the oxidation and reduction characteristics of adsorbed films of O and OH radicals derived from water oxidation. Throughout all this work the reference electrode was a bubbling hydrogen electrode in the same solution to which all potentials are referred (HRE potentials).

RESULTS

Open-circuit potentials

Open-circuit potentials attained within a few minutes after the release of the potentiostatic circuit holding the electrode at 50 mV are shown for both ruthenium and rhodium in Table 1. These initial potentials represent less than 1 mV change in 5 min, though a very slow rise to higher values took place over a period of hours. Where only one value is quoted in Table 1, it is the initial value. It is apparent from the Tables that there is some tendency for the open-circuit potentials to fall with temperature, presumably reflecting the increasing ease of formation of equilibrium oxide coverage as temperature rises. Open-circuit potentials noted are somewhat similar to those observed on iridium in the same electrolyte[5], and appreciably lower than those on platinum[6].

TABLE 1

OPEN-CIRCUIT POTENTIALS ON BRIGHT PRE-REDUCED RHODIUM AND RUTHENIUM ELECTRODES, OXYGEN-SATURATED SOLUTION

Temp./°C	*Potential/mV (HRE)*	
	Rh	*Ru*
22.0	847 (858)	899 (903)
52.1	840 (897)	867 (880)
76.1	880 (904)	814 (862)
95.9	878	
104.0		790 (880)
116.0	858	
136.1	843	793

Values in parentheses were attained after 24 h at open circuit.

Tafel plots

Tafel plots were made at a number of temperatures in the range 22.0°–136.1° C. Electrodes were pulsed between 50 mV and open circuit to desorb trace impurities[5], and steady-state (less than 2 mV in 2 min) galvanostatic data were obtained. In some cases, electrodes were examined after they had been allowed to remain at open circuit for long periods in the solution (24 h). Such plots are discussed below.

Figures 1 and 2 show Tafel plots obtained by the pulsing technique on rhodium and ruthenium electrodes. For the rhodium electrode plots, it is not easy to fit accurate values to Tafel slopes at the higher temperatures studied but straight portions occur over ranges of less than one decade. Slopes in this range are close to RT/F, *i.e.*, the same as on bare platinum[6,7]. At low temperatures ($< 76.0°$ C) a longer Tafel range occurs with a slope of RT/F, with an increase in slope at higher current densities.

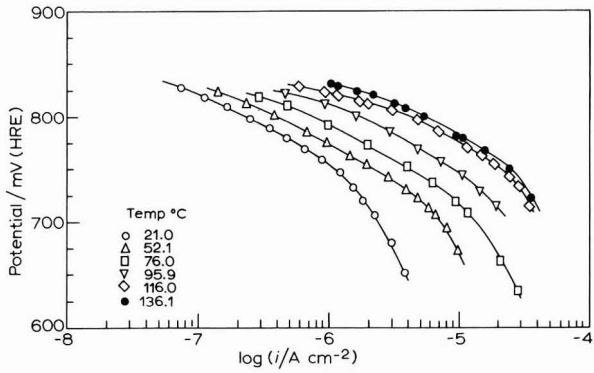

Fig. 1. Tafel plots on rhodium electrodes.

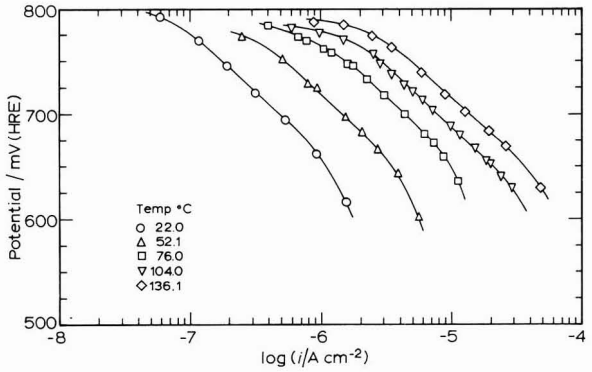

Fig. 2. Tafel plots on ruthenium electrodes.

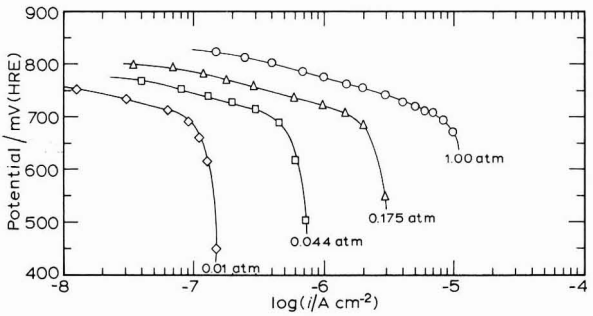

Fig. 3. Tafel plots of rhodium at 52.1°C at different O_2 partial pressures; purified 85% H_3PO_4.

On ruthenium electrodes, slopes are close to $2RT/F$ at low temperatures, but are essentially independent of temperature, so that $1/\alpha$ falls to about 1.42 at 136.1° C.

Values for the Tafel slope $1/\alpha$ and i_0 (corrected for oxygen partial pressure assuming a first-order process, as determined below) on each electrode are given in Tables 2 and 3. The i_0 values were obtained by extrapolating the Tafel line back to the theoretical reversible potential[6] at each temperature.

TABLE 2

KINETIC DATA FOR OXYGEN REDUCTION ON RHODIUM

Temp./°C	*Slope/mV*	$1/\alpha$	$i_0/A\ cm^{-2}$ (*corr. for* pO_2)
22.0	60	1.03	4.3×10^{-15}
52.1	64	0.99	6.4×10^{-14}
76.1	68	1.00	5.6×10^{-13}
95.9	73	1.00	5.3×10^{-12}
116.0	75	0.97	4.1×10^{-11}
136.1	75	0.92	1.4×10^{-10}

TABLE 3

KINETIC DATA FOR OXYGEN REDUCTION ON RUTHENIUM

Temp./°C	*Slope/mV*	$1/\alpha$	$i_0/A\ cm^{-2}$ (*corr. for* p_{O_2})
22.0	115	1.97	6.2×10^{-12}
52.1	115	1.79	3.1×10^{-11}
76.1	115	1.69	1.5×10^{-10}
104.0	115	1.54	4.3×10^{-10}
136.1	115	1.42	2.4×10^{-9}

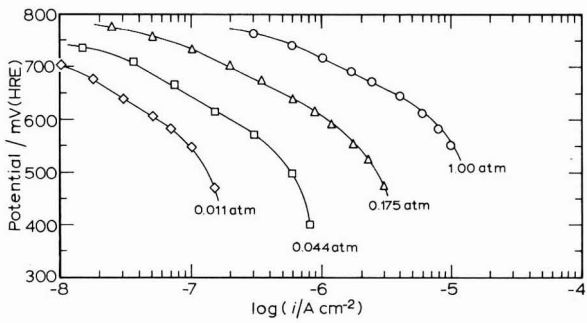

Fig. 4. Tafel plots of ruthenium at 52.1°C at different O_2 partial pressures; purified 85% H_3PO_4.

Oxygen reaction order

Tafel plots obtained at four oxygen partial pressures are shown in Figs. 3 and 4. These results were obtained in the same way as in previous work on platinum[6], gold[5], and iridium[5] electrodes. In each case, an approximately first-order reaction mechanism takes place at constant potential.

Activation energy

Arrhenius plots of i_0 *vs.* $1/T$ are shown for electrodes of both metals (Figs. 5 and 6). Activation energies* at the reversible potential are 22.0 ± 1.5 kcal** for

* No correction has been made for changes in oxygen solubility, or water or H^+ activity as a function of temperature, as in previously reported data.

** 1 cal. ≡ 4.184 J.

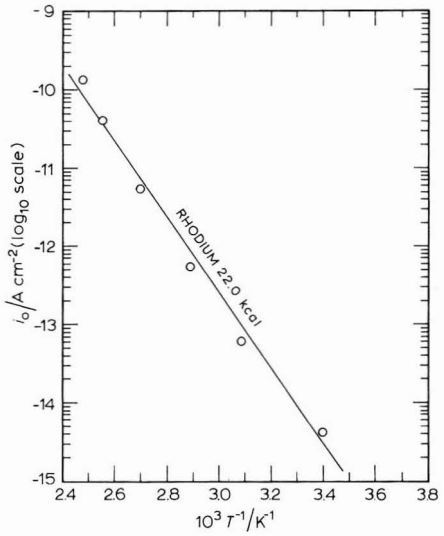

Fig. 5. Arrhenius plot of i_0 values for oxygen reduction on bright rhodium in 85% orthophosphoric acid.

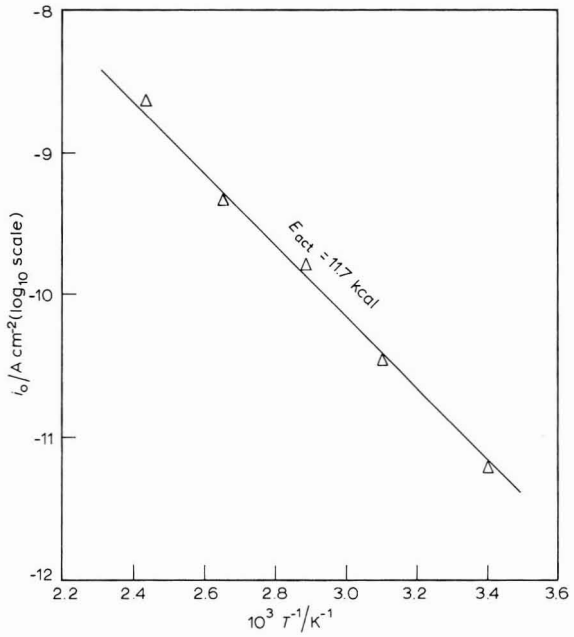

Fig. 6. Arrhenius plot of i_0 values for oxygen reduction on bright ruthenium in 85% orthophosphoric acid.

rhodium, close to the value previously reported for oxide-free platinum (22.9 kcal)[6]. The value experimentally measured on ruthenium is much lower (11.7 ± 0.5 kcal), but this figure is lower than might be expected owing to the temperature-independence of the Tafel slope on this metal. If α had been temperature-independent on ruthenium,

the corresponding activation energy value would have been approximately 17.0 kcal, somewhat less than the corresponding value on iridium, assuming a temperature-dependent value of α for that metal (17.9 kcal compared with the measured value of 12.6 kcal)[5].

DISCUSSION

Variation of α with temperature

On oxide-free iridium, ruthenium, and gold electrodes the Tafel slope for oxygen reduction is very nearly temperature-independent. It is not easy to explain this fact in a convincing manner. However, it implies that the entropy of activation is potential-dependent[8], assuming that the potential-independent part of the heat of activation, *i.e.*, the chemical heat of activation, remains constant. If the chemical heat of activation depends on potential, (for example, if heats of adsorption of reaction intermediates are potential-dependent) two parallel mechanisms are implied, one being favored at high potentials, the other at the low-potential end of the plot. Such a dual mechanism would almost certainly produce a nonlinear Tafel plot.

Slopes almost independent of temperature have been noted by other workers for oxygen evolution electrode systems and are not a new phenomenon[8,9]. Several possible explanation for the variation of α with temperature may be suggested.

(1) Change in *entropy of activation*, which indicates variation in the probability formation of an activated complex (or an active site) with potential. This may be the result of a real change in the number of available sites on the metal surface as a result of impurity adsorption or desorption. It may also be accompanied by the change in chemical heat of activation (a separate phenomenon) due to alteration in electronic structure of the metal surface as a result of the presence of the adsorbate, so that the heat of adsorption of reaction intermediates changes.

(2) Change in the probability of active site formation as a function of potential because of changes in the oxygen adsorbate coverage on the electrode, the same factors operating as in (1). An increase in the potential-dependence of heat of adsorption with temperature due to the changes in double-layer structure* causing increasing bond polarization is also formally possible. For oxygen reduction on ruthenium and iridium, interaction between neighboring adsorbed $-O$ and $-OH$ groups may be temperature-dependent, so there is a tendency for the heat of adsorption of reaction intermediates to change from Langmuir to Temkin (or other coverage-dependent) conditions at high temperatures. The effect of this would be to give a value of α that increases with temperature, assuming a constant symmetry factor. Neither (1) nor (2) is considered likely to apply on gold electrodes, as the tendency of this metal to adsorb either oxygen or impurities is small on the potential range in which data were obtained[5].

(3) Variation of the symmetry factor with temperature; the two previous explanations have assumed a constant symmetry factor. If the Morse function of the reacting species becomes steeper as the temperature increases because of modifications in double-layer structure, then an increase in β will be observed from the nominal

* For instance, changes in specific adsorption of anions.

value of 0.5. This is considered to be the most probable explanation for the changes in α with temperature in oxygen reduction on gold[5].

Impurity effects

Rhodium electrodes are very sensitive to the presence of trace impurities that are not removed by normal preelectrolysis or oxidative treatment of the electrolyte. Such impurities are probably traces of organic polymers and certain foreign specifically adsorbed ions. In phosphoric acid, polyphosphate may be responsible, though Bockris *et al.*[10] consider the $H_2PO_4^-$ ion itself responsible for phenomena associated with strong adsorption, which on platinum occurs in the 400–700 mV (HRE) range[6]. The general effect of this time-dependent phenomenon, noted by Müller and Nekrasov[11] in dilute sulfuric acid, is to progressively poison the platinum electrode with increasing potential, resulting in very steep steady-state Tafel slopes (for instance, as noted by Bianchi and Mussini[12] in chloride solutions).

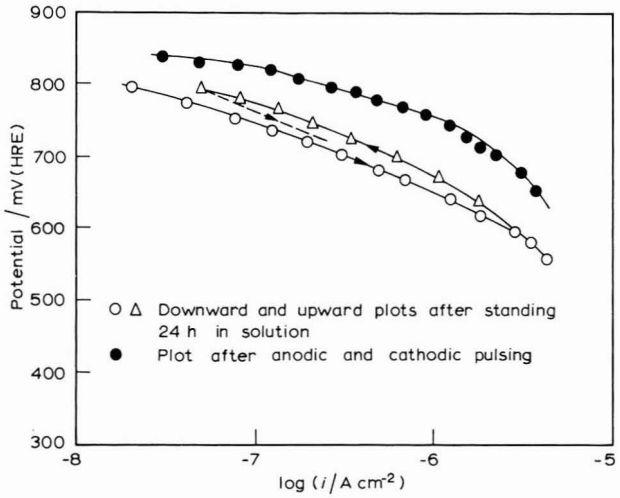

Fig. 7. Tafel plots on rhodium showing desorption–adsorption hysteresis at 22.0°C.

At potentials of about 700 mV, very steep Tafel slopes are noted on rhodium before the limiting current region is reached (for example, the plot for 76.1° C in Fig. 1). The points on such plots are time-dependent and higher values, corresponding to approximately RT/F slopes, are observed immediately after pulsing. Similar steep slopes have been noted at high current densities in previous work[1]. This effect is probably due to an adsorption-dependent change of mechanism.

A Tafel plot of oxygen reduction on a rhodium electrode that had been allowed to stand for 24 h at open circuit is shown in Fig. 7. In the initial steady-state downward plot, points were taken after 10 min at each current density. The second (upward) plot shows similar ascending points taken after the plotting direction was reversed from the highest current density studied. A further reversal of the plotting direction led to a curve between the two. The final plot (clean surface) was obtained after pulsing to desorb impurities and has a somewhat lower slope than the two previous sets of

data, at considerably higher potentials. In each case, an increasing slope at higher current densities is apparent, reflecting a change in mechanism. It is possible that this hysteresis is caused to some extent by increasing irreversible adsorption of oxygen radicals (or oxide formation) when electrodes stand for some time at open circuit, but adsorption of capillary-active impurities is probably the major influence.

Iridium and ruthenium electrodes*, in contrast to those of rhodium, show deactivation effects that are more apparent at high potentials (Tafel plots taken after standing for long periods in the electrolyte tend to have *lower* slopes than those obtained by pulsing) so that the initial and pulsed plots become identical at sufficiently high current densities. It is interesting to note in this connection that steady-state oxygen reduction Tafel plots of slopes less than $2RT/F$ in acid solution have been observed on ruthenium and iridium by Gnanamuthu and Petrocelli[2].

Reduction mechanism

Previous publications have dealt with the question of oxygen reduction on oxide-free platinum[6] and oxide-free gold and iridium[5] in acid media, in particular 85% orthophosphoric acid.

These metals, like rhodium and ruthenium, show a first-order dependence for oxygen reduction. This implies a reductive sequence in which the stoichiometric number is unity in the rate-determining step. Gold, iridium, and ruthenium electrodes gave Tafel slopes of about $2RT/F$ for oxygen reduction. Assuming the Langmuir isotherm holds for any adsorbed intermediates and neglecting reactions with 2-electron charge transfers**, it has been shown previously[5] that such data are only explicable in terms of a charge transfer reaction without previous charge transfer as the rate-determining step. A useful list of mechanisms that have been proposed for the oxygen electrode reaction on noble metals has been provided by Gnanamuthu and Petrocelli[2]. In each case, these mechanisms are given theoretical Tafel slopes, calculated assuming Langmuir adsorption occurs. These authors have in certain cases made corrections for possible incomplete transfer of charge across the double layer, for instance when an electron is transferred to a neutral species specifically adsorbed on the electrode surface (presumably within the double layer) without simultaneous transfer of a proton from the solution. If such a reaction occurs, higher-than-normal Tafel slopes may be predicted. Only two reactions satisfy the necessary Tafel slope and stoichiometric number conditions for ruthenium, gold, and iridium. These are

(i) $O_2 + e^- \rightarrow O_2^-$

(ii) $S + O_2 + H^+ + e^- \rightarrow SO_2H$

Gnanamuthu and Petrocelli[2] have pointed out that the Tafel slope of (i) may be appreciably higher than $2RT/F$, owing to the charge transfer across a potential barrier less than that for the metal–solution interface. On this basis, (ii) is the most probable rate-determining step, and pH-dependence measurements have shown it to be the most probable reaction on gold[5] and platinum[6]. *Slow* proton addition, as a subsequent step, to O_2^- is improbable in acid solution; hence, the same reaction is

* Hysteresis effects of the same type as those on rhodium were also observed on electrodes of these metals.
** These are assumed to require too-high an activation energy.

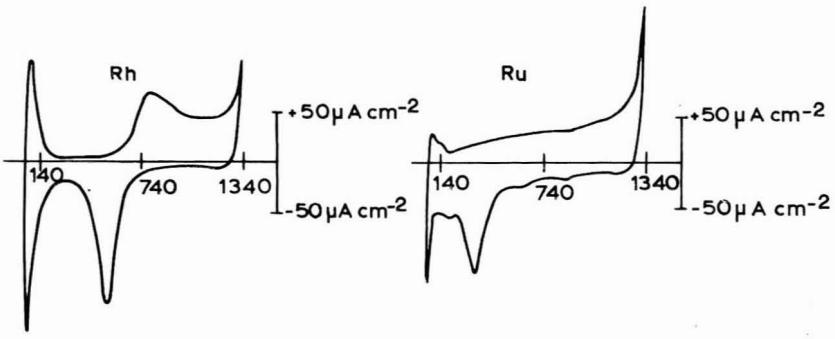

Fig. 8. Cyclic voltammetric scans at 26 mV s^{-1}, nitrogen-saturated 85% orthophosphoric acid at 95.9°C (horizontal scale = mV (HRE)).

almost certainly also applicable to iridium and ruthenium electrodes. A cyclic voltammetric scan on ruthenium is shown in nitrogen-saturated 85% orthophosphoric acid in Fig. 8. It is evident from the scan that coverages of oxygen or OH radicals derived from water oxidation are relatively high at potentials corresponding to the oxygen reduction Tafel range. Adsorption of oxygen starts at even lower potentials than on iridium. Under equilibrium conditions, therefore, high coverages of O and OH may be expected on the electrode; hence, adsorption of O_2H will be Langmuirian.

On platinum, the experimental Tafel slope (about RT/F) was interpreted in terms of a Temkin isotherm operating for adsorbed O and OH on the electrode[6,7]. Linear coverage–potential plots for these species are observed on platinum.

For the equilibrium

$$Pt + H_2O \rightleftarrows Pt - OH + H^+ + e^-$$

which represents the reaction for adsorption of intermediates on the electrode, we may write

$$\theta/(1-\theta) = k[H^+] \exp(-\Delta G/RT) \exp(FV/RT) \quad (1)$$

where θ is the coverage in OH, ΔG is the standard free energy of adsorption of OH (defined at $\theta = 1/2$), k is a constant, and F, V, R, and T have their usual meanings.

Taking logarithms and neglecting variations of $\log[\theta/(1-\theta)]$ in the medium coverage range ($0.1 > \theta > 0.9$), we have

$$\log[H^+] - \Delta G/RT = -FV/RT + \text{const.} \quad (2)$$

or

$$\log[H^+] - \Delta H/RT = -FV/RT + \text{const.} \quad (3)$$

where ΔH is assumed to be coverage-dependent, and ΔS, the standard entropy of activation, is assumed in this model to be coverage-independent[13]. Hence,

$$\log[H^+] - \Delta H/RT + [f(r, \theta - \tfrac{1}{2})]/RT = -FV/RT + \text{const.} \quad (4)$$

where ΔH is the heat of adsorption of OH at $\theta = \frac{1}{2}$ (standard state), and $f(r, \theta - \frac{1}{2})$ is a coverage-dependent part of the heat of adsorption, r being a constant. Under Temkin conditions,

$$f(r, \theta - \tfrac{1}{2}) = r\theta - r/2 \tag{5}$$

Hence,

$$\log [H^+) + r\theta/RT = -FV/RT \tag{6}$$

where $V = 0$ corresponds to a limitingly low θ at $[H^+] = 1$. This is in agreement with the experimentally observed linear coverage–potential relationship in the medium coverage ($0.1 > \theta > 0.9$) range[7,14]. It is assumed that the heat of adsorption of the product of the rate-determining step, $-O_2H$, the individual coverage of which is comparatively low, varies with the total coverage[15] of oxygenated material on the electrode surface in the same way as predicted by eqn. (6).

The rate equation for reaction (ii) may be written

$$i = kF[H^+]p_{O_2} \exp(-\beta r\theta/RT) \exp(-\beta FV/RT) \tag{7}$$

assuming adsorption of O_2 molecules to be Langmuirian, where k is a constant, and β is the symmetry factor. Hence, substituting eqns. (6) and (7), with $\beta = \frac{1}{2}$ we obtain

$$i = kF[H]^{\frac{3}{2}} p_{O_2} \exp(-FV/RT)$$

which is in accordance with the observed Tafel slopes[6] and the pH-dependence[7] on platinum electrodes.

It is probable that the same type of mechanism applies to rhodium.

Rhodium electrodes with reproducibly clean surfaces show the same Tafel slope and oxygen reaction order as platinum, and cyclic scans on rhodium electrodes (Fig. 8) show striking similarity to those on platinum, though O or OH adsorption starts at lower potentials. Böld and Breiter[16] have explained the flat-topped anodic adsorption curve in terms of a Temkin isotherm. It thus seems probable that a Temkin isotherm can also be assumed for the adsorption of O_2H, the product of the rate-determining step.

It is also interesting to note that the activation energy on oxide-free rhodium at the reversible potential (22.0 kcal, Fig. 5) is close to the value for platinum (22.9 kcal)[6].

ACKNOWLEDGEMENT

The author wishes to thank the sponsors of the Target Fuel Cell Program and Pratt and Whitney Aircraft Division of United Aircraft Corporation for permission to publish this work. The help of the members of IGT who assisted in the preparation of the publication is also greatly appreciated.

SUMMARY

Cathodic reduction of oxygen has been studied on bright oxide-free rhodium and ruthenium electrodes in purified 85% orthophosphoric acid as a function of temperature. Tafel slopes on reproducibly clean rhodium electrodes are close to RT/F; on ruthenium the corresponding value is about $2RT/F$. The Tafel slope on ruthenium did not have the theoretical temperature-dependence. A similar effect was previously noted on gold and iridium electrodes under the same conditions[5]. On

rhodium an apparent increase in Tafel slope occurs at higher current densities. This may indicate a change in mechanism. Ruthenium behaves like iridium[5] in the presence of impurities: These result in deactivated electrodes with lower Tafel slopes.

The exchange current on rhodium was about 2 orders of magnitude less than that on platinum (slope also RT/F)[6] under the same conditions. The value of i_0 on ruthenium was similar to that noted on iridium (about 10^{-11} A cm^{-2}) under the same conditions. Oxygen reduction is first-order on these metals. Activation energies at the reversible potential were determined to be 22.0 ± 1.5 kcal on rhodium, similar to the value (22.9 kcal) reported on platinum[6], and 11.7 ± 0.5 kcal on ruthenium, somewhat less than the value (12.6 kcal) on iridium[5].

The suggested rate-determining step on these metals is

$$O_2 + H^+ + e^- \rightarrow O_2H_{ads}$$

On rhodium, it occurs under Temkin adsorption conditions in the potential range where medium coverages of adsorbed O and OH radicals (from water oxidation) are present on the electrode. On ruthenium, high coverages of these radicals occur, and adsorption is Langmuirian.

REFERENCES

1 J. P. Hoare, *Electrochim. Acta*, 11 (1966) 203; 13 (1968) 417.
2 D. S. Gnanamuthu and J. V. Petrocelli, *J. Electrochem. Soc.*, 114 (1967) 1036.
3 A. Damjanovic, A. Dey and J. O'M. Bockris, *J. Electrochem. Soc.*, 113 (1966) 739.
4 A. J. Appleby, *J. Electroanal. Chem.*, 24 (1970) 97.
5 A. J. Appleby, *J. Electroanal. Chem.*, 27 (1970) 325.
6 A. J. Appleby, *J. Electrochem. Soc.*, 117 (1970) 328.
7 A. Damjanovic and V. Brusić, *Electrochim. Acta*, 12 (1967) 615.
8 J. N. Agar, *Discussions Faraday Soc.*, 1 (1947) 81.
9 W. Roiter and R. Jampolskaja, *Acta Physicochim. U.R.S.S.*, 7 (1937) 247.
10 J. O'M. Bockris, B. D. Cahan and G. E. Stoner, *Chem. Instrumentation*, 1 (1969) 273.
11 L. Müller and L. N. Nekrasov, *Dokl. Akad. Nauk SSSR*, 154 (1964) 437.
12 G. Bianchi and T. Mussini, *Electrochim. Acta*, 10 (1965) 445.
13 R. Parsons, *Trans. Faraday Soc.*, 54 (1958) 1053.
14 H. Wroblowa, M. L. B. Rao, A. Damjanovic and J. O'M. Bockris, *J. Electroanal. Chem.*, 15 (1967) 139.
15 B. E. Conway and E. Gileadi, *Trans. Faraday Soc.*, 58 (1962) 2493.
16 W. Böld and M. Breiter, *Electrochim. Acta*, 5 (1961) 169.

ELECTROANALYTICAL CHEMISTRY AND INTERFACIAL ELECTROCHEMISTRY
Elsevier Sequoia S.A., Lausanne – Printed in The Netherlands

OXYGEN REDUCTION ON PLATINUM–RUTHENIUM ALLOY ELECTRODES IN 85% ORTHOPHOSPHORIC ACID

A. J. APPLEBY
Institute of Gas Technology Chicago, Illinois (U.S.A.)
(Received April 14th, 1970)

INTRODUCTION

A number of studies of oxide-free alloy systems for oxygen electrode kinetics in dilute acid solutions at room temperature have been reported. The system most widely studied has been gold–palladium[1-3], but platinum–rhodium[4] and platinum–gold[1,2] have also received consideration. Studies on gold–palladium[1] have shown that gold-rich alloys behave with the characteristic $2RT/F$ Tafel slope of gold until a composition of about 40 atom percent of palladium is reached, at which point the alloy shows the RT/F Temkin-type Tafel slope[5] characteristic of palladium, and suddenly shows much greater activity. Gold appeared to act as an inert dilutant as far as activity was concerned; no synergistic effects were noted. A further series of studies carried out by Hoar and Brooman[6,7] on Pt–Ru, Pt–Rh, and Pt–Ir alloys containing low atomic percentages of the alloying metal indicated that, at least under the conditions of study in dilute sulfuric acid at room temperature, such alloys were more active for oxygen reduction than platinum itself. The rate enhancement for such alloys over pure platinum has been noted for gas-phase catalysis processes. In particular, Bond and Webster[8,9] have shown that coreduced Pt–Ru oxides gave a more reactive catalyst than either metal alone for certain hydrogenation processes. Other examples of marked synergistic effects have also been reported[10].

Accordingly, an investigation was carried out on one of the above alloy systems. The platinum–ruthenium system was chosen, as platinum and ruthenium show different Tafel slopes for the reaction

$$O_2 + H^+ + e^- \rightarrow O_2H \text{ (adsorbed)}$$

which is rate-determining for oxygen reduction in acid solution on noble metals that are not oxidized[5,11-13]. The difference in Tafel slopes arises from the type of isotherm involved in the adsorption of the O_2H radical on the electrode surface. On platinum, the heat of adsorption is potential-dependent (Temkin dependence), and the Tafel slope is thus influenced by this consideration, giving a value of RT/F rather than the expected $2RT/F$ slope for a discharge process without previous charge transfer[5,11]. On ruthenium, the slope is approximately $2RT/F$, and the Langmuir isotherm applies[13]. This consideration and the fact that platinum is the most active metal at about 800 mV, pure ruthenium being the least active of the above alloying metals at the same potential, indicate that divergencies in behavior should be more marked for intermediate Pt–Ru alloys than for any other of the above alloy systems.

EXPERIMENTAL

A series of alloys was obtained containing 8, 18, 40, and 60 atom percent of ruthenium and platinum, all in the solid solution range*. The 8 and 18 atom percent alloys were commercial products (Engelhard Industries Inc.) in the form of flat rolled sheets, 0.01 in thick. The 40 and 60 atom percent alloys were prepared by vacuum induction melting of the powdered metals (Metals Research Ltd., Cambridge, England), and samples, in the form of flat disks, were cut from the interior of small castings using a diamond saw. Samples of each alloy were ground and polished with alumina powders, were spot welded to gold wires, and were then subjected to a standard cleaning procedure. This consisted of washings in concentrated HCl, conductivity water, and the electrolyte (purified 85% orthophosphoric acid), followed by potentiostatting for 2 h at 50 mV (HRE) to reduce any superficial oxide coating before measurements were made.

The electrochemical cell used was the same all-silica equipment in a thermostatic oil bath used in previous work[14]. All polarization measurements were conducted galvanostatically. The electrolyte was purified using a series of hydrogen peroxide treatments[14]. To avoid the possibility of contamination of the electrode surface by traces of dissolved platinum, a gold counter-electrode was used. The reference electrode was a bubbling hydrogen electrode in the same solution, to which all potentials throughout this paper are referred.

RESULTS

Open-circuit potentials

Open-circuit potentials attained immediately (within 5 min) after the release of the potentiostatic current holding the electrodes at 50 mV are shown in Table 1. After some hours, a slow rise to higher values occurs. In each case, the higher value at each temperature was attained after 2–3 h in the solution.

TABLE 1

OPEN-CIRCUIT POTENTIALS ON PURE PLATINUM, RUTHENIUM, AND ALLOYS

Temp./°C	*Pt*	*Pt-8 Atom % Ru*	*Pt-18 Atom % Ru*	*Pt-40 Atom % Ru*	*Pt-60 Atom % Ru*	*Ru*
			E/mV (HRE)			
22.0	1020[a]	995–1011	998–1018	938–1004	916–938	899–903[b]
52.1	~1000	990–1021	988	985	883	867–880
76.0	~1000	1000	985	966–989	890–928	814–862
104.0	980–1000	993–1020	985–1003	958–995	910	790–880
136.1	~1000	985	~980	938	915	793

[a] Polished surface. [b] 21.0°C.

* Ruthenium is not miscible with platinum throughout the whole range of compositions. There is a considerable difference in lattice energies; ruthenium is h.c.p., not f.c.c.

Tafel plots

A pulsing technique (described earlier for platinum[11]) was used in order to ensure that the surface of each electrode was in a reproducibly clean condition, free from adsorbed trace impurities (for example, adsorbed anions such as polyphosphates) and from any build-up of irreversibly adsorbed oxygen.

Before each galvanostatic point was taken, the electrode was pulsed between open circuit and 50 mV, and allowed to reach its final potential value at each applied cathodic current density. Potentials obtained in this manner slowly decayed (at a few mV per hour) from a maximum value. This may be attributed to slow deactivation by diffusion of foreign specifically adsorbed ions from the solution, and possibly build-up of phase oxide. In each case, the maximum potential value was plotted. Electrodes were never taken more anodic than 1000 mV (HRE) to avoid surface composition changes.

Tafel data on clean surfaces

Data were obtained for surfaces in the "clean" condition at 22.0°, 52.1°, 76.1°, 104.0°, and 136.1°C. Tafel plots for each alloy at the above temperatures are shown in Figs. 1 and 2. Included are previous data on ruthenium[13] and rolled annealed platinum[11] together with a plot on alumina-polished platinum at 22°C.

Tables 2–5 give values of Tafel slopes, $1/\alpha$ values, and i_0 values for the alloys corrected for oxygen partial pressure assuming a first-order reduction reaction. The latter were obtained by extrapolating the Tafel line to the theoretical open-circuit potential at each temperature[11].

DISCUSSION

It has been previously shown that experimental data for oxygen reduction on oxide-free platinum in acid solution are in accordance with the reaction[5,11]

$$S + O_2 + H^+ + e^- \rightarrow S\text{–}O_2H\ *$$

as rate-determining step. This is in agreement with the first-order dependence noted for oxygen reduction on platinum in both dilute perchloric[5] and concentrated orthophosphoric acid[11]. The reaction has an experimental Tafel slope of RT/F, which is not explicable unless it is assumed that the adsorption of the O_2H radical is potential-dependent (Temkin conditions). At potentials above about 700 mV (HRE), oxygen or OH radicals are absorbed on platinum electrodes in coverages that are linearly potential-dependent[5,15]. This implies that the heat of adsorption of these radicals is linearly coverage-dependent, at least in the range $0.1 < \theta < 0.9$, where θ is the coverage (that is, the Temkin isotherm applies). It is assumed that the coverage of O_2H is low, but that the heat of adsorption of this intermediate follows the same Temkin isotherm as the other oxygenated species on the electrode, so that its heat of adsorption depends on the *total* coverage[16].

We may write the rate equation to the above reaction as

$$i = Fkp_{O_2}[H^+] \exp\left[-(\beta FV/RT) - (\beta r\theta/RT)\right] \quad (1)$$

where R, T, F, and V have their usual meanings; β is the symmetry factor, r is the change

* S is a surface adsorption site on the metal substrate.

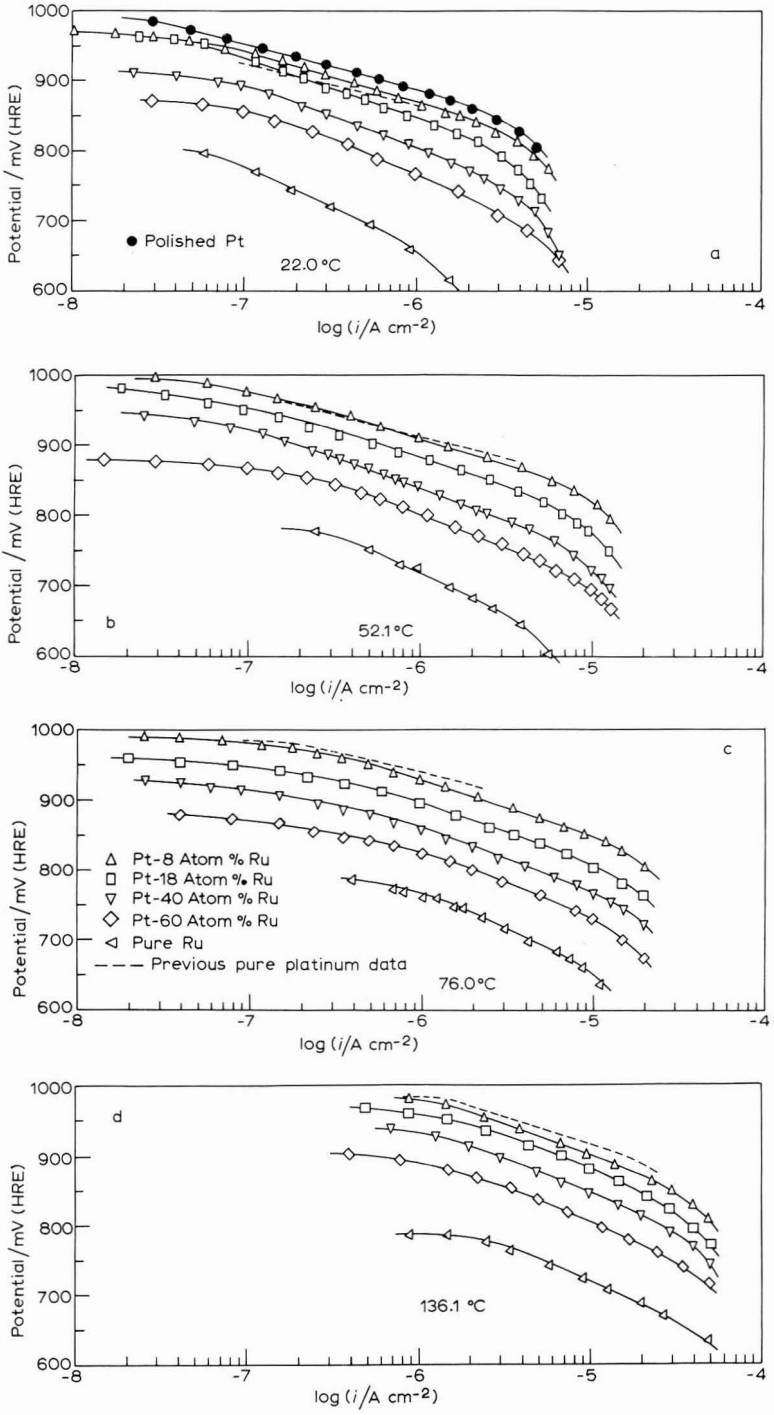

Fig. 1. Temperature-dependence of oxygen reduction on platinum, ruthenium, and alloys.

in heat of adsorption of O_2H as θ (the coverage of *all* oxygenated species) goes from low to high values; and k is a constant. It is assumed that the heat of adsorption of O_2 molecules on the electrode may be neglected[11].

Assuming that the Temkin isotherm applies to adsorbed O and OH on the electrode surface, it can be shown that, for the equilibrium

$$S+H_2O \rightleftarrows S-OH+H^+ +e^-$$

in the range of intermediate coverages[15] of OH

$$\log [H^+]+r\theta/RT = FV/RT \qquad (2)$$

TABLE 2

OXYGEN REDUCTION ON PLATINUM-8 ATOM PERCENT RUTHENIUM

Temp./°C	*Slope/ mV decade*$^{-1}$	$1/\alpha$	$i_0/A\ cm^{-2}$
22.0	73	1.25	4.2×10^{-12}
52.1	75	1.16	4.5×10^{-11}
76.1	77	1.13	1.7×10^{-10}
104.0	83	1.11	2.4×10^{-9}
136.1	86	1.06	$\sim1.8\times10^{-8}$

TABLE 3

OXYGEN REDUCTION ON PLATINUM-18 ATOM PERCENT RUTHENIUM

Temp./°C	*Slope/ mV decade*$^{-1}$	$1/\alpha$	$i_0/A\ cm^{-2}$
22.0	80	1.37	6.0×10^{-12}
52.1	82	1.27	5.1×10^{-11}
76.1	85	1.25	1.7×10^{-10}
104.0	90	1.20	1.7×10^{-9}
136.1	91	1.11	$\sim1.4\times10^{-8}$

TABLE 4

OXYGEN REDUCTION ON PLATINUM-40 ATOM

Temp./°C	*Slope/ mV decade*$^{-1}$	$1/\alpha$	$i_0/A\ cm^{-2}$
22.0	89	1.52	6.8×10^{-12}
52.1	92	1.43	4.9×10^{-11}
76.1	92	1.35	1.4×10^{-10}
104.0	95	1.27	1.6×10^{-9}
136.1	98	1.20	9.0×10^{-9}

TABLE 5

OXYGEN REDUCTION ON PLATINUM-60 ATOM PERCENT RUTHENIUM

Temp./°C	*Slope/ mV decade*$^{-1}$	$1/\alpha$	$i_0/A\ cm^{-2}$
22.0	95	1.62	6.3×10^{-12}
52.1	99	1.54	4.1×10^{-11}
76.1	102	1.50	1.8×10^{-10}
104.0	103	1.38	7.8×10^{-10}
136.1	105	1.30	6.0×10^{-9}

Substituting this eqn. in (1), we obtain, with $\beta=\frac{1}{2}$,

$$i\propto p_{O_2}[H^+]^{\frac{3}{2}}\exp(FV/RT) \qquad (3)$$

which is in agreement with the observed Tafel slope and pH-dependence in dilute acid[5].

In a recent publication the corresponding process on ruthenium was studied[13]. It was found that oxygen reduction was again first order and that the Tafel slope on clean ruthenium surfaces was about $2RT/F$ (Figs. 1 and 2). On ruthenium, high coverages of O and OH are noted in the oxygen reduction Tafel range; thus, it is probable that Langmuirian adsorption occurs. Although no data on the pH-dependence of ruthenium oxygen reduction electrodes in dilute acid solution have been

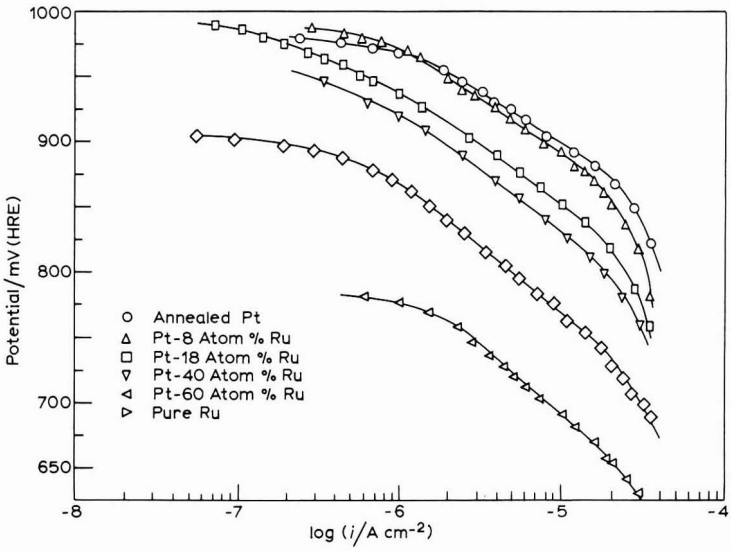

Fig. 2. Oxygen electrode on platinum, ruthenium, and alloys at 104.0°C in purified 85% orthophosphoric acid.

obtained, it is reasonable to suppose that the same rate-determining step applies on this metal, although with a Langmuir isotherm Tafel slope of $2RT/F$. This has been discussed in detail elsewhere[13].

Earlier data obtained on ruthenium indicated that the Tafel slope on this metal was essentially temperature-independent[13]. This may indicate a tendency toward Temkin adsorption conditions at higher temperatures. On alloys of platinum and ruthenium the same rate-determining reaction occurs, with a degree of Temkin-type adsorption (indicated by the Tafel slope), depending on composition.

From the data quoted in Tables 2–5 for the alloys at each temperature, it is evident that there is a tendency for i_0 to decrease as the composition moves from pure platinum to pure ruthenium at the lower temperatures studied. This improvement is, however, offset at practical operating potentials (for instance, around 900, or lower, mV) by the steady increase in the Tafel slope with alloy composition. At such potentials, log current is approximately proportional to the platinum content of the alloy, an effect similar to that noted by Hoare[4] for platinum–rhodium. At high temperatures, the tendency of i_0 to *decrease* as the composition moves from pure platinum to pure ruthenium indicates a still more marked dependence of log current on composition. At about 76°C, the i_0 values for the whole series of alloys, platinum, and ruthenium are much the same. As a consequence of the Temkin adsorption isotherm operating for the adsorbed reaction product, the rate of reaction on platinum is artificially lowered by the change in heat of adsorption of the reaction intermediates as overpotential decreases. This results in considerable heat of activation at the reversible potential compared with the corresponding value at relatively high overpotentials. For ruthenium there is no change in Tafel slope with temperature; therefore, the heat of activation is potential-independent. Figure 3 shows Arrhenius plots of the i_0 values for pure ruthenium and the alloys together with the plot previously obtained on pure

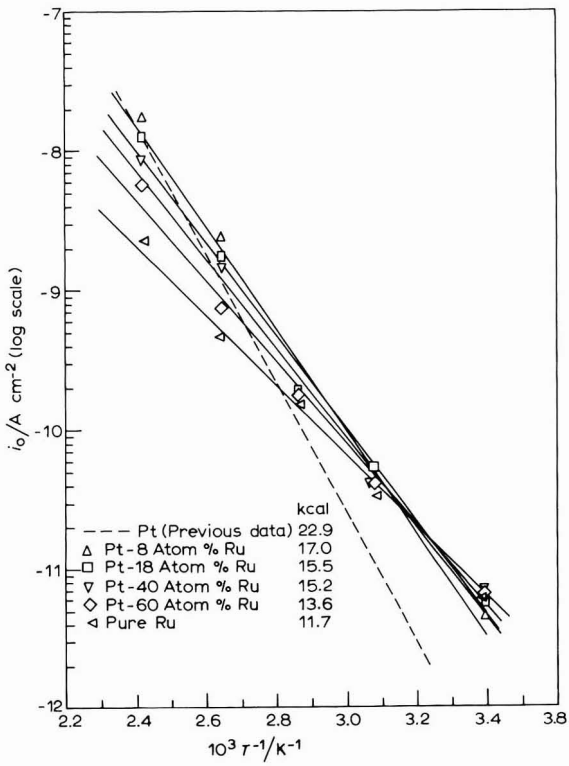

Fig. 3. Arrhenius plots of exchange current densities on platinum, ruthenium, and alloys.

platinum[11]. This Figure shows that there is a steady increase in activation energy with an increase in platinum content, as expected, and that the Arrhenius plots intersect one another in the middle range of temperatures.

It should be noted that all data on platinum electrodes were obtained on rolled, annealed surfaces[11], whereas alloy electrodes were mechanically polished. Accordingly, data have been plotted for a similarly prepared platinum surface at 22.0°C. A slightly *increased* activity (by approximately a factor of 2) was noted, compared with the same sample of platinum in the annealed condition.

ACKNOWLEDGEMENT

The author wishes to thank the sponsors of this work under the TARGET Fuel Cell Program, and Pratt and Whitney Aircraft Division of United Aircraft Corporation for permission to publish this paper. The help of the various members of IGT who assisted in preparation is also greatly appreciated.

SUMMARY

There is no evidence that the platinum–ruthenium alloys are ever better than similarly prepared pure platinum surfaces for oxygen reduction in acid solutions

under clean conditions at practical working potentials; however, platinum alloy electrodes containing small percentages of ruthenium are apparently more active under contaminated conditions than pure platinum. Since adsorbed impurities donate electrons to the *d*-bands of the electrode, thus reducing its power to adsorb electrode reaction intermediates, we would expect that the materials containing a larger number of *d*-orbital vacancies per atom would be less affected by the impurities. Platinum has 0.6 vacancies per atom and ruthenium[17] 2.2, so that platinum alloys containing small amounts of ruthenium, with intrinsic activities close to that of platinum, are more active than platinum itself when contaminated.

For the alloys, a "compensation effect" between the heat of activation and preexponential factor is noted so that rates on the alloys, pure platinum, and pure ruthenium are much the same in the 75°–100°C range. Platinum, however, has the greatest heat of activation (22.9 ± 0.9 kcal) at the reversible potential, and for alloys the value falls with increasing ruthenium content to the value of approximately 11.7 ± 0.5 kcal on ruthenium. Owing to the increasing Tafel slope with alloy ruthenium content, platinum-rich compositions are always more active for oxygen reduction in the 900 mV (HRE) range or below even at low temperatures where ruthenium-rich i_0 values are favorable.

REFERENCES

1 A. Damjanovic and V. Brusić, *Electrochim. Acta*, 12 (1967) 1171.
2 D. S. Gnanamuthu and J. V. Petrocelli, *J. Electrochem. Soc.*, 114 (1967) 1036.
3 A. Damjanovic, V. Brusić and J. O'M. Bockris, *J. Phys. Chem.*, 71 (1967) 2741.
4 J. P. Hoare, *Electrochim. Acta*, 14 (1969) 797.
5 A. Damjanovic and V. Brusić, *Electrochim. Acta*, 12 (1967) 615.
6 E. W. Brooman and T. P. Hoar, *Platinum Metals Rev.*, 9 (1966) 122.
7 T. P. Hoar and E. W. Brooman, *Electrochim. Acta*, 11 (1966) 545.
8 G. C. Bond and D. E. Webster, *Proc. Chem. Soc.*, (1964) 328.
9 G. C. Bond and D. E. Webster, *Platinum Metals Rev.*, 9 (1965) 12.
10 D. W. McKee and F. J. Norton, *J. Phys. Chem.*, 68 (1964) 481.
11 A. J. Appleby, *J. Electrochem. Soc.*, 117 (1970) 382.
12 A. J. Appleby, *J. Electroanal. Chem.*, 27 (1970) 325.
13 A. J. Appleby, *J. Electroanal. Chem.*, 27 (1970) 335.
14 A. J. Appleby, *J. Electroanal. Chem.*, 24 (1970) 97.
15 H. Wroblowa, M. L. B. Rao, A. Damjanovic and J. O'M. Bockris, *J. Electroanal. Chem.*, 15 (1967) 139.
16 B. E. Conway and E. Gileadi, *Trans. Faraday Soc.*, 58 (1962) 2439.
17 M. L. B. Rao, A. Damjanovic and J. O'M. Bockris, *J. Phys. Chem.*, 67 (1963) 2508.

ELECTROANALYTICAL CHEMISTRY AND INTERFACIAL ELECTROCHEMISTRY
Elsevier Sequoia S.A., Lausanne – Printed in The Netherlands

PROTONEN- UND ELEKTRONEN-TRANSFER AN INHIBITORBEDECKTEN ELEKTRODEN*

B. KASTENING UND L. HOLLECK

Forschungsabteilung Angewandte Elektrochemie, Kernforschungsanlage Jülich GmbH, Jülich (Deutschland)
Chemisches Institut der Hochschule, Bamberg (Deutschland)

(Eingegangen am 9. März, 1970)

EINLEITUNG

Es ist aus der heterogenen Katalyse bekannt, dass an einer Phasengrenze chemische Reaktionen ablaufen können, die in homogener Phase praktisch nicht zu beobachten sind, dass aber auch die in homogener Phase möglichen Reaktionen an der Phasengrenze oftmals über einen anderen Mechanismus, zumindest aber mit anderer Geschwindigkeit vor sich gehen als im homogenen Phaseninnern. In vielen Fällen beruht dies auf einem Eingriff der chemischen Substanz der anderen Phase, in zahlreichen anderen Fällen bewirken allein die an der Phasengrenze veränderten physikalischen Parameter einen anderen Mechanismus bzw. andere Geschwindigkeit. Gelegentlich ist es aber auch einfach so, dass die Grenzfläche—bei einer gewissen Verweilzeit der reagierenden Teilchen an ihr—zum blossen Ort des Rendezvous wird, an dem die Teilchen eine vernünftige Chance haben, sich zu treffen, während sie sich im homogenen Innern nur allzu selten begegnen. Hier handelt es sich also darum, dass für die Geschwindigkeit der Reaktion eine andere Gesetzmässigkeit gilt, dass Grenzflächen- anstelle von Volumenkonzentrationen eingehen.

All dies gilt auch für eine Elektrode, also die Phasengrenze zwischen Metall und Elektrolytlösung. Als besonderes Charakteristikum tritt hinzu, dass hier neben anderen chemischen Reaktionen auch Ladungsübergänge zum Metall möglich sind. Ausserdem spielen physikalische Parameter hier eine besondere Rolle: Die Struktur der elektrochemischen Doppelschicht beeinflusst nicht nur Ladungsübergänge, sondern kann auch für die Geschwindigkeit anderer an der Phasengrenze ablaufender Reaktionen von wesentlicher Bedeutung sein. Im Elektrodenpotential hat man eine Grösse, die sowohl für die Struktur der Doppelschicht, die Feldwirkung auf adsorbierte Moleküle und deren Wechselwirkung mit dem Elektrodenmaterial massgeblich ist, als auch die Grenzflächenkonzentration solcher Moleküle beeinflussen kann. Diese Grenzflächenkonzentration Γ_M ist aber für die Geschwindigkeit der Heterogenreaktion—sei es ein Elektronentransfer oder eine chemische Reaktion wie der heterogene Protonentransfer—massgeblich. Bezeichnet man mit q die Elektrodenfläche, so ist der molare Umsatz in der Zeiteinheit für den Elektronentransfer gegeben durch

$$dn/dt = i/zF = k_e q \Gamma_M \quad (1)$$

* Auszugsweise vorgetragen anlässlich der 19. CITCE-Tagung, Sept. 1968, Detroit/Mich., USA.

wo k_e die exponentiell vom Potential abhängige Geschwindigkeitskonstante des Elektronentransfers ist (Dimension s^{-1}) und anschaulich die reziproke Lebensdauer adsorbierter Moleküle in bezug auf den Ladungsaustausch darstellt. Entsprechend gilt für den heterogenen Protonentransfer von einem gelösten Donatormolekül, dessen Lösungskonzentration (im Falle von Konzentrationspolarisation: in Grenzflächennähe) c_D sei:

$$dn/dt = k_p q c_D \Gamma_M \tag{2}$$

Die Geschwindigkeitskonstante k_p des heterogenen Protonentransfers (Dimension $M^{-1}\ s^{-1}$) stellt die reziproke Lebensdauer adsorbierter Moleküle in bezug auf den Protonentransfer dar (bezogen auf die Einheitskonzentration des Donators).

Für den Fall, dass die reagierenden Moleküle nur schwach adsorbiert sind, also einen geringen Bedeckungsgrad aufweisen ($\theta \ll 1$), kann eine lineare Adsorptionsisotherme

$$\Gamma_M = \gamma c_M \tag{3}$$

angenommen werden, wo γ ein Adsorptionskoeffizient ist (Dimension cm), dessen anschauliche Bedeutung diejenige Schichtdicke der Lösung ist, in der sich gleich viele Moleküle befinden wie in der Adsorptionsschicht gleichen Querschnitts.

Nur unter der Voraussetzung der Gültigkeit von Gl. (3) mit konstantem γ sind die sogenannten "heterogenen Geschwindigkeitskonstanten", die hier mit k'_e bzw. k'_p bezeichnet werden sollen und die die unanschaulichen Dimensionen cm s^{-1} bzw. cm s^{-1} M^{-1} besitzen, wenn die Ansätze (1) und (2) mit der Lösungskonzentration c_M anstelle der Grenzflächenkonzentration Γ_M gebildet werden, konzentrationsunabhängig. Diese Konstanten sind in Wahrheit zusammengesetzte Grössen:

$$k'_e = \gamma k_e \tag{4}$$

$$k'_p = \gamma k_p \tag{5}$$

woraus sich ihre unanschauliche Dimension erklärt.

In der vorliegenden Arbeit sollen Elektronen- und Protonentransferprozesse unter Wirkung vorherrschend adsorbierter Inhibitoren untersucht werden. Da unter diesen Bedingungen die reagierenden Moleküle nur einen geringen Bruchteil der Adsorptionsschicht ausmachen, kann die Gültigkeit von Gl. (3) vorausgesetzt werden. Obgleich in diesem Falle k'_e und k'_p konzentrationsunabhängig sind (und nur diese zusammengesetzten Grössen der unmittelbaren elektrochemischen Messung zugänglich sind), sollen die entsprechenden Beziehungen hier dennoch mit den Einzelgrössen γ und k_e bzw. k_p geschrieben werden, um die Verhältnisse durchsichtiger zu gestalten:

$$dn/dt = i/zF = k_e q \gamma c_M \tag{6}$$

$$dn/dt = k_p q \gamma c_D c_M \tag{7}$$

Die Einzelgrössen zeigen nämlich eine ganz unterschiedliche Beeinflussung durch die für den Umsatz massgeblichen Parameter, das Potential und die Inhibitor-Lösungskonzentration c_I, und nur der summarische Einfluss wird in den Grössen k'_e bzw. k'_p wiedergegeben.

Die thermodynamische Gleichgewichtskonstante γ ist im allgemeinen in einem relativ breiten Potentialbereich erheblich weniger potentialabhängig als

die Geschwindigkeitskonstante k_e. Dies gilt zumal—worauf besonders hingewiesen werden soll—in Gegenwart eines vorherrschend adsorbierten Inhibitors. In diesem Falle entfällt nämlich weitgehend der Einfluss einer bevorzugten Adsorption des Lösungsmittels, der sonst beiderseits des Potentials maximaler Adsorption zu einer Schwächung der letzteren führt, solange nicht auch die Adsorption des Inhibitors merklich abnimmt: in die Schicht der organischen Inhibitormoleküle werden die organischen Moleküle des reagierenden Stoffes gegenüber einem Einbau von Lösungsmittel (vor allem Wasser) bevorzugt aufgenommen. Dagegen hängt die Konstante γ recht empfindlich von der Lösungskonzentration c_I des Inhibitors ab, da bei Zunahme von c_I die Adsorptionstendenz des Inhibitors verstärkt wird, so dass die Moleküle M fortschreitend verdrängt werden und γ abnimmt. Hierfür wurde in vorhergehenden Arbeiten[1,2] der Zusammenhang

$$\gamma = \text{const}\ c_I^{-\kappa} \tag{8}$$

theoretisch abgeleitet und experimentell verifiziert. Der Exponent κ hat dabei die Bedeutung

$$\kappa = P_M/P_I \tag{9}$$

wobei P_M und P_I den Flächenbedarf (in $Å^2$/Molekül) der beiden Molekülsorten angeben. In die Konstante "const" gehen vor allem die Adsorptionsenergien beider Molekülsorten sowie deren Wechselwirkung in der Adsorptionsschicht ein. γ hängt daher sowohl über κ als auch über "const" stark von der Art des jeweiligen Inhibitors ab.

Von den kinetischen Konstanten ist in erster Linie k_e potentialabhängig, und zwar in der üblichen exponentiellen Weise (gegebenenfalls ist eine Korrektur erforderlich, um durch ein ψ-Potential dem Potentialabfall in der diffusen Doppelschicht Rechnung zu tragen). Bei der Konstanten k_p liegen nur sekundäre Einflüsse des Potentials, vor allem infolge Veränderung der Moleküleigenschaften unter der Wirkung eines veränderten Feldes, vor. Von der Inhibitorkonzentration c_I sollten diese Konstanten hingegen praktisch unabhängig sein, weil bei vorherrschender Inhibitoradsorption angenommen werden kann, dass das reagierende Molekül sich stets isoliert in einer Umgebung von Inhibitormolekülen befindet, und es daher für seine Lebensdauer hinsichtlich der betreffenden Reaktion (nicht hinsichtlich seiner Desorption) unerheblich ist, wie gross das durch die Inhibitorkonzentration geregelte Verhältnis Inhibitor: reagierender Stoff ist. Indessen können die Geschwindigkeitskonstanten von der Art des jeweiligen Inhibitors abhängen, da durch Wechselwirkungen mit den Inhibitormolekülen sowie durch die Dicke der Inhibitor-Molekülschicht die zum Elektronenaustausch führende Wechselwirkung mit der Elektrode sowie der Zutritt des Donatormoleküls zum adsorbierten Molekül M beeinflusst wird.

Insgesamt ergeben sich somit folgende Abhängigkeiten

	Einfluss von:		
	Art des Inhibitors	*Konzentration c_I des Inhibitors*	*Potential*
γ	stark	stark	schwach
k_e	merklich	unbedeutend	stark
k_p	merklich	unbedeutend	schwach

EXPERIMENTELLES

Die Untersuchungen wurden bei Zimmertemperatur mit der konventionellen polarographischen Technik durchgeführt; Bezugselektrode war eine gesättigte Kalomelelektrode (GKE). Das Lösungsmittel war Wasser mit einem Zusatz von 10% Methanol, um auch bei Anwendung schlecht löslicher Inhibitoren bzw. Depolarisatoren unter vergleichbaren Bedingungen zu arbeiten.

Die Konzentration des Inhibitors wurde stets wenigstens so gross gewählt, dass sein Adsorptionsgleichgewicht praktisch vom Beginn der Tropfzeit an eingestellt war und keine Konzentrationspolarisation des Inhibitors vorlag.

ERGEBNISSE

Nitrobenzol

Das bei der Reduktion von Nitrobenzol primär entstehende Radikalanion besitzt in alkalischer Lösung eine beschränkte Stabilität. Die Stabilisierung erfolgt durch Dismutation in homogener Lösung, durch direkte Aufnahme eines zweiten Elektrons mit nachfolgender rascher Weiterreduktion oder durch heterogene Protonenübertragung und nachfolgende rasche Weiterreduktion des ungeladenen Radikals[3]

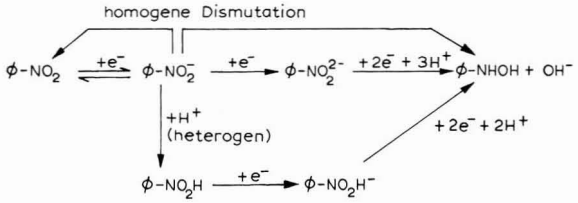

Die homogene Dismutation[4] wurde nach elektrolytischer Erzeugung des Radikalanions getrennt von der Elektrode mit Hilfe der Elektronenspinresonanz im Bereich pH 6 bis 13 untersucht[5] (vergl. hierzu auch E.S.R.-Untersuchungen mit interner Radikalerzeugung[6]). Diese Reaktion, die im wesentlichen nach dem Zeitgesetz zweiter Ordnung verläuft, führt bei schwach alkalischen und saueren Lösungen zu einer Überhöhung der ersten Reduktionsstufe von Nitrobenzol. Diese Überhöhung ist jedoch nur auf die Wirkung der homogenen Dismutation allein beschränkt, wenn die Lösung einen so starken Inhibitor enthält, dass nicht nur die direkte Elektronenaufnahme erst bei negativeren Potentialen bemerkbar wird, sondern auch ein heterogener Protonentransfer ausgeschaltet ist, insbesondere in Gegenwart von Triphenylphosphinoxid oder Campher. Aus der Überhöhung lässt sich in diesem Falle die homogene Geschwindigkeitskonstante feststellen; die entsprechenden Werte stimmen mit den in homogener Lösung ermittelten überein[7].

In Abwesenheit von Inhibitoren sind die heterogenen Folgeprozesse stets so rasch, dass nur eine 4-Elektronenstufe in Erscheinung tritt, und zwar in stärker alkalischen Lösungen (pH > 10) infolge direkten Elektronentransfers, in schwächer alkalischen und saueren Lösungen (pH < 10) infolge heterogenen Protonentransfers auf das Radikalanion.

Bei Gegenwart schwacher Inhibitoren beruht die Überhöhung der Stufe in

saueren Lösungen (je nach der Depolarisator-Konzentration von etwa pH 8...9 abwärts) auf der nebeneinander erfolgenden homogenen Dismutation und heterogenem Protonentransfer. Im Bereich um pH 9 ist die Überhöhung in diesem Falle auf den heterogenen Protonentransfer allein beschränkt, so dass sich dessen summarische Geschwindigkeitskonstante $k'_p = \gamma k_p$ ermitteln lässt.

Bei schlechter Trennung der beiden Reduktionsstufen ist die vollständige Beziehung für die Stromstärke i als Funktion der Geschwindigkeitskonstanten k'_e und k'_p anzuwenden:

$$i/i_d = (1+\lambda)^{-1}\{1+(3+4\lambda)\bar{F}(\chi_1)\} \tag{10}$$

wo i_d den diffusionsbedingten Grenzstrom der 1-Elektronenreduktion, $\bar{F}(\chi_1)$ die Koutecký-Funktion mit

$$\chi_1 = (k'_e + k'_p c_D)(12\,\tau/7\,D)^{\frac{1}{2}}/(1+\lambda) \tag{11}$$

$$\lambda = \exp[(F/RT)(E-E_0)] \tag{12}$$

bedeuten (E_0 = Standard-Redoxpotential des 1-elektronigen Primärvorgangs). Die Geschwindigkeitskonstante k'_p für den Protonentransfer lässt sich dann als potentialunabhängiger Anteil der Summe $(k'_e + k'_p c_D)$ bei Auftragung der letzteren gegen das Potential ermitteln. Bei Ausbildung eines potentialunabhängigen Grenzstromes vereinfacht sich die Beziehung (mit $\lambda \to 0$, $k'_e \to 0$) zu

$$i/i_d = 1+3\bar{F}(\chi_1) \tag{13}$$

mit

$$\chi_1 = k'_p c_D (12\,\tau/7\,D)^{\frac{1}{2}} \tag{14}$$

In Abb. 1 sind polarographische Stromspannungskurven von Nitrobenzol bei pH 9.4 in Gegenwart verschiedener Konzentrationen des schwachen Inhibitors Benzonitril wiedergegeben. Die Geschwindigkeitskonstanten des Elektronentransfers k'_e und des heterogenen Protonentransfers $k'_p c_D$ sind in Abb. 2 als Funktion der Inhibitor-Konzentration im doppelt-logarithmischen Massstab aufgetragen, entsprechend der für beide Konstanten gültigen Beziehung

$$k' = \gamma k = \text{const}\; c_I^{-\kappa} k \tag{15}$$

bzw.

$$\log k' = \text{const}' + \log k - \kappa \log c_I \tag{16}$$

Während bei niedrigen Inhibitor-Konzentrationen die beiden Geschwindigkeitskonstanten von c_I annähernd unabhängig werden, da hier die fortschreitende Desorption des Inhibitors dessen Wirkung gering werden lässt, ist bei höheren Konzentrationen der nach Gl. (16) erwartete geradlinige Verlauf in etwa erfüllt, wie dies auch früher mit Nitro- und Azo-Verbindungen aufgefunden wurde[1,2]. Für den Exponenten κ ergeben sich die Werte 1.2 (bei Protonentransfer) bzw. 2.8 (bei Elektronentransfer). Ähnliche Ergebnisse, $\kappa = 1.8$ für Protonen- und $\kappa \cong 4$ für Elektronentransfer, wurden mit p-Tolunitril als Inhibitor erhalten.

Die experimentell bestimmten Konstanten k'_e und k'_p sind von Art und Konzentration des Leitelektrolyten abhängig. Um die Ursachen dieses Einflusses zu

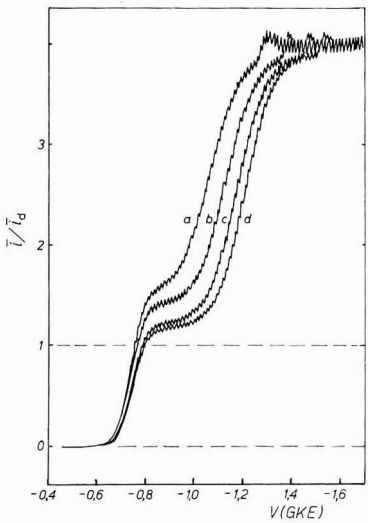

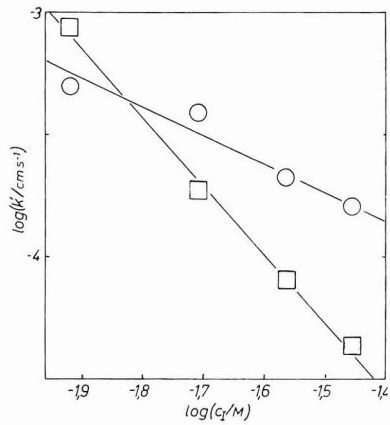

Abb. 1. Polarographische Stromspannungskurven von Nitrobenzol (10^{-3} *M*), pH 9.4, Zusatz von Benzonitril: (a) 0.12, (b) 0.2, (c) 0.28, (d) 0.36 %.

Abb. 2. Abhängigkeit der Geschwindigkeitskonstanten für Protonen- und Elektronentransfer von der Inhibitor-Lösungskonzentration, zufolge Abb. 1. (○) $k'_p c_D$, (□) k'_e (für -1.0 V, GKE).

TABELLE 1

FORMALE GESCHWINDIGKEITSKONSTANTEN FÜR ELEKTRONEN- UND PROTONEN-TRANSFER BEI DER NITROBENZOL-REDUKTION IN GEGENWART VON 0.05% *p*-TOLUNITRIL IN VERSCHIEDENEN ELEKTROLYTLÖSUNGEN

Leitelektrolyt	*pH*	$k'_p c_D \times 10^3/cm\ s^{-1}$	$k'_e \times 10^3/cm\ s^{-1}$ (*bei* -1 *V GKE*)
0.02 *M* NaH_2BO_3 0.01 *M* H_3BO_3	9.4	0.4	1.2
0.1 *M* NaH_2BO_3 0.05 *M* H_3BO_3	9.4	0.9	7
wie vor $+10^{-3}$ *M* $N(C_2H_5)_4^+$	9.4	0.7	110
wie vor $+2.5 \times 10^{-3}$ *M* $N(C_2H_5)_4^+$	9.4	1	490
0.1 *M* NH_4^+ 0.2 *M* NH_3	9.7	6	80
0.1 *M* NH_4^+ 0.05 *M* NH_3	9.0	8	80
0.015 *M* KH_2PO_4 0.028 *M* Na_2HPO_4	7.4	60[a]	[b]

[a] Dieser Wert ist geringfügig zu gross, da bei diesem pH-Wert bereits die homogene Dismutation einen Beitrag leistet.

[b] k'_e kann hier nicht bestimmt werden, da der Diffusions-Grenzstrom wegen des hohen Wertes von $k'_p c_D$ bereits bei Potentialen erreicht wird, bei denen k'_e noch nicht merkliche Werte annimmt.

klären, wurden einige orientierende Versuche durchgeführt, bei denen NH_4^+ als Leitelektrolyt-Kation und Puffersäure bzw. $N(C_2H_5)_4^+$ als Zusatz zum Leitelektrolyten (Puffersystem) verwendet wurden. In Gegenwart von 0.05% *p*-Tolunitril als Inhibitor ergaben sich die in Tabelle 1 aufgeführten Werte.

Benzaldehyd

Die Höhe der polarographischen Stufe von Benzaldehyd sinkt—in Abwesenheit von Inhibitoren—in alkalischen Lösungen mit wachsendem pH-Wert von dem Wert für einen 2-Elektronen-Vorgang (Produkt: Benzylalkohol) auf denjenigen für einen 1-Elektronen-Vorgang (Produkt: Hydrobenzoin) ab[4,8]. In Gegenwart starker Inhibitoren (Triphenylphosphinoxid) bleibt die Stufe auch in neutralen bis saueren Lösungen auf die Höhe des 1-Elektronen-Vorgangs beschränkt, bis das Desorptionspotential des Inhibitors erreicht wird (Abb. 3). Daraus kann geschlossen werden, dass die 2-Elektronen-Reduktion eine Heterogen-Reaktion voraussetzt, und zwar—da ein potentialunabhängiger Grenzstrom vorliegt—eine chemische Heterogenreaktion, der der Transfer des zweiten Elektrons als rasche Folgereaktion angeschlossen ist. Wegen der pH-Abhängigkeit des Grenzstromes handelt es sich offenbar wieder um einen heterogenen Protonentransfer, der mit der homogenen Dimerisierung in Konkurrenz tritt, in Gegenwart starker Inhibitoren jedoch ausgeschaltet wird. (Ein direkter Transfer eines zweiten Elektrons auf das primäre Radikalanion erfolgt erst bei wesentlich negativeren Potentialen und ist nur in Anwesenheit gewisser Kationen —wie Cs^+—sichtbar.) Der Mechanismus der Reaktion kann danach wie folgt formuliert werden:

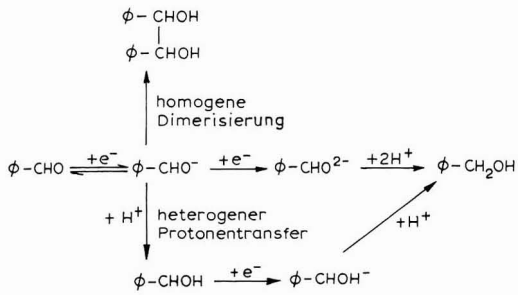

Diese Annahme wird gestützt durch das Verhalten von 2,6-Dichlorbenzaldehyd (Abb. 4). Hier ist der Grenzstrom im schwach alkalischen Bereich auch in Gegenwart eines starken Inhibitors gegenüber dem Wert für einen 1-Elektronenvorgang überhöht, und zwar in einem von der Konzentration des Inhibitors abhängigen Ausmass. Dies beruht offenbar auf einer besseren Adsorbierbarkeit des entsprechenden Radiakalanions gegenüber demjenigen von Benzaldehyd. Auf den merkwürdigen Verlauf der Stromspannungskurve in Abwesenheit von Inhibitoren sowie die Tatsache, dass in einem gewissen Potentialbereich die Stromstärke ohne Inhibitoren geringer als mit diesen ist, wird in der Diskussion noch einzugehen sein.

Sauerstoff

Ein weiteres Beispiel für einen am Elektrodenprozess beteiligten heterogenen Protonentransfer stellt die Reduktion von Sauerstoff dar, über die an anderer Stelle

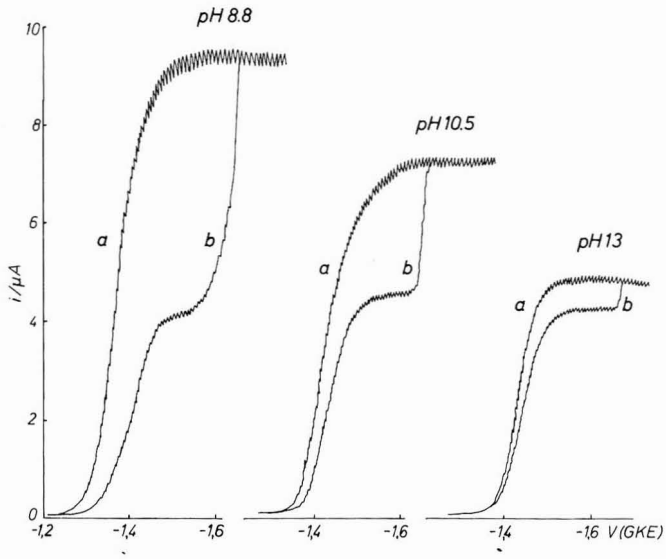

Abb. 3. Polarographische Stromspannungskurven von Benzaldehyd (10^{-3} *M*) bei verschiedenen pH-Werten. (a) ohne Zusatz, (b) mit 0.05% Triphenylphosphinoxid.

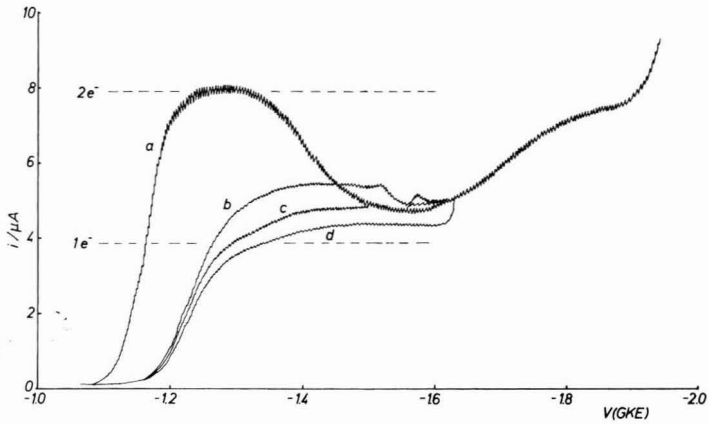

Abb. 4. Polarographische Stromspannungskurven von 2,6-Dichlorbenzaldehyd (10^{-3} *M*), pH 10.5, Zusatz von Triphenylphosphinoxid: (a) 0, (b) 0.008, (c) 0.016, (d) 0.075%.

ausführlicher berichtet wird[9]. Während in alkalischen Lösungen in Abwesenheit von Inhibitoren ein reversibler 2-Elektronenvorgang vorliegt (Abb. 5, Kurve a)

$$O_2 + 2e^- + H_2O \rightleftharpoons HO_2^- + OH^- \qquad (17)$$

bleibt die Reduktion in Gegenwart gewisser starker Inhibitoren (Triphenylphosphinoxid, Campher) auf einen 1-Elektronen-Vorgang beschränkt (Abb. 5, Kurve f). Erst bei niedrigeren pH-Werten wächst die Stufenhöhe auf diejenige eines 2-Elektronen-Vorgangs (Abb. 5, Kurven c, d, e). Da die Grenzstromstärken in diesem Falle von der Inhibitor-Lösungskonzentration unabhängig sind, beruht der Stromanstieg

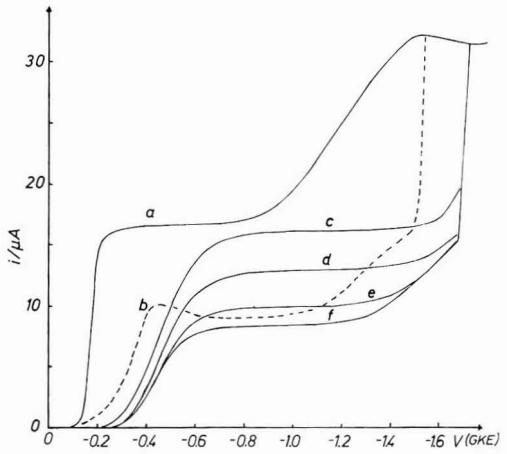

Abb. 5. Polarographische Stromspannungskurven von Sauerstoff (gesättigte Lösung). (a) pH 13, ohne Zusatz; (b) pH 13, 0.01% Triphenylphosphinoxid; alle weiteren Kurven mit 0.05% Triphenylphosphinoxid, (c) pH 5.2; (d) pH 7.9; (e) pH 9.6; (f) pH 11.5 bis 13.

offenbar auf einer homogenen Dismutation. Bei niedrigeren Inhibitor-Konzentrationen (Abb. 5, Kurve b, und ähnlich bei schwächeren Inhibitoren) ist die Stromstärke hingegen auch in stärker alkalischen Lösungen in einem gewissen Potentialbereich grösser, als der 1-Elektronen-Reduktion entspricht; erst mit negativer werdendem Potential sinkt die Stromstärke auf die 1-Elektronen-Reduktion ab. Die starke Abhängigkeit des auftretenden (nicht strömungsbedingten) Maximums von der Inhibitor-Konzentration zeigt, dass der zugrundeliegende Vorgang eine heterogene Reaktion ist, offenbar der Protonentransfer (von einem Wassermolekül) auf das primär gebildete O_2^-, wobei sich die sofortige Weiterreduktion des Radikals HO_2 anschliesst. Es liegt daher wahrscheinlich folgender Mechanismus zugrunde:

homogene Dismutation
(erst bei pH < 11 merklich)

$$O_2 \xrightarrow{+e^-} O_2^- \xrightarrow[(+H_2O-OH^-)]{\text{heterogener Protonentransfer}} HO_2 \xrightarrow{+e^-} HO_2^-$$

In homogener Lösung mit pH > 11 scheint das Superoxidion O_2^- (oder ein nicht reduzierbares Folgeprodukt, z.B. das Dimere O_4^{2-}) während der Dauer eines polarographischen Tropfens stabil zu sein.

DISKUSSION

Grenzflächenaktive Stoffe bilden oberhalb gewisser Mindestkonzentrationen auf der Elektrodengrenzfläche eine annähernd lückenlose monomolekulare Adsorptionsschicht, deren Eigenschaften sich auch bei stärkerer Variation der Lösungskonzentrationen nicht merklich ändern. Trotzdem liegt ein erheblicher und eigentümlicher Einfluss der Lösungskonzentration auf heterogen ablaufende Prozesse wie

Elektronen- und Protonentransfer vor. Diese Beobachtung kann—wie bereits früher erörtert—nur so verstanden werden, dass die Substratmoleküle in die Adsorptionsschicht eingebettet werden und dort reagieren. Ein Transport von Elektronen durch die Adsorptionsschicht auf ausserhalb befindliche Substratmoleküle, wie er für den Elektronentransfer grundsätzlich auch diskutiert werden könnte, findet dagegen —jedenfalls bei den von uns früher und in dieser Arbeit untersuchten Systemen— nicht (oder nicht mit merklicher Geschwindigkeit) statt.

Dass die beiden Geraden in Abb. 2 eine unterschiedliche Neigung besitzen, verdient eine besondere Betrachtung. Der Neigungsfaktor κ stellt nach Gl. (9) das Verhältnis des Flächenbedarfs von Radikalanion und Inhibitormolekül dar. Da vorausgesetzt werden kann, dass Protonen- und Elektronentransfer in der gleichen Umgebung von Inhibitormolekülen stattfinden, P_I also in beiden Fällen gleich gross ist (aus Messungen der Grenzflächenspannung als Funktion der Inhibitor-Lösungskonzentration ergab sich für Benzonitril $P_I = 24$ Å^2/Molekül[1]), ist dieses Ergebnis so zu deuten, dass das Radikalanion in zwei verschiedenen Orientierungen mit unterschiedlichem Flächenbedarf (Elektronentransfer: $P_M = 68$ Å^2/Molekül; Protonentransfer: $P_M = 29$ Å^2/Molekül) in die Inhibitorschicht eingebaut wird. Die Lage, bei der ein Elektronentransfer stattfindet, entspricht offenbar einer Anordnung mit dem Benzolring parallel zur Elektrodenfläche; der Elektronentransfer ist in diesem Falle durch die innige Wechselwirkung des π-Elektronensystems des Moleküls mit den Elektronen des Metalls begünstigt. Dagegen ist das Molekül in der anderen Lage mit dem Benzolring senkrecht zur Grenzfläche und der anionischen Gruppe $-NO_2^-$ zur Lösung hin orientiert; dies begünstigt den Zutritt eines von der Lösung kommenden Donatormoleküls. Die Verhältnisse sind in Abb. 6 schematisch skizziert. Für die verschiedenen Anordnungen gelten natürlich auch unterschiedliche Adsorptionsenergien, so dass auch die Konstante "const." in Gl. (8) für die beiden Lagen unterschiedliche Werte besitzen sollte.

Grundsätzlich könnte der unterschiedliche Flächenbedarf auch durch Adsorption verschieden stark solvatisierter Radikalanionen gedeutet werden. Dann wäre jedoch der Elektronentransfer zum stärker solvatisierten Ion begünstigt— entgegen der allgemeinen Erfahrung, dass der Elektronentransfer mit zunehmender Solvatation langsamer wird.

Aus den Angaben in Tabelle 1 für Borat- bzw. Phosphatpuffer kann geschlossen werden, dass in diesen Fällen das solvatisierte Proton der vorherrschend wirksame Donator und eine Donatorwirkung von H_3BO_3 bzw. $H_2PO_4^-$ untergeordnet ist. Hiermit ergibt sich die formale Konstante $k'_{p(H_{aq}^+)} = 10^6$ cm s^{-1} M^{-1}. Merkliche Donatorwirkung zeigt auch das Ammoniumion, für das ein Wert von etwa $k'_{p(NH_4^+)} = 60$ cm s^{-1} M^{-1} folgt. (Einflüsse der elektrochemischen Doppelschicht

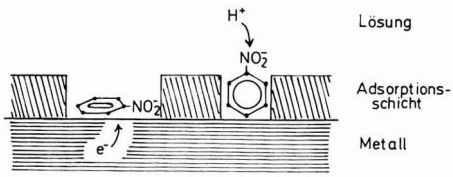

Abb. 6. Schematische Darstellung der beiden Orientierungen des Nitrobenzol-Radikalanions für Elektronen- bzw. Protonentransfer in einer Adsorptionsschicht von Benzonitril.

—Dissoziationsfeldeffekt, Änderung der Ionenkonzentrationen gegenüber dem Lösungsinnern durch das ψ-Potential— sind bei der Berechnung dieser Werte unberücksichtigt geblieben.) Vergleicht man den Wert für das hydratisierte Proton mit dem von Koopmann und Gerischer[6] auf anderem Wege, in Abwesenheit von Inhibitoren, gefundenen Wert für die "wahre" Geschwindigkeitskonstante $k_{p(H^+_{aq})} = 3.4 \times 10^9\ M^{-1}\ s^{-1}$, so folgt—unter Vernachlässigung zusätzlicher Einflüsse der veränderten Umgebung auf die Protonentransfergeschwindigkeit—aus Gl. (5) für den Adsorptionskoeffizienten in Gegenwart von 0.05% p-Tolunitril ein Wert $\gamma \sim 3 \times 10^{-4}$ cm. Dieser Wert dürfte die richtige Grössenordnung darstellen. Für das (wahrscheinlich etwas besser adsorbierte) p-Nitrochlorbenzol wurde in Abwesenheit von Inhibitoren ein Wert von $\gamma \sim 2 \times 10^{-3}$ cm, in Gegenwart des starken Inhibitors Triphenylphosphinoxid (Konzentration 0.005...0.1%) Werte von $\gamma = 0.5 \ldots 3 \times 10^{-5}$ cm gefunden[10].

Die Wirkung verschiedenartiger Inhibitoren auf Elektronen- und Protonentransfer-Prozesse muss in diesem Zusammenhang noch etwas ausführlicher diskutiert werden. Zunächst beruht ihre unterschiedliche Wirkung auf ihrem Einfluss auf γ infolge der verschiedenen Adsorptionsenergien (sowie verschiedener Wechselwirkungsenergien mit dem eingebetteten elektroaktiven Molekül). Daneben ist aber auch die Frage wesentlich, in welchem Ausmass der betreffende Inhibitor verschiedene Orientierungsmöglichkeiten der eingebetteten Moleküle zulässt. Der Wert für P_M beim Elektronentransfer auf das Nitrobenzol-Radikalanion in einer Adsorptionsschicht von Triphenylphosphinoxid ($P_M = 30$ Å^2/Molekül) zeigt, dass dieser Inhibitor—im Gegensatz zu Benzonitril und p-Tolunitril—eine für den Elektronenübergang günstige Parallel-Orientierung des Radikalanions praktisch gar nicht zulässt, so dass auch der Elektronentransfer über die ungünstige Orientierung mit dem Ring senkrecht zur Elektrode verlaufen muss; dies führt—wie schon früher diskutiert—zu einer zusätzlichen Erhöhung der Aktivierungsenergie. Dass in diesem Falle trotz offenbar allein vorliegender Orientierung senkrecht zur Elektrode der Protonentransfer praktisch ganz ausgeschaltet ist, kann zum Teil an dem sehr geringen Wert des Adsorptionskoeffizienten γ, daneben aber wohl auch an der grösseren Dicke der monomolekularen Adsorptionsschicht dieses voluminöseren Inhibitormoleküls liegen, die auch das senkrecht orientierte Radikalanion noch hinreichend vom Zutritt des Protonendonators abschirmt. (Ähnliches gilt für Campher als Inhibitor.) Dagegen können auch grössere Moleküle trotz starker Adsorption schwächere Inhibitoren für den Protonentransfer sein, wenn sie nämlich—wie bei Methylcellulosen oder Gelatine—entweder infolge ihres Quellungsvermögens Elektrolytlösung mit in die Adsorptionsschicht einbauen oder gar selbst als Protonenüberträger wirken können. (Vergl. hierzu die Deutung der Wirkung von Gelatine auf die Wasserstoff-Stufe[11] und die Reduktion von Azo- und Azoxybenzol[12].)

Für das Auftreten eines potentialunabhängigen Grenzstromes, der durch die Geschwindigkeit des Protonentransfers bedingt wird, wie dies in den hier erörterten Fällen vorliegt, ist vorauszusetzen, dass nicht nur die Geschwindigkeitskonstante k_p, sondern auch der Adsorptionskoeffizient γ keine merkliche Änderung mit dem Potential erfährt. In Abwesenheit von Inhibitoren ändert sich γ zwar merklich schwächer als die Elektronentransfer-Geschwindigkeitskonstante k_e, aber doch nicht unerheblich mit dem Potential (abgesehen von einem engen Potentialbereich maximaler Adsorption), verursacht im wesentlichen durch die bei stärker positiven oder negati-

ven Potentialen bevorzugte Adsorption des Lösungsmittels (H_2O). Dies dürfte auch die Ursache für den merkwürdigen Verlauf (Abb. 4, Kurve a) der Stromstärke bei der Reduktion von 2,6-Dichlorbenzaldehyd* in Abwesenheit von Inhibitoren sein: Mit wachsend negativem Potential wird die Adsorption des zugehörigen Radikalanions derart geschwächt, dass der einer Aufnahme des zweiten Elektrons vorgelagerte heterogene Protonentransfer langsamer als die homogene Dimerisierung erfolgt. (Ein Einfluss des ψ-Potentials, wie er zur Deutung ähnlicher Erscheinungen insbesondere mit anorganischen mehrwertigen Anionen herangezogen wird, dürfte im vorliegenden Falle auszuschliessen sein, da bei den sehr negativen Potentialen, bei denen die Erscheinung beobachtet wird, das ψ-Potential sich mit dem Elektrodenpotential nicht sehr erheblich ändert, im Gegensatz zu Potentialen in der Nähe des Nulladungspotentials.)

Beim Vorliegen einer Adsorptionsschicht eines organischen Inhibitors hingegen kann angenommen werden, dass sich der Adsorptionskoeffizient des Substratmoleküls über einen sehr breiten Potentialbereich bis in die Nähe des Desorptionspotentials des Inhibitors kaum ändert, da der Einbau von Lösungsmittelmolekülen (insbesondere Wasser) in diese Schicht—vor allem in deren dem Metall zugewandten, hydrophoben Gruppierungen—sehr erschwert ist gegenüber dem Einbau organischer Moleküle. Dies dürfte die Ursache für die in Gegenwart des Inhibitors beobachteten potentialunabhängigen Grenzströme in Abb. 5 sein. Im Bereich um -1.5 V (GKE) kommt es bei der kleinsten angewandten Inhibitorkonzentration sogar zu einem quasi katalytischen Einfluss des Inhibitors auf den Heterogenvorgang: Die Stromstärke wird grösser als in Abwesenheit des Inhibitors, da das Radikalanion in die Schicht der organischen Inhibitormoleküle in höherer Konzentration aufgenommen wird als in eine Schicht von Lösungsmittelmolekülen (H_2O).

Bei der Reduktion von Sauerstoff sinkt die Geschwindigkeit des heterogenen Protonentransfers, der oben als Ursache für den über die 1-Elektronen-Reduktion hinausgehenden Strom (Abb. 5, Kurve b) bezeichnet wurde, in Gegenwart des Inhibitors mit negativer werdendem Potential ab. Dies ist am einfachsten dadurch zu deuten, dass das Superoxidion O_2^- nicht bevorzugt in die Adsorptionsschicht eingebaut wird, sondern mit negativer werdendem Potential wegen seiner starken Solvatation desorbiert wird. Es sinkt daher nicht der Wert der Geschwindigkeitskonstante, sondern derjenige des Adsorptionskoeffizienten γ.

Nach den Angaben in Tabelle 1 sind Tetraäthylammoniumionen ohne Einfluss auf die Geschwindigkeit des Protonentransfers; die Erhöhung der letzteren durch Ammonium-Ionen wurde oben auf deren Wirkung als zusätzliche Protonendonatoren zurückgeführt. Beide Ionenarten—insbesondere die schon bei kleiner Konzentration wirksamen Tetraäthylammonium-Ionen—beeinflussen jedoch erheblich die Geschwindigkeit des Elektronentransfers. Dieser Einfluss kann als eine Wirkung auf die Geschwindigkeitskonstante k_e, auf den Adsorptionskoeffizienten γ oder auf die Radikalanionen-Konzentration c_M in der Nähe der Adsorptionsschicht diskutiert werden. Eine Beeinflussung von k_e sowie von c_M kann durch eine Änderung des ψ-Potentials in der an die Adsorptionsschicht angrenzende Helmholtz-Ebene erfolgen: werden die Ionen NH_4^+ und besonders NR_4^+ in einer zweiten Schicht adsorbiert, so wird hier das ψ-Potential in positiver Richtung verschoben und damit die Konzen-

* Ähnliches wurde auch mit *o*-Chlorbenzaldehyd beobachtet[13].

tration von Anionen in der diffusen Doppelschicht erhöht und der für k_e wirksame Potentialunterschied zwischen Metall und dem Ort des adsorbierten Substratmoleküls vergrössert. (Bei einem Einfluss über c_M sollte grundsätzlich die gleiche Wirkung auch auf den Protonentransfer erfolgen. Da hierfür zugleich aber die Konzentration c_D des Donators H_{aq}^+ massgeblich ist und diese im gleichen Masse verringert wird, wie sich diejenige der Anionen erhöht, entfällt ein solcher Einfluss des ψ-Potentials. Bei NH_4^+ als Donator wäre die Konzentration in der sekundären Adsorptionsschicht massgeblich; eine eigene Rückwirkung über das ψ-Potential liesse sich hiervon nicht abtrennen.)

Ein Einfluss auf k_e wie auf γ könnte dadurch zustandekommen, dass die Kationen NH_4^+ bzw. NR_4^+ mit dem Radikalanion zugleich in dieselbe Lücke in der Adsorptionsschicht eingebaut werden. Infolge der damit verbundenen Änderung der Umgebung würde sich k_e ändern; der bevorzugte Einbau eines solchen Ionenpaares würde γ erhöhen. Wegen des unbeeinflussten Protonentransfers sollte dieser Effekt jedoch nur die "Parallellage" betreffen, während sich die Kationen auf den Einbau der Radikalanionen mit senkrecht zur Grenzfläche orientierten Ringen nicht auswirkt. Dem steht entgegen, dass auch in Gegenwart von Triphenylphosphinoxid als Inhibitor, bei dem nach obigen Erörterungen auch der Elektronentransfer mit den "senkrecht" orientierten Radikalanionen erfolgt, ein merklicher Beschleunigungseffekt durch NH_4^+-Gegenwart zu beobachten ist.

Der Einfluss von NH_4^+ und NR_4^+ auf k_e' (Veränderungen von c_M in der diffusen Doppelschicht infolge veränderten ψ-Potentials sind in diese Konstante einbezogen) ist daher wahrscheinlicher auf die vorhergenannten Wirkungen des ψ-Potentials zurückzuführen. Entgegen unserer früher geäusserten Vermutung[2] zeigt eine überschlägige Berechnung, dass auch der Einfluss veränderter Leitsalzkonzentration (d.h. der Kationen K^+, Na^+) auf k_e' durch deren Wirkung auf das ψ-Potential erklärt werden kann.

DANK

Dem Bundesministerium für Wirtschaft danken wir für die Unterstützung dieser Arbeit. Dank sagen möchten wir auch Herrn Prof. Dr. D. Jannakoudakis (Thessaloniki), der eine Reihe von Messungen durchführte.

ZUSAMMENFASSUNG

Chemische Oberflächenreaktionen, wie sie vor allem in der heterogenen Katalyse massgeblich sind, spielen neben Ladungsübergängen auch im Ablauf von Elektrodenprozessen eine wichtige Rolle; besondere Bedeutung kommt dem heterogenen Protonentransfer zu. Untersuchungen mit aromatischen Carbonyl- und Nitroverbindungen sowie mit Sauerstoff zeigen, dass ein Protonentransfer ebenso wie der Ladungsaustausch mit der Elektrode auch dann noch stattfinden kann, wenn die Elektrode nahezu vollständig mit Inhibitormolekülen belegt ist. Für die Geschwindigkeit des Protonen- ebenso wie des Elektronenübergangs ist dabei die neben dem Inhibitor in der Adsorptionsschicht noch vorhandene Grenzflächenkonzentration des reagierenden Stoffes massgeblich. Diese Grenzflächenkonzentration steht über eine früher abgeleitete Beziehung mit der Lösungskonzentration des Inhibitors

im Zusammenhang, wenn die Vorgänge an homogenen Oberflächen (Quecksilber) ablaufen. Polarographische Untersuchungen mit Nitroverbindungen zeigen, dass das Produkt der primären Elektrodenreaktion (das Radikalanion) zwei verschiedene Orientierungen in der Adsorptionsschicht einnehmen kann, wobei die eine (mit dem Ring parallel zur Grenzfläche) den Elektronenübergang von der Elektrode, die andere (senkrecht zur Grenzfläche, mit der Gruppe $-NO_2^-$ zur Lösung) den Protonentransfer aus der Lösung begünstigt.

SUMMARY

Chemical reactions at surfaces, important in heterogeneous catalysis, may also play a role—besides that of charge transfer—during electrode processes; heterogeneous proton transfer is of particular significance. Investigations with aromatic carbonyl and nitro compounds, as well as with oxygen, show that proton transfer —like electron transfer—takes place even at electrodes almost completely covered with inhibitor molecules. The rate of proton transfer, like that of electron transfer, under these conditions depends on the surface concentration of the reacting species present in the adsorption layer besides the inhibitor. The dependence of this surface concentration on the bulk concentration of the inhibitor is given by a previously derived relation for processes taking place at a homogeneous surface (mercury). Polarographic investigations with nitro compounds show that the product of the primary electrode reaction, the anion radical, can arrange itself in two different ways within the adsorption layer. One of the two orientations—with the ring plane parallel to the electrode surface—favours electron transfer from the electrode, while the other —perpendicular to the electrode with the $-NO_2^-$ group towards the solution— favours proton transfer from the solution.

LITERATUR

1 L. HOLLECK, B. KASTENING UND R. D. WILLIAMS, *Z. Elektrochem.*, 66 (1962) 396; B. KASTENING, *Ber. Bunsenges. Phys. Chem.*, 68 (1964) 979.
2 B. KASTENING UND L. HOLLECK, *Talanta*, 12 (1965) 1259.
3 L. HOLLECK UND B. KASTENING, *Rev. Polarog. (Kyoto)*, 11 (1963) 129.
4 B. KASTENING UND L. HOLLECK, *Z. Elektrochem.*, 63 (1959) 166.
5 B. KASTENING, *Z. Anal. Chem.*, 224 (1967) 196; B. KASTENING UND S. VAVŘIČKA, *Ber. Bunsenges. Phys. Chem.*, 72 (1968) 27.
6 R. KOOPMANN UND H. GERISCHER, *Ber. Bunsenges. Phys. Chem.*, 70 (1966) 127.
7 B. KASTENING, *J. Electroanal. Chem.*, 24 (1970) 417.
8 L. HOLLECK UND H. MARSEN, *Z. Elektrochem.*, 57 (1953) 301.
9 B. KASTENING UND G. KAZEMIFARD, *Ber. Bunsenges. Phys. Chem.*, 74 (1970) 551.
10 B. KASTENING, H. GARTMANN UND L. HOLLECK, *Electrochim. Acta*, 9 (1964) 741.
11 L. HOLLECK, J. M. ABD-EL-KADER UND A. M. SHAMS-EL-DIN, *J. Electroanal. Chem.*, 17 (1968) 401.
12 G. HOLLECK UND L. HOLLECK, *Naturwissenschaften*, 51 (1964) 433; L. HOLLECK UND G. HOLLECK, *Z. Naturforsch.*, 19b (1964) 162.
13 L. HOLLECK UND H. MARSEN, *Z. Elektrochem.*, 57 (1953) 944.

ELECTROANALYTICAL CHEMISTRY AND INTERFACIAL ELECTROCHEMISTRY
Elsevier Sequoia S.A., Lausanne – Printed in The Netherlands

HALF-WAVE POTENTIAL SHIFTS AT ROTATING DISK ELECTRODES OXIDATION OF N,N,N′,N′-TETRAMETHYL-*p*-PHENYLENEDIAMINE

ROBERT H. PHILP, JR.*
Department of Chemistry, University of South Carolina, Columbia, S. C. 29208 (U.S.A.)
(Received August 11th, 1969; in revised form January 9th, 1970)

INTRODUCTION

The utility of the rotating disk electrode (RDE) in studies of the kinetics of processes coupled to electrochemical reactions is well established[1-3].

Galus and Adams[4] showed that an equation for the current–potential curve for the kinetic case:

$$R \rightleftharpoons O + ne \tag{1}$$

$$O \xrightarrow{k} Z \tag{2}$$

can be derived by simple combination of the reaction layer model with the mass transport equations for the RDE. The equation for the half-wave potential of an oxidation wave can be written:

$$E_{\frac{1}{2}}^{k} = E^0 + (RT/nF) \ln (0.62\, D^{\frac{1}{6}} \omega^{\frac{1}{2}} k^{-\frac{1}{2}} v^{-\frac{1}{6}}) \tag{3}$$

where $E_{\frac{1}{2}}^{k}$ is the half-wave potential in the presence of kinetic complications, ω is the angular velocity (radians s^{-1}), v is the kinematic viscosity, and k is the pseudo-first order rate constant for transformation (2). The other symbols have their usual significance and all diffusion coefficients are assumed equal. A more exact equation, based on the derivation of Tong[5] *et al.* is:

$$E_{\frac{1}{2}} = E^0 - (RT/nF) \ln (1.61\, k^{\frac{1}{2}} v^{\frac{1}{6}} D^{-\frac{1}{6}} \omega^{-\frac{1}{2}}) \coth (1.61\, k^{\frac{1}{2}} v^{\frac{1}{6}} D^{-\frac{1}{6}} \omega^{-\frac{1}{2}}) \tag{4}$$

At values of $(k^{\frac{1}{2}}/\omega^{\frac{1}{2}}) > 10$, with typical values of D and v, eqn. (4) becomes identical with (3).

Curves of potential shift as a function of $\log \omega$ calculated from eqn. (4) over the range of rotation rates employed in this study are shown in Fig. 1. At $k = 10^2$ s^{-1} the system is indistinguishable from the uncomplicated case (1), while at about $k = 10^5$ s^{-1} the slope has reached the value of $(0.030/n)$ V predicted by eqn. (3).

It should thus be possible, under experimental conditions where eqn. (3) is valid, to detect reactions of kinetic type (1)–(2) by noting that a plot of the measured $E_{\frac{1}{2}}$ *vs.* $\log \omega$ is linear with a slope of $(0.059/2n)$ V. The reaction chosen to test this relation was the second one-electron step in the oxidation of N,N,N′,N′-tetramethyl-*p*-phenylenediamine (TMPPD). While the complete course of the oxidation of this

* Experimental work done at Kansas University.

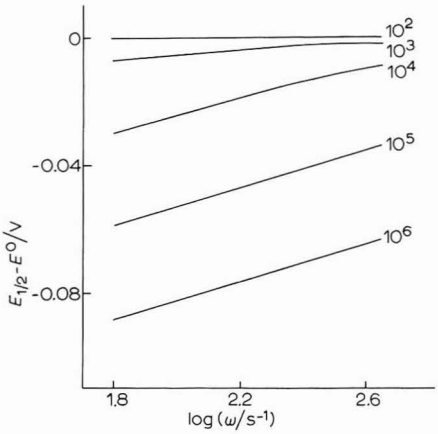

Fig. 1. Potential shift *vs.* log ω for indicated values of the rate constants. Values used in calculation: $D = 5.0 \times 10^{-6}$ cm^2 s^{-1}, $\nu = 0.01$ cm^2 s^{-1}, $n = 1$.

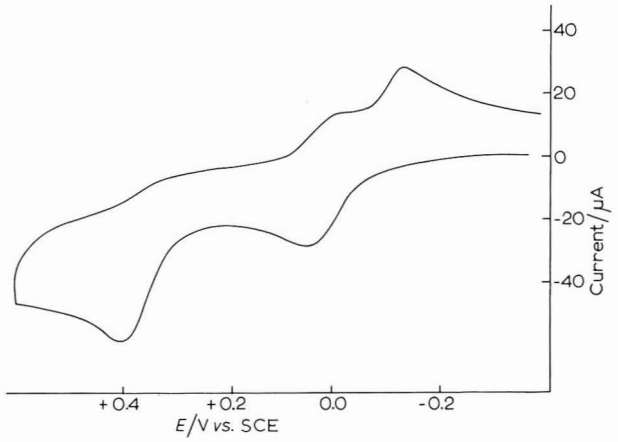

Fig. 2. Cyclic voltammogram of TMPPD at pH 9.8. Scan rate 2V min^{-1}

compound has not been elucidated, it appears that at pH 9.8 the system is relatively straightforward and conforms to the kinetic type being considered.

EXPERIMENTAL

All current–potential curves were obtained using standard three-electrode circuitry of the type described by Booman[6]. Polarization rate in the RDE studies was 200 mV/min. The rotating disk assembly has been described by Galus and Adams[7]. Platinum electrodes initially pretreated by Fe(II) in 1 *M* H_2SO_4 were employed. The active area of the RDE was 0.066 cm^2. Britton–Robinson buffers 0.2 *M* in Na_2SO_4 were prepared from doubly distilled water. The TMPPD was 5×10^{-4} *M* prepared by direct weighing of the dihydrochloride.

RESULTS

A cyclic voltammogram for TMPPD at pH 9.8 is shown in Fig. 2. On subsequent sweeps an anodic peak at about -0.1 V develops which is apparently the reoxidation of the system giving the cathodic peak at -0.12 V. The peak potentials of this system agree to within 10 mV with those for *p*-benzoquinone under the same experimental conditions. This relatively simple cyclic behavior is consistent with the overall scheme:

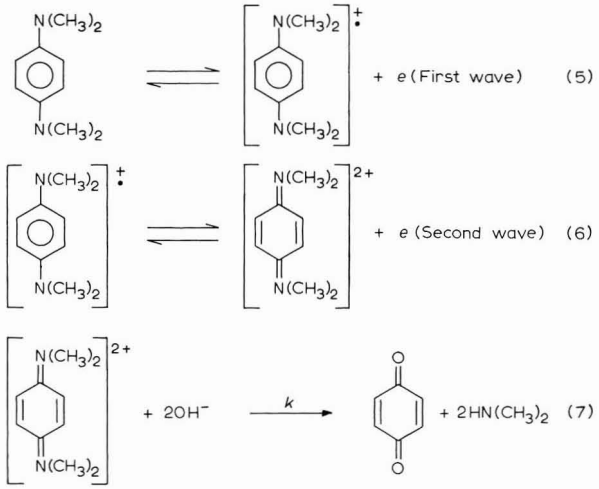

The RDE current–potential curves for TMPPD at pH 9.8 are given in Fig. 3. The limiting currents were linear with $\omega^{\frac{1}{2}}$ through the range of rotation rates employed. The ratio of limiting currents (second wave/first wave) was independent of rotation rate. The slopes of the least squares limiting current *vs.* $\omega^{\frac{1}{2}}$ lines are 1.40 ± 0.04 and 1.21 ± 0.02 μA $s^{\frac{1}{2}}$ for the first and second waves respectively. From the first wave, by assuming a value of 0.01 $cm^2\ s^{-1}$ for ν, a diffusion coefficient of 0.48×10^{-5} $cm^2\ s^{-1}$ for TMPPD is calculated. This is in good agreement with values given for similiar compounds[5].

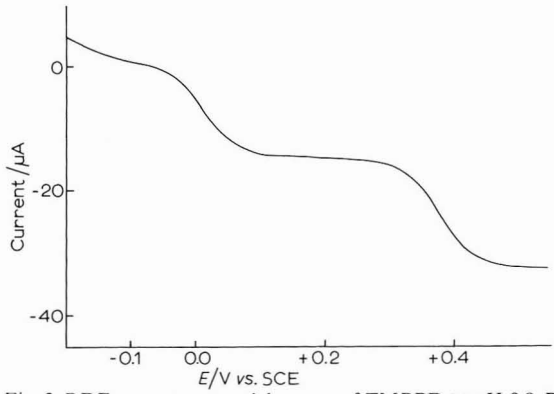

Fig. 3. RDE current–potential curves of TMPPD at pH 9.8. Rotation rate 20 rev. s^{-1}.

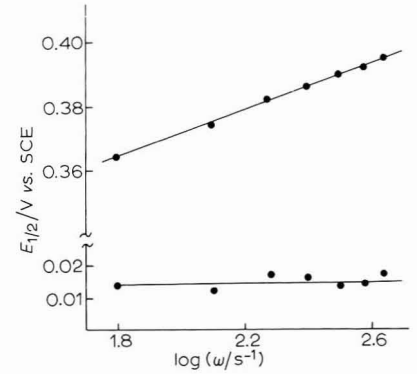

Fig. 4. Half-wave potentials from RDE current–potential curves.

The half-wave potentials as a function of log ω are shown in Fig. 4. The $E_{\frac{1}{2}}$ of the second wave shows a clear linear dependence on log ω although the slope is somewhat high (0.035 V) compared to that predicted by eqn. (3). No trend in the $E_{\frac{1}{2}}$ of the first wave is noted although the scatter is bad. This scatter reflects some difficulty in making very accurate $E_{\frac{1}{2}}$ measurements on the first wave due to the onset of cathodic limiting processes which can be seen near 0 V in Fig. 3. The second curve, on the other hand, is near the classical shape and amenable to quite accurate $E_{\frac{1}{2}}$ measurement. All $E_{\frac{1}{2}}$ values are means of values taken from two sets of curves. The first series was started at 10 rev. s^{-1} and increased to 70 rev. s^{-1}. The second was started at 70 rev. s^{-1} and decreased to 10 rev. s^{-1}. At the same rotation rate the $E_{\frac{1}{2}}$ of the second wave never differed by more than 2 mV between the two sets. The shape of the second wave did not change with rotation rate. Fast electron transfer is indicated by the slope of the wave ($E_{\frac{3}{4}} - E_{\frac{1}{4}} = 0.055 \pm 0.001$ V) which did not vary with rotation rate.

It thus appears that detection of kinetic type (1)–(2) can be accomplished by simple measurement of $E_{\frac{1}{2}}$ as a function of log ω. With the range of RDE rotation rates normally available one would expect the most useful study to be for reactions with k values from 10 to 10^3 s^{-1}. For faster reactions a linear relation between $E_{\frac{1}{2}}$ and log ω serves only to fix a lower limit on the value of the rate constant. The value of the rate constant for reaction (7) at pH 9.8 is thus indicated as $> 10^4$ s^{-1}.

It should be noted that a totally irreversible electron transfer would also be expected to show a linear relation between $E_{\frac{1}{2}}$ and log ω. In this case, however, the slope would be $(0.059/2\alpha n)$ V at 25°C. This possibility is not consistent with the strong indication that the second wave of TMPPD is a rapid one-electron step.

SUMMARY

Equations for $E_{\frac{1}{2}}$ of current–potential curves at the rotating disk electrode in the case of rapid electron transfer followed by pseudo-first order transformation of the product are discussed. In cases where $k^{\frac{1}{2}}/\omega^{\frac{1}{2}} > 10$, a linear relation between $E_{\frac{1}{2}}$ and log ω having a slope of $0.059/2n$ V is indicative of this kinetic type.

The cyclic voltammetry of N,N,N′,N′-tetramethyl-*p*-phenylenediamine at pH 9.8 indicates that the second step in the oxidation conforms to this reaction scheme. Measured $E_{\frac{1}{2}}$ values at the rotating disk electrode of the first wave were independent of ω in the region 10–70 rev. s^{-1}. The $E_{\frac{1}{2}}$ of the second wave is linear with log ω in

this region indicating a rate constant $>10^4\ s^{-1}$ for the deamination of the quinone diimine formed in this step.

REFERENCES

1 V. G. LEVICH AND J. KOUTECKY, *Zh. Fiz. Khim.*, 32 (1958) 1565.
2 A. C. RIDDIFORD, in P. DELAHAY (Ed.), *Advances in Electrochemistry and Electrochemical Engineering, Vol. 4*, Interscience, New York, 1966, p. 103.
3 P. A. MALACHESKY, L. S. MARCOUX AND R. N. ADAMS, *J. Phys. Chem.*, 70 (1966) 4068.
4 Z. GALUS AND R. N. ADAMS, *J. Electroanal. Chem.*, 4 (1962) 248.
5 L. K. J. TONG, K. LIANG AND W. R. RUBY, *J. Electroanal. Chem.*, 13 (1967) 245.
6 G. L. BOOMAN, *Anal. Chem.*, 29 (1957) 213.
7 Z. GALUS AND R. N. ADAMS, *J. Phys. Chem.*, 67 (1963) 866.

ELECTROANALYTICAL CHEMISTRY AND INTERFACIAL ELECTROCHEMISTRY
Elsevier Sequoia S.A., Lausanne – Printed in The Netherlands

ELECTROCHEMICAL REDUCTION OF PARABANIC ACID: PRODUCTS AND MECHANISM

GLENN DRYHURST*, BARBARA H. HANSEN AND EDWARD B. HARKINS
Department of Chemistry, University of Oklahoma, Norman, Oklahoma (U.S.A.)
(Received March 23rd, 1970)

INTRODUCTION

Parabanic acid appears to be a major product formed upon electrochemical[1-4], enzymic[5-7] and photochemical reaction[8] of many naturally occurring biologically important purines. The electrochemical reduction of parabanic acid itself has not, however, been studied in detail even though polarography provides an elegant and simple method for its determination[9].

Hladik[10] has postulated that parabanic acid is reduced at mercury electrodes in a two-electron, two-proton reaction to 5-hydroxyhydantoin, although this was supported only by the value of the diffusion current constant. In buffer solutions, above about pH 4.6, which contained phosphate, a post wave was observed which Hladik attributed to reduction of the anionic form of parabanic acid, since its first pK_a is between about 6.1 and 6.2[10,11]. Struck and Elving[9] briefly re-examined the polarography of parabanic acid and concluded that the post wave was probably due to reduction of a phosphate complex of parabanic acid. No significant data on the detailed mechanism of the electrode process or on the nature of the phosphate complex were presented in this latter report.

It has been found that both parabanic acid and its mono- and di-methyl derivatives are formed in many electrochemical reactions of certain biologically important purines. Accordingly, the electrochemical reduction of each of these compounds has been further investigated with a view to understanding more thoroughly the electrochemical mechanism, products and nature of the phosphate complexes postulated. Detailed study was confined to parabanic acid itself.

EXPERIMENTAL

Chemicals

Parabanic acid was obtained from Eastman and was sufficiently pure to be used without further purification. Methyl- and dimethyl parabanic acid were synthesized according to Blitz and Topp[12]. Glyoxylic acid was obtained by passing its magnesium salt, prepared according to Hawk *et al.*[13], through a strongly acid ion exchange resin (Dowex 50–X8). Buffer solutions were prepared from reagent grade chemicals to give an ionic strength of 0.5 *M* at the pH value concerned. Argon (Linde) used for

* To whom further correspondence should be directed.

deoxygenating purposes was equilibrated with water; no other purification was necessary.

Apparatus

Polarograms were recorded on a Sargent Model XV polarograph using a water jacketted cell maintained at 25° ±0.1°C containing a saturated mercurous sulfate reference electrode (MSE). All potentials are referred to the MSE at 25°C (MSE has a potential of 0.40 V *vs.* the saturated calomel electrode[14]). The dropping mercury electrode had normal *m* and *t* values and employed triply distilled mercury. The preparation of pyrolytic graphite electrodes has been described elsewhere[1], as has the apparatus for cyclic voltammetry, controlled potential electrolysis, coulometry and lyophylization[15,16]. Ultraviolet absorption spectra were recorded on a Perkin Elmer–Hitachi Model 124 spectrophotometer; infrared spectra were recorded on a Beckman IR8 spectrophotometer. Mass spectra were recorded on a Hitachi MS-18 mass spectrometer.

Polarographic procedure

Approximately 20 ml of test solution which was normally about 0.5 m*M* with respect to the appropriate parabanic acid (and freshly prepared) was transferred to the polarographic cell and deoxygenated with argon for at least 10 min and then polarographed. No maximum suppressors were employed. A portion of the buffer solution was treated identically to obtain the background current which was subtracted from the total current. The half-wave potential, $E_{\frac{1}{2}}$, and limiting current were determined graphically from the average of the recorder trace.

Coulometry

A measured volume of background solution was electrolyzed at a massive mercury pool electrode at the appropriate potential in the working electrode compartment until a titration coulometer[17] gave a very small constant titration rate. Then sufficient of the appropriate parabanic acid was introduced to give a resulting solution of about 0.5–1m*M*. The electrolysis was then continued until the current had decayed to close to background level and the resulting solution showed no polarographic wave (or only a very small polarographic wave) in the region expected for parabanic acid (*vide infra*).

Macroscale electrolysis

This was essentially identical to that described under *Coulometry* except that about ten times more parabanic acid was employed. The background employed was always 1 *M* HOAc. At apparent completion of the electrolysis the solution in the working electrode compartment was shell frozen onto the walls of a 500 ml flask and lyophilized. The resultant product was a white fluffy powder which was extremely hygroscopic.

Thin layer chromatography

The most useful thin layer plate was a Brinkman MN-Polygram Cellulose 300 impregnated with a fluorescent indicator. Two solvent systems were employed; n-butanol–acetic acid–water (BAW) in the ratio 60–15–25% respectively, and

n-propanol–water (PW) in the ratio 70–30% respectively. All positive identifications were made by parallel behavior of reference compounds and components of the electrolysis product. Urea was detected with Ehrlich's reagent ($r_f = 0.50$) using the BAW solvent. In the same solvent system two fluorescing spots ($r_f = 0.23$, 0.41) were also observed. In PW solvent, glycolic acid was detected with neutral alcoholic bromocresol green ($r_f = 0.56$–0.59); this corresponded with one of the u.v. active spots, the other had a lower r_f value of 0.46. As a result of these separations, urea and glycolic acid were identified in the electrolysis along with a further u.v. active species having r_f values of 0.23 and 0.46 in BAW and PW solvents respectively. On the basis of other information it is probable that these latter spots are due to 5-hydroxyhydantoin. In no case was glyoxylic acid detected in the electrolysis product.

Mass spectra

Mass spectrometry of the product showed several significant peaks above background. A peak corresponding to mass 116 corresponds to the parent ion of 5-hydroxyhydantoin; a peak at mass 60 corresponds to urea. Most of the ions of lower masses could be readily rationalized on the basis of the known or expected fragmentation patterns for these two compounds. No peak was observed that corresponded to the parent ion of glycolic acid. However, under the conditions of heat and vacuum extant in the mass spectrometer it is likely that dehydration and polymerization of glycolic acid might readily occur. Mass spectrometry appeared therefore to confirm the presence of 5-hydroxyhydantion and urea.

RESULTS AND DISCUSSION

Parabanic acid

Below pH 5.3 parabanic acid shows a single well-formed polarographic reduction wave, the half-wave potential for which shifts linearly more negative with increasing pH (wave I, Fig. 1A). Between pH 5.6 and 7 in McIlvaine (phosphate, citrate, chloride) two waves appear (Fig. 2A). The more positive and larger of these waves follows the same pH dependence as wave I; the more negative wave (wave II) is generally more drawn out, is smaller than wave I and is essentially pH independent (Fig. 1A). In acetate-containing buffers between pH 5.6 and 6.3 only wave I appears, although $E_{\frac{1}{2}}$ occurs 40–50 mV more positive than in McIlvaine buffers. Above pH 7, wave II is not observed. The shift of the half-wave potential for wave I with pH follows the relationship, $E_{\frac{1}{2}}/\mathrm{V} = -0.926$–$0.058$ pH. Between pH 0 and 7 the diffusion current constant ($I = i_d/Cm^{\frac{2}{3}}t^{\frac{1}{6}}$) for wave I lies between 4.4 and 5.7 which is indicative of a process involving between 2 and 3 electrons transferred per molecule of parabanic acid which is reduced. Above pH 7 the hydrolysis of parabanic acid to oxaluric acid is too rapid to allow accurate measurement of the diffusion current constant. Oxaluric acid has been studied polarographically[18] and does not give rise to any waves in the potential range of interest in this study. Over the range pH 5.5–6.5, parabanic acid did not give rise to wave II in citrate buffers which did not contain phosphate. However, in buffers prepared solely from the appropriate sodium salts of phosphoric acid, between pH 5.2 and 6.8 both wave I and wave II were observed (Fig. 2D).

In acetate buffers below pH 5 wave I is entirely under diffusion control as evidenced by the temperature and droptime dependence of the wave. Over the pH region

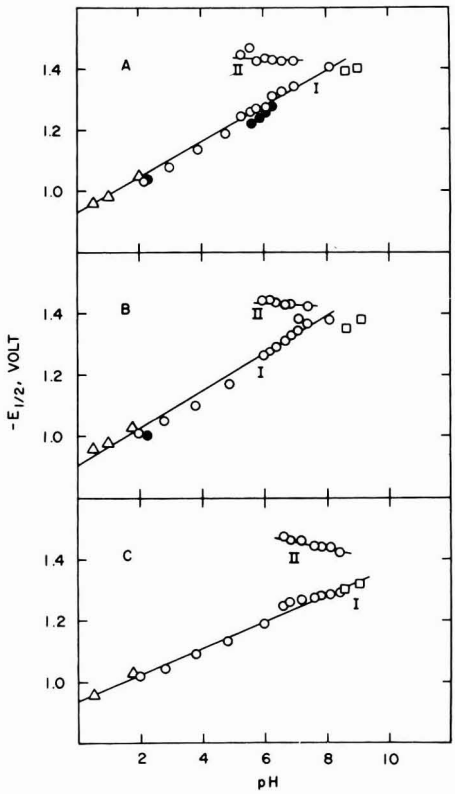

Fig. 1. Variation of $E_{\frac{1}{2}}$ with pH for waves I and II of: (A) parabanic acid, (B) methylparabanic acid, (C) dimethylparabanic acid. Buffer systems: (○) McIlvaine, (△) chloride, (●) acetate, (□) ammonia.

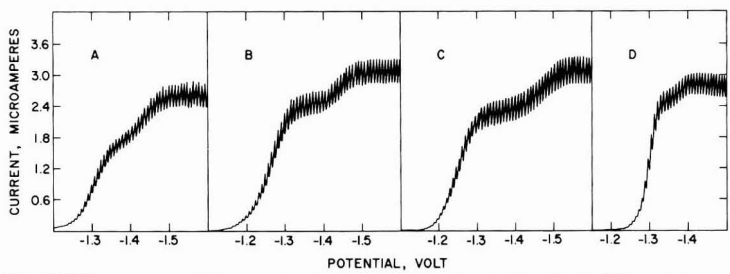

Fig. 2. Polarograms of: (A) parabanic acid in McIlvaine buffer pH 6.1, (B) methylparabanic acid in McIlvaine buffer pH 6.0, (C) dimethylparabanic acid in McIlvaine buffer pH 6.6, (D) parabanic acid in Na_2HPO_4–$NaHPO_4$ buffer pH 5.4. Concn. Approx. 0.5 mM in each case.

where both waves I and II appear distinctly, *i.e.* pH 5.5–7, parabanic acid decomposes at a slow but perceptible rate so that it was not possible to obtain meaningful data from the droptime and temperature dependence of the waves. Polarograms run in a series of McIlvaine buffers between pH 5.3 and 7 showed that above about pH 5.6 the relative heights of waves I and II were very approximately constant; the ratio i_1 (wave II)/i_1 (wave I) over this latter pH range was 0.48 ± 0.21. The uncertainty in these

data reflect again the decomposition of parabanic acid solutions at these pH regions.

At low pH, *e.g.* 1 *M* HOAc pH 2.3, the diffusion current for parabanic acid is linearly dependent upon concentration.

Methyl parabanic acid

Below pH 6, methylparabanic acid shows a single pH dependent wave (wave I) which shifts linearly more negative with increasing pH, $E_{\frac{1}{2}}/\mathrm{V} = -0.902-0.061$ pH. In McIlvaine buffers between pH 6 and 7.4 a second wave appears (wave II) (Fig. 2B) which is always smaller than wave I and which is almost pH independent (Fig. 1B). At higher pH, again only a single wave is observed. Between pH 0.5 and 7 the diffusion current constant for wave I is constant at 3.6 ± 0.2 which suggests a two-electron polarographic process. Below pH 5 in acetate buffers wave I is entirely under diffusion control as evidenced by its droptime and temperature dependence. Decomposition of methylparabanic acid at pH regions where waves I and II are observed was sufficiently rapid so that droptime and temperature studies could not be meaningfully carried out. Over the pH range 6.0–7.4 there was no systematic change in the relative heights for waves I and II; the ratio i_1 (wave II)/i_1 (wave I) was 0.37 ± 0.15.

Dimethyl parabanic acid

Below pH 6.6 dimethylparabanic acid gives only a single polarographic wave (wave I) which shifts linearly more negative with pH, $E_{\frac{1}{2}}/\mathrm{V} = -0.937-0.043$ pH (Fig. 1C). Between pH 6.6 and 8.4 in McIlvaine buffers a second wave appears (wave II) (Fig. 2C) which appeared to shift to slightly more positive potential with increasing pH. However, the instability of dimethylparabanic acid, especially at the higher pH values, along with the closeness of the two waves made very accurate measurements of $E_{\frac{1}{2}}$ for wave II difficult. At higher pH only a single wave was observed. Between pH 0.5 and 7.2 the value of the diffusion current constant was 3.6 ± 0.4. At low pH the single wave I was entirely under diffusion control. Instability of dimethylparabanic acid at pH values where both waves I and II were observed precluded the study of droptime and temperature. As with the other acids, the ratio i_1 (wave II)/i_1 (wave I) was fairly constant at 0.39 ± 0.11 in McIlvaine buffers between pH 6.6 and 8.4.

Coulometry

At pH 2.3, coulometry at a potential corresponding to the crest of the polarographic wave of parabanic acid gave an average faradaic n value of 1.9 e. Such electrolyses took between 2–3 h to reach essentially completion; it was often noted that polarography of the resultant solution showed a very small wave close to that expected for parabanic acid, which increased very slowly in height with standing time. Coulometry of methylparabanic acid at low pH gave an average faradaic n value of 1.7 and for dimethylparabanic acid a value of 1.9 was obtained.

Macroscale electrolysis

Exhaustive electrolysis of parabanic acid in1 *M* HOAc of a 5–10 m*M* solution until complete removal of all polarographic waves took four days or longer. The resultant product (isolated by lyophilization) was an off-white and extremely hygroscopic solid. Thin layer chromatography and mass spectrometry revealed that urea, 5-hydroxyhydantoin and glycolic acid were present in the electrolysis product.

Cyclic voltammetry

The slope of the polarographic wave, particularly at low pH, of parabanic acid suggested a reversible reaction. Cyclic voltammetry at pyrolytic graphite and mercury electrodes did not give any anodic peaks characteristic of a reversible process at any pH.

MECHANISM

The magnitude of the diffusion current constant and coulometry of dilute solutions suggests that the polarographic process associated with wave I in the absence of phosphate involves transfer of two electrons per molecule of parabanic acid (and its methylated derivatives) reduced. In order to gain further mechanistic information, a wave analysis, at various pH values using the well known log-plot or ($E_{\frac{3}{4}}$–$E_{\frac{1}{4}}$) methods, was carried out to evaluate the number of electrons and protons involved in the rate, or potential, controlling processes. In summary, it was found that below pH 1 (parabanic acid), 2.8 (methylparabanic acid), and 4.8 (dimethylparabanic acid), and above pH 8 (all acids), that the rate-controlling step involved two electrons and two protons. In the intermediate pH regions the potential-controlling step was found to involve two electrons but only a single proton.

The decomposition of all the parabanic acids above pH 8 was very rapid so that wave analysis data in this region might involve considerable error. In view of the presence of 5-hydroxyhydantoin (II, eqn. 1) in the product of macroscale electrolysis, the following primary electrochemical mechanisms can be written (eqn. 1 a, b).

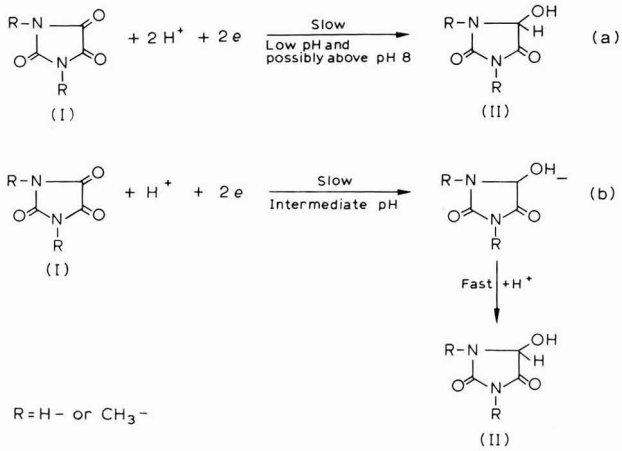

(1)

Prolonged electrolysis of parabanic acid itself, however, results not only in 5-hydroxyhydantoin but also in urea and glycolic acid. Hydrolysis of 5-hydroxyhydantoin (eqn. 2) would be expected to yield urea and glyoxylic acid[19] (II, eqn. 2).

(2)

Glyoxylic acid, is however, polarographically reducible in a apparent kinetically controlled process[20,21]. Polarograms of authentic glyoxylic acid in 1 *M* HOAc showed a small well-formed wave, $E_{\frac{1}{2}} = -0.95$ V. Accordingly, any glyoxylic acid produced upon hydrolysis of 5-hydroxyhydantoin would be reduced to glycolic acid the known electrochemical product[20]. In view of the continued presence of small amounts of hydantoin even after prolonged electrolysis, it is likely that the rate of its hydrolysis is slow. Formation of glyoxylic acid by this route nicely accounts for the small polarographic wave observed at potentials close to those expected for parabanic acid after coulometry or macroscale electrolysis, which slowly increased in height upon standing.

Because of the instability of parabanic acid above pH 5 it is difficult to obtain information on the chemical and electrochemical processes responsible for waves I and II. Wave I, however, is undoubtedly due to reduction of free parabanic acid as evidenced by the pH and wave analysis data. Wave II is clearly dependent upon the presence of large excesses of phosphate and must be reduction of a phosphate complex of parabanic acid. The approximately constant height of wave II relative to wave I, regardless of the pH of the McIlvaine buffer system, over the limited pH regions at which it is observed would tend to suggest complexation with one or other of the predominant phosphate ions in solution, namely $H_2PO_4^-$ or HPO_4^{2-} which are always present in all buffers in very large excess over the particular parabanic acid. By approximate analogy with Pasternak's[22] suggestions regarding borate complexes of 1,2-diketones, several possible parabanic acid–phosphate complexes might be expected. However, in view of the presence of large excesses of the $H_2PO_4^-$ and HPO_4^{2-} species, and the pH independence of the polarographic wave for the complex, it is likely that the complex would be of the type shown in eqns. (3a or 3b).

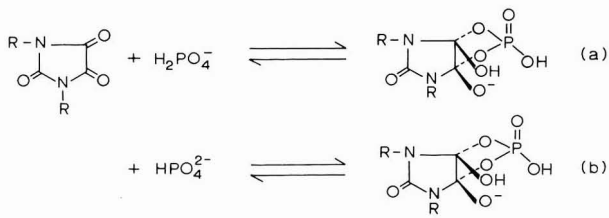

(3)

Since protonation of the reducible carbonyl group takes place upon complexation (this might occur *via* a hydrogen-bonded structure), the mechanism of polarographic reduction can be represented by eqn. (4) which accounts for the virtual pH independence of wave II.

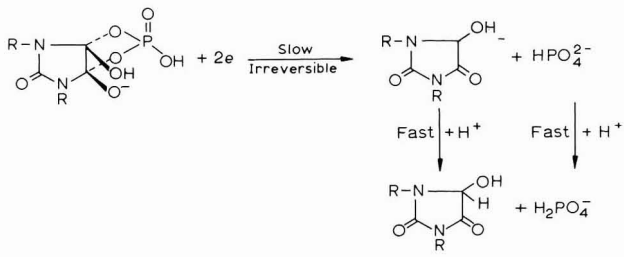

(4)

Approximate wave slope data confirm the rate controlling process in this mechanism.

It is likely that the formation constant for such a phosphate complex is very small so that it is only observed in the presence of very large excesses of phosphate and that minor relative changes in phosphate concentration at higher pH have only minor effect on the solution concentration of the complex.

The disappearance of wave II below pH 5–6 no doubt reflects instability at moderately high proton concentrations.

ACKNOWLEDGEMENT

The authors would like to thank the National Science Foundation which partially supported the work described through Grant No. GP 8151 and the National Aeronautics and Space Administration which provided fellowship support (B.H.H.) during part of the work.

SUMMARY

The polarographic reduction of parabanic acid, methylparabanic acid and dimethylparabanic acid has been investigated over a wide range of pH.

The primary electrochemical reaction involves overall two-electrons and two-protons to give the corresponding 5-hydroxyhydantoin. At low pH and possibly at moderately high pH, the rate controlling step involves two-electrons and two-protons; at intermediate pH values a two-electron, one-proton rate controlling process is operative. 5-Hydroxyhydantoin appears to be slowly hydrolyzed to glyoxylic acid and urea so that prolonged electrolysis (in 1 *M* HOAc) of parabanic acid gives a mixture of 5-hydroxyhydantoin, urea and the reduction product of glyoxylic acid, namely glycolic acid.

In phosphate-containing buffers between approximately pH 6 and 8 all the parabanic acids give a very weak complex with phosphate which is reduced at more negative potentials than the free acids in an essentially pH independent process. On the basis of the phosphate species present in solution and the pH independence of the complex wave, a tentative structure has been proposed for the complex.

REFERENCES

1 G. DRYHURST AND P. J. ELVING, *J. Electrochem. Soc.*, 115 (1968) 1014.
2 W. A. STRUCK AND P. J. ELVING, *Biochemistry*, 4 (1965) 1343.
3 G. DRYHURST, *J. Electrochem. Soc.*, submitted for publication.
4 G. DRYHURST AND B. H. HANSEN, *work in progress.*
5 E. S. CANELLAKIS AND P. P. COHEN, *J. Biol. Chem.*, 213 (1955) 385.
6 K. G. PAUL AND Y. AVI-DOR, *Acta Chem. Scand.*, 8 (1954) 637.
7 G. SOBERON AND P. P. COHEN, *Arch. Biochem. Biophys.*, 103 (1963) 331.
8 J. S. SUSSENBACH AND W. BERENDS, *Biochem. Biophys. Acta*, 95 (1965) 185.
9 W. A. STRUCK AND P. J. ELVING, *Anal. Chem.*, 36 (1964) 1374.
10 V. HLADIK, *Sb. Mezinar. Polarogr. Sjezdu, 1st Congr.*, Pt. 1, (1951) 686.
11 G. KORTÜM, W. VOGEL AND K. ANDRUSSOW, *Dissociation Constants of Organic Acids in Aqueous Solutions*, Butterworths, London, 1961, p. 526.
12 H. BLITZ AND E. TOPP, *Ber.*, 46 (1913) 1387.
13 P. B. HAWK, B. L. OSER AND W. H. SUMMERSON, *Practical Physiological Chemistry*, Blakiston Co., St. Louis, 1947, p. 1227.

14 J. J. LINGANE, *Electroanalytical Chemistry*, Interscience Publishers, New York, 2nd edn., 1966, p. 363.
15 G. DRYHURST, *J. Electrochem. Soc.*, 116 (1969) 1097.
16 G. DRYHURST, *J. Electrochem. Soc.*, 116 (1969) 1411.
17 See ref. 14, pp. 457–458.
18 G. DRYHURST AND P. J. ELVING, *Anal. Chem.*, 40 (1968) 492.
19 C. T. GRAY, M. S. BROOKE AND J. C. GERHART, *J. Bacteriol.*, 81 (1961) 755.
20 J. KŮTA, *Collection Czech. Chem. Commun.*, 24 (1959) 2532.
21 V. S. BEZUGLYI, V. N. DMITRIEVA, T. S. TARASYUK AND N. A. IZMAILOV, *Zh. Obshch. Khim.*, 30 (1960) 2415.
22 R. PASTERNAK, *Helv. Chim. Acta*, 30 (1947) 1984.

ELECTROANALYTICAL CHEMISTRY AND INTERFACIAL ELECTROCHEMISTRY
Elsevier Sequoia S.A., Lausanne – Printed in The Netherlands

REDUCTION MECHANISM OF NITROGEN COMPOUNDS AT THE DME*

I. Di-n-PROPYL-N-NITROSOAMINE

F. PULIDORI, G. BORGHESANI, C. BIGHI AND R. PEDRIALI
Department of Chemistry, University of Ferrara (Italy)
(Received March 2nd, 1970; in revised form April 24th, 1970)

The polarographic reduction of N-nitrosoderivatives of aliphatic, cycloaliphatic and aromatic amines has already been the subject of various studies. While some of them are mainly of analytical character[1-5,15] in others attempts have been made to elucidate, although incompletely and qualitatively, the mechanism of the electrode reduction of the =N–N=O group and to establish the influence of the molecular skeleton on the reducibility of this group[6-11].

Martin and Tashdijan[6], for example, consider the process as controlled by diffusion, although considering the possibility of a more complicated control. According to Lund[8], the electroreduction of N-nitroso compounds is irreversible and diffusion controlled both in strong acid and alkaline media, involving respectively 4 and 2 electrons. At intermediate pH, the nature of the rate-determining step has not been established. In alkaline medium the reduction products are said to be a secondary amine and N_2O. Holleck and Schindler[9] consider that the process takes place through a hydroxylamine intermediate, which is also the reduction product in alkaline medium. In acid medium the electrolysis product is the corresponding hydrazine. Polarographic and spectroscopic studies on various N-nitrosoamines led Zharadnik *et al.*[11] to propose a mechanism involving kinetic complications.

It remains therefore to establish the nature and the details of the electroreduction mechanism of this class of compound, which are important, *inter alia*, for the electrochemical preparation of asymmetric hydrazines, which are of interest for their biological activity, etc.

EXPERIMENTAL

Di-n-propyl-N-nitrosoamine (DNPNA) was prepared by the method of Lemal *et al.*[12]. The product used had the following physical properties: b.p. 90°C/13 Torr; $n_D^{25} = 1.44165$; $d_4^{25} = 0.91101$; $\varepsilon_{25} = 33.80$[14]. The ir spectrum was identical with that reported by Tarte[13]. Dielectric and vapour pressure measurements[14,16] excluded the possibility of dimerization equilibria.

The supporting electrolyte consisted of Britton–Robinson buffer containing 20% by volume of EtOH. Below pH 2 the measurements were made in H_2SO_4 containing 20% of EtOH. All the products used were of analytical grade.

The polarographic measurements were carried out in a three electrode cell

* This work was carried out with the financial support of the National Research Council (C.N.R.).

with an Amel model 557/SU potentiostat with a model 563 programming unit. The half-wave potentials are referred to a saturated calomel electrode (SCE). Capillary constants were as follows: $m = 2.7$ mg s^{-1}; $t = 3.0$ s for $h_{Hg} = 76$ cm.

pH-measurements were made with an Amel pH-meter, model 331 and were all carried out at temperatures kept constant to $\pm 0.1°C$.

The spectrophotometric measurements were made with an Optica CF4 instrument.

All solutions were deaerated with high purity nitrogen for 20 min before recording a polarogram. During the course of the measurements a nitrogen atmosphere was maintained above the solutions.

RESULTS

The reduction of DNPNA takes place irreversibly. This can be demonstrated by:

(*a*) the absence of cathanodic waves in d.c. polarography,

(*b*) the number of electrons taking part in the process, together with the slopes of the semilogarithmic polarographic graphs,

(*c*) the dependence of $E_{\frac{1}{2}}$ on the drop time,

(*d*) the slope of the current–potential curves in cyclic voltammetry.

EtOH was added to the buffer in order to ensure complete solubility over the whole pH range for all the members of the N-nitrosoamines series.

The polarographic behaviour of DNPNA, is summarized in Fig. 1.

At low pH, DNPNA gives rise to a single irreversible cathodic wave whose half-wave potential $E_{\frac{1}{2},1}$ shifts towards more negative values with increasing pH (Fig. 1, IB). The height of this wave, $i_{l,1}$, is constant at pH values $\leqq 4$. With further increase in pH the height of the wave starts to diminish and finally disappears at pH values of about 8. At the same time $i_{l,1}$ exhibits a kinetic character as shown by the $i_{l,1}$ *vs.* $\sqrt{h_{Hg}}$ curves (Fig. 2).

In the pH region in which the height of the first wave decreases (Fig. 1, IA), a

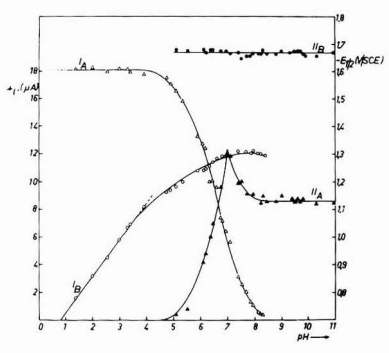

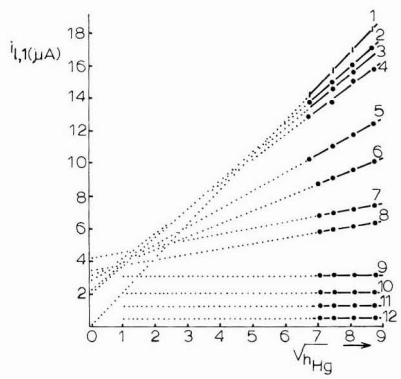

Fig. 1. Dependence of the limiting current (A) and half-wave potentials (B) of the first (I) and second (II) wave of DNPNA on pH. $C = 1 \times 10^{-3}$ *M*; B.R. buffer + 20% EtOH; $h_{Hg} = 76$ cm; $t = 25°$.

Fig. 2. Dependence of the first wave of 1×10^{-3} *M* DNPNA on h_{Hg} at various pH values: (1) 1.40–4.75, (2) 4.89, (3) 5.09, (4) 5.34, (5) 6.21, (6) 6.44, (7) 6.76, (8) 6.94, (9) 7.38, (10) 7.68, (11) 7.85, (12) 8.15.

second irreversible wave (Fig. 1, IIA) is present at more negative potentials. Its height $i_{l,2}$ increases with increasing pH up to a constant value ($=\frac{1}{2}\, i_{l,1}$ at pH $\leqq 4$) in the pH range where the first wave no longer exists. Under these conditions, height experiments seem to indicate a diffusion controlled process. $E_{\frac{1}{2},2}$ is pH independent and varies between -1.670 and -1.680 V/SCE (Fig. 1, IIB).

The number of electrons involved in the first wave, determined by constant-potential electrolysis, varied between 3.8 and 4.1, *i.e.* 4 F mol^{-1}. The second wave involves therefore 2 F mol^{-1} of depolarizer.

Using the spectrophotometric method of McKennis and Yard[17], the presence of the corresponding hydrazine was recognized as the reduction product in the electrolysis in strong acid medium. However, it has not yet been possible to show the presence of the N-hydroxylamine derivative at higher acid pH values, as suggested by other authors[9].

The corresponding secondary amine is obtained by the large-scale electrolysis of the N-nitrosoamine at a mercury cathode in the diffusion region of the second wave. From the results obtained at pH 2, at various concentrations and various h_{Hg}, a diffusion current constant of 7.2 ± 0.1 and a diffusion coefficient $D = 8.8 \pm 0.3 \times 10^{-6}$ cm^2 s^{-1} are obtained, in substantial agreement with those reported in the literature for analogous compounds[8,9,18].

At pH 2, the temperature coefficient of the limiting current is of the order of 1.7%/°C, thus indicating a diffusion-controlled process (Table 1).

The activation energy of the diffusion step, which controls the overall process under these conditions, was evaluated from the dependence of D on the temperature. At pH 6.93 the temperature coefficient of $i_{l,1}$ tends to increase with a decrease in the drop time (Table 2) and also with increasing pH without, however, appreciably exceeding 2%/°C (Table 3).

In the Tables 1, 2 and 3 are also reported the slopes of the semilogarithmic curves at, respectively, pH 2, pH 6.93, and pH 7.47 as well as the interpolated values of $E_{\frac{1}{2},1}$. Table 1 also gives the depolarization potentials of the process of the first wave. It can be seen that the temperature coefficient of $E_{\frac{1}{2},1}$ is negative and increases

TABLE 1

CHARACTERISTICS OF THE FIRST WAVE OF DNPNA AT A CONCENTRATION OF 1×10^{-3} *M* AT VARIOUS TEMPERATURES

B.R. buffer + 20% EtOH; $h_{Hg} = 76$ cm; pH = 2

t/°C	$i_{l,1}/\mu A$	$-E_{\frac{1}{2}}/V\,(SCE)$	$10^6\, D/cm^2\, s^{-1}$	$-b/V$	$-E_d/V\,(SCE)$	
8	12.7	0.860	4.93	0.090	0.685	—
12	14.0	0.861	5.81	0.091	0.691	—
16	15.2	0.860	6.75	0.093	0.694	—
22	17.2	0.865	8.33	0.093	0.695	—
25	18.3	0.858	8.84	0.092	0.696	—
30	19.8		10.54			—
34	21.2	0.856	11.84	0.093	0.703	two slopes
40	22.5	0.864	13.73	0.101	0.710	two slopes
46	24.3	0.860	15.16	0.098	0.712	two slopes

Mean temp. coefficient of $i_{l,1} = 1.67$%/°C log $D = -1.070 - (1.187 \pm 30)/T$; $\Delta H_{diff.} = 5400 \pm 200$ cal mol^{-1}

b = slope of the functions $E = f(\log [i/(i_l - i)])$.

TABLE 2

DEPENDENCE OF $i_{1,1}$ OF DNPNA AT A CONCENTRATION OF 1×10^{-3} M ON TEMPERATURE AT VARIOUS HEIGHTS OF THE MERCURY RESERVOIR

B.R. buffer + 20% EtOH; pH 6.93

$t/°C$	$i_{1,1}/\mu A$				$-E_{\frac{1}{2}}/V\,(SCE)$	$-b/V$
	50 *cm*	56 *cm*	66 *cm*	76 *cm*		
12	4.4	4.4	4.4	4.4	1.269	0.120
15	4.7	4.7	4.7	4.8	1.277	0.116
19	4.8	4.9	5.1	5.3	1.128	0.122
25	5.3	5.5	5.7	6.0	1.289	0.122
29	5.9	6.0	6.2	6.4	1.298	0.116
34	6.4	6.6	6.8	7.3	1.307	0.108
40	6.8	7.2	7.5	8.0	1.313	0.110
Temp. coefficient						
	1.7	1.85	1.93	2.16%/°C	−1.6 mV/°C	

TABLE 3

DEPENDENCE OF $i_{1,1}$ OF DNPNA AT A CONCENTRATION OF 1×10^{-3} M ON TEMPERATURE

B.R. buffer + 20% EtOH; pH 7.47; $h_{Hg} = 76$ cm

$t/°C$	$i_{1,1}/\mu A$	$-E_{\frac{1}{2}}/V\,(SCE)$	$-b/V$
25	2.8	1.312	0.104
33	3.2	1.319	0.096
42	3.7	1.337	0.078

Temp. coefficient 2.01%/°C; −1.47 mV/°C. b = slope of the function $E = f\{\log[i/(i_l - i)]\}$

with pH. The depolarization potentials E_d (Table 1) shift towards more negative values with rising temperature. The influence of temperature on the shape of the first wave of DNPNA has also been studied in aqueous buffer. The results are given schematically in Table 4.

Tables 5 and 6 summarize the data of the logarithmic analysis of the first DNPNA wave at various pH with and without added EtOH. Table 5 also shows the dependence of $E_{\frac{1}{2},1}$ on the drop time in the pH range in which $i_{1,1}$ is constant. $E_{\frac{1}{2},1}$, at least up to pH 4, is a linear function of the pH:

$$E_{\frac{1}{2}} = (-0.592 \pm 0.006) - (0.132 \pm 0.002)\,\text{pH} \quad \text{for} \quad h_{Hg} = 76\ \text{cm},$$

which is valid for solutions in EtOH. In an aqueous medium the function is also linear, but the slope is $dE_{\frac{1}{2}}/d\text{pH} = -0.101 \pm 0.002$ V/pH. Owing to the irreversibility of the process, it is possible to write:

$$dE_{\frac{1}{2}}/d\text{pH} = 0.059\, m/\alpha n_a$$

where n_a is the number of electrons involved in the slow stage of the process, α is the transfer coefficient, and m is the corresponding number of protons involved. The values of αn_a obtained under various pH, concentration and temperature conditions,

TABLE 4

LOGARITHMIC ANALYSIS OF THE FIRST REDUCTION WAVE OF DNPNA

DNPNA 1×10^{-3} M in B.R. buffer pH 1.85, without EtOH, at various temperatures: $h_{Hg} = 76$ cm

$t/°C$	$i/\mu A$	$-E_{\frac{1}{2}}/V(SCE)$	$-b/V$
5	11.7	0.807	0.104
10	12.8	0.810	0.103
15	14.1	0.811	0.106
20	15.4	0.816	0.107
25	17.2	0.819	0.107
30	18.0	0.821	0.112
35	19.2	0.824	0.106
39,5	20.8	0.829	0.104
44	22.1	0.831	0.105

Temp. coefficient of the limiting current = 1.74%/°C
Temp. coefficient of $E_{\frac{1}{2}} = -0.64$ mV/°C
The data of Tables 4 and 6 were obtained with a different capillary ($t = 4.36$ s; $m = 8.29$ mg s^{-1} at -0.9 V/SCE)
Diffusion current constant (at $t = 25°C$) = 8.7.

TABLE 5

LOGARITHMIC ANALYSIS OF THE FIRST WAVE OF DNPNA

DNPNA at a concentration of 1×10^{-3} M at various pH values; $t = 25°C$; B.R. buffer + 20% EtOH; b = slope of the linear function $E = E_{\frac{1}{2}} - b \log[i/(i_l - i)]$; B = slope of the linear function $E_{\frac{1}{2}} = f(\log t_d)$

pH	h_{Hg}/cm	b/V	$-E_{\frac{1}{2}}/V(SCE)$	$log(t_d/s)$	B/V
2.0	76	0.092	0.858	0.466	0.060
	66	0.093	0.856	0.530	
	56	0.091	0.851	0.599	
2.55	76	0.096	0.924	0.461	0.073
	66	0.098	0.926	0.525	
	56	0.097	0.914	0.596	
3.00	76	0.099	0.988	0.459	0.078
	66	0.101	0.982	0.523	
	56	0.101	0.977	0.591	
3.30	76	0.105	1.036	0.456	—
	66	0.109	1.026	0.519	
3.92	76	0.106	1.109	0.456	0.078
	66	0.112	1.104	0.514	
	56	0.119	1.098	0.577	

are all in the range between 0.47 and 0.60. Considering $n_a = 1$, a number m of protons at least equal to the electrons involved in the rate-controlling step is obtained.

DISCUSSION

From the reported data, the hypothesis of a protonation equilibrium:

TABLE 6

LOGARITHMIC ANALYSIS OF THE FIRST REDUCTION WAVE OF DNPNA
DNPNA at a concentration of 1×10^{-3} M in B.R. buffer without EtOH at various pH values; $t = 25°C$; $h_{Hg} = 76$ cm

pH	$i/\mu A$	$-E_{\frac{1}{2}\,extr.}/V(SCE)$	$-b/V$
1.85	17.20	0.819	0.108
2.46	17.16	0.895	0.114
2.69	17.20	0.936	0.116
2.86	17.68	0.954	0.119
3.37	16.80	1.023	0.104
4.19	17.68	1.095	0.087
4.53	17.04	1.116	0.082
5.46	16.20	1.135	0.106
5.90	14.52	1.175	0.120

$dE_{\frac{1}{2}}/dpH$ (range 1.8–4) $= -0.101$ V.
N.B. The values of b relate to the central section of the function $E = f[\log i/(i_l - i)]$.

$$B + H^+ \underset{k_d}{\overset{k_r}{\rightleftharpoons}} BH^+ \tag{1}$$

(where BH^+ is the conjugate acid of the base B = DNPNA) prior to the electrochemical step, seems to be supported. BH^+ is reduced more easily than B, and an increase in the hydrogen ion concentration therefore displaces $E_{\frac{1}{2},1}$ towards more positive potentials. B is reduced without direct intervention of protons, as shown (Fig. 1, IIB) by $E_{\frac{1}{2},2}$, pH-independent. Over the whole range of potentials in which the first wave appears, chemical reaction (1) precedes the irreversible charge-transfer reactions:

$$BH^+ + n_a e \xrightarrow[\text{slow}]{k_f} BH \tag{2}$$

$$BH + (n - n_a)e + (m-1)H^+ \xrightarrow[\text{fast}]{} \text{products} \tag{3}$$

For the second wave it seems reasonable to write the overall process as

$$2B + 4e + 3H_2O \rightarrow 2\,\begin{matrix} R \\ R \end{matrix}\!\!>\!N\text{–}H + N_2O + 4OH^- \tag{4}$$

which is also irreversible.

The equation for kinetically limited currents according to Brdička and Wiesner[19–21] or rigorously according to Koutecky[22] is:

$$i_{k,BH^+} = i_{d,B} \cdot \frac{0.886\, M(K_f k_r [H^+]^2 t_d)^{\frac{1}{2}}}{1 + 0.886\, M(K_f k_r [H^+]^2 t_d)^{\frac{1}{2}}} \tag{5}$$

where i_{k,BH^+} = kinetic current of BH^+ (μA); $i_{d,B}$ = limiting diffusion current of B under the same conditions (μA); $M = (D_{BH^+}/D_B)^{\frac{1}{2}}$; $K_f = [BH^+]/[B][H^+]$ (l mol^{-1}) the formal equilibrium constant of reaction (1); k_r = formal rate constant for the formation of BH^+ (l mol^{-1} s^{-1}); t_d = drop time of the capillary (s). Putting $D_{BH^+} = D_B$ and $0.886\ (K_f k_r [H^+]^2 t_d)^{\frac{1}{2}} = \lambda$ (dimensionless parameter) eqn. (5) can be written as follows:

$$i_{k,BH^+} = i_{d,B} \cdot \lambda/(1+\lambda) \quad (6)$$

For i_k and i_d to be distinguishable, $\lambda/(1+\lambda)$ must be at least less than 0.9. Particularly when $\lambda < 0.1$, *i.e.* when the limiting current of the process reduces to at least $\frac{1}{10}$ of its maximum value in acid medium, $\lambda/1+\lambda \cong \lambda$ and the limiting current is totally kinetic as shown by height experiments.

Under such conditions,

$$i_{k,BH^+} = i_{d,B} \cdot 0.886(K_f k_r [H^+]^2 t_d)^{\frac{1}{2}} \quad (7)$$

Using experimental data for $i_{l,1}$ that satisfy these conditions and substituting in eqn. (7) the experimental values of K_f, $[H^+]$, t_d, and $i_{d,B}$ (18.1 μA), it is possible to estimate k_r, the rate constant of the preceding protonation reaction.

The experimental value $K_f = 0.14$ obtained by the u.v. spectra of DNPNA in solutions of sulphuric acid containing 20% of EtOH, agrees substantially with the data given by Layne *et al.*[23] for other N-nitrosoamines. It is emphasized in this respect that an appreciable displacement of the u.v. absorption maximum towards smaller wavelengths is shown only for high concentrations of the acid ($> 2\ M$), which demonstrates the difficulty of the protonation of B in solution. The mean value of k_r $(8.7 \pm 1.2) \times 10^{13}$ l mol^{-1} s^{-1} evaluated from experiments under different pH or t_d conditions seems to be paradoxial. Values of this order of magnitude have been found by other authors for other compounds:

N-Nitrosopyrrolidine	$k_r = 5 \times 10^{14}$ l mol^{-1} s^{-1}	(ref. 11)
Isonicotine	$k_r = 0.13 \times 10^{13}$ l mol^{-1} s^{-1}	(ref. 24)
Hydroxylamine	$k_r = 1.9 \times 10^{13}$ l mol^{-1} s^{-1}	(ref. 25)
Azobenzene-*p*-monocarboxylic acid	$k_r = 5.15 \times 10^{13}$ l mol^{-1} s^{-1}.	(ref. 26)

However, it has been known for some time[27,28] that the rates of fast recombination reactions in solution such as, for example, the transfer of H^+ to a base, reach an upper value limited by the diffusion rate of the H^+ towards the base (Debye limit $\cong 10^{11}$ l mol^{-1} s^{-1}). In fact, limiting values of rate constants for proton transfer in recombination processes of the order of 10^{10}–10^{11} l mol^{-1} s^{-1} have been found:

$H^+ + CH_3COO^- \rightarrow CH_3COOH$	$k_r =$ values between 2.6 and 9×10^{10} l mol^{-1} s^{-1} by various techniques[29]; polarographically 4×10^{10};
$H^+ + H_2PO_4^{2-} \rightarrow H_3PO_4$	$k_r = 9 \times 10^{10}$ l mol^{-1} s^{-1} polarographically[30];
$H^+ + OH^- \rightarrow H_2O$	$k_r = 1.4 \times 10^{11}$ l mol^{-1} s^{-1} from relaxation measurements[31].

On this basis it is legitimate to consider that the high value of k_r obtained must be attributed to the inadequacy of Koutecký's model in our case. In fact, no doubt exists concerning the value of K_f used in eqn. (7) inasmuch as the difficulty of the protonation of the aliphatic N-nitrosoamines, which add a single proton to the oxygen at low temperatures and in highly concentrated acids, has also been shown by means of n.m.r.[32]. The only advantage offered by eqn. (7), in the logarithmic form:

$$\log(i_k/i) = \text{const.} + x \log [H^+] \quad (8)$$

is that of showing the reaction order of the kinetic step with respect to the proton. From the experimental data a function is obtained which, in the pH range where the process is kinetically controlled, assumes a linear form with a unit slope, in agreement with eqn. (1) (Fig. 3).

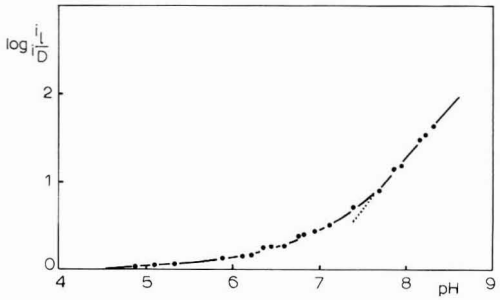

Fig. 3. $\log i_{l,1}/i_D$ *vs.* pH of the first wave of 1×10^{-3} *M* DNPNA in B.R. + 20% EtOH; $h_{Hg} = 76$ cm; $t = 25°C$.

Various hypotheses have been put forward[33] to justify polarographic values of k_r higher than the Debye limit, such as general acid catalysis of reaction (1), or, in the case of reaction layers of a molecular order of size, a greater supply of protons from the dissociation of the acids of the buffer and variations in K_f under the action of the electric field. When the reaction takes place in such thin layers, it assumes a more or less heterogeneous nature and Fick's diffusion laws are no longer applicable. This is equivalent to assuming, in the present case, that the protonation reaction preceding the charge transfer has a superficial nature, or that it takes place (or largely) on the surface of the electrode with the participation of the adsorbed depolarizer in its inactive form.

The problem of the "surface" kinetic current has been treated previously by Mairanovski[34,35], on the assumption of adsorption of the depolarizer. The surface concentration of the adsorbate may be greater by orders of magnitude than its concentration in the bulk of the solution, even in the most unfavourable case of sparingly adsorbable substances.

If adsorption is neglected and equations valid for "bulk" kinetic waves are used, unacceptably high values of k_r are obtained. Besides the concentration effect, the rate of the "surface" reaction may be influenced by an increase in the reactivity of the adsorbed molecules under the polarizing effect of the electric field[36,37].

The increase in the rate of the preceding protonation reaction, due to the factors mentioned above, causes the polarographic wave of the protonated species (active species of the first wave) to be observed experimentally even in a pH range in which it should not appear. Consequently, there is a subsequent increase in the apparent value of the polarographic dissociation constant of the protonated species (pK_a^*) in comparison with the real dissociation constant (pK_a). Surface kinetic currents can therefore appear even at pH values higher by 7–8 units than the actual pK_a value of the electroactive species as observed by Mairanovski *et al.*[38] in the case of pyridine N-oxide ($pK_a^* = 7.5$; $pK_a = 0.8$; $\Delta pK_a = 6.7$). The latter value is too high in relation to the model of Brdička and Koutecký[20], which is valid for "bulk" kinetic waves and

according to which ΔpK_a expressed by means of the relation

$$\log k_r[H^+] = pK_a^* - pK_a + 0.105 - \log t_d \quad (9)$$

cannot exceed 4–5 units. In the present case, $pK_a^* = 6.55$ (Fig. 1); $pK_a = -0.85$; $\Delta pK = 7.4$.

In fact drop time curves indicate that DNPNA is adsorbed over the potential range 0 to -1.5 V (SCE). Otherwise detailed analysis of all the experimental data supports qualitatively, for the present, the hypothesis of the surface nature of the protonation kinetics. Furthermore the adsorption of the inactive depolarizer displaces $E_{\frac{1}{2},1}$ towards more positive values, as shown by a comparison of measurements taken in the presence and absence of EtOH. The latter is in fact simultaneously adsorbed on the electrode and interferes with adsorption of the base, which is therefore reduced at more negative potentials (Tables 4 and 6). It can then be observed that the slope of the linear functions $E_{\frac{1}{2},1} = f(\log t_d)$ in the pH range in which $i_{l,1} \cong i_d = \text{const.}$ is clearly greater than half the slope of the corresponding semilogarithmic plots, as could be predicted for a simple irreversible charge transfer (Table 5).

Moreover, in the absence of EtOH, and for $i_{l,1} \cong i_{d,B} = \text{const.}$, $dE_{\frac{1}{2}}/dpH = -0.101$ V is always smaller than the value of b of the semilogarithmic graphs (Table 6), between -0.108 V and -0.119 V, in contrast with the prediction for a case of preceding protonation in the bulk of the solution, in which the slope b of the function $E_{\frac{1}{2}}$ *vs.* pH should always be equal to the slope b of the semilogarithmic plots. However, the observed behaviour satisfies the characteristics of quasi-diffusive surface waves for which, as a rule, $dE_{\frac{1}{2}}/dpH$ is always smaller than b of the semilogarithmic graphs, with a difference that tends to increase as $E_{\frac{1}{2}}$ is displaced from the potential of maximum adsorption, as for example by increasing pH. In the presence of EtOH this correlation does not seem to be maintained, even though (Table 5) the slope of the semilogarithmic curves increases progressively with a rise in pH. The high value of $dE_{\frac{1}{2}}/dpH$, in this case -0.130 V per pH unit, is obviously connected with the influence of the organic solvent.

In all cases, complication of the reduction process is shown by the shape of the semilogarithmic curves which often have an irregular shape with the appearance of breaks, which are always more frequent as the pH is increased.

Measurements as a function of temperature are also in favour of the hypothesis of surface protonation of adsorbed DNPNA molecules. An increase in t decreases the degree of adsorption of the inactive species and therefore the rate v_k of the surface protonation reaction. This decrease may be compensated to a greater or smaller degree by an increase in the specific rate constant k_r, at least in a certain temperature range.

In the pH range in which $i_{l,1} \cong i_{d,B} = \text{const.}$, v_k is always greater than the diffusion rate v_d, for which the temperature coefficient of $i_{l,1}$ is of the order of magnitude required by diffusion (Table 1). Under these conditions, and in the presence of EtOH, $E_{\frac{1}{2},1}$ is little affected by t, although there is a certain tendency for its displacement towards more negative values. However this displacement is observed unequivocally if one considers the depolarization potentials (Table 1). At the same time, there is an increase in the values of b of the semilogarithmic plots which can be justified if the decrease in adsorption with temperature is considered.

The corresponding measurements in the absence of EtOH (Table 4) show more

clearly the negative coefficient of $E_{\frac{1}{2}}$, the increase in b of the semilogarithmic graphs, and the extension of the corresponding linear section with an increase in t.

For pH values at which $i_{l,1}$ ($\ll i_d$) is largely under kinetic control, an increase in temperature does not involve a high thermal coefficient of $i_{l,1}$ as could be predicted for an ordinary kinetic process. In fact, at pH 6.93 (Table 2) values between 1.7 and 2 %/°C are obtained. Nevertheless, from an examination of Table 2 the values obtained at various heights of the Hg reservoir can be justified if they are considered in the following way. At low temperatures adsorption is favoured; the surface concentration of the inactive species increases and should therefore increase the rate v_k of the kinetic step. Nevertheless, the value of k_r for this latter process has undergone a more drastic decrease, which largely compensates the increase connected with the greater surface concentration; finally, if v_k becomes smaller than the diffusion rate v_d of DNPNA, $i_{l,1}$ is independent of the pressure of Hg. At higher temperatures the decrease in the adsorption is largely compensated by the increase in k_r; consequently, v_k may became greater than v_d and $i_{l,1}$ must take a course that tends to pass progressively under diffusive control. The values of b of the corresponding semilogarithmic graphs are the highest and are practically constant (Table 2). The value of $dE_{\frac{1}{2}}/dt$ is negative and fairly high (Table 3).

The role of the electrode potential E is, however, fundamental, inasmuch as along a given curve different adsorption conditions may exist at different potentials. A displacement of E towards more cathodic values brings about a decrease in the adsorption and therefore in the rate of the kinetic stage, while the rate of electron transfer v_e increases correspondingly. For sufficiently negative values of E, the increase in v_e no longer succeeds in compensating the decrease in v_k, so that there is a decrease in the limiting current with increasing potential $-E$. This has been clearly observed in the case of other members of the homologous series (diisobutyl derivative, unpublished work). The surface nature of the first wave of DNPNA therefore seems adequately confirmed, so that the following scheme of the corresponding electroreduction process can be proposed

(a) $B \xrightarrow{\text{diff.}} B_s$

(b) $B_s \rightleftarrows B_{s,ads}$

(c) $B_{s,ads} + H^+ \underset{K_d}{\overset{k_r}{\rightleftarrows}} BH^+_{ads}$

(d) $BH^+_{ads} + n_a e \xrightarrow[\text{slow}]{k_f} BH_{ads}$

(e) $BH + (n-n_a)e + (m-1)H^+ \rightarrow$ products .

The value of k_r of the surface protonation reaction (c) can, in our opinion be estimated only when quantitative data on the adsorption are available.

A more accurate analysis of the second wave of DNPNA over its whole range of existence is not possible, since it is frequently superimposed on the discharge of the support. Consequently, for the moment the scheme given above remain valid. Further work is now programmed for other terms of this class of compounds.

SUMMARY

The polarographic behaviour of di-n-propyl-N-nitrosoamine (DNPNA) has been investigated in buffered solutions over a range of pH, temperature, drop time, and with and without added EtOH.

The reduction mechanism is complex and depends on pH. At higher acidic, neutral or weakly alkaline pH values, the first irreversible reduction wave of DNPNA, related to its protonated form, is limited by the rate of the protonation reaction, while at lower pH values it is diffusion controlled.

The rate constant of the preceding protonation reaction has been calculated according to Koutecky. The value obtained, as well as all the experimental results, indicate the surface character of the kinetically limited process.

REFERENCES

1 A. A. Smales and H. H. Wilson, *J. Soc. Chem. Ind. London*, 67 (1948) 210.
2 F. L. English, *Anal. Chem.*, 23 (1951) 344.
3 M. Leclercq, *Mem. Poudres*, 35 (1953) 365.
4 E. A. M. F. Dahamen, D. Vader and J. D. Van Der Haase, *Z. Anal. Chem.*, 186 (1962) 161.
5 O. G. Devik, *Acta Chem. Scand.*, 21 (1967) 2302.
6 R. B. Martin and M. O. Tashdijan, *J. Phys. Chem.*, 60 (1956) 1028.
7 R. N. Haszeldine and J. Jander, *J. Chem. Soc.*, (1954) 691.
8 H. Lund, *Acta Chem. Scand.*, 11 (1957) 990.
9 L. Holleck and R. Schindler, *Z. Elektrochem.*, 62 (1958) 492.
10 E. Laviron and P. Fournari, *Bull. Soc. Chim. France*, (1966) 518.
11 R. Zharadnik, E. Svatek and M. Chvapil, *Chem. Listy*, 51 (1957) 2232.
12 D. M. Lemal, F. Menger and E. Coats, *J. Am. Chem. Soc.*, 86 (1964) 2395.
13 P. Tarte, *Bull. Soc. Chim. Belges.*, 63 (1954) 525.
14 C. Bighi, G. Gilli and F. Pulidori, *Ann. Univ. Ferrara Sez. 5*, Vol. II, 18 and 19 (1968).
15 H. Burghardt, H. Jager and M. Von Stackelberg, *J. Electroanal. Chem.*, 17 (1968) 191.
16 S. D. Christian and P. Klaeboe, *Acta Chem. Scand.*, 21 (1967) 2293.
17 H. McKennis and A. S. Yard, *Anal. Chem.*, 26 (1954) 1960.
18 P. Lanza, A. Del Marco, A. F. McKay and G. Semerano, *Contr. Teor. Sper. Pol. Vol. III, Suppl. Ric. Sci.* (1956) 116.
19 R. Brdička and K. Wiesner, *Collection Czech. Chem. Commun.*, 12 (1947) 39, 138.
20 R. Brdička and J. Koutecký, *Collection Czech. Chem. Commun.*, 12 (1947) 337.
21 K. Wiesner, *Anal. Chem.*, 27 (1955) 1712.
22 J. Koutecký, *Chem. Listy*, 47 (1953) 323; *Collection Czech. Chem. Commun.*, 18 (1953) 597.
23 W. S. Layne, H. H. Jaffé and H. Zimmer, *J. Am. Chem. Soc.*, 85 (1963) 1816.
24 J. Volke and V. Volkova, *Collection Czech. Chem. Commun.*, 20 (1955) 1332.
25 Z. Vodrazka, *Chem. Listy*, 45 (1951) 293.
26 P. Ruetschi and G. Trumpler, *Helv. Chim. Acta*, 35 (1953) 1947.
27 M. V. Smoluchowski, *Z. Physik. Chem.*, 92 (1917) 129; L. Onsager, *J. Chem. Phys.*, 2 (1934) 599.
28 P. Debye, *Trans. Electrochem. Soc.*, 82 (1942) 265.
29 A. Bewick, N. Fleischmann and J. N. Hiddleston, *Polarography 1964*, Vol. 1, McMillan, London, 1966, p. 63.
30 H. W. Nurnberg, G. Van Riesenbeck and M. Von Stackelberg, *Collection Czech. Chem. Commun.*, 26 (1961) 126.
31 N. Eigen and L. De Maeyer, *Z. Elektrochem.*, 59 (1955) 986.
32 S. J. Kuhn and J. S. McIntyre, *Can. J. Chem.*, 44 (1966) 105.
33 H. Strehlow, *Z. Elektrochem.*, 64 (1960) 45.
34 S. G. Mairanowski, *Electrochim. Acta*, 9 (1964) 803.

35 S. G. MAIRANOWSKI, *Catalytic and Kinetic Waves in Polarography*, Plenum Press, New York, 1968, p. 129.
36 B. L. TIMAN, *Dokl. Akad. Nauk SSSR*, 112 (1957); *Zh. Fiz. Khim.*, 31 (1957) 2143; 33 (1959) 1189.
37 A. VINCENZ-CHODKOWSKA AND Z. R. GRABOWSKI, *Electrochim. Acta*, 9 (1964) 789.
38 S. G. MAIRANOWSKI, N. V. BARASHKOVA AND F. D. ALESHEV, *Zh. Fiz. Khim.*, 36 (1962) 562.

ELECTROANALYTICAL CHEMISTRY AND INTERFACIAL ELECTROCHEMISTRY
Elsevier Sequoia S.A., Lausanne – Printed in The Netherlands

AN ELECTRONIC INSTRUMENT FOR CYCLIC CHRONOPOTENTIOMETRY

T. RABUZIN, G. SMILJANIĆ AND F. JOVIĆ
Department of Electronics, Institute "Rudjer Bošković", Zagreb (Yugoslavia)
(Received April 3rd, 1970)

INTRODUCTION

Cyclic chronopotentiometry (c.c.p.) is a method of electrolysis with a constant current which is successively reversed each time the potential of the working electrode reaches certain predetermined upper and lower levels. The method has been devised by Herman and Bard[1], who also described the first, simple electron-tube commutator. Later, Herman and Bard[2] described a new system for cyclic chronopotentiometry based on Philbrick tube type operational amplifiers employing electronic switching. Both Sturrock[3] and Rabuzin and Pravdić[4] applied mechanical switching, the result of which were instruments capable, more or less, of semiquantitative work. The development of the theory of consecutive electrochemical–chemical reaction mechanisms by Bard and Herman[5,6], and recently also by Vuković and Pravdić[7], necessitated fast and precise instrumentation.

A unit of this type has been devised and is presented here.

1. THE ELECTRONIC SYSTEM FOR CYCLIC CHRONOPOTENTIOMETRY

The basic concept of the system is similar to the one previously described by Rabuzin and Pravdić[4]. The system presented here is more versatile, all solid state and it has no mechanical switching elements in the commutator. It has also facilities for transition time measurements by pulse counting and storage.

The schematic diagram of the system is shown in Fig. 1.1. The system operates as follows: First the binaries Bi_1 and Bi_2 are reset by means of switch S_3, so that they are in the state "0". The output potential of gate G_1 is $+10$ V when both its inputs are in the state "1", and it is $\emptyset$ V if any input is in the state "0". The gate G_2 has the output potential -10 V when its inputs are in the state "1" and it has zero potential when one of them is in the state "0". So, when the binaries Bi_1 and Bi_2 are reset, the outputs of gates G_1 and G_2 are $\emptyset$ V. Therefore, the output of the amplifier A_1 is also $\emptyset$ V, and no current flows from its output into the electrochemical cell, which is in the feedback loop of the amplifier A_2. In this state of the binary Bi_1, the potentiostat A_3 is connected with the cell through the electronic switches ES_1 and ES_2. The starting value of the potential between the working (W) and reference (R) electrodes of the cell can be adjusted by means of the potentiometer P_3.

After adjustment of the starting potential, the measuring process can be started by means of switch S_5, which sets the binary Bi_1 in state "1". In this state of the

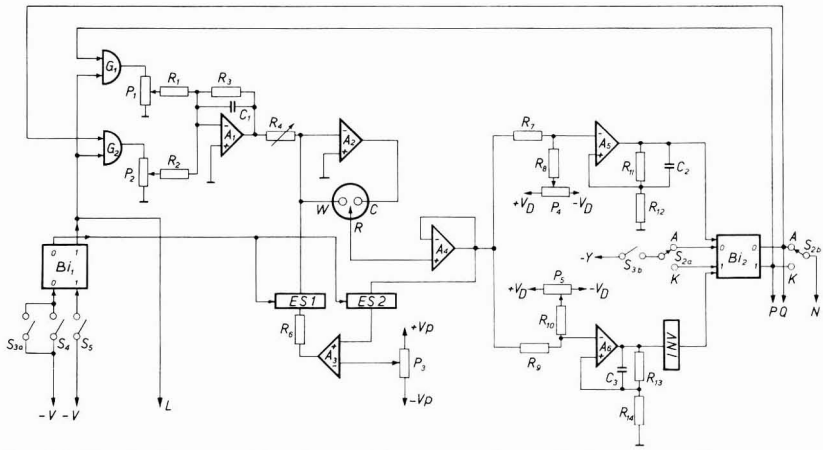

Fig. 1.1. Circuit diagram of the electronic instrument for cyclic chronopotentiometry.

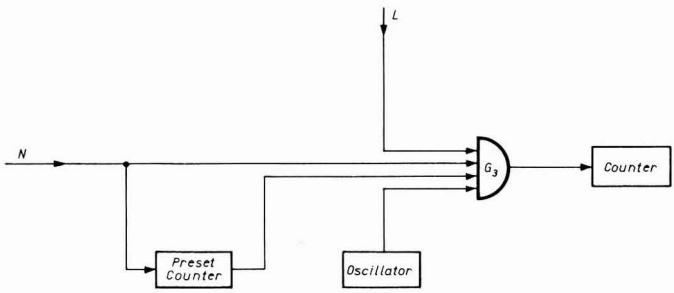

Fig. 1.2. The arrangement for time measurements in cyclic chronopotentiometry.

binary Bi_1, the electronic switches ES_1 and ES_2 are open and the potentiostat A_3 is disconnected from the cell in a very short time (0.1 μs). If switch S_2 is in the position "A", the output of gate G_1 has the potential of $\emptyset$ V, while the output potential of gate G_2 is -10 V, and the measurement is started with the anodic process. The magnitude of the current into the cell can be adjusted by means of the potentiometer P_2 and variable resistor R_4. In this case the potential between the reference and working electrodes is negative going and when it reaches the preset value (the transition potential) determined by the potentiometer P_5, the discriminator A_6 switches, giving a positive voltage step on its output. This step is by means of the inverter INV inverted to a negative one, which triggers the binary Bi_2, and it switches into the other stable state. The switching cycle is correspondingly repeated.

The process of cyclic chronopotentiometry can be stopped by means of switch S_4, which sets the binary Bi_1 into the state "0" again, setting the output of gates G_1 and G_2 in the state "0".

The transition time measurements can be made in several ways. In this system two arrangements are provided.

The arrangement for time measurements is shown in Fig. 1.2. It operates in the following manner: The pulses from the oscillator are applied to the input of the counter through gate G_3, which is controlled by the binary Bi_1, binary Bi_2 and by the preset

counter. During the measurement the preset counter is set sequentially to 1,2,3,...etc. counts and so the counter registers the duration of 1,2,3,...etc. transition periods. Which transition periods—cathodic or anodic—will be measured, depends on the position of switch S_{2b}.

An alternative arrangement can be realized using a multichannel time interval measuring system. In Fig. 1.3. the required additional circuitry is shown. When the

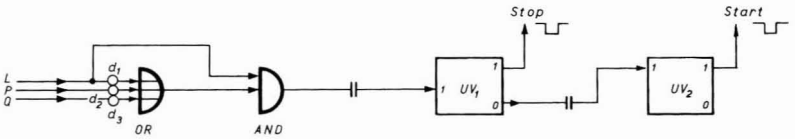

Fig. 1.3. The additional circuit for time measurements with the time interval measuring system.

measurement process is started by switch S_5, the binary Bi_1 gives a signal to the input of OR gate, through the differentiator d_1, which gives a signal to the input of the AND gate. The AND gate is controlled also by the binary Bi_1, so the signals which come to the P and Q input of the OR gate from the binary Bi_2 through the differentiators d_2 and d_3 can pass through the AND gate and trigger the univibrator UV_1 only during the process of measurement. The first signal coming from the binary Bi_1 triggers the univibrator UV_1, which produces a short pulse. The first pulse from UV_1 serves to reset the multichannel time interval measuring system ("stop" pulse). A short time later (about 15 μs), when the univibrator UV_1 returns into its stable state, it triggers the univibrator UV_2. The output pulse from the univibrator UV_2 opens the first channel of the device for the transition time measurements ("start" pulse). The pulses from the oscillator are counted now until the "stop" pulse, which is generated by the univibrator UV_1 when the first transition time (anodic or cathodic) is over and then are stored in the first channel of the memory. The second pulse, coming from the univibrator UV_2, opens the second channel of the device and the timing pulses are now counted and stored later on in the second channel of the memory, etc.

2. THE TIME INTERVAL MEASURING SYSTEM

Transition time measurements performed in the manner as shown in Fig. 1.2. are tedious and time consuming. Moreover the results obtained from several measurements are not as good as the results obtained from a single one. So, an attempt was made to measure 20 successive time intervals and to store the results in a 20-channel core memory. The principle of measurements was explained above (description of Fig. 1.3). Ten anodic and ten cathodic transition times can be measured in one measurement cycle using a 20-word memory. Twenty channels were chosen since this gives a satisfactory amount of information. After a measurement cycle, the results can be read out visually in a binary code, or transmitted to an external digital unit.

The problem consists in measuring the time intervals between the "start" and "stop" pulses shown in Fig. 1.3. When a measurement cycle is started, a "stop" pulse appears first. The time relationship is shown in Fig. 2.1. A time interval of 15 μs after every "stop" pulse is reserved for storing the data obtained into the appropriate memory channel. Thus each measured time interval is shorter by approximately

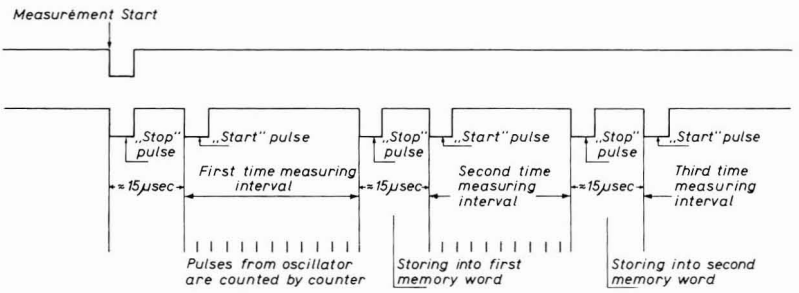

Fig. 2.1. Time relationship of the time interval measurement.

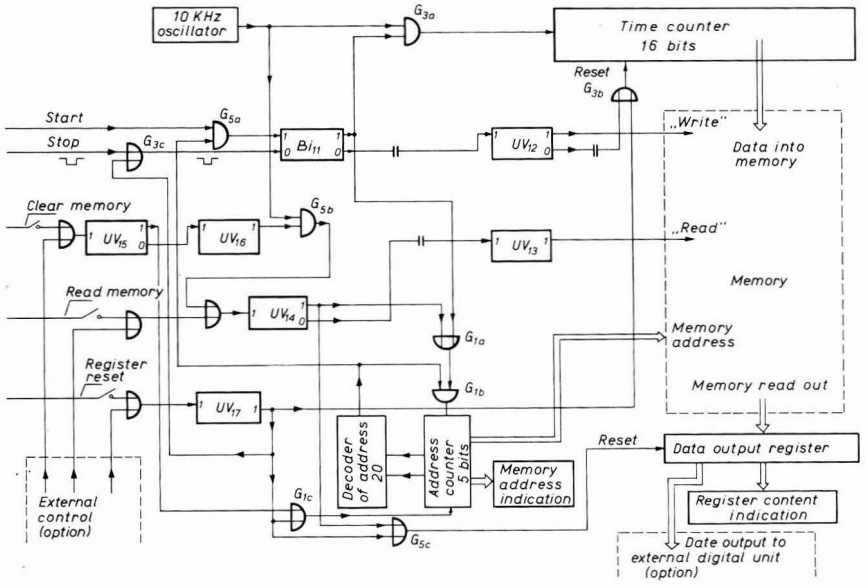

Fig. 2.2. Logic Diagram of the time interval measuring system.

15 μs than the real anodic or cathodic transition time. The transition times are in fact determined by the leading edges of two successive "stop" pulses. This is not a serious problem because in the application considered the transition time and measured time intervals are much larger than 15 μs.

Time interval measurement is based on a well known principle: pulses from an oscillator of known and stable frequency are counted by a binary counter.

A specific feature of the system presented here is that 20 successive time intervals can be measured. The time between two successive time interval measurements is too small to enable the reading or printing of the information obtained by measurement. So data are first stored in the core memory and then read out when the measurement is over. The logic diagram of the operation is given in Fig. 2.2.

A "start" pulse sets the bistable Bi_{11}, which opens gate G_{3a}. The pulses from the 10 kHz oscillator are counted by the "time counter". A "stop" pulse resets Bi_{11} and gate G_{3a} closes. The measured duration of the time interval is given by the number of

pulses counted multiplied by 100 μs if the 10 kHz oscillator is used. Bistable Bi_{11} after closing gate G_{3a}, also triggers the univibrator UV_{12}, which generates the "write" pulse for the memory, and thus the data from the counter are stored in an appropriate memory location. After storing the data, UV_{12} resets the time counter, which is now ready to measure the next time interval. The time counter, as well as the memory words, has 16 bits. Therefore the maximum time interval which can be measured in the present system is approximately 6.5 s.

Before starting the measurement cycle the whole time measuring system must be reset. This can be done by pressing the button "register reset", clearing the "time counter", "address counter", "data output register" and bistable Bi_{11}. The first "start" pulse sets Bi_{11} which opens gate G_{3a} as described above. Bi_{11} sends also a pulse to the "address counter" through gates G_{1a} and G_{1b}. Therefore the first time interval is stored in the first memory location. The second "start" pulse sends the second pulse to the memory address counter and the measured second time interval is stored in the second location of the core memory, etc. At the end of a measurement cycle, the measured 20 time intervals are stored in 20 successive memory locations. When the address 20 is reached, a decoder closes gate G_{5a}, and the measuring cycle is completed.

To read the data stored in the memory, one must first press the button "register reset", in order to clear the memory address counter. Then, pressing the button "read memory", the univibrator UV_{14} is triggered and the "data output register" is cleared to be able to receive data from the memory. A pulse is also sent through gates G_{1a} and G_{1b} to the address counter, which now gives the address of the first memory word. Then the univibrator UV_{13} is triggered generating the memory "read" pulse. Thus the content of the first memory word is transferred to the "data output register". The content of this register is displayed by neon indicators in a binary code. It can be transferred also to a computer or some other digital system. Pressing the button "read memory" the second time, the second memory word is read out and so on until the 20th memory word is read. The memory address is also indicated by neon indicators in a binary code.

When all data are read out from the memory, the memory is cleared and a new measurement can begin. However, sometimes it might be necessary to clear the memory quickly. This can be done by the "clear memory" button. Pressing the button, the memory address counter is cleared first and then the univibrator UV_{16} opens gate G_{5b}, triggering UV_{14} with the oscillator pulses in the same way as it was triggered by the "read memory" button. UV_{14} is triggered at least 20 times and thus the memory is cleared.

The necessary pulses for register reset, memory read and memory clear can be obtained from an external control as indicated in Fig. 2.2.

The time interval measuring system described above is realised using integrated circuits. To simplify the design, relatively slow memory cores were used. The 20-channel time interval measuring system was described in more detail in another paper[8].

ACKNOWLEDGEMENT

The authors are indebted to Dr. V. Pravdić, who initiated and stimulated this work, and also to Mr. I. Kontušić who constructed and tested all instruments.

SUMMARY

Cyclic chronopotentiometry, a technique of special merit in the study of coupled chemical and electrochemical reaction mechanisms, requires comparatively elaborate electronic instrumentation. A description of an electronic commutator based on solid state operational amplifiers and integrated circuitry is given, featuring short switching times, precise and independent forward and back electrolysis current sources, floating working electrode potential discriminators and a timing oscillator. Information storage (transitions times) is achieved with a time measuring system having a 20-channel memory unit. Successive measurement of 20 time intervals is thus possible. The time measurement system enables the read-out of data in a binary system. Alternatively, data can be transmitted to a computer.

The whole system is used in studying oxidation–reduction mechanisms of complex ions in aqueous solution and is characterized by versatility and precision.

REFERENCES

1 H. B. HERMAN AND A. J. BARD, *Anal. Chem.*, 35 (1963) 1121.
2 H. B. HERMAN AND A. J. BARD, *Anal. Chem.*, 37 (1965) 590.
3 P. E. STURROCK, *J. Electroanal. Chem.*, 8 (1964) 425.
4 T. RABUZIN AND V. PRAVDIĆ, *J. Electroanal. Chem.*, 9 (1965) 435.
5 A. J. BARD AND H. B. HERMAN, *Polarography 1964*, McMillan, London, 1966, pp. 373 ff.
6 H. B. HERMAN AND A. J. BARD, *J. Electrochem. Soc.*, 115 (1968) 1028.
7 M. VUKOVIĆ AND V. PRAVDIĆ, *Croat. Chem. Acta*, 42 (1970) 21.
8 G. SMILJANIĆ AND F. JOVIĆ, *Elektroteknika*, 1970, No. 1.

ELECTROANALYTICAL CHEMISTRY AND INTERFACIAL ELECTROCHEMISTRY
Elsevier Sequoia S.A., Lausanne – Printed in The Netherlands

ELECTRON PHOTOEMISSION AS A NEW METHOD FOR STUDYING THE ELECTRIC DOUBLE LAYER STRUCTURE AND THE KINETICS OF ELECTROCHEMICAL REACTIONS

Z. A. ROTENBERG, V. I. LAKOMOV AND YU. V. PLESKOV
Institute of Electrochemistry, the Academy of Sciences of the USSR, Moscow (U.S.S.R.)

(Received April 6th' 1970)

INTRODUCTION

In our previous communication[1] we considered some regularities in photoemission from metals into electrolyte solutions: the influence of the electrode potential, metal nature and indifferent electrolyte concentration. This paper presents the results of more recent studies both on the photoemission proper (effect of specific adsorption, Section I) and on further transformations of hydrated electrons in the solution (effect of the acceptor concentration on photocurrent and the dependence of photocurrent on potential, Section II), as well as on the transformation of the reaction products of hydrated electrons and acceptors (as exemplified by atomic hydrogen reactions, Section III, and unstable ion-radical NO_3^{2-}, Section IV).

The experimental procedure used was the same as already described[1]. All measurements were carried out on a mercury electrode illuminated with a light beam, wavelength 365 nm. The potentials are referred to a saturated calomel electrode.

I. EFFECT OF SPECIFIC ADSORPTION ON PHOTOEMISSION

Earlier we showed[1] that the "red boundary" (more precisely, the threshold potential φ_0) of the extrinsic photoeffect at the metal–electrolyte solution interface does not depend on the metal nature, on its zero charge potential, in particular, and is unambiguously determined by the incident quantum energy and by the reference electrode potential. φ_0 should remain constant also in the case of surfactant adsorption shifting the zero charge potential if the conditions of the applicability of the threshold approximation[2] are fulfilled. According to this approximation, if its de-Broglie wavelength is greater than the thickness of the region of decay of the surface forces, the emitted electron is not affected by the detailed potential distribution in this region. In this case the emission energetics are affected only by the difference between the initial and final electron states, which is wholly determined by the electrode potential.

For experimental verification of this assumption, we measured[3] the photocurrents in 0.1 *M* KF, KBr and KI solutions, as well as in 0.1 *M* KF solutions in the presence of tetrabutylammonium (TBA) cation and thiourea (TU). All these substances shift significantly the zero charge potential of mercury*. Nitrous oxide was

* In 0.1 *M* KBr and KI solutions the zero charge potentials are more negative than in 0.1 *M* KF by 0.1 and 0.26 V, respectively[4]. TBA shifts the zero charge potential in the positive direction[5] by approximately 0.2 V, TU—in the negative direction, by 0.3 V in 0.1 *M* TU solution[6,7].

used as an electron acceptor ("scavenger") in solution. The threshold potential was found by means of the "$\frac{5}{2}$-law"[2]: by extrapolating[1] the dependence $j^{0.4}$–φ to the current $j=0$.

The experimental results for 0.1 M KF, KBr and KI solutions are given in Fig. 1 (in the Figs. photocurrent values are expressed in arbitrary units). It is clear from the Figure that the threshold potential φ_0 is the same for all solutions, being close to -0.2 V. The difference in φ_0 for the three anions does not exceed the experimental error (± 20 mV) and is much less than the difference of the zero charge potentials.

The effect of the adsorption of TBA cation on the photocurrent is shown in Fig. 2. In the presence of TBA the current diminishes by a factor of approximately two. At potentials from -0.4 to -1.0 V for all TBA concentrations the $j^{0.4}$–φ dependence is practically linear. At higher negative potentials the experimental values deviate from

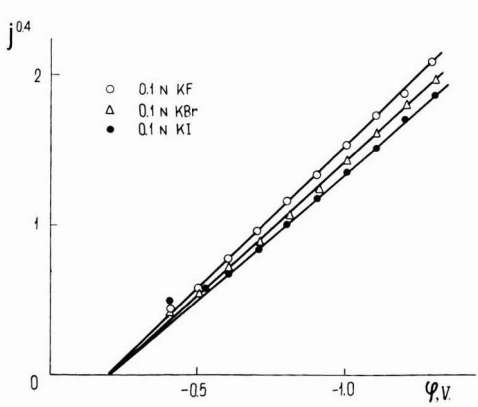

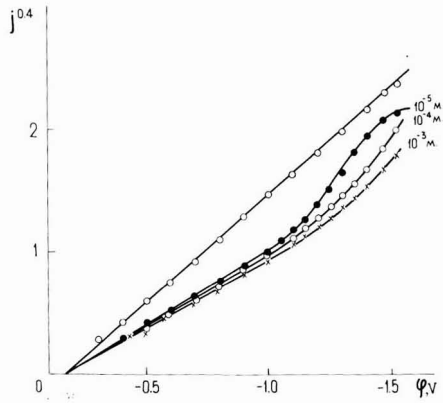

Fig. 1. $j^{0.4}$–φ plots in 0.1 M KF, KBr and KI solns. satd. with N_2O.

Fig. 2. $j^{0.4}$–φ plots in 0.1 M KF soln. (top straight line) and in the same soln. with tetrabutylammonium bromide addition.

the straight line. The potential at which this deviation starts is more negative the higher the TBA concentration in solution. In the region of a linear relationship between $j^{0.4}$ and φ the photocurrent diminishes slightly with increasing TBA concentration, the threshold potential being the same for all concentrations and coinciding with φ_0 in the absence of TBA.

The effect of TBA on the photocurrent value is completely determined by its specific adsorption on the mercury surface*, namely, by the effect of adsorption on the electron density on the metal surface. Secondary bulk reactions involving TBA can be neglected owing to its low concentration in solution. The photocurrent increase at negative potentials can be explained as being due to TBA desorption from the electrode surface.

The results of the experimental study on the effect of TBA on photocurrent are in a qualitative agreement with the literature data on hydrogen overvoltage[11] and the

* In the potential range where the $j^{0.4}$–φ dependence is linear the surface coverage of mercury with TBA cation is as much as 1, unlike Br^- and I^-, for which the surface coverage[8-10] in this range of potentials and concentrations is much less than 1.

differential capacity of the double layer[10].

We also studied the influence of a thiourea (TU) addition on the photoeffect. Introduction of TU into the solution considerably reduces the value of the photocurrent observed (the effect increasing with increase in TU concentration), but has little effect on the nature of the potential dependence of photocurrent and practically does not change the threshold potential φ_0. The effect of TU in reducing the magnitude of photocurrent is probably due to the participation of TU molecules in the competing scavenging of the hydrated electrons[12] (the scavenging rate constants for N_2O and TU are 9×10^9 and 5×10^9 l mol^{-1} s^{-1}, respectively). If the TU^- radicals formed are subsequently oxidized on the electrode, a decrease of photocurrent should be observed.

It can be concluded from the above results that the specific adsorption of ions and neutral molecules does not greatly affect the nature of the photocurrent–potential dependence and the threshold potential of the photoeffect, if the wavelength of emitted electrons is greater than the adsorption layer thickness.

A different picture is to be expected if the above conditions are not fulfilled. Thus, we showed[1] that in dilute electrolyte solutions ($\leqq 10^{-1}$ M) the "$\frac{5}{2}$-law" is not valid due to the increased value of the ψ_1-potential in the diffuse part of the double layer. In this case the dependence of the photocurrent j on the electrode potential φ can be described by an approximate formula

$$j = A[\varphi_0 - (\varphi - \psi_1)]^{\frac{5}{2}}, \tag{1}$$

where A is a constant associated with the nature of the metal and the quantum yield of the photoeffect. As is clear from this formula, the shift of ψ_1 in the negative direction leads to a decrease of photocurrent. In the derivation of formula (1), it is of no importance whether the ψ_1-potential arises merely as the result of dilution of the solution, or is of an "adsorption" origin (*i.e.* due to specific adsorption on the electrode from solution with a low overall electrolyte concentration). For the potential drop in the diffuse part of the double layer to affect significantly the photocurrent, the thickness of this part must be greater than the electron wavelength. For electrons with energy 0.3–1 eV, which are obtained upon illumination of mercury with a beam of light with wavelength 365 nm in the potential range from -0.6 to -1.3 V, the electron wavelength varies within 10–25 Å. Thus, for the condition of the threshold approximation to be violated, the experiments must be carried out in dilute ($\leqq 0.01$ M) electrolyte solutions.

In fact, if we compare the photocurrents in 0.01 M KF and KI solutions, we see[13] that in the region of iodine adsorption, from -0.6 to -1.0 V, the photocurrent in KI is appreciably lower than in KF (at more negative potentials the curves practically merge). This is due to a change in the electric double layer structure. Iodine adsorption involves an increase in the negative value of ψ_1* and, according to formula (1) leads to a photocurrent decrease.

Thus, specific adsorption, if combined with a low overall solution concentration, affects the nature of the dependence of the electron photoemission current on potential.

Another case when the condition of threshold approximation is violated is the adsorption on the electrode of ions and molecules whose size (and hence the thickness

* In the case of specific adsorption ψ_1 is understood to be the potential in the outer Helmholtz plane.

of this adsorption layer) is greater than the electron wavelength. In this case adsorption directly affects photoemission in concentrated (with respect to indifferent electrolyte) solutions as well. We used as adsorbate particles the molecules of cetyl alcohol $CH_3(CH_2)_{14}CH_2OH$, palmitic $CH_3(CH_2)_{14}COOH$ and myristic $CH_3(CH_2)_{12}COOH$ acids, as well as dimethyldidodecylammonium ion. As regards the first three compounds, they are known[14] to form at the mercury/solution interface continuous layers, the thickness of which, *e.g.* for cetyl alcohol, is about 19 Å (*i.e.* is comparable with the wavelength of the emitted electron). Adsorption was carried out by the method of "rubbing" the mercury electrode with a small crystal of organic substance at the potential of maximum adsorption (−0.7 V).

Figure 3 shows the curves for the photocurrent on a "clean" mercury electrode in 0.1 *M* KF solution and on the electrode covered with cetyl alcohol. At potentials from −0.6 to −1.2 V, alcohol adsorption reduces the photocurrent by a factor of some tens. The current rise below or at −1.2 V is evidently due to disintegration of the

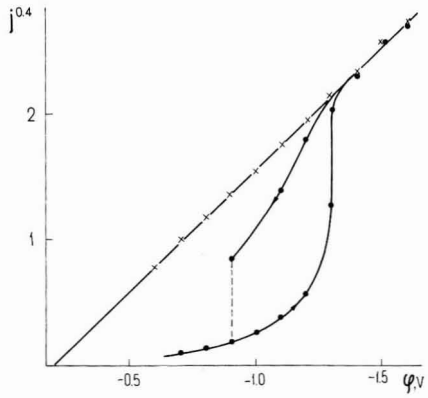

Fig. 3. $j^{0.4}$–φ plots in 0.1 *M* KF soln. for "clean" mercury surface (×) and for mercury covered with a cetyl alcohol film (•). Direction of potential variation is shown by arrows.

organic substance layer at a large negative surface charge. If the electrode potential is again shifted into the region of more positive values, the photocurrent value at the initial moment will be the same as on a "clean" electrode surface. However, in the course of time the alcohol monolayer on the electrode is spontaneously restored (as was clear from the differential capacity and hydrogen overvoltage measurements[14]), and the photocurrent drops again.

The other substances listed above have the same effect, but their influence is not so strong.

The effect of adsorption of "bulky" organic molecules on the electron photoemission can be accounted for by the appearance in this case, as it were, of a new phase between metal and solution. The electron work function in this case is greater than for the metal/water system, and therefore the hydrocarbon interlayer acts as an energy barrier for emitted electrons. Moreover, there are no electron acceptors within the adsorption layer. These two facts lead to a decrease of the photocurrent measured.

II. EFFECT OF THE ELECTRON ACCEPTOR CONCENTRATION ON THE PHOTOCURRENT VALUE AND ON THE CHARACTER OF ITS DEPENDENCE ON POTENTIAL*

The photocurrent in electrochemical systems, arising during electrode illumination, is determined both by the photoemission act proper and by the nature of the interaction of emitted electrons with condensed medium. Under the conditions when all electrons are captured by acceptors the photocurrent observed experimentally coincides with the emission current. If there are few acceptors and part of the electrons return to the electrode, the measured photocurrent is less than the emission current, and the general character of the photocurrent dependence on potential changes. The theoretical and experimental aspects of this problem are treated below.

In accordance with the concepts developed[2,15-17], emitted electrons undergo the following consecutive transformations in the solution: thermalization, solvation and capture of solvated electrons by acceptors. Then the equation for the photocurrent, taking account of these transformations, can be written as

$$j = A \int_0^{\eta} \varepsilon^{\frac{3}{2}} \mathrm{d}\varepsilon \int_0^{\infty} \mathrm{f}(x, \varepsilon)(1 - \mathrm{e}^{-\lambda x})\mathrm{d}x \,, \tag{2}$$

where ε is the energy of emitted electrons, $\eta = \hbar\omega - \hbar\omega_0 - \mathrm{e}\varphi$, $\hbar$ is the Planck constant, ω the light frequency, $\hbar\omega_0$ the electron work function at the potential $\varphi = 0$, $\lambda = (kc_\mathrm{A}/D)^{\frac{1}{2}}$, k the rate constant of the interaction of solvated electrons with acceptors the concentration of which is c_A and D the diffusion coefficient of solvated electrons. The function $\mathrm{f}(x, \varepsilon)$ introduced in eqn. (2) describes the distribution in the direction normal to the electrode surface of solvated electrons formed from emitted electrons with initial energy ε. For $\mathrm{f}(x, \varepsilon)$ the relation $\int_0^{\infty} \mathrm{f}(x, \varepsilon)\mathrm{d}x = 1$ is valid.

On the basis of the "Theorem of the mean", eqn. (2) can be rewritten as follows

$$j = A \int_0^{\eta} \varepsilon^{\frac{3}{2}} (1 - \mathrm{e}^{-\lambda \bar{x}(\varepsilon)}) \mathrm{d}\varepsilon \,, \tag{3}$$

where $\bar{x}(\varepsilon)$ is a certain value of the coordinate x within the variation range of the function $\mathrm{f}(x, \varepsilon)$. It gives the mean-weighted value of a distance at which the electrons with initial energy ε undergo solvation. Since $\bar{x}(\varepsilon)$ is a function of energy, the character of the dependence of photocurrent on η (or potential) should, generally speaking, differ from that for the emission current, which is equal to [2,15]

$$j \sim \int_0^{\eta} \varepsilon^{\frac{3}{2}} \mathrm{d}\varepsilon \sim (\hbar\omega - \hbar\omega_0 - \mathrm{e}\varphi)^{\frac{5}{2}} \tag{4}$$

To characterize qualitatively the general form of the dependence thus obtained, let us consider two limiting cases. At a low acceptor concentration, when for all $\varepsilon \leqq \eta$ the condition $\lambda\bar{x}(\varepsilon) \ll 1$ is valid,

$$j \sim \lambda \int_0^{\eta} \bar{x}(\varepsilon) \varepsilon^{\frac{3}{2}} \mathrm{d}\varepsilon \tag{5}$$

The presence in eqn. (5) of the additional factor $\bar{x}(\varepsilon)$ dependent on energy distinguishes it from the equation for photoemission current. The explicit form of $\bar{x}(\varepsilon)$ can be, in

* This Section is based on the results of a study carried out together with A. M. Brodsky.

principle, estimated from experiment.

On the other hand, if the acceptor concentration is such that for fast electrons the inequality $\lambda\bar{x}(\varepsilon) > 1$ is valid, eqn. (3) can be written approximately as

$$j \sim \int_{\varepsilon_0}^{\eta} \varepsilon^{\frac{3}{2}} \mathrm{d}\varepsilon ,$$

where ε_0 is the energy at which $\lambda\bar{x}(\varepsilon_0) = 1$. After integration we obtain

$$j \sim \{(\hbar\omega - \hbar\omega_0 - \mathrm{e}\varphi)^{\frac{5}{2}} - \varepsilon_0^{\frac{5}{2}}\} . \tag{6}$$

At $\varepsilon_0 < \eta$ from eqn. (6) we have

$$j^{0.4} \simeq \{(\hbar\omega - \hbar\omega_0 - \mathrm{e}\varphi) - 0.4\, \varepsilon_0^{\frac{5}{2}}/\bar{\eta}^{\frac{3}{2}}\} , \tag{7}$$

where $\bar{\eta}$ is the mean value of $\eta = \hbar\omega - \hbar\omega_0 - \mathrm{e}\varphi$ in the region examined.

The effective threshold potential φ_0, determined from experimental data by extrapolation of the linear plots $j^{0.4}$–φ, according to eqn. (7) will shift in the negative direction with respect to the "true" threshold potential* $\hbar\omega - \hbar\omega_0$ by $0.4\, \varepsilon_0^{\frac{5}{2}}/\bar{\eta}^{\frac{3}{2}}$.

Figure 4 shows the dependences of the photocurrent raised to the power 0.4 on potential, for various hydrogen ion concentrations, H_3O^+ used as an acceptor. The total electrolyte concentration (HCl + KCl) was kept constant (1 *M*). As is clear from the Figure, for all $c_{H_3O^+}$ the experimental data fall well enough on straight lines. With decreasing $c_{H_3O^+}$, the threshold potential φ_0 shifts in the negative direction down to $c_{H_3O^+} = 0.01$ *M*, remaining practically constant (-0.25 ± 0.03 V) for $c_{H_3O^+}$ values below this. A similar effect was also observed in neutral solutions when nitrous oxide was used as an electron acceptor.

A shift of the threshold potential occurs also in the case of specific adsorption of TBA cation in *acid* solutions, when the near-the-electrode concentration of hydrogen ions decreases appreciably due to the ψ_1-effect. As was pointed out in Section I, specific adsorption of TBA in *neutral* solutions (acceptor N_2O) practically does not affect φ_0.

Figure 5 shows the dependence of the threshold potential φ_0 on $c_{H_3O^+}{}^{-\frac{1}{2}}$. At $c_{H_3O^+}{}^{-\frac{1}{2}} \to 0$, φ_0 tends to the "true" threshold potential $\hbar\omega - \hbar\omega_0$, the numerical value of which is equal to 0.00 ± 0.04 V. The value thus obtained differs from that given earlier[1] for solutions dilute with respect to acceptors. With the threshold potential value known, it is possible to determine the "true" electron work function for the mercury/water system at the zero charge potential. It will be equal to $\hbar\omega - \mathrm{e}\varphi_0 + \mathrm{e}\varphi_{q=0} = 3.38 - 0.43 = 2.95 \pm 0.1$ eV.

Thus, the "true" work function is lower than that measured in dilute acceptor solutions[1] by approximately 0.3 eV.

As has been pointed out earlier, the shift of φ_0 is due to the change in character of the potential dependence of photocurrent. To calculate the dependence correctly it is necessary to know the explicit form of the function $\bar{x}(\varepsilon)$. In Fig. 4 the dependence of photocurrent on potential is shown for 0.01 *N* H_3O^+ by a dashed line, plotted in the coordinates $j^{\frac{1}{3}}$–φ. In other words, here we assumed that in the range of parameters

* It should be noted that the effective shift of the threshold potential does not reflect the changes in the "true" electron work function for the metal/water system, but results from the change in the character of the potential dependence of photocurrent, the experimental data being treated by the same graphical method (extrapolation of the $j^{0.4}$–φ plots).

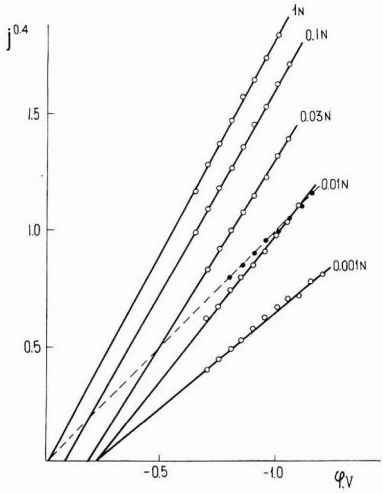

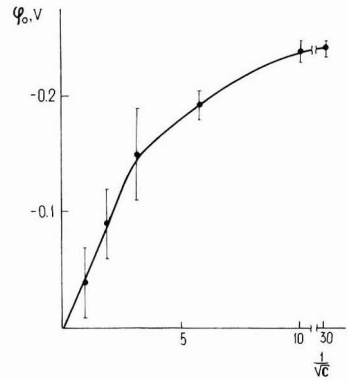

Fig. 4. $j^{0.4}$–φ plots for various hydrogen ion concns. at a constant (1 M) overall concn. of the electrolyte (HCl + KCl). (------) $j^{\frac{1}{2}}$–φ plot.

Fig. 5. Dependence of the threshold potential φ_0 on $c_{H_3O^+}{}^{-\frac{1}{2}}$.

under consideration* $\bar{x}(\varepsilon) = a\sqrt{\varepsilon}$. As is clear from the Figure, in this case the threshold potential practically coincides with the "true" threshold potential. Hence it can be concluded that the distance from the electrode surface at which electrons are preferentially hydrated increases with their energy ε as $\sqrt{\varepsilon}$. The numerical value of the coefficient a, relating $\bar{x}(\varepsilon)$ to $\sqrt{\varepsilon}$, can be readily found from the experimental dependence of photocurrent on the acceptor concentration.

We measured[18] the dependence of photocurrent on the concentration of hydrated electron acceptors (H_3O^+ and NO_3^-) at a fixed potential and constant overall electrolyte concentration. At low acceptor concentrations c_A, the photocurrent is proportional to $\sqrt{c_A}$; with increasing c_A, the photocurrent tends to the limiting value (photoemission current).

In 1 M supporting electrolyte solutions at a potential -1 V the extrapolated section of the "photocurrent–acceptor concentration" curve, where the law $j \sim \sqrt{c_A}$ is valid, intersects with the saturation current near $c_{H_3O^+} \approx 0.1\ N$**. At this concentration $\int_0^\eta \varepsilon^{\frac{1}{2}}\,d\varepsilon = a(0.1\ k/D)^{\frac{1}{2}} \int_0^\eta \varepsilon^2\,d\varepsilon$ (see eqns. (4) and (5)) or $a = 3(D/k)^{\frac{1}{2}}\eta^{-\frac{1}{2}}$. Since η (potential as referred to the threshold potential) was chosen close to 1, $a \approx 3(D/k)^{\frac{1}{2}}$. It should be noted that at $c_{H_3O^+} = 0.01\ M$, $\lambda\bar{x}(\eta) = 0.3$, *i.e.* at lower concentrations the condition $\lambda\bar{x}(\eta) \ll 1$ is fulfilled and the limiting law (5) is valid.

By means of the explicit form of the function $\bar{x}(\varepsilon)$ it is possible to find the dependence of photocurrent on the potential and on the acceptor concentration in a

* Actually, the function $\bar{x}(\varepsilon)$ is probably of a more complex form. It follows from general considerations that it must rise from a certain non-zero value at $\varepsilon \approx 0$ up to energies of the order of some fractions of the energy of electronic excitation of water (*i.e.* ≈ 0.5 eV) when $\bar{x}(\varepsilon)$ should reach an approximately constant value. It is clear from the form of eqn. (7) that the general dependence of photocurrent on potential at $\eta > \varepsilon_0$ is only slightly affected by the concrete form of $\bar{x}(\varepsilon)$.

** In more dilute solutions with respect to the supporting electrolyte the intersection point lies at lower acceptor concentrations.

wide range of arguments. Thus, for example, substituting into formula (3) $\bar{x}(\varepsilon) = g(D/k)^{\frac{1}{2}}\sqrt{\varepsilon}$, after integration we arrive at the equation:

$$j \sim \{\tfrac{1}{5}\eta^{\frac{5}{2}} - (24/g^5 c_A^{\frac{5}{2}}) + [\exp(-gc_A^{\frac{1}{2}}\eta^{\frac{1}{2}})/g^5 c_A^{\frac{5}{2}}] \times (\eta^2 g^4 c_A^2 + 4\eta^{\frac{3}{2}} g^3 c_A^{\frac{3}{2}} + 12\,\eta g^2 c_A + 24\,\eta^{\frac{1}{2}} g c_A^{\frac{1}{2}} + 24)\} \quad (8)$$

The parameter g depends on the supporting electrolyte concentration. As has been mentioned above, in 1 M solutions $g \approx 3$. Figure 6 shows the curves calculated ac-

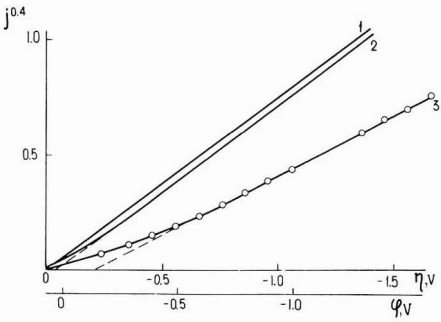

Fig. 6. $j^{0.4}$–φ curves calcd. by means of eqn. (8) for various acceptor concns., $g = 3$. (1) $c_A \to \infty$, (2) $c_A = 1$ M, (3) $c_A = 0.1$ M, (○) experiment (0.1 M KF solution satd. with N_2O).

cording to eqn. (8) and plotted in coordinates $j^{0.4}$–φ for three acceptor concentrations. At a distance from the threshold in these coordinates the $j^{0.4}$–φ dependence is approximately linear, the marked deviation from linearity being observed at more negative φ, the lower the acceptor concentration. The theoretical equation (8) describes the experimental data fairly well for nitrous oxide, shown in the Figure by circles*. The calculated and the experimental curves were superimposed at negative potentials. Since here the deviation of the experimental data from the "$\frac{5}{2}$-law" is observed far ($\gg kT/e$) from the threshold, it cannot be explained by a "thermal tail".

It should be noted that eqn. (8), which contains the explicit dependence of photocurrent on the acceptor concentration, at large λ differs significantly from the equations proposed earlier[16] on the basis of model concepts.

It is clear from Fig. 6 that the threshold potential value determined by extrapolation of the $j^{0.4}$–φ plot depends essentially on the potential range over which extrapolation is performed. The nearer this range is to the threshold, the more positive is the value of φ_0. This can probably account for the anomalous dependence of φ_0 on the quantum energy given in ref. 19.

Thus, the correct value of the electron work function for the metal/solution system can be obtained only at a large acceptor concentration; in solutions dilute

* The concentration of a saturated solution of N_2O in 0.1 M KF (0.025 M) is lower than the concentration $c_A = 0.1$ M, for which curve 3 is plotted. This difference, however, is compensated for by the fact that in 0.1 M KF solution the value of g is somewhat higher than that found experimentally in 1 M KCl solution (see above, $g = 3$), it follows from the measured values of $\bar{x}$. As a result, the apparent threshold is the same in these two solutions, which fact served as a criterion in choosing a solution for comparison of experimental with calculated curves.

with respect to acceptors it is necessary to introduce a correction into the measured threshold value, allowing for the return of electrons to the electrode*.

The experimentally obtained dependence of photocurrent at a fixed potential on the acceptor concentration c_A was made use of to calculate $\bar{x}$—the mean distance from the electrode at which the emitted electrons undergo hydration[18]. Unlike other investigators[16], we did not make any assumptions regarding the explicit form of the function f(x). As shown in ref. 17, if the main change of f(x) occurs at a small enough distance from the electrode, irrespective of the concrete form of f(x), at small c_A the following expression is valid for the photocurrent

$$j = I\bar{x}(kc_A/D)^{\frac{1}{2}} \tag{9}$$

Here $\bar{x}$ is averaged over the energies of emitted electrons, I—the emission current. If k and D are known, it is possible to determine $\bar{x}$. In 1 M indifferent electrolyte solutions $\bar{x} \approx 20$ Å and in 0.01 M solutions $\bar{x}$ increases to 80–100 Å**.

III. INVESTIGATION OF THE KINETICS OF ELECTROCHEMICAL TRANSFORMATION OF ATOMIC HYDROGEN ON A MERCURY ELECTRODE BY THE EXTRINSIC PHOTOEFFECT METHOD

In this section we shall show how it is possible to use photoemission for the study of the kinetics of electrochemical transformation of atomic hydrogen, which is a product of interaction between a hydrated electron and H_3O^+ ion:

$$e_{aq} + H_3O^+ = H + H_2O \tag{A}$$

In a wide potential range (from -0.7 to -1.5 V) the hydrogen atom mainly enters into a reduction reaction

$$H + HS + e = H_2 + S \tag{B}$$

Here S is the proton source; this, in principle, can be H_3O^+ or H_2O. At more positive potentials, along with this reaction, atomic hydrogen ionization is also of importance

$$H + H_2O = H_3O^+ + e \tag{C}$$

leading to a decrease of the experimentally measured cathodic photocurrent which was first observed by Barker *et al.*[16].

Thus, photoemission is a source of atomic hydrogen near the electrode surface (a more convenient one than those used earlier[20]).

Let us write the basic kinetic equations for the reaction. The experimentally measured photocurrent in the electrochemical system is determined by the relation

$$j = I_e + \vec{j} - \overleftarrow{j} \tag{10}$$

where I_e is the emission current minus the current of the return to the electrode of

* In comparative measurements (*i.e.* in the cases when the change in the value of φ_0 is of interest rather than its accurate value) at a constant (even if a low one) acceptor concentration this fact can be ignored (see ref. 1 and Section I of the present paper). The same is true for Section III, except for Fig. 10, which was obtained at a varying acceptor concentration. It proved in that case, however, that if instead of making use of the "$\frac{5}{2}$-law" for extrapolation, we vary somewhat the exponent, the final form of Fig. 10 is almost the same.

** We assumed that k/D depends only slightly on the ionic strength of the solution.

unreacted electrons, $\vec{j}$ the cathodic current of reaction (B) and $\overleftarrow{j}$ the current of atomic hydrogen ionization.

A hydrogen atom can participate in reactions (B) and (C) either being adsorbed on the metal surface, or dissolved in the near-the-electrode solution layer. If the removal of atomic hydrogen proceeds simultaneously by both mechanisms, under steady state conditions the following equations are valid:

$$I_e = (k_0 + \vec{k}_1 + \overleftarrow{k}_1) c_H(0) \tag{11a}$$

$$k_0 c_H(0) = (\vec{k}_2 + \overleftarrow{k}_2)\theta \tag{11b}$$

$$j = I_e + (\vec{k}_1 - \overleftarrow{k}_1) c_H(0) + (\vec{k}_2 - \overleftarrow{k}_2)\theta \tag{11c}$$

Here k_0 is the rate constant* of atomic hydrogen adsorption, $\vec{k}_1$ and $\overleftarrow{k}_1$ the rate constants of cathodic removal and ionization of atomic hydrogen directly from solution, respectively, $\vec{k}_2$ and $\overleftarrow{k}_2$ the respective rate constants for adsorbed hydrogen, $c_H(0)$ the near-the-electrode concentration of hydrogen atoms and θ the surface coverage with adsorbed hydrogen. In the derivation of eqns. (11) we neglected the recombination of hydrogen atoms in the solution and on the electrode surface**. Since reaction (B) can proceed with the simultaneous participation of water molecules and hydrogen ions, the rate constants $\vec{k}_1$ and $\vec{k}_2$ of cathodic removal of atomic hydrogen can be represented as the sum of two terms $\vec{k}_i = \vec{k}_i' + \vec{k}_i'' X$. Here $\vec{k}_i'$ and $\vec{k}_i''$ are the rate constants of atomic hydrogen removal involving water and hydrogen ions, respectively, and X the mole fraction of H_3O^+ (the mole fraction of water at small X is close to unity).

The elimination of θ and $c_H(0)$ from eqns. (11) leads to the following expression for the current

$$j = 2 I_e \left\{ \frac{\vec{k}_1}{k_0 + \vec{k}_1 + \overleftarrow{k}_1} + \frac{\vec{k}_2 k_0}{(k_0 + \vec{k}_1 + \overleftarrow{k}_1)(\vec{k}_2 + \overleftarrow{k}_2)} \right\} \tag{12}$$

In the limiting case, when the oxidation reactions can be neglected ($\overleftarrow{k}_1 = \overleftarrow{k}_2 = 0$), $j = 2 I_e \sim (\varphi_0 - \varphi)^{\frac{5}{2}}$, and the "$\frac{5}{2}$-law" is valid for the photocurrent (see footnote on page 411). The rate constants for electrochemical reactions contained in eqn. (12) in their turn are a function of the electrode potential. Therefore, the dependence of j on φ in the general case is no longer described by the "$\frac{5}{2}$-law", but is of a more complex character. It is rather difficult to verify experimentally the general eqn. (12). To simplify the problem let us consider some particular cases, which are probably realized in experiment.

(*a*) Cathodic and anodic removal of atomic hydrogen occurs without passing through the adsorption stage. For this mechanism $k_0 = 0$ and $j = I_e[2\,\vec{k}_1/(\vec{k}_1 + \overleftarrow{k}_1)]$.

---

* The rate constants in eqns. (11) are expressed in electrical units.

** As can been shown by a simple estimate, under the usual intensity of illumination the diffusion time of hydrogen atoms from the region of their formation in the solution to the electrode surface (*i.e.* to a distance of some tens of Å) is much less than their recombination time. On account of low θ on mercury, the rate of surface recombination of hydrogen atoms can also be neglected.

Taking into consideration the dependence of the rate constants $\vec{k}_1$ and $\overleftarrow{k}_1$ on potential*, we obtain the following kinetic equation

$$\varphi = [2.3\ RT/(\alpha_1+\beta_1)F][\log\gamma + \log(\vec{k}'_{10}+\vec{k}''_{10}\,X)/\overleftarrow{k}_{10}] \tag{13}$$

where $\gamma=(2\ I_e-j)/j$. It can be readily shown that $\gamma=\overleftarrow{j}/\vec{j}$.

(*b*) Atomic hydrogen enters into cathodic and anodic electrochemical reactions only in the adsorbed state. In this case $\vec{k}_1=\overleftarrow{k}_1=0$ and

$$\varphi = [2.3\ RT/(\alpha_2+\beta_2)F][\log\gamma + \log(\vec{k}'_{20}+\vec{k}''_{20}\,X)/\overleftarrow{k}_{20}]\,. \tag{14}$$

(*c*) Atomic hydrogen is removed from the surface by the mechanism of electrochemical desorption and is simultaneously oxidized from the near-the-electrode layer ($\vec{k}_1=\overleftarrow{k}_2=0$). Then $j=k_0/(k_0+\overleftarrow{k}_1)$ and

$$\varphi = (2.3\ RT/\beta_1 F)[\log\gamma + \log(k_0/\overleftarrow{k}_{10})]\,. \tag{15}$$

Some other particular cases are possible, but for them more complex dependences of φ on γ are obtained. Equations (13)–(15) describe the kinetics of two conjugate processes—cathodic (B) and anodic (C). In their form these equations are quite similar to the equations for the slow discharge, the only difference being that here in place of the discharge current we have the parameter γ. It follows from eqns. (13)–(15) that a linear relationship should exist between φ and $\log\gamma$, the slope of the straight line characterizing the transfer coefficient of the corresponding reaction. To determine γ it is necessary to know the current $2\ I_e$ in the absence of atomic hydrogen oxidation. This can be found either by extrapolating the linear section of the $j^{0.4}$–φ plot** into the potential range in which the dependence is no longer linear, or by measuring the photocurrents with other acceptors whose products of interaction with hydrated electrons are not oxidized on the electrode. This requirement is met, for instance, by nitrous oxide which after electron capture forms the $OH^{\cdot}$ radical. This is reduced on the electrode to hydroxyl ion in the whole potential range under consideration. To calculate γ by the second method, the curves of the photocurrent for N_2O and H_3O^+ should be normalized in the region of the linear $j^{0.4}$–φ dependence to the same current value. Equations (13)–(15) will be compared below with the experimentally observed $-\varphi$–$\log\gamma$ dependence in order to determine the real mechanism of electrochemical transformation of atomic hydrogen on mercury.

Figure 7 gives the dependences of photocurrent on potential plotted in the coordinates $j^{0.4}$–φ for three solutions with different H_2SO_4 concentrations: 0.0005, 0.005 and 0.05 *M* at constant (0.5 *M*) overall electrolyte concentration. At negative potentials ($\varphi < -0.6$ V) the $j^{0.4}$–φ dependence is linear for all H_3O^+ concentrations. At more positive potentials than -0.6 V a deviation from the straight line in the direction of smaller current values is observed, which is associated with the beginning of hydrogen oxidation.

---

* $\vec{k}_i=\vec{k}_{i0}\exp(-\alpha_i F\varphi/RT)$; $\overleftarrow{k}_i=\overleftarrow{k}_{i0}\exp(\beta_i F\varphi/RT)$. We assumed the transfer coefficients α_i for reactions (B) proceeding *via* interaction with water and *via* that with hydrogen ions, to be the same.

** Estimates show that a certain deviation from linearity at low acceptor concentrations (see Section II) does not introduce any significant errors into these measurements.

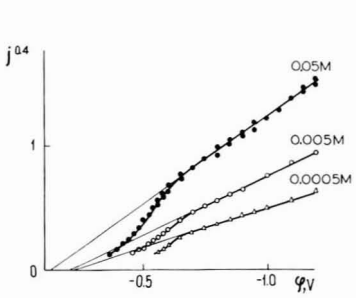

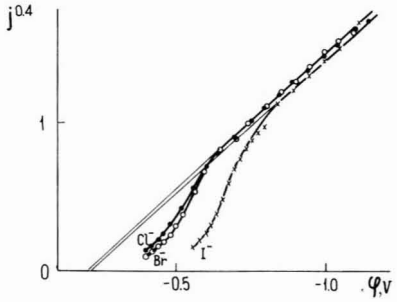

Fig. 7. $j^{0.4}$–φ plots in $K_2SO_4 + H_2SO_4$ solns. Overall electrolyte concn. 0.5 *M*, H_2SO_4 concns. indicated on Figure.

Fig. 8. $j^{0.4}$–φ plots in 0.1 *M* KCl, KBr and KI solns. containing 0.01 *M* HCl.

In Fig. 8 similar curves are given for 0.1 *M* KCl, KBr and KI solutions containing 0.01 *M* HCl. Here, as well as in the previous case, a decay of photocurrent is observed, which, when passing from Cl^- to I^-, starts at more negative potentials.

The experimental data obtained, replotted in the coordinates φ–log γ, are shown in Fig. 9*. It is clear from the Figure that there is a linear relationship between φ and log γ, the slopes of the straight lines being close to 120 mV for K_2SO_4 and to 100 mV for KCl, KBr and KI solutions. Specific adsorption of Br^- and Cl^- has little effects on γ, whereas I^- greatly increases the anodic, as compared to the cathodic, current.

As follows from eqns. (13)–(15), in the case of electrochemical transformations of atomic hydrogen the relationship between φ and log γ in the simplest cases must be linear. The experimental data in Fig. 9 show that this is true for all electrolytes studied. Thus, one of the three particular cases considered is realized experimentally.

The main criteria to be used in choosing between these three mechanisms are: the slope of the straight line φ–log γ, determining the transfer coefficient of the corresponding reaction; the effect of the solution pH on the character of the φ–log γ dependence; the influence of specific adsorption.

For a quantitative study of the effect of the solution pH it is convenient to introduce the potential φ^*, at which cathodic and anodic currents are equal, *i.e.* $\gamma = 1$. Then for different mechanisms of hydrogen removal, the dependence of φ^* on pH will differ. In particular, if ionization does not proceed *via* the adsorption step and the cathodic process is the electrochemical desorption, φ^* should not depend on pH (see eqn. (15)). Figure 10 shows the dependence of φ^* on the hydrogen ion concentration obtained in the range of $c_{H_3O^+}$ from 10^{-3} to 1 *N* in solutions with 0.5 *M* overall electrolyte concentration. As is clear from the Figure, with increasing solution acidity, φ^* rises monotonically, the greatest change of φ^* being observed for high $c_{H_3O^+}$. In the range of low acid concentrations (10^{-2}–10^{-3} *N*) φ^* practically does not depend on pH. This character of φ^*–pH dependence is at variance with eqn. (15), *i.e.* with the mechanism where atomic hydrogen is ionized without being adsorbed on the electrode

* The limiting values of the currents ($2I_e$) for K_2SO_4 solutions were found by extrapolation of linear sections of $j^{0.4}$–φ plots and for KCl, KBr and KI from the values of photocurrents measured in neutral solutions saturated with N_2O.

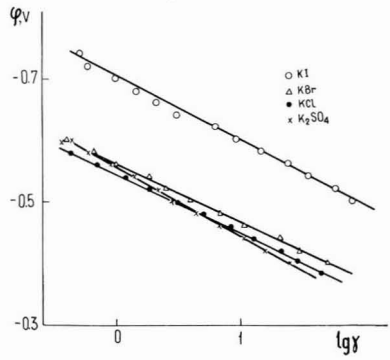

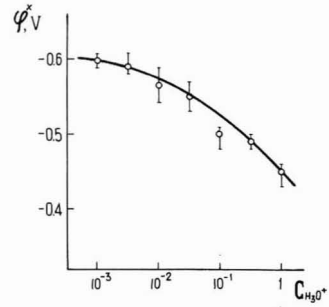

Fig. 9. φ–log γ dependence for 0.45 M K_2SO_4+0.005 M H_2SO_4 soln. and for 0.1 M KCl, KBr and KI solns. containing 0.01 M HCl.

Fig. 10. φ^* dependence on the hydrogen ion concn. (gram equiv. per liter) in solns. with 0.5 M overall electrolyte ($K_2SO_4+H_2SO_4$) concn.

and the cathodic process is ordinary electrochemical desorption. Therefore, in all probability one of the two possible mechanisms of hydrogen atoms removal is realized: both conjugate reactions proceed without passing *via* the adsorption step, or, on the other hand, adsorbed hydrogen participates in both reactions. It is impossible to choose unambiguously between these two mechanisms on the basis of the experimental data available, since the same kinetic law is valid in both cases.

The kinetic equations for these two mechanisms deduced above describe adequately the experimental data given in Fig. 9, if one of the conjugate reactions —ionization or electrochemical desorption*—is activationless[21] ($\alpha+\beta=\frac{1}{2}$). If it is atomic hydrogen ionization which is the activationless reaction, at negative potentials it must become an activation reaction, *i.e.* in the straight line φ–log γ in the range of negative potentials a change in the slope should be expected from 120 mV to 60 mV. We could not detect this experimentally (perhaps, due to a large error in the determination of γ near the beginning of the photocurrent decay).

On the other hand, if electrochemical desorption is the activationless process and ionization the activation one, at more positive potentials the latter must also become activationless. This is due to the fact that at a potential of about -0.45 V (in the absence of specific adsorption) the ordinary hydrogen ion discharge turns into a barrierless one[21]. In this case parameter γ should reach a limiting value which will remain constant with further potential increase. As is clear from Fig. 9, over the whole potential range accessible for measurement the straight lines φ–log γ have the same slope**.

Thus, from the experimental results presented above we cannot give a conclusive answer to the question which of the two reactions is activationless. It can be only affirmed that one of them must be by all means activationless. Additional data must be available for final solution of this problem.

---

* Irrespective of the detailed mechanism of hydrogen removal, for convenience we shall call the cathodic process "electrochemical desorption".

** It should be borne in mind, however, that at very positive potentials determination of γ becomes inaccurate.

According to Krishtalik[21], activationless hydrogen ionization should start at more positive potentials than approximately -0.45 V. At more negative potential values, ordinary discharge and hence ionization, are observed. Comparing Krishtalik's results with ours, we can suppose that in all probability electrochemical desorption is the activationless step, atomic hydrogen ionization proceeding by the ordinary mechanism with $\beta=\frac{1}{2}$. It should be noted, however, that this comparison is not rigorous, since hydrogen atoms arriving at the surface from solution are not equivalent in point of energy to those arising during discharge[20]. Therefore, it is not impossible that in our case hydrogen ionization can become activationless at a different potential value.

As has been pointed out earlier, electrochemical desorption can proceed by two independent mechanisms: with participation of hydrogen ions, or of water molecules. In the former case according to eqn. (14) the potential φ^* should, with pH increasing by unity, shift in the negative direction by 116 mV. In the case of desorption *via* reaction with water molecules φ^* does not depend on pH at all. Experimental data given in Fig. 10 show that both H_3O^+ ions and water molecules participate in electrochemical desorption. From the analysis of the curve in the Figure it was found that in 1 N acid solution the rate of atomic hydrogen removal *via* reaction with H_3O^+ ions is approximately 50 times as high as that involving water molecules. In less concentrated acid solutions ($c_{H_3O^+} < 10^{-2}$ N) electrochemical desorption of atomic hydrogen occurs mainly with participation of water. The mechanism of electrochemical hydrogen desorption in acid solutions *via* interaction with water molecules was first suggested by Krishtalik[22] to explain the experimental data on the barrierless discharge.

Specific anion adsorption accelerates the ionization reaction (if it is an activation one), since the potential drop in the dense part of the double layer becomes more positive. At the same time, specific anion adsorption should increase the rate of the activationless electrochemical desorption *via* reaction with hydrogen ions since a negative ψ_1 enhances the hydrogen ion concentration at the electrode. As is clear from Fig. 9, Cl^- and Br^- have little effect on γ, whereas I^- greatly increases γ^*. These data can be explained only by the fact that iodide adsorption affects hydrogen ionization more strongly than electrochemical desorption (due, in particular, to the participation in the latter reaction not only of hydrogen ions, but also of water molecules**).

IV. INVESTIGATION OF THE UNSTABLE ION-RADICAL NO_3^{2-} REACTIONS***

In the case of electron photoemission into a nitrate solution the hydrated electron is captured by NO_3^- ion to form the unstable ion-radical NO_3^{2-}, which is partly oxidized on the electrode (at sufficiently positive potentials) and partly disintegrates in the solution bulk. The product of this disintegration—the OH· radical—is irreversibly reduced on the mercury electrode over the whole potential range studied. The NO_3^{2-} oxidation decreases and the OH· reduction increases the photocurrent

* The lower slope of the straight line φ–log γ in the case of specific anion adsorption is due to the fact that with potential increasing in the positive direction effective ψ_1 becomes more negative.

** The effect of specific adsorption of I^- can be explained in a similar manner if it is assumed that hydrogen ionization is the activationless reaction.

*** This Section is based on the results of a study carried out together with V.V. Eletsky.

measured[16].

The solution of a set of differential equations describing the diffusion and reactions of hydrated electron and NO_3^{2-} leads with the use of ref. 17 to the following expression for the photocurrent:

$$j = 2\Big\{ I - e \int_0^\infty f(x)\exp(-\lambda x)\,dx + \\ - [ek_{ox}/(\lambda_d D' + k_{ox})][\lambda^2/(\lambda^2 - \lambda_d^2)] \times \\ \times \int_0^\infty f(x)[\exp(-\lambda_d x) - \exp(-\lambda x)]\,dx \Big\} \qquad (16)$$

Here $\lambda = (kc_A/D)^{\frac{1}{2}}$; $\lambda_d = (k_d/D')^{\frac{1}{2}}$; I is the emission current, $c_A = c_{NO_3^-}$, D and k are the diffusion coefficient of hydrated electron and the rate constant of its interaction with NO_3^-, D', k_d and k_{ox} are the diffusion coefficient of NO_3^{2-} and the rate constants of its bulk disintegration and oxidation on the electrode, respectively, with $k_{ox} = k_{ox,0} \times \exp(\beta F\varphi/RT)$; $f(x)$ is the function of the hydrated electron source, averaged over the emitted electron energies (*cf.* p. 407).

The second term in the right-hand side of formula (16) describes the return to the electrode of the hydrated electrons which were not captured by acceptors, the third term—the reactions with participation of NO_3^{2-}. At sufficiently negative potentials, when NO_3^{2-} is not oxidized ($k_{ox} \ll \lambda_d D'$) the third term is zero. At sufficiently positive potentials, where all NO_3^{2-} particles reaching the electrode surface are oxidized ($k_{ox} \gg \lambda_d D'$), the third term does not depend on k_{ox}. In both limiting cases the photocurrent being measured is to the first approximation proportional to the emission current I, *i.e.* is described by the "$\frac{5}{2}$-law" with the same threshold potential φ_0.

It proved in experiment that in sufficiently concentrated $NaNO_3$ solutions (10^{-2}–1 mol/l) the $j^{0.4}$–φ plot has in fact two approximately linear sections at high and at low potentials, separated by the region of monotonic photocurrent decay (Fig. 11, curve I). At potentials more negative than -1.2 V NO_3^{2-} is not oxidized on a mercury electrode. In the potential range more positive than -0.7 V the oxidation rate reaches its limiting value (determined by the rate of supply of NO_3^{2-} to the electrode surface). It is significant that here the photocurrent does not vanish (as in the case of the H_3O^+ acceptor, see above), since a fraction of NO_3^{2-} manages to disintegrate in solution and thus escape oxidation.

On addition to the solution of small amounts (10^{-4} mol/l) of tetrabutylammonium, in the region of TBA adsorption (more positive than -1.3 V) the S-shaped curve changes to a straight line (Fig. 11, curve 2). Undoubtedly, TBA has two distinct effects: (*a*) it decreases the photoemission rate (*cf.* p. 405 and Fig. 2) and (*b*) inhibits the electrooxidation of NO_3^{2-}, which is responsible for the disappearance of the photocurrent decay at positive potentials.

From the dependence of photocurrent j on potential φ (in the range from -0.7 to -1.2 V), using eqn. (16), we determined the transfer coefficient of the electrooxidation reaction of NO_3^{2-}: $\beta \approx 0.25$.

To determine the rate constant of the bulk disintegration of NO_3^{2-} let us consider the case of high NO_3^- concentration where all hydrated electrons are captured in the solution ($\lambda x \gg 1$ in the range of x where $f(x)$ is different from zero). If $\lambda_d x \ll 1$ as

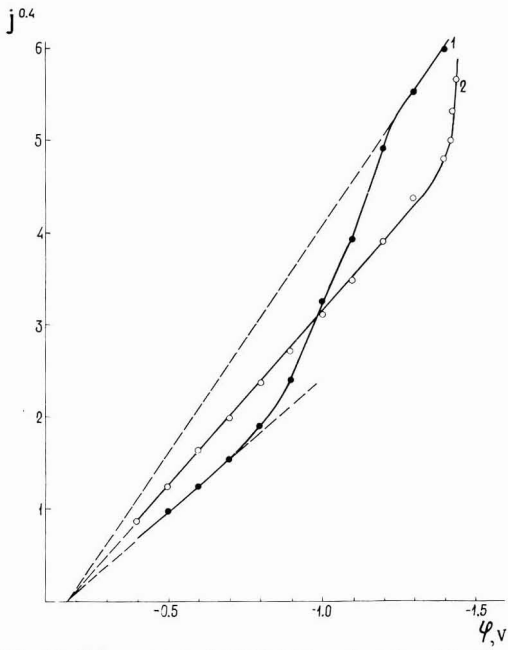

Fig. 11. $j^{0.4}$–φ plot in 1 M $NaNO_3$ soln. (1) and in the same soln. with 10^{-4} M TBA addition (2).

well, in the range of positive potentials, where the oxidation rate of NO_3^{2-} is high ($k_{ox} \gg \lambda_d D'$), the photocurrent is $j = 2\,I\bar{x}\lambda_d = 2\,I\bar{x}(k_d/D')^{\frac{1}{2}}$ (*cf.* eqn. (9)).

The emission current I and the quantity $\bar{x}$ have been determined from the section of the $j^{0.4}$–φ straight line obtained at negative potentials, j measured at positive potentials; assuming $D' \approx 10^{-5}$ cm^2 s^{-1}, we found $k_d = 6 \times 10^6$ s^{-1}.

Thus, from the measurements of the extrinsic photoeffect at the metal–electrolyte interface it is possible to obtain important information on the kinetics of both homogeneous and heterogeneous (electrode) reactions which is not accessible to usual electrochemical methods of investigation.

ACKNOWLEDGEMENTS

We wish to express our thanks to A. N. Frumkin, L. I. Krishtalik, A. M. Brodsky and Yu. Ya. Gurevich for detailed discussion of this paper and V. V. Eletsky for experimental assistance.

SUMMARY

The effect of various factors on the electron photoemission proper and on further transformations in solution of hydrated electrons and the products of their interaction with acceptors has been studied.

Specific adsorption does not change the photoemission threshold if the adsorption layer thickness remains less than the de-Broglie wavelength of emitted electrons. Otherwise adsorption has a strong effect on photoemission.

At low acceptor concentrations, when a large portion of emitted electrons is not captured in solution but returns to the electrode, the dependence of photocurrent on electrode potential is no longer described by the "$\frac{5}{2}$-law". The mean distance from the electrode at which emitted electrons undergo hydration has been estimated. The electron work function for the mercury/aqueous solutions system at the potential of zero charge is 3.0 eV.

The photoemission method has been applied to the investigation of the kinetics of electrochemical transformation of atomic hydrogen on the mercury electrode. It has been shown that atomic hydrogen enters into both conjugate reactions—ionization and cathodic reduction—being in the same initial state (adsorbed on the electrode or dissolved in electrolyte). One of these reactions (apparently, electrochemical desorption) is activationless. The electrochemical desorption reaction occurs with the participation both of hydrogen ions and water.

The rate constant of bulk disintegration of unstable ion-radical NO_3^{2-} has been measured as well as its oxidation transfer coefficient on mercury.

REFERENCES

1 YU. V. PLESKOV AND Z. A. ROTENBERG, *J. Electroanal. Chem.*, 20 (1969) 1.
2 A. M. BRODSKY AND YU. YA. GUREVICH, *Electrochim. Acta*, 13 (1968) 1245.
3 Z. A. ROTENBERG AND YU. V. PLESKOV, *Elektrokhimiya*, 5 (1969) 982.
4 D. C. GRAHAME, E. M. COFFIN, J. I. CAMMINGS AND M. A. POTH, *J. Amer. Chem. Soc.* 74 (1952) 1207.
5 A. N. FRUMKIN, V. S. BAGOTSKY, Z. A. IOFA AND B. N. KABANOV, *Kinetika Elektrodnykh Prozessov*, Izdatel'stvo Moskovskogo Universiteta, Moscow, 1952.
6 R. PARSONS, *Proc. Royal Soc. London*, 261A (1961) 79.
7 F. W. SCHAPINK, M. OUDEMAN, K. W. LEU AND J. N. HELLE, *Trans. Faraday Soc.*, 56 (1960) 415.
8 D. C. GRAHAME AND B. A. SODERBERG, *J. Chem. Phys.*, 22 (1954) 449.
9 D. C. GRAHAME, *J. Am. Chem. Soc.*, 80 (1958) 4201.
10 A. N. FRUMKIN AND B. B. DAMASKIN, *Dokl. Akad. Nauk SSSR*, 129 (1959) 862.
11 A. N. FRUMKIN in P. DELAHAY (Ed.), *Advances in Electrochemistry and Electrochemical Engineering*, Vol. I, 1961.
12 G. C. BARKER, *Electrochim. Acta*, 13 (1968) 1221.
13 Z. A. ROTENBERG AND YU. V. PLESKOV, *Elektrokhimiya*, 6 (1970) 418.
14 A. GORODETSKAYA AND A. N. FRUMKIN, *Dokl. Akad. Nauk SSSR*, 18 (1938) 649; N. V. NIKOLAEVA, A. N. FRUMKIN AND Z. A. IOFA, *Zh. Fiz. Khim.*, 26 (1952) 1326.
15 A. M. BRODSKY AND YU. YA. GUREVICH, *Zh. Eksperim. i. Teor. Fiz.*, 54 (1968) 213.
16 G. C. BARKER, A. W. GARDNER AND D. C. SAMMON, *J. Electrochem. Soc.*, 113 (1966) 1182.
17 YU. YA. GUREVICH AND Z. A. ROTENBERG, *Elektrokhimiya*, 4 (1968) 984.
18 V. I. LAKOMOV, V. V. ELETSKY, Z. A. ROTENBERG AND YU. V. PLESKOV, *Elektrokhimiya*, 6 (1970) 415.
19 R. DE LEVIE AND J. C. KREUSER, *J. Electroanal. Chem.*, 21 (1969) 221.
20 A. N. FRUMKIN, *Zh. Fiz. Khim.*, 31 (1957) 1875.
21 L. I. KRISHTALIK, *Usp. Khim.*, 34 (1965) 1841.
22 L .I. KRISHTALIK, *Elektrokhimiya*, 4 (1968) 877.

ELECTROANALYTICAL CHEMISTRY AND INTERFACIAL ELECTROCHEMISTRY
Elsevier Sequoia S.A., Lausanne – Printed in The Netherlands

POLAROGRAPHISCHE UNTERSUCHUNGEN AM ADENOSIN-5'-TRIPHOSPHAT (ATP)

H. SOHR, KH. LOHS UND G. KÖNIG

Institut für Biophysik, Berlin-Buch, der Deutschen Akademie der Wissenschaften zu Berlin (D.D.R.)

(Eingegangen am 11. Februar, 1970)

Nucleotide und Nucleoside sind—vorallem wegen ihrer vielfältigen Funktionen im biochemischen Geschehen der Zelle—Gegenstand umfangreicher physikochemischer Untersuchungen. Die Gleichstrompolarographie hat dabei bisher vergleichsweise keine wesentliche Rolle gespielt. Den seinerzeit von Heath[1] veröffentlichten Ergebnissen, z.B. an Adenosinmonophosphat, folgten erst viel später weitere Untersuchungen dieser Art auch am Adenin[2,3]. Der Grund dafür ist möglicherweise darin zu suchen, dass diese Methode bei den genannten Verbindungen hinsichtlich der Analytik nicht konkurrenzfähig und bezüglich des Studiums der physikochemischen Eigenschaften nicht aussagekräftig genug war.

Kürzlich wurden Arbeiten bekannt, die die teilweise sehr hohe und stark differenzierte Oberflächenaktivität dieser Verbindungen nutzten und mittels der Tensammetrie und der Differentialkapazitätsmessungen durch eine geeignete Messbrücke zu interessanten Ergebnissen gelangten[4,5].

Eine zusammenfassende Darstellung der Anwendung der verschiedenartigen polarographischen Methoden bezüglich dieser Verbindungen ist von Janik und Elving gegeben worden[6].

Wir haben uns im Rahmen dieser Arbeit vorallem mit polarographischen Untersuchungen des Adenosin-5-triphosphats (ATP) beschäftigt, da diese Substanz in der biologischen Zelle eine bevorzugte Stellung unter den Nucleotiden einnimmt.

EXPERIMENTELLES

Die gleichstrompolarographischen und tensammetrischen Messungen wurden mit einem Polarographen vom Typ GWP 563 (Akademiewerkstätten der Deutschen Akademie der Wissenschaften zu Berlin) durchgeführt. Das Gerät ermöglicht neben der Aufnahme von polarographischen Kurven tensammetrische Messungen bei 78 Hz und Wechselspannungen zwischen 2 und 100 mV. Die i–t-Kurven sind nach der von Volke vorgeschlagenen Methode mit dem gleichen Gerät registriert worden[7].

Als Zelle diente ein abgeschlossenes, temperierbares Gefäss, dessen Bezugselektrode (gesättigte Kalomelelektrode) über eine Salzbrücke mit der Zelle verbunden war. Die verwendeten Jenaer Stumpfkapillaren hatten folgende Konstanten: (t = Tropfzeit (s), m = Ausflussgeschwindigkeit (mg s^{-1}), die in 0.5 N Na_2SO_4-Lösung bei offenen Stromkreis bestimmt wurden), Kapillare 1 (K1) $t = 6.1$, $m = 0.927$; Kapillare 2 (K2) $t = 6.0$, $m = 1.23$; Kapillare 3 (K3), $t = 8.2$, $m = 0.554$; Kapillare 4 (K4) $t = 4.2$, $m = 1.81$; Kapillare 5 (K5) $t = 32.0$, $m = 0.102$.

Alle Messungen sind bei $25 \pm 0.2°$ C durchgeführt worden. Die für die Messungen vorbereiteten Lösungen wurden 20 Minuten mit nachgereinigtem Stickstoff, der zusätzlich über Aktivkohle und danach durch eine Lösung mit gleicher Zusammensetzung wie die Messlösung geleitet wurde, vom Sauerstoff befreit.

Das ATP (Dinatriumsalz) wurde von der Firma FERAK (Berlin-West) bezogen und das verwendete Tributylphosphat (TBP) ist selbst hergestellt und jeweils frisch destilliert worden.

Da das ATP mit abnehmenden pH-Wert eine zunehmende Hydrolysetendenz zeigt[8], ist diese Substanz in entsprechender Konzentration unmittelbar vor der Messung mit einer Mikropipette nach der Entlüftung zur Messlösung gegeben worden, wobei die Konzentration der ATP-Lösung so gewählt wurde, dass die Volumen- und pH-Änderung der Messlösung vernachlässigbar war. Die vorbereitete ATP-Lösung hatte einen pH-Wert $= 9.5$. Bei diesem pH-Wert, bei dem das ATP als ATP^{4-} vorliegt[9], ist die Hydrolysetendenz sehr gering, d.h., diese Lösungen sind im Kühlschrank längere Zeit haltbar. Der pH-Wert der Messlösung wurde autotitrimetrisch auf 5.0 eingestellt. Da Cu(II)-Ionen die Hydrolyse von ATP beschleunigen und das Maximum bei pH $= 5.5$ liegt[10,11] wurde darauf geachtet, dass die Zeit der unmittelbaren Messung möglichst 10 Minuten nicht überschritt. Sie betrug im allgemeinen 3 Minuten, wodurch auch der zeitabhängigen Adsorption des ATP an den Gefässwänden entgegengewirkt wurde.

Als Grundelektrolyt diente fast ausschliesslich Na_2SO_4. Die Reinigung erfolgte so, dass das käufliche Produkt (p.A.) zweimal in bidest. H_2O umkristallisiert und danach bei 500° C geglüht wurde. Die übrigen Salze sind ebenfalls durch Umkristallisation gereinigt worden. Zur Herstellung der Messlösungen diente bidest. H_2O. Nach jeder Messreihe wurde die Zelle mit konz. Schwefelsäure (p.A.) gereinigt. Die im folgenden als Grundlösung bezeichnete Lösung hatte die Zusammensetzung: 0.5 *N* Na_2SO_4, 3×10^{-3} *M* $CuSO_4$, 5×10^{-4} *M* TBP.

ERGEBNISSE

Wir konnten nachweisen, dass in Gegenwart verschiedener Adenosin-5′-phosphate Ni(II)-Vorwellen auftraten, die vergleichsweise schon von vielen Autoren an anderen Systemen nachgewiesen und interpretiert (z.B. von Mark *et al.*[12-14]) und in ihrem Prinzip auf Heyrovský zurückgeführt werden können[15]. Die letzten zusammenfassenden Darstellungen dieses Gebiets wurden von Mairanovsky und Calusaru gegeben[16,17]. Da sich jedoch bei den Adenosin-5′-phosphaten keine wesentlich neuen Gesichtspunkte ergaben, ist dieses Problem nicht weiter bearbeitet worden.

Unerwartet günstige Ergebnisse erhielten wir hingegen, als wir feststellten, dass Adenosin-5′-phosphate vorallem das ATP schon in Spurenkonzentrationen in einem bestimmten Potentialbereich die z.B. durch TBP verursachten Deformationen der gleichstrompolarographischen Cu(II)-Welle wieder z.T. aufheben können. Wir fanden, dass schon eine 10^{-9} *M* ATP-Konzentration eine diesbezüglich signifikante Zunahme der Stromstärke verursacht. Um diese später noch ausführlich zu diskutierenden Phänomene näher zu untersuchen, waren zunächst einige tensammetrische Messungen nötig, wobei vorallem der Potentialbereich der Adsorption von ATP sowie seine Oberflächenaktivität untersucht wurden.

In Abb. 1 sind einige tensammetrische Kurven in Abhängigkeit von der ATP-

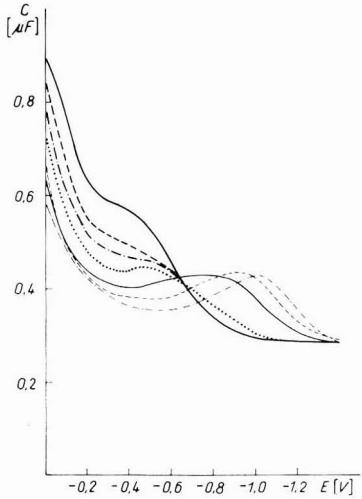

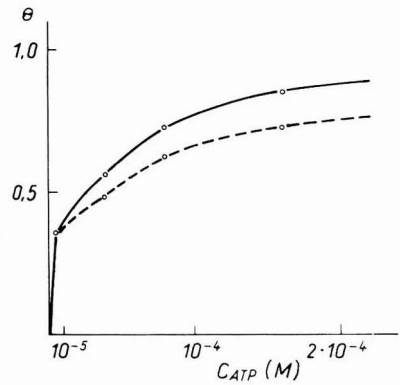

Abb. 1. Tensammetrische Kurven von ATP in McIlvaine-Pufferlösung +0.5 *N* Na_2SO_4, pH = 5.0. ATP Konzentrationen: (——) 0, (– – – –) 4.9×10^{-6}, (— · — · —) 3.9×10^{-5}, (.....) 7.8×10^{-5}, (——) 6.25×10^{-4}, (– – – –) 2.5×10^{-3}, (– · – · –) 5×10^{-3} *M*. E = 10 mV; (K1).

Abb. 2. Adsorptionsisothermen von ATP in McIlvaine-Pufferlösung +0.5 *N* Na_2SO_4, pH = 5.0. (——) −0.2 V, (– – – –) −0.4 V; (K1).

Konzentration in McIlvaine-Puffer dargestellt (da die Oberflächenaktivität beim ATP pH-abhängig ist[18] und die eingangs erwähnte Hydrolysetendenz zu berücksichtigen ist, sind die Messungen vergleichsweise zunächst in Pufferlösung gemacht worden). Bei den weiteren Untersuchungen konnte unter Berücksichtigung der eingangs erwähnten Bedingungen auf die Verwendung von Pufferlösungen verzichtet werden.

Im Unterschied zu den von Vetterl[5] unter ähnlichen Bedingungen gemessenen tensammetrischen Kurven des Adenosins bildet sich beim ATP kein zweites Adsorptionsgebiet aus. Da das ATP bei pH = 5.0 hauptsächlich als $ATPH^{3-}$ vorliegt, ist eine derartige Assoziation der adsorbierten Moleküle, wie sie von Vetterl beim Adenosin festgestellt wurde, nicht möglich. Somit unterscheiden sich das Adenosin und das ATP in ihren Kurvenbildern beträchtlich. Das Adenosin-5′-diphosphat (ADP) und das entsprechende Monophosphat (AMP) sind eher mit dem ATP aus den eben genannten Gründen vergleichbar als mit dem Adenosin[18]. In Abb. 2 sind die Adsorptionsisothermen bei zwei verschiedenen Potentialen dargestellt (die Kurven für −0.2 und −0.3 V liegen zwischen den beiden abgebildeten Kurven). Der Bedeckungsgrad wurde nach der bekannten Beziehung

$$\theta = (C_0 - C_1)/(C_0 - C)$$

ermittelt. C_0 = Differentialkapazität der Grundlösung, C_1 = Differentialkapazität bei der jeweiligen ATP-Konzentration, C = Differentialkapazität bei maximaler ATP-Bedeckung. Obgleich die Auswertung bei konstantem Potential auf diese Weise nicht ganz exakt ist (da die Frequenz einen Einfluss haben kann), weist der ermittelte Adsorptionskoeffizient ($\beta = 1.5 \times 10^5$ 1/Mol) dennoch die beträchtliche Oberflächenaktivität des ATP deutlich aus.

Der Kurvenverlauf der Adsorptionsisothermen ist typisch für geladene oberflächenaktive Substanzen, d.h. a (Wechselwirkungskoeffizient) ist negativ[19].

Desweiteren untersuchten wir den Einfluss von ATP auf die tensammetrischen Kurven des TBP, da diese Substanz für die Deformation der Cu(II)-Welle eingesetzt wurde. Wie aus Abb. 3 ersichtlich ist, wird selbst bei einer ATP-Konzentration von

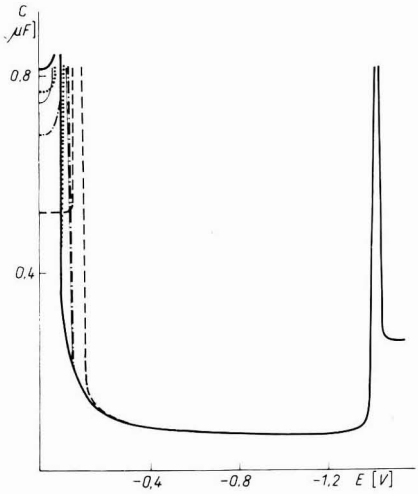

Abb. 3. Tensammetrische Kurven von TBP (5×10^{-4} M) in 0.5 N Na_2SO_4, pH = 5.0 in Abhängigkeit von der ATP Konzentration: (——) 0, (– – – –) 10^{-3}, (–·–·–) 10^{-4}, (——) 10^{-5}, (.....) 10^{-6} M, $E = 10$ mV; (K1).

10^{-6} M noch eine, wenn auch geringe, Verschiebung des Adsorptionspeaks des Tributylphosphats erreicht. Damit ist zunächst die Schlussfolgerung naheliegend, dass die noch zu besprechenden Stromstärkeerhöhungen durch Einfluss geringer Mengen ATP damit in Zusammenhang gebracht werden müssen. Allerdings muss erwähnt werden, dass Adenosin den gleichen Effekt zeigt, obgleich es nur eine geringfügige Veränderung der Stromstärke—verglichen mit dem ATP—bewirkt.

Die in die Messlösung eingebrachte ATP-Konzentration bewirkt, dass infolge der vergleichsweise hohen Konzentration an Cu(II)-Ionen und der pk_A-Werte[20] (der bei dem angegebenen pH-Wert möglichen Cu-ATP-Komplexe) die ATP-Moleküle nahezu quantitativ als ATP-Komplexe vorliegen. Deshalb wurde der Einfluss verschiedener 2-wertiger Kationen auf die Oberflächenaktivität an der Hg-Elektrode untersucht. Da Cu(II) hierfür ungeeignet ist, wurde in Gegenwart von Ni(II) gemessen, dass bezüglich der Komplexbildungstendenz mit ATP gewisse Parallelen erlaubt; ausserdem wurde Mg(II) eingesetzt. Von dem Letzteren ist bekannt, dass es im Gegensatz zu Cu(II) und Ni(II) nahezu keine Wechselwirkung mit der in C_6-Stellung befindlichen NH_2-Gruppe des Adenins eingeht und auch keine Dimerisierungstendenz zeigt, sondern sich auf β- und γ-ständige Phosphorylgruppen beschränkt[21]. Diese unterschiedliche Komplexbildungstendenz ist aus den Abb. 4 und 5 ersichtlich. Da unter dem Einfluss der Mg(II)-Ionen die Oberflächenaktivität sich nur wenig von derjenigen in Abwesenheit von Mg(II)-Ionen unterscheidet, ist der Einfluss der Ni(II)-Ionen wesentlich stärker ausgeprägt. Während beim Mg(II) bei dem angegebenen pH-Wert das $(ATPHMg)^-$ vorherrschend ist,

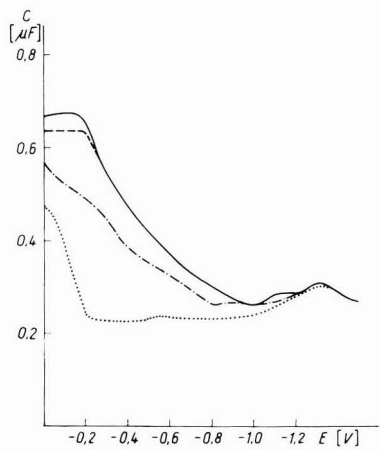

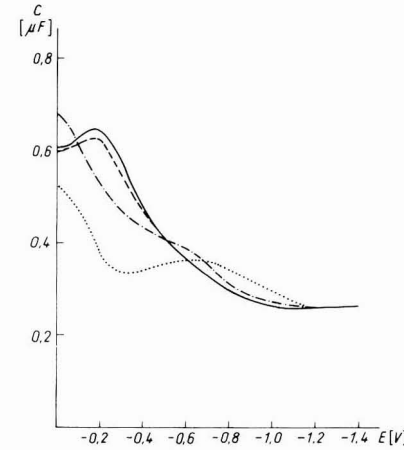

Abb. 4. Tensammetrische Kurven von ATP in 0.5 N Na_2SO_4 in Gegenwart von 5×10^{-3} M $NiSO_4$, pH = 5.0. ATP-Konzentrationen: (——) 0, (– – –) 10^{-6}, (–·–·–) 10^{-5}, (.....) 10^{-3} M, $E = 10$ mV; (K1).

Abb. 5. Tensammetrische Kurven von ATP in 0.5 N Na_2SO_4 in Gegenwart von 5×10^{-3} M $MgSO_4$, pH = 5.0. ATP-Konzentrationen: (——) 0, (– – –) 10^{-6}, (–·–·–) 10^{-5}, (.....) 10^{-3} M, $E = 10$ mV (K1).

bestehen bei den Schwermetallionen, vorallem beim Cu(II), weitere Möglichkeiten zur Komplexbildung, nämlich $[ATPCu(OH)]^{3-}$ sowie $[ATPCu(OH)]_2^{6-}$ und $[ATPCu(OH)_2]^{4-}$. Bei pH 5.5 besteht nach verschiedenen Autoren ein Maximum für die Dimerenbildung $[ATPCu(OH)_2]^{6-}$. Diesen Dimeren kann man sicher auch eine grössere Oberflächenaktivität zurechnen, wie in Abb. 5 zu sehen ist. Diese Dimeren haben nach den genannten Autoren folgende Anordnung[10,22]:

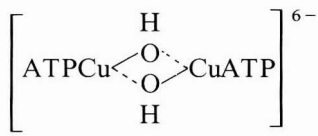

Von Brintzinger wurde die Dimerisierungstendenz in der Reihenfolge:

$$Cu(II) > Zn(II) > Ni(II) > Co(II) > Mn(II) > Mg(II)$$

angegeben[23]. Die pk_A-Werte für die Dimerisierung liegen weit höher als jene für die Monomeren[22].

Einschränkend sei erwähnt, dass bisher keine komplexchemischen Untersuchungen vorliegen, die unseren Konzentrationsverhältnissen entsprechen ($[Cu^{2+}] = 10^{-4}$ bis 3×10^{-3} M und $[ATP] = 1.25 \times 10^{-9}$ bis 4×10^{-7} M).

Allerdings würde sich dieser Sachverhalt infolge der hohen Oberflächenaktivität des ATP an der Hg Oberfläche bei den entsprechenden Potentialwerten wesentlich günstiger gestalten.

GLEICHSTROMPOLAROGRAPHISCHE UNTERSUCHUNGEN

In Abb. 6 sind die gleichstrompolarographischen Kurven des Cu(II) in Gegenwart von TBP und in Abhängigkeit von verschiedenen ATP-Konzentrationen darge-

stellt. Die Grundkurve gibt dabei den Verlauf der durch die Anwesenheit von TBP deformierten Cu(II)-Welle wieder, während die übrigen Kurven den Einfluss steigender Mengen an ATP zeigen. Die Zunahme der Stromstärke infolge des ATP-Einflusses ist auf den Potentialbereich beschränkt, wo vermutlich das ATP an der Hg-Oberfläche, wenn auch in sehr geringem Masse, adsorbiert ist. Wir haben, wie aus den vorausgegangenen Abbildungen hervorgeht, den Nachweis der Adsorption bis 10^{-6} M geführt. Es kann aber als sicher gelten, dass auch bei wesentlich niedrigeren Konzentrationen noch ATP adsorbiert wird, obgleich dann der Nachweis mittels Tensammetrie nicht mehr möglich ist. Allerdings ist dies noch kein schlüssiger Beweis für die Zunahme der Stromstärke in Abb. 6, da Adenosin in dem angegebenen Konzentrationsbereich nur bei den höchsten Konzentrationen (4×10^{-7} M) eine geringe Stromstärkezunahme ergibt, obgleich die Oberflächenaktivität des Adenosins mit der des ATP verglichen werden kann.

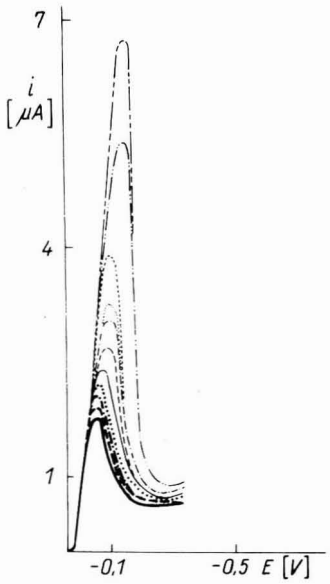

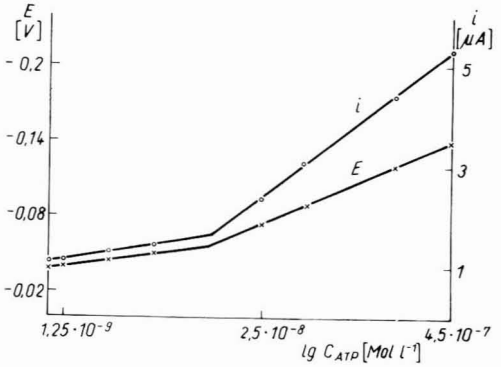

Abb. 6. Abhängigkeit der gleichstrompolarographischen Kurven der Grundlösung von der ATP Konzentration. ATP-Konzentrationen: (——) 0, (– – –) 1.25×10^{-9}, (–·–·–) 2.5×10^{-9}, (.....) 5×10^{-9}, (——) 7.5×10^{-9}, (– – – –) 1.25×10^{-8}, (–·–·–·–) 2×10^{-8}, (.....) 2.5×10^{-8}, (_ _ _ _) 5×10^{-8}, (–·–·–·–) 2×10^{-7}, (——————) 4×10^{-7} M; (3). Der Anstieg der Kurven auf den Stromstärkewert i_D wurde nicht mit gezeichnet.

Abb. 7. Abhängigkeit der Stromstärke (i) bzw. des Potentials E des Maximums von der ATP-Konzentration in Grundlösung (K3).

Bei der Prüfung der Abhängigkeit der Stromstärke durch ATP von der Cu(II)-Konzentration erhielten wir Kurven, wie sie für katalytische Wellen charakteristisch sind (Abb. 7). Auch die Abhängigkeit der Stromstärke zeigte charakteristische Merkmale der katalytischen Wellen (Abb. 8). Es geht schon aus Abb. 8 hervor, wo neben der Abhängigkeit der Stromstärke des Peaks auch die Abhängigkeit der Peakpotentiale dargestellt ist, dass zwei Vorgänge hierbei eine Rolle spielen.

i–t-Kurven

Um diese Prozesse näher zu untersuchen, wurde die Abhängigkeit der Peakhöhe von der Tropfzeit und die Abhängigkeit der *i–t*-Kurven vom Potential am 1. Tropfen mit einer langsam tropfenden Kapillare (*t* etwa 30 s) untersucht. Was die Tropfzeitabhängigkeit anbetrifft, kann man zunächst feststellen, dass im ersten ATP-Konzentrationsbereich bis zum Schnittpunkt der beiden Geraden in Abb. 8 die Peakhöhe unabhängig von der Tropfzeit ist, während im zweiten Konzentrationsbereich

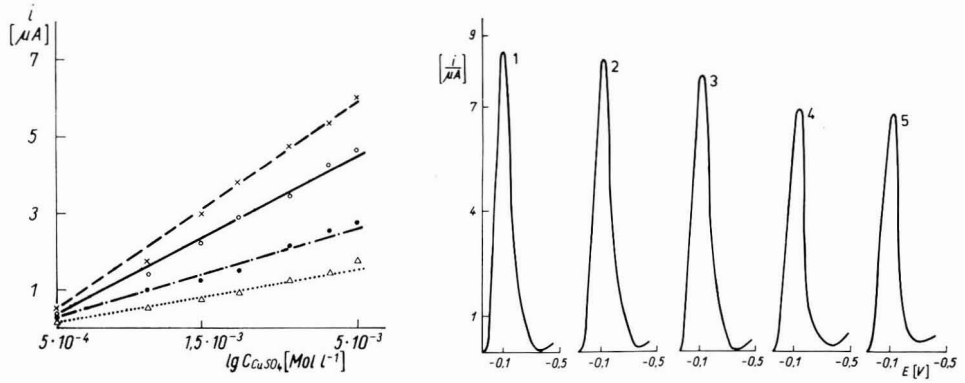

Abb. 8. Abhängigkeit der Stromstärke (*i*) des Maximums (bezogen auf die Stromstärkewerte der Grundlösung bei gleichem Potential) von der Konzentration des $CuSO_4$ (K3) ATP-Konzentrationen: (—·—·—) 5×10^{-8}, (... △...) 2.5×10^{-8}, (——×——) 4.5×10^{-7}, (—○—) 2×10^{-7} *M*.

Abb. 9. Tropfzeitabhängigkeit der polarographischen Kurve der Grundlösung + 10^{-3} *M* KCl in Gegenwart von 4.5×10^{-7} *M* ATP (K4). (1) $t = 1.73$, (2) $t = 2.06$, (3) $t = 2.50$, (4) $t = 4.2$, (5) $t = 6.5$ s.

eine Zunahme der Höhe umgekehrt proportional zur Tropfzeit vorliegt (Abb. 9). Aufschlussreicher für die Charakterisierung der beiden Prozesse sind allerdings die *i–t*-Kurven.

In der folgenden Tabelle sind die β-Werte ($i = t^{\beta}$) in Abhängigkeit von der ATP-Konzentration dargestellt. Die *i–t*-Kurven wurden beim Potential des durch die Zugabe von ATP verursachten Strompeaks registriert.

TABELLE 1

ABHÄNGIGKEIT DES EXPONENTEN β VON DER ATP-KONZENTRATION BEIM PEAKPOTENTIAL

Grundlösung: 0.5 *N* Na_2SO_4, 3×10^{-3} *M* $CuSO_4$, 5×10^{-4} *M* TBP, pH = 5.0. In Abwesenheit und in Gegenwart von 10^{-3} *M* KCl (β_{KCl})

E_{Peak}/V	*ATP Konzentration/[M]*	β_{KCl}	β
−0.03	0	0.98	1.20
−0.04	1.25×10^{-9}	1.08	1.19
−0.04	2.5×10^{-9}	1.08	1.16
−0.05	5×10^{-9}	1.07	1.18
−0.06	2.5×10^{-8}	1.51	1.23
−0.07	5×10^{-8}	1.59	1.26
−0.11	2×10^{-7}	1.51	1.40
−0.14	4.5×10^{-7}	1.55	1.41

DISKUSSION

Aus den bisherigen Darlegungen geht hervor, dass die Komplexbildung zwischen ATP und Cu(II) für den Stromanstieg von grosser Bedeutung sein muss, wobei vor allem die Komplexbildung auf der Hg-Oberfläche wichtig ist. Obwohl bereits in der Lösung ATP-Cu-Komplexe gebildet werden, haben diese Komplexe für den unmittelbaren Elektrodenprozess jedoch keine Bedeutung, da sie in vernachlässigter kleiner Konzentration vorliegen. Lediglich ihre Adsorptionstendenz auf der Hg-Oberfläche ist von Bedeutung, welche schon eingangs erwähnt wurde.

Nachfolgend sind die pk-Werte der Adeninnucleotide (monomere Komplexe) und die Abstufung der mit unserer Methode gemessenen Empfindlichkeit (Zunahme der Peakstromhöhe) Zusammengestellt:

$$\begin{array}{ccccc} \text{ATP} & > & \text{ADP} & > & \text{AMP} \gg \text{Adenosin} \\ (pk = 6.13)^{22} & & (pk = 5.9)^{24} & & (pk = 3.18)^{24}\ (pk = 0.84)^{25} \end{array} \quad (1)$$

Auf Grund der unterschiedlichen Verfahren und der ebenso unterschiedlichen Methoden bei der Bestimmung der pk-Werte ist ein Vergleich exakt nicht möglich. Die obengenannten Werte wurden von verschiedenen Autoren gemessen und geben die Tendenz der Abstufung wieder. Die pk-Werte der Dimerisierung sind hierbei allerdings nicht berücksichtigt, da sie nur für ATP und ADP ermittelt wurden[25], sie liegen wesentlich höher[22].

Da auf Grund der Ergebnisse für die Reaktion an der Elektrodenoberfläche die Dimerisierung eine Rolle spielen muss, ist die dem Durchtrittsprozess vorgelagerte chemische Substitutionsreaktion wie folgt zu formulieren:

$$2\,[\text{ATPH}]_{ads}^{3-} + 2\,[\text{Cu}(\text{H}_2\text{O})_6]^{2+} \rightleftarrows [(\text{Cu ATPOH})_2]_{ads}^{6-} + 10\,\text{H}_2\text{O} + 4\,\text{H}^+ \quad (2)$$

Allerdings kann nicht ausgeschlossen werden, dass auch noch andere Cu-ATP-Komplexe in der Adsorptionsschicht gebildet werden.

Mit der obengenannten Gl. (2) ist aber noch keine Erklärung für die in Abb. 8 dargestellten Kurven, sowie für die starke Änderung der β-Werte im Verlauf der ATP-Konzentrationserhöhung (vor allem in Gegenwart von 10^{-3} M KCl) gegeben. Die von uns gemessenen β-Werte von 1.5 und darüber deuten auf Maxima 1. Art hin, d.h. von einer bestimmten ATP-Konzentration an (10^{-8} M) beginnt auf der Hg-Oberfläche trotz der Bedeckung mit oberflächenaktiven Substanzen eine Oberflächenströmung einzusetzen, wobei auch Potentialänderungen auftreten können[26]. Infolge der positiven Oberflächenladung der Hg-Tropfen in dem bestimmten Potentialbereich muss die Bewegung an der Hg-Oberfläche vom Tropfenhals zum Tropfenscheitel gerichtet sein und somit die Potentialdifferenz nach negativen Werten verschoben werden, wie das auch von uns gemessen wurde.

Die ungewöhnlich hohen β-Werte auch in Abwesenheit von ATP deuten auf einen Beschleunigungseffekt in Gegenwart von TBP hin.

Wir nehmen an, dass es sich dabei um einen Struktureffekt der Adsorptionsschicht des TBP handelt, d.h. die tetraedrisch strukturierten TBP-Moleküle verändern etwas die Lage zueinander in der Adsorptionsschicht, wodurch die Phosphorylgruppen näher aneinander rücken und somit günstigere Bedingungen für die stufenweise komplexe Substitution ergeben. Die Differentialkapazität ändert sich dabei nicht merklich, da die Alkylgruppen dabei immer zur Hg-Oberfläche zeigen[27].

Was den Einfluss von Cl^- Ionen (ClO_4^--Ionen sind ebenfalls in dieser Weise wirksam) anlangt, so besteht keine völlige Klarheit. Es ist aber anzunehmen, dass ein Einfluss auf die chemischen Reaktionen in der Adsorptionsschicht vorliegt. Möglicherweise können diese Anionen anstelle der OH-Ionen an der Dimerisierung der Cu-ATP-Komplexe in der Adsorptionsschicht teilnehmen.

ZUSAMMENFASSUNG

Im Rahmen elektrochemischer Studien an biologisch bedeutsamen Nukleotiden und Nukleosiden wurde anhand tensammetrischer Messungen gezeigt, dass ATP eine sehr hohe Oberflächenaktivität an der Hg-Elektrode besitzt. Die Oberflächenaktivität dieser Substanz ist u.a. von der Komplexbildung in der Lösung abhängig. Mit Übergangsmetallionen bilden sich im Bereich um pH = 5.0 Dimerenkomplexe aus, wodurch die Oberflächenaktivität gesteigert wird.

Diese Ergebnisse werden im Zusammenhang mit der Ausbildung von gleichstrompolarographischen Stromstärkepeaks in Gegenwart von Spurenkomplexen an ATP und Cu(II)-Ionen betrachtet. Diese Stromstärkepeaks treten bei Potentialen auf, bei denen die Cu(II)-Welle grösstenteils durch das ebenfalls in der Lösung vorhandene TBP inhibiert ist.

Die Zunahme der Stromstärke durch gesteigerte Mengen an ATP ergibt keine einfache funktionelle Abhängigkeit, sondern die Ergebnisse weisen darauf hin, dass ein zusätzlicher stromstärkesteigernder Vorgang eine Rolle spielt. Es wurde der Nachweis geführt, dass es sich dabei um Oberflächenströmungen auf der Hg-Elektrode handelt.

SUMMARY

In the field of electrochemical studies of biologically important nucleotides and nucleosides, it was shown by means of tensammetric measurements that ATP has a very high surface activity at the Hg electrode. The surface activity of the substances depends *inter alia* on the complex formation in solution. In the region of pH = 5.0 it forms dimeric complexes with transition metal ions which cause an increase in the surface activity.

These results are considered in relation with the formation of d.c. polarographic current peaks in the presence of trace complexes of ATP and Cu(II) ions. These current peaks occur at potentials at which the Cu(II) wave is largely inhibited by the TBP also present in the solution.

The increase in the current due to increased amount of ATP follows no simple functional dependence, but the results suggest that an additional current-increasing reaction plays a role. It is suggested that this may be connected with surface streaming of the Hg-electrode.

LITERATUR

1 J. HEATH, *Nature*, 158 (1946) 23.
2 N. G. LUTHY UND B. LAUB, *J. Pharm. Pharmacol.*, 8 (1956) 410.
3 F. A. MCGINN UND G. B. BROWN, *J. Am. Chem. Soc.*, 82 (1960) 3193.
4 V. VETTERL, *Collection Czech. Chem. Commun.*, 31 (1966) 2105.

5 V. VETTERL, *J. Electroanal. Chem.*, 19 (1968) 169.
6 B. JANIK UND P. J. ELVING, *Chem. Rev.*, 68 (1968) 295.
7 J. VOLKE, *Z. Anal. Chem.*, 224 (1967) 41.
8 D. A. KALBHEN UND H. J. KOCH, *Z. Klin. Chem.*, 5 (1967) 299.
9 E. MARTELL UND G. SCHWARZENBACH, *Helv. Chim. Acta*, 39 (1956) 653.
10 M. TETAS UND J. M. LOWENSTEIN, *Biochemistry*, 2 (1963) 351.
11 T. G. SPIRO, W. A. KJELLSTROM, M. ZEYDEL UND R. A. BUTOW, *Biochemistry*, 7 (1968) 859.
12 H. B. MARK JR., *J. Electroanal. Chem.*, 7 (1964) 276.
13 H. B. MARK JR. UND L. R. MCCOY, *Rev. Polarog. Kyoto*, 14 (1967) 122.
14 L. R. MCCOY, H. B. MARK JR. UND L. GIERST, *J. Phys. Chem.*, 72 (1968) 4637.
15 J. HEYROVSKÝ UND J. BABICKA, *Collection Czech. Chem. Commun.*, 2 (1930) 270.
16 C. G. MAIRANOVSKY, *Katalytische und kinetische Stufen in der Polarographie*, Verlag "Wissenschaft" Moskau, 1966.
17 A. CALUSARU, *J. Electroanal. Chem.*, 15 (1967) 269.
18 H. SOHR, bisher unveröffentlichte Ergebnisse.
19 W. LORENZ, F. MÖCKEL UND W. MÜLLER, *Z. Physik. Chem., (N.F.)* 25 (1961) 1199.
20 R. PHILIPPS, *Chem. Rev.*, 66 (1966) 501.
21 I. FELDMANN UND E. KEIL, *J. Am. Chem. Soc.*, 87 (1965) 3281.
22 M. M. KHAN UND A. E. MARTELL, *J. Phys. Chem.*, 66 (1962) 10.
23 H. BRINTZINGER, *Helv. Chim. Acta*, 44 (1961) 1199.
24 P. W. SCHNEIDER UND H. BRINTZINGER, *Helv. Chim. Acta*, 47 (1964) 992.
25 T. M. M. KHAN UND A. E. MARTELL, *J. Am. Chem. Soc.*, 84 (1962) 3037.
26 M. V. STACKELBERG UND H. FASSBENDER, *Z. Elektrochem.*, 62 (1968) 834.
27 H. SOHR, Publ. in Vorbereitung.

ELECTROANALYTICAL CHEMISTRY AND INTERFACIAL ELECTROCHEMISTRY
Elsevier Sequoia S.A., Lausanne Printed in The Netherlands

MILLICOULOMETRIC DETERMINATION OF n AND D WITH A MODIFIED DME AND EVALUATION OF THE NUMBER OF H_3O^+ IONS INVOLVED IN A POLAROGRAPHIC PROCESS

C. BIONDI AND L. BELLUGI
Istituto di Chimica Generale ed Inorganica, Università degli Studi, Roma (Italy)
(Received April 3rd, 1970)

INTRODUCTION

Many publications have dealt with the coulometric and millicoulometric determination of the number of electrons involved in a process at the dropping mercury electrode (DME)[1-10]. This work presents a simple cell by which it is possible to evaluate for diffusion controlled processes the number of electrons involved, n, and, independently, the diffusion coefficient D, of the depolarizer. For the determination of D, it is not necessary to know the concentration of the depolarizer. The cell can also be utilized in some cases for the determination of the number of H_3O^+ or OH^- ions involved in an electrode reaction.

THEORY

For a system that yields a diffusion controlled current the decrease of the concentration with the time during the electrolysis follows the equation[11]

$$dc_{(t)}/dt = i_{d(t)}/nFv \tag{1}$$

In eqn. (1) v and c_t are, respectively, the volume of the solution and the concentration of the depolarizer at a time t after the beginning of the electrolysis; F and n are the Faraday (96500 C) and the number of electrons for the process, respectively, and $i_{d(t)}$ is the diffusion current at time t. For processes at the DME, provided that the bulk of the solution during the electrolysis can be considered homogeneous with respect to its concentration, an equation for the average polarographic diffusion current may be introduced in eqn. (1).

It is known that the Ilkovic equation does not take into account the curvature of the electrode surface: this neglect may result in calculated currents different from those observed. Several equations have been derived which take into account the curvature of the DME, such as the one given by Koutecký[12]:

$$i_d = 0.627\, nFm^{\frac{2}{3}}\tau^{\frac{1}{6}}cD^{\frac{1}{2}}\left[1+3.4\,\frac{\tau^{\frac{1}{6}}D^{\frac{1}{2}}}{m^{\frac{1}{3}}}+\left(\frac{D^{\frac{1}{2}}\tau^{\frac{1}{6}}}{m^{\frac{1}{3}}}\right)^2\right] \tag{2}$$

If the quadratic term in eqn. (2) is neglected, the resulting equation is similar to those obtained by several authors[13-15], which differ only in the value of the con-

stant A:

$$i_d = 0.627\, nFm^{\frac{2}{3}}\tau^{\frac{1}{6}}cD^{\frac{1}{2}}\left(1 + \frac{A\tau^{\frac{1}{6}}D^{\frac{1}{2}}}{m^{\frac{1}{3}}}\right) \tag{3}$$

Since the quadratic term in the Koutecký equation amounts to at most 1%, we can neglect it for the purpose of the present application, so that the combination of eqns. (1) and (3) gives

$$dc_t/c_t = -(0.627\, m^{\frac{2}{3}}\tau^{\frac{1}{6}}D^{\frac{1}{2}}/v)[1+(A\tau^{\frac{1}{6}}D^{\frac{1}{2}}/m^{\frac{1}{3}})]dt \tag{4}$$

which, by integration and transformation into decimal logarithms, yields

$$\log(c_t/c_0) = -0.627\, m^{\frac{2}{3}}\tau^{\frac{1}{6}}D^{\frac{1}{2}}(1+Am^{-\frac{1}{3}}\tau^{\frac{1}{6}}D^{\frac{1}{2}})t/2.303\, v \tag{5}$$

In eqn. (5), c_0 is the concentration of the solution at the beginning of the electrolysis, D is the diffusion coefficient ($cm^2\ s^{-1}$), τ and m are, respectively, the drop time (s) and the mercury rate of flow ($g\ s^{-1}$), and A ($g^{\frac{1}{3}}\ cm^{-1}$) is a constant.

Under the stated conditions we have

$$i_{d(0)} = Kc_0 = sh_0 \tag{6}$$

and

$$i_{d(t)} = Kc_t = sh_t \tag{7}$$

where s is the recorder sensitivity, $i_{d(0)}$ and $i_{d(t)}$ are, respectively, the average diffusion current at the beginning of the electrolysis and at time t, h_0 and h_t are the corresponding recorder deflections, and K is a proportionality constant which corresponds to i_d/c in eqn. (3).

From (5), (6) and (7) we obtain:

$$\log(c_t/c_0) = \log(i_{d(t)}/i_{d(0)}) = \log(h_t/h_0) = -\vartheta t \tag{8}$$

where

$$\vartheta = 0.627\, m^{\frac{2}{3}}\tau^{\frac{1}{6}}D^{\frac{1}{2}}/2.303\, v + 0.627\, Am^{\frac{1}{3}}\tau^{\frac{1}{3}}D/2.303\, v \tag{9}$$

For experiments made with a given cell and electrode, several quantities which appear in eqn. (9) are either constant, like A and v, or may be considered constant, like m, since, for aqueous solutions and with a constant value of mercury pressure on the DME, its value is virtually independent of the solution or the potential of the electrode[16]. The quantities τ and D depend on the particular depolarizer and medium used, but, for a particular experiment, τ is constant and D is essentially constant since it varies only slightly with the concentration. If these conditions are satisfied, then the quantity ϑ is a constant for a given experiment and a plot of $\log(h_t/h_0)$ *vs.* time (or of $\log h_t$ *vs.* time) will give a straight line whose slope is ϑ. From ϑ it is possible to calculate, at least in principle, the value of D of the depolarizer, since all the other quantities in eqn. (9) are either known or measurable by simple means. It can be noted that the concentration does not appear in eqn. (9), so that D can be evaluated independently from a knowledge of c, the depolarizer concentration.

From eqns. (5), (6) and (7), the quantity of electricity used during an electrolysis that lasts t s can be obtained:

$$Q = \int_0^t i_t dt = \int_0^t i_0\, 10^{-\vartheta t}\, dt = (i_0 - i_t)/2.303\, \vartheta$$

The number of moles of the depolarizer correspondingly consumed at the electrode is $\Delta M = v(c_0 - c_t)$.

Since $nF\Delta M = Q$, it follows that the number of electrons involved in the reaction is:

$$n = (i_0 - i_t)/2.30\, F\vartheta\Delta M = 4.50 \times 10^{-6}\, i_0/\vartheta v c_0 \qquad (10)$$

An equation equivalent to (10) has already been applied to the calculation[4-7] of n, but the results have not been quite satisfactory.

EXPERIMENTAL

The apparatus used in this work is a polarographic cell whose nitrogen inlet permits a mercury pool to be used (Fig. 1). The DME capillary, ground at its tip,

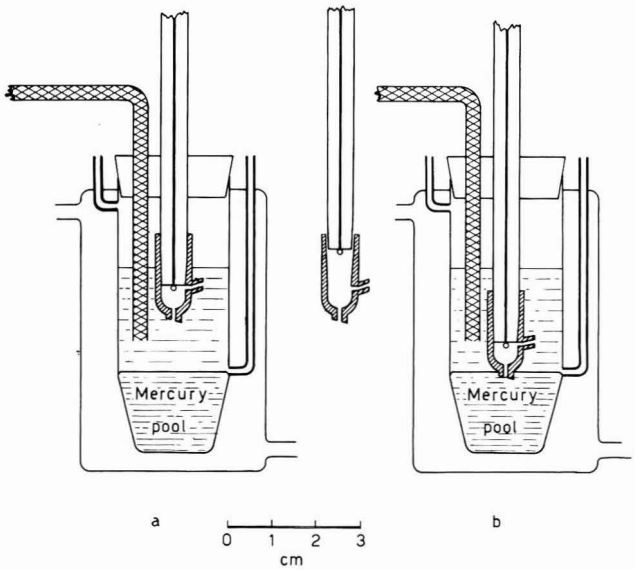

Fig. 1. Exptl. arrangement of the cell: (a) for normal polarograms, (b) for millicoulometry.

accommodates semi-permanently the microcell, ground likewise in the inner part of the top. The microcell has two openings, one on the side (length 0.2 cm, inside diameter 0.1 cm) at the level of the tip of the capillary, and one at the bottom (diameter 0.15 cm). The diameter of the microcell is 0.52 cm and its height about 0.70 cm; the volume, as measured with a microsyringe, is $v = 0.104 \pm 0.003$ ml. The characteristics of the capillary in 0.1 M KNO_3 at -1.00 V *vs.* SCE, under the mercury pressure used for all the experiments (120 cm), are $\tau = 7.9$ s and $m = 1.78 \times 10^{-3}$ g s^{-1} ($m^{\frac{2}{3}}\tau^{\frac{1}{6}} = 2.08 \times 10^{-2}$ g$^{\frac{2}{3}}$ s$^{-\frac{1}{2}}$).

When the cell, mounted on the capillary, is dipped in the mercury pool, it fills with the metal; if it is then raised, the mercury is replaced by the solution and the apparatus is ready to be used. Some care has to be used in order to avoid gas bubbles in the cell. In the position shown in Fig. 1a, a normal polarogram can be recorded

since the mercury drops falling through the lower opening allow fresh solution to come in from the side tube: polarograms recorded with and without the microcell, in otherwise identical conditions, gave the same results. In order to perform a microcoulometry, the cell is lowered so that the bottom opening becomes closed by the mercury pool, as in Fig. 1b. In this position (due to the high surface tension at the mercury–solution interface) the cell encloses a definite and reproducible volume of the solution. The side opening permits the electric contact to be established, while its geometry minimizes interdiffusion of the internal and external portions of the solution. A chronometer and the polarograph are started simultaneously so that the current is recorded while a known, constant potential difference is applied between the DME and a reference electrode, which is connected by an agar–agar salt bridge to the solution. The applied potential is chosen so as to correspond to the establishment of the diffusion current of the depolarizer: the electrolysis may be operated until about 20–30% of the depolarizer has reacted. The curves obtained in these experiments are of the type shown in Fig. 2b. A Sargent XXI polarograph was used: potentials are referred to the SCE and are uncorrected for *IR* drop. Values of the

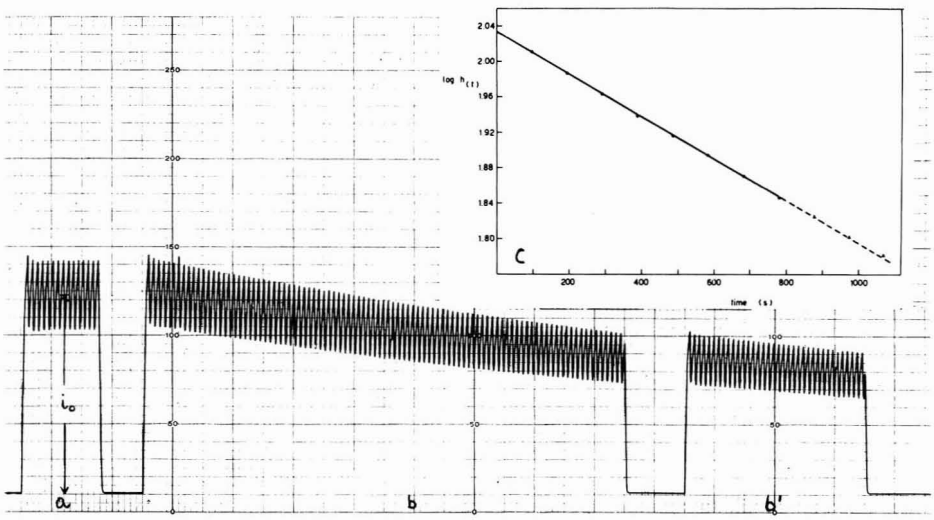

Fig. 2. Current–time curves for 1.12×10^{-3} *M* $TlNO_3$ in 0.1 *M* KNO_3; -1.20 V; $s = 0.06$ μA/mm, (a) Open cell, (b) closed cell, (b′) expt. (b), after about 100 s with the electrical circuit open, (c) plot of expt. (b) (full line) and b′ (broken line).

average diffusion current (recorded without damping) were measured at half of the oscillations and are corrected for the residual current.

The temperature for all experiments was $25.0 \pm 0.1°$ C. Analytical grade reagents were used to prepare the solutions which were deoxygenated with purified nitrogen. The value of the drop time was measured several times for each experiment: in all the cases considered in this paper, no change in drop time was detected during a single experiment.

In addition to the microcell already described, a slightly smaller one was made, (volume $= 0.098 \pm 0.003$ ml) and fitted to a capillary with the following characteristics:

$\tau = 4.9$ s, $m = 1.33 \times 10^{-3}$ g s^{-1} in 0.1 M KNO_3 at -1.00 V under a mercury pressure of 120 cm. Both cells gave concordant results, so that we report only those obtained with the first cell.

RESULTS AND DISCUSSION

Evaluation of n

In order to test the performance of the microcell in relation to eqns. (9) and (10), the behaviour of several species (whose diffusion coefficients and number of electrons involved in the respective electrode reactions were known) were examined.

Some typical results obtained with a solution of 1.18×10^{-3} M $Zn(ClO_4)_2$ and 0.1 M KNO_3 at -1.40 V are reported in Table 1 and in Fig. 3, where the values of $\log h_t$ as a function of time are plotted for four experiments. The values of ϑ and n are found reproducible within about 1 %. The values of n obtained by means of eqn. (10) are within 1 % of the true value: it is therefore reasonable to assume that the diffusion

TABLE 1

	$c_0 \times 10^3$/ mol l^{-1}	Supporting electrolyte	E_{app}/ V vs. SCE	Electrolysis time/s	$i_{d(0)}/\mu A$	$i_{d(t)}/\mu A$	$\vartheta \times 10^4/s^{-1}$	n
1.	1.18	0.1 M KNO_3	-1.40	970	7.80	5.55	1.43	2.02
2.	1.18	0.1 M KNO_3	-1.40	638	7.80	6.33	1.45	1.99
3.	1.18	0.1 M KNO_3	-1.40	1010	7.80	5.46	1.46	1.97
4.	1.18	0.1 M KNO_3	-1.40	582	7.80	6.46	1.45	2.01
							$\vartheta_{(av.)} = 1.45 \mp 0.01$	
							$n_{(av.)} = 1.99 \pm 0.02$	

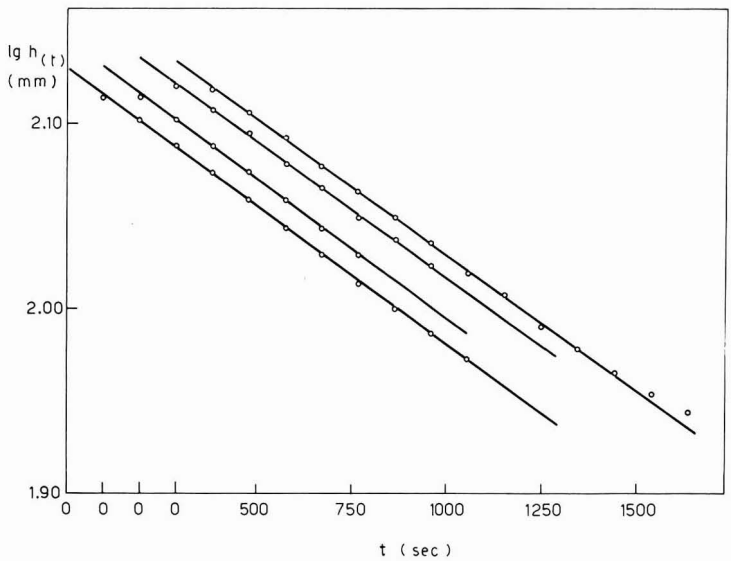

Fig. 3. Application of eqn. (8) to the cathodic currents of a 1.18×10^{-3} M solution of $Zn(ClO_4)_2$ in 0.1 M KNO_3; -1.40 V (see Table 1).

current values $i_{d(t)}$, during the electrolysis and at its end (about 15 min from the start of the experiments), are quite close to those corresponding to a homogeneous solution of concentration c_t. Were this not the case, a higher or lower value of ϑ would be obtained, while the ratio $4.50 \times 10^{-6}\ i_0/vc_0$ in eqn. (10) would of course retain its value; under these conditions, values of n above or below the true values would be found. Moreover, this substantial homogeneity of the solution, at least at the end of the electrolysis, has often been checked noting that the value of the current recorded at the end of an experiment is the same, within experimental error, as that found after some time (of the order of 1–2 min) has elapsed since the end of electrolysis with the polarographic circuit open and the microcell closed. During this time a possible inhomogeneity would presumably have disappeared, or at least undergone a modification, so that a change in the value of the current should have been found. The results of an experiment of this kind are shown in Fig. 2b, b′ and c.

Deviations from the linearity of the log h_t–time plots develop for electrolysis times longer than about 1000 s (depending on the particular species examined); this effect should be related to the building up of the concentration gradient between the electrolyzed portion of the solution and its bulk, so that some depolarizer diffuses inside the microcell through the side opening. However, during this time interval of 1000 s, some 20–30 % of the depolarizer can react at the electrode thus permitting the evaluation of ϑ and the detection of possible electrochemical processes of the reaction products by recording again the polarogram of the electrolyzed solution. It is also possible to characterize the reaction products by other methods, since, by withdrawing the microcell from the solution, its content can be recovered.

The results obtained for several species are shown in Fig. 4 and Table 2.

For the H_3O^+ ion, we have electrolyzed solutions of $HClO_4$ in 0.1 *M* KCl and 0.1 *M* KNO_3, at -1.65 V; in both cases the same value of ϑ was obtained. The solutions used contained $HClO_4$ of low enough concentration that waves exhibiting a regular plateau could be obtained. Under these conditions and for potentials between -1.60 and -1.70 V it is also found that the current follows the equation $i_d = Kc$. The value of ϑ for the OH^- ion has been obtained for concentrations less than 10^{-3} *M*, so that the relation $i_d = Kc$ is valid.

Evaluation of D

It is known that while the derivation of the Koutecky equation is quite rigor-

TABLE 2

Species	$c_0 \times 10^3$/ *mol* l^{-1}	*Supporting electrolyte*	E_{app}/ *V vs. SCE*	$\vartheta_{(av.)} \times 10^4/s^{-1}$	$\vartheta_{(av.)}\tau^{-\frac{1}{6}} \times 10^2/s^{-7/6}$	$n_{(av.)}$	$D \times 10^6$/ $cm^2\ s^{-1}$
Zn^{2+}	1.18	0.1 *M* KNO_3	−1.40	1.45	1.03	1.99	6.38^{18}
Cd^{2+}	0.59	0.1 *M* KNO_3 + 5×10^{-3} *M* $HClO_4$	−0.96	1.50	1.07	1.99	6.90^{18}
Pb^{2+}	0.57	0.1 *M* KNO_3	−1.00	1.64	1.17	2.02	8.28^{18}
Tl^+	1.08	0.1 *M* KNO_3	−1.20	2.50	1.78	1.00	18.20^{18}
OH^-	0.65	1.0 *M* KNO_3	+0.20	4.16	2.96	0.98	44.50^{26}
H_3O^+	0.63	0.1 *M* KCl	−1.65	6.00	4.38	0.98	86.30^{18}
	0.44	0.1 *M* KNO_3					

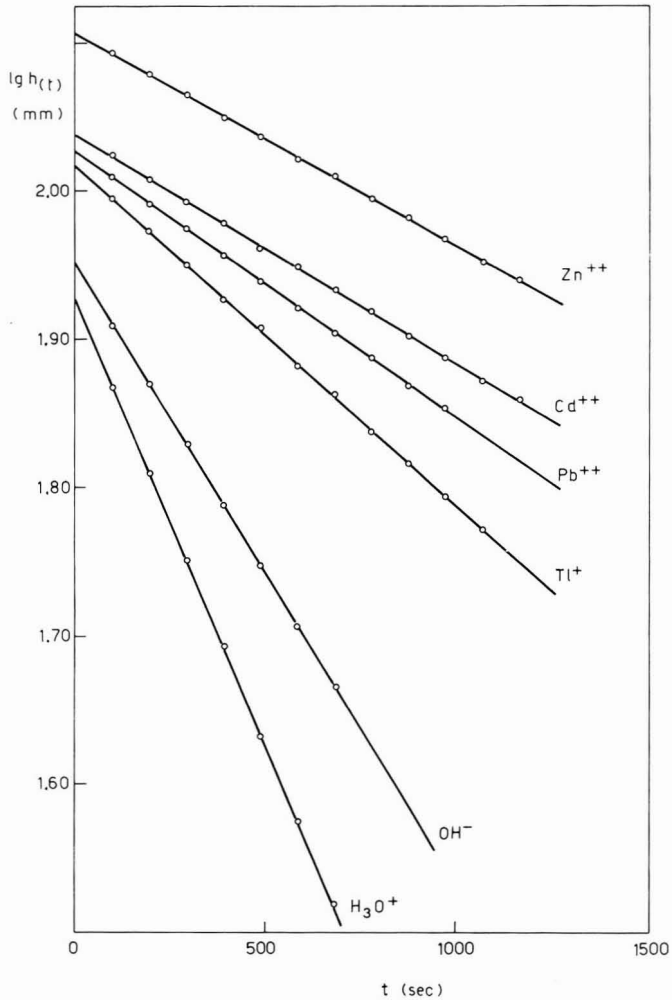

Fig. 4. Application of eqn. (8) to the currents of solutions of $Zn(ClO_4)_2$, $Cd(ClO_4)_2$, $Pb(NO_3)_2$, $TlNO_3$, NaOH, $HClO_4$ (see Table 2).

ous, its applicability in practical circumstances cannot be expected to hold with analogous rigor. In particular, the discrepancies can be expected to depend on the value of the constant of the correction term, so that instead of its theoretical value[17] ($A = 3.4626\ g^{\frac{1}{3}}\ cm^{-1}$) other values must be used in practice in order to apply the equation to polarographic data. As a consequence, the direct application of eqn. (9) to the evaluation of D, which depends on a precise knowledge of the A value, is not feasible. For our purposes, we shall use a relative method taking advantage of known values of D obtained from the literature. It is possible to make a standardization plot so that by interpolation unknown values of D for other depolarizers can be obtained from their ϑ values. In order to have a diagram valid for the different species, irrespective of the particular value of τ at which the corresponding ϑ's are evaluated, we can

rewrite eqn. (9) in the form:

$$\vartheta\tau^{-\frac{1}{6}} = aD^{\frac{1}{2}} + b\tau^{\frac{1}{6}}D \tag{11}$$

where $a = 0.627\ m^{\frac{2}{3}}/2.303\ v$ and $b = 0.627\ m^{\frac{1}{3}}\ A/2.303\ v$.

The plot of Fig. 5 shows the experimental values of $\vartheta\tau^{-\frac{1}{6}}$ for the different depolarizers *versus* the square root of their (known) diffusion coefficients, measured in the same media that we have used[18,26].

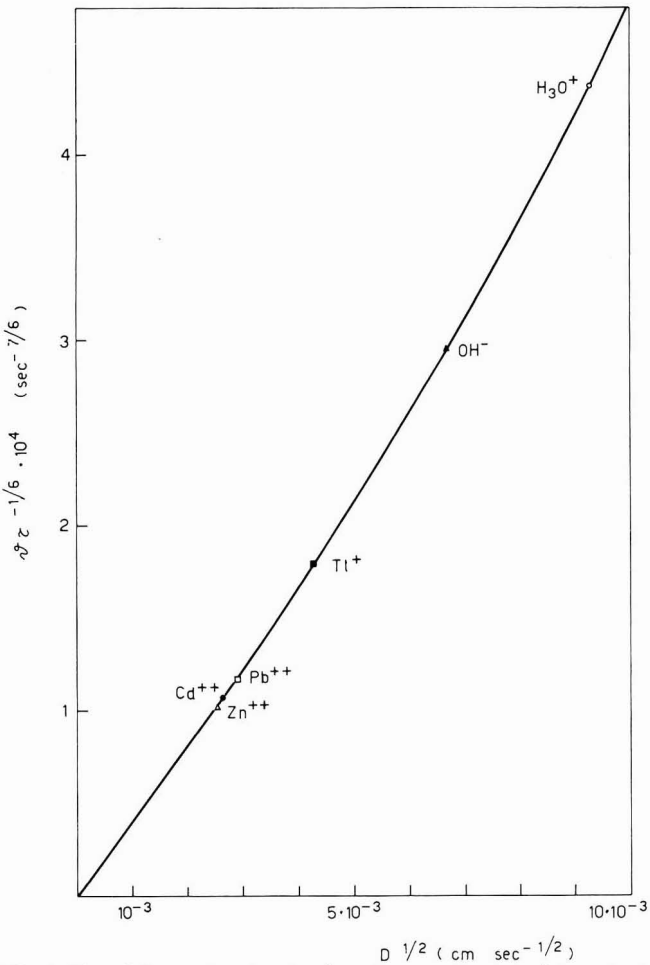

Fig. 5. Plot of the exptl. values $\vartheta\tau^{-\frac{1}{6}}$ *vs.* known values of $D^{\frac{1}{2}}$ (eqn. (11)).

The full line drawn in the Figure has been calculated making use of eqn. (11) with $A = 2.3\ g^{\frac{1}{3}}\ cm^{-1}$ and $\tau = 7.5$ s which is the average value of the experimentally measured τ's, for all the species considered, which involve a wide range of applied potentials.

On the other hand, the value of A has been deduced from the parameters of

the straight line, Fig. 6, which results from the graph of eqn. (9) written in the form:

$$\vartheta\tau^{-\frac{1}{6}}D^{-\frac{1}{2}} = a + b\tau^{\frac{1}{6}}D^{\frac{1}{2}} \qquad (11')$$

From the intercept, the value $a = 3.80 \times 10^{-2}$ is found and, from the slope, $b = 0.72$, so that it follows that $(b/a)m^{\frac{1}{3}} = A = 2.3\ \mathrm{g}^{\frac{1}{3}}\ \mathrm{cm}^{-1}$.

From the experimental value of a, a value of the microcell volume, $v = 0.105$ ml is found, in good agreement with the measured value (0.104 ml).

It can be seen from Fig. 5 that the experimental values of $\vartheta\tau^{-\frac{1}{6}}$ closely follow the parabolic curve of eqn. (11) with $A = 2.3\ \mathrm{g}^{\frac{1}{3}}\ \mathrm{cm}^{-1}$; variations of $\tau^{\frac{1}{6}}$ (in the second term of the equation) bring about differences which are lower than the experimental error.

The experimental data obtained with the second microcell have been treated in the same way: the results agree closely with those found with the first cell, with the notable exception of the value of the constant which is in this case $A = 2.0\ \mathrm{g}^{\frac{1}{3}}\ \mathrm{cm}^{-1}$.

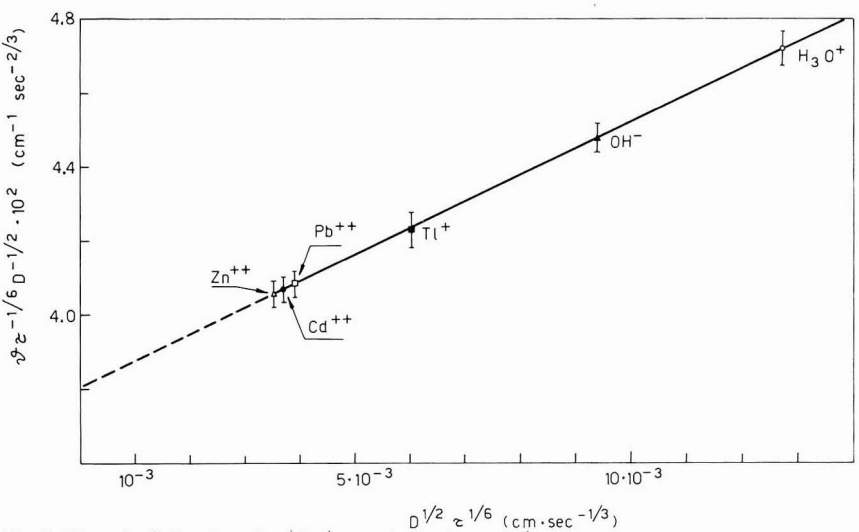

Fig. 6. Plot of calcd. values $\vartheta\tau^{-\frac{1}{6}}D^{-\frac{1}{2}}$ *vs.* calcd. values of $\tau^{\frac{1}{6}}D^{\frac{1}{2}}$ (eqn. (11')).

These results show that, at least in the limits of our experimental error (which we estimate at about 1 % in the values of ϑ), the experimental data may be adequately correlated by means of eqn. (3).

The graph of Fig. 6 shows that, under our conditions, for a given electrode A is really constant: different electrodes, however, exhibit different A values, a result which may be related to the depletion effect, which may differ from electrode to electrode.

Evaluation of n_H and n_{OH}

Dissolved oxygen can be titrated polarographically by adding a solution of standardized acid[19]; the H_3O^+ wave at the DME will appear only when its flux at the electrode is greater than the flux of the oxygen, taking into account the fact that four H_3O^+ are used up for every oxygen molecule reduced. This concept of equi-

valence of fluxes has been utilized for studies on anomalous waves[20,21], and its use has been suggested for the determination of the number of H_3O^+ involved in a polarographic process[19].

For a diffusion limited electrode reduction, the average current of the depolarizer is given by eqn. (3). From eqns. (3) and (9) it follows that the average number of moles of the depolarizer reaching the electrode per unit time is

$$\varphi_D = i_{d(D)}/nF = 2.303\ vc_D\ \vartheta_D \tag{12}$$

Correspondingly, the average number of equivalents of H_3O^+ ions reaching the electrode per unit time is

$$\varphi_H = i_{d(H)}/F = 2.303\ vc_H\ \vartheta_H \tag{12'}$$

In eqns. (12) and (12'), ϑ_H and ϑ_D are the rates of decrease of the current, respectively for the H_3O^+ ions and for the depolarizer (see D evaluation), both measured with the same electrode and cell, at the same potential and with the same mercury pressure used for the flux experiments; c_D and c_H are the bulk concentrations of the depolarizer and of the H_3O^+ ions. Provided that neither the depolarizer, nor the reduction products, take part in acid–base equilibria under the conditions of the experiments, it follows from (12) and (12') that when the amount of H_3O^+ ions taken up by the electrode reaction corresponds exactly to that reaching the electrode, the following equation is satisfied:

$$c_H^*\,\vartheta_H = n_H c_D\,\vartheta_D \tag{13}$$

In eqn. (13) n_H is the number of H_3O^+ ions involved in the reduction for each depolarizer particle, and c_H^* is a particular value of the H_3O^+ bulk concentration.

A reduction wave for H_3O^+ can then be polarographically recorded only if $c_H > c_H^*$, and eqn. (13) then becomes:

$$c_H\,\vartheta_H = i_H/2.3\ vF + n_H c_D\,\vartheta_D \tag{13'}$$

where i_H is the current due to excess H_3O^+.

From a graph of i_H *vs.* c_H, obtained at constant c_D, the value c_H^* may be evaluated.

Since by using the microcell ϑ_H and ϑ_D can be obtained in virtually the same conditions of the flux experiments (with the possible exception of the drop time), by applying eqn. (13) or (13') the value of n_H can be found.

It may be convenient to apply a correction to these equations in the case that ϑ_D and ϑ_H are obtained under quite different values of drop time.

The ϑ values can be transformed to those that would be found were the relative experiments performed with the same drop time as the flux experiments, thus:

$$\frac{\vartheta_D}{\vartheta_D'} = \frac{\tau^{\frac{1}{6}}\,(m^{\frac{1}{3}} + AD^{\frac{1}{2}}\tau^{\frac{1}{6}})}{\tau'^{\frac{1}{6}}\,(m^{\frac{1}{3}} + AD^{\frac{1}{2}}\tau'^{\frac{1}{6}})} \approx \left(\frac{\tau}{\tau'}\right)^{\frac{1}{6}} \tag{14}$$

$$\frac{\vartheta_H}{\vartheta_H''} \approx \left(\frac{\tau}{\tau''}\right)^{\frac{1}{6}} \tag{14'}$$

In these equations ϑ_D and ϑ_H are values related to the drop time, τ, of the flux experiments, ϑ_D' and ϑ_H'' are values obtained at drop times τ' and τ'', respectively. By

using eqns. (14) and (14'), eqn. (13) becomes:

$$c_H^* \vartheta_H'' (\tau'/\tau'')^{\frac{1}{6}} \cong n_H \vartheta_D' c_D \tag{15}$$

A similar method can be applied for oxidation reactions in alkaline solutions. In this case, the concentration and the diffusion coefficient of the OH^- ion are involved and eqn. (13) becomes

$$\vartheta_{OH} c_{OH}^* = n_{OH} \vartheta_D c_D \tag{16}$$

For reduction reactions in basic media and for oxidation reactions in acid solutions, the methods just described cannot be applied. For these conditions, however, a different approach can often be used by recording the anodic wave of the OH^- ion or the cathodic wave of the H_3O^+ ion (produced during the millicoulometry) and comparing them to those recorded before the electrolysis.

P-Benzoquinone

Millicoulometric determinations have been performed with a 4.85×10^{-4} M solution of *p*-quinone (Q), 1.58×10^{-3} M $HClO_4$ and 0.1 M KNO_3 at -0.80 V. Under these conditions, a value $D = 9.05 \times 10^{-6}$ cm^2 s^{-1} can be evaluated; the number of electrons found by eqn. (10) is $n = 1.99$ (Table 3a).

TABLE 3a
p-Quinone

$c_0 \times 10^3$/ mol l^{-1}	*Supporting electrolyte*	E_{app}/ *V vs. SCE*	$\vartheta_{(av.)} \times 10^4/s^{-1}$	$\vartheta_{(av.)} \tau^{-\frac{1}{6}} \times 10^2/s^{-7/6}$	$n_{(av.)}$	$D \times 10^6$/ $cm^2\ s^{-1}$
0.485	0.1 M KNO_3 + 1.58×10^{-3} M $HClO_4$	-0.80	1.84	1.27	1.99	9.05
1.45	Phosphate buffer 0.1 M pH 7.0	-0.80	1.70	1.20	1.98	8.45

TABLE 3b

$c_H \times 10^3/mol\ l^{-1}$	0.477	0.701	0.811	1.04	1.16	1.58
$i_H/\mu A$	1.80	3.95	5.20	7.75	8.80	12.90
$[Q] = 4.85 \times 10^{-4}$ M						

Polarographic curves have been obtained for solutions containing a constant concentration of Q 4.85×10^{-4} M, and increasing concentrations of $HClO_4$, between 4.77×10^{-4} M and 1.58×10^{-3} M. The graph of the excess hydrogen ion diffusion current (at -1.65 V) *versus* the analytical concentration of the strong acid gives $c_H^* = 3.0 \times 10^{-4}$ M for zero current (Table 3b). Since in 0.1 M KNO_3, $\vartheta_H = 6.0 \times 10^{-4}$, application of eqn. (15) gives $n_H = 2.02$.

It is known[22] that the overall reduction of Q follows the reaction (H_2Q is hydroquinone) $Q + 2\ H_3O^+ + 2e \rightarrow H_2Q + 2\ H_2O$ so we conclude that the millicoulometric method gives in this case reasonably accurate values of n and n_H.

The value of D obtained in these conditions for the quinone is appreciably different from that ($D = 8.4 \times 10^{-6}$ cm^2 s^{-1}) reported in the literature[23]. The latter

value has been obtained, however, in a phosphate buffer at pH 7.0; a better accord results ($D = 8.45 \times 10^{-6}$ cm^2 s^{-1}) when ϑ is measured in the same medium (Table 3a).

Chromate ion

Chromate ion gives, in alkaline media, a well developed diffusion controlled reduction wave[24].

Millicoulometric experiments were carried out with a 1.26×10^{-4} *M* solution of K_2CrO_4, 4.54×10^{-4} *M* NaOH and 0.1 *M* KNO_3, at -1.24 V. At the end of the electrolysis, the anodic wave of the OH^- ions was recorded and compared with the wave corresponding to the OH^- concentration in the bulk of the solution, recorded with the cell open, before the electrolysis. An increase in the OH^- concentration, ($\Delta[OH^-]$) was found. The fraction of CrO_4^{2-} ion transformed during the electrolysis is obtained from the decrease of its wave. From the ratio $\Delta[OH^-]/\Delta[CrO_4^{2-}]$ a value $n_{OH} = 3.96$ is obtained (Table 4) for the number of OH^- ions produced for every CrO_4^{2-} ion reduced. From the millicoulometric data (Table 4) a value $n = 3.01$ is evaluated, so that the reduction reaction for CrO_4^{2-} ion can be written $CrO_4^{2-} + 3e + 2H_2O \rightarrow CrO_2^- + 4\ OH^-$, in accord with other data[24].

The ϑ obtained gives for this ion a value of *D* about 9 % lower than that which may be calculated from conductivity data[25] (1.07×10^{-5} cm^2 s^{-1}). However, it is known that differences of this order of magnitude are also found for the *D* values of other species, when data obtained at high dilution and at $\mu = 0.1$ are compared.

TABLE 4
K_2CrO_4

$c_0 \times 10^3$/ mol l^{-1}	Supporting electrolyte	E_{app}/ V vs. SCE	$\vartheta_{(av.)} \times 10^4$/s^{-1}	$\vartheta_{(av.)} \tau^{-\frac{1}{6}} \times 10^2$/s$^{-7/6}$	$n_{(av.)}$	$D \times 10^6$/ cm^2 s^{-1}
0.126	0.1 *M* KNO_3 + 4.54×10^{-4} *M* NaOH	-1.24	1.82	1.29	3.01	9.75

Electrolysis time/s	CrO_4^{2-}		OH^-		$\Delta[CrO_4^{2-}]$/mol	$\Delta[OH^-]$/mol	n_{OH}
	$i_0/\mu A$	$i_t/\mu A$	$-i_0/\mu A$	$-i_t/\mu A$			
679	1.55	1.04	3.30	4.50	4.30×10^{-9}	1.70×10^{-8}	3.96

CONCLUSION

In order to obtain the *n* value of a depolarizer from its rate of current decrease the electrolysis of a relatively small volume of solution has been performed by some authors[4-7], who have applied equations equivalent to eqn. (10) to the evaluation of the data.

Too high values of *n* have been found, with errors of the order of 10 %; these systematic errors have been related either to a partial redissolution of the metals from the amalgams (formed in the reduction of the respective ions[28]) or to a depletion effect in the vicinity of the electrode[6,27].

The present results are not compatible with the first explanation; as for the second, we feel that a depletion effect near the electrode would result in a faster decrease of the current and in a lower value of n (rather than higher) for continuous electrolysis experiments which involve the transformation of only a portion of the depolarizer (of the order of 20%). We are inclined to assume another possibility. During the electrolysis, the drops fall and continuously transport some of the depleted solution towards the bottom of the cell, where, in the absence of an efficient mechanism of stirring, a region of lower than average concentration forms. Under these conditions, in regions relatively close to the electrode, there is higher concentration than average which, in turn, would give a higher current than that which would be recorded if the solution were homogeneous. This would lead to a lower value for ϑ and a higher n would be found (eqn. (10)).

The improved results obtained with the cells used in the present work may be attributed to their quasi-hemispherical geometry and small capacity, which possibly allow a better homogenization of the enclosed solutions, operated by the mercury drops which fall from the electrode. While in principle it would be safer to use a three-electrode system for the electrolyses[10] (particularly when operated for long times), in the present cases no difficulties have been encountered by using the two-electrode arrangement. With these modified electrodes some difficulties and the related errors may also be eliminated, such as those encountered in keeping the volume constant while deaerating the solutions, or those inherent in the use of a reference electrode with a bridge in contact with the contents of the cell. In the latter case, some of the depolarizer may diffuse in the bridge, or some of the electrolytic solution of the bridge may be transferred in the cell during the electrolysis, thus altering the volume of the solution and its composition. From a practical point of view the cell does not need to be detached from the electrode other than in exceptional circumstances, since the rigid system cell–electrode can be easily cleaned once removed from the polarographic cell.

Repeated determinations of ϑ, if needed, are easily made by redipping the capillary two or three times in the mercury pool and withdrawing it, so that a fresh sample can be subjected to electrolysis. The ratio i_0/c_0, needed to evaluate n from eqn. (10), is obtained with the cell not in contact with the mercury pool, Fig. (1a), a condition which permits also the recording of a conventional polarogram. It would not be correct to obtain i_0/c_0 from the i_0 value of a coulometric experiment, since the first drop does not encounter any transference of concentration polarization, so that a higher current is recorded (Fig. 2a, b, c). The transference effect makes itself felt for the drops following: the adoption of a practical value of the constant A takes it into account.

There are limitations to the practical advantages of the cell proposed here. Some experience is needed in order to obtain the best results; it is important, of course, to avoid vibrations while the electrolyses are performed. Great care has to be used in grinding the DME, since only with difficulty can it be unclogged once the capillary becomes contaminated during the grinding operations. Moreover, the applicability of the modified electrode, as presented here (and of eqns. (9), (10), (15) and (16)) is limited to diffusion controlled processes; n_H or n_{OH} values can be evaluated by eqns. (15) or (16) only when the depolarizers and the reaction products do not establish acid–base equilibria under the experimental conditions.

From eqn. (9) it can be seen that the rate of decrease of the current, for a given cell and electrode, depends practically only on the value of D, not on the value of n nor on the depolarizer concentration in the solution. It follows that, since in general D changes only slightly with c, the same value of ϑ should be found for a depolarizer in a rather extended range of its concentration values in a given medium. Differences larger than expected from the estimated experimental errors among the values of ϑ found at different concentrations of a depolarizer, will then point to difficulties in the applicability of eqns. (9), (10) and (15) or (16). One such case would be a possible chemical interaction of the electrode reaction products with the untransformed depolarizer before it reaches the electrode surface. Difficulties of this kind have already been discussed in the literature[29].

In conclusion, while we believe that the modified electrode used in the present work cannot be used (because of uncertainties in the value of the constant A in eqn. (9)) to evaluate absolute values of D, its standardization with species of known diffusion coefficients permits unknown values of D for other species to be found, with errors of the order of 2–4%. In particular, it could be useful when it is not possible, or is difficult, to know the concentration of the depolarizer as for some systems of biological interest. For the evaluation of n, and of n_H or n_{OH}, it is of course necessary to know the depolarizer concentration.

ACKNOWLEDGEMENT

One of us (L.B.) is grateful to the National Research Council of Italy for the grant of a research fellowship.

SUMMARY

A DME connected with a microcell is proposed for the millicoulometric determination of n and D of electroactive species; the apparatus may also be employed for the evaluation of the number of H_3O^+ or OH^- ions involved in an electrode process. These applications are possible, with some limitations, provided that the electrochemical reactions are diffusion controlled; for the determination of D, the concentration of the depolarizer need not be known.

REFERENCES

1 J. J. LINGANE, *J. Am. Chem. Soc.*, 67 (1945) 1916.
2 E. VECCHI, *Atti Ist. Veneto Sci., Lettere Arti, Parte II*, 107 (1949) 181.
3 L. MEITES AND T. MEITES, *J. Am. Chem. Soc.*, 72 (1950) 3686.
4 G. A. GILBERT AND E. K. RIDEAL, *Trans. Faraday Soc.*, 47 (1951) 396.
5 P. LANZA AND A. CORBELLINI, *Rend. Accad. Nazl. Lincei, Classe Sci. Fis. Mat. Nat.*, 6 (1952) 406.
6 S. BOGAN, L. MEITES, E. PETERS AND J. M. STURTEVANT, *J. Am. Chem. Soc.*, 73 (1951) 1584.
7 G. F. REYNOLDS AND H. J. SHALGOSKY, *Anal. Chim. Acta*, 10 (1954) 386.
8 T. DE VRIES AND J. L. KROON, *J. Am. Chem. Soc.*, 75 (1953) 2486.
9 R. D. WEAVER AND G. C. WHITNACK, *Anal. Chim. Acta*, 18 (1958) 51.
10 J. MASEK, *J. Electroanal. Chem.*, 1 (1960) 416.
11 P. DELAHAY, *New Instrumental Methods in Electrochemistry*, Interscience Publishers, New York, 1954, p. 294.
12 J. KOUTECKÝ, *Czech. J. Phys.*, 2 (1953) 50.

13 J. J. LINGANE AND B. A. LOVERIDGE, *J. Am. Chem. Soc.*, 72 (1950) 438.
14 H. STREHLOW AND M. VON STACKELBERG, *Z. Elektrochem.*, 54 (1950) 51.
15 T. KAMBARA AND J. TACHI, *Bull. Chem. Soc. Japan*, 23 (1950) 226.
16 J. HEYROVSKÝ AND J. KŮTA, *Principles of Polarography*, Publishing House of the Czechoslovak Academy of Sciences, Prague, 1966 p. 37.
17 J. NEWMAN, *J. Electroanal. Chem.*, 15 (1967) 309.
18 J. HEYROVSKÝ AND J. KŮTA, *Principles of Polarography*, Publishing House of the Czechoslovak Academy of Sciences, Prague, 1966, p. 106.
19 J. M. KOLTHOFF AND J. J. LINGANE, *Polarography, Vol. 1*, Interscience Publishers, New York, 2nd edn., 1952, p. 110.
20 J. J. LINGANE, *Ph. D. Thesis*, University Minnesota, 1938.
21 J. J. LINGANE AND L. W. NIEDRACH, *J. Am. Chem. Soc.*, 71 (1949) 196.
22 J. M. KOLTHOFF AND J. J. LINGANE, *Polarography, Vol. 1*, Interscience Publishers, New York, 2nd edn., 1952, p. 248.
23 J. M. KOLTHOFF AND J. J. LINGANE, *Polarography, Vol. 1*, Interscience Publishers, New York, 2nd edn., 1952, p. 252.
24 J. M. KOLTHOFF AND J. J. LINGANE, *Polarography, Vol. 2*, Interscience Publishers, New York, 2nd edn., 1952, p. 455.
25 J. HEYROVSKÝ AND J. KŮTA, *Principles of Polarography*, Publishing House of the Czechoslovak Academy of Sciences, Prague, 1966, p. 105.
26 R. N. ADAMS, *Electrochemistry at Solid Electrodes*, Marcel Dekker, New York, 1969, p. 221.
27 J. HEYROVSKÝ AND J. KŮTA, *Principles of Polarography*, Publishing House of the Czechoslovak Academy of Sciences, Prague, 1966, p. 277.
28 P. DELAHAY, *New Instrumental Methods in Electrochemistry*, Interscience Publishers, New York, 1954, p. 295.
29 L. MEITES, *Polarographic Techniques*, Interscience Publishers, New York, 2nd edn., 1965, p. 527.

ELECTROANALYTICAL CHEMISTRY AND INTERFACIAL ELECTROCHEMISTRY
Elsevier Sequoia S.A., Lausanne – Printed in The Netherlands

UNTERSUCHUNGEN ZUR BESTIMMUNG VON AUSTAUSCHSTROMDICHTEN AN REDOXSYSTEMEN DES KOBALTS MIT UNTERSCHIEDLICHEN LIGANDEN

H. BARTELT

Sektion Chemie der Humboldt-Universität zu Berlin, 108 Berlin, Bunsenstr. 1 (D.D.R.)

(Eingegangen am 3. Februar 1970)

1. EINLEITUNG

In der homogenen Kinetik sind Redoxreaktionen vom Typ

$$Ox_1 + Red_2 \rightarrow Ox_2 + Red_1 \qquad (1)$$

in grosser Zahl untersucht worden, deren Ergebnisse in zusammenfassenden Artikeln dargelegt wurden[1-3]. Beschränkt man sich bei der Auswahl der Redoxsysteme auf Reaktionen die nach dem outer-sphere-Mechanismus verlaufen, dann gewinnen die Ergebnisse dieser homogenen Austauschvorgänge noch an Bedeutung, weil es mit Hilfe einer von Marcus[4] entwickelten Beziehung

$$k_{12} = (k_{11} \cdot k_{22}/K_{12} \cdot f)^{\frac{1}{2}} \qquad (2)$$

möglich wird die homogene Geschwindigkeitskonstante (k_{11} oder k_{22}) eines der beiden Redoxsysteme bei Kenntnis von k_{12} und k_{11} oder k_{22} zu berechnen.

Die Übertragung dieser Vorstellungen auf elektrochemische Durchtrittsreaktionen, die ebenfalls nach dem outer-sphere-Mechanismus ablaufen sollten, erscheint zunächst wenig erfolgversprechend. In vorangehenden Untersuchungen[5-7] an Redoxsystemen des Kobalts konnten wir durch die Bestimmung der Austauschstromdichten von $Co(Diamin)_3^{2+}/Co(Diamin)_3^{3+}$-Redoxsystemen an Platinelektroden nachweisen, dass die Geschwindigkeitskonstanten für den Elektronenaustausch zwischen beiden Redoxpartnern des Kobalts empfindlich durch die Art der Liganden beeinflusst werden. Weiterhin konnte gezeigt werden, dass sich die Gleichgewichtspotentiale dieser Redoxsysteme nur um maximal 20 mV ändern, wenn man vom Redoxsystem

$Co\ en_3^{2+}/Co\ en_3^{3+}$, $E_0 = -495 \pm 2$ mV zum Redoxsystem
$Co\ chn_3^{2+}/Co\ chn_3^{3+}$, $E_0 = -515 \pm 2$ mV übergeht.*
(Alle Potentialangaben gegen G.K.E.)

Diese verhältnismässig geringe Differenz der Gleichgewichtspotentiale bewog uns zur Untersuchung von Redoxsystemen, die wir in Anlehnung an die Gl. (1) wie folgt formulieren können:

* In dieser Arbeit bedeuten: en—Äthylendiamin, pn—1,2-Propandiamin, bn—2,3-Butandiamin, chn—1,2-Cyclohexandiamin.

$$Co(L_a)_3^{2+} \rightarrow Co(L_a)_3^{3+} + e \quad (3)$$
$$Co(L_b)_3^{2+} \leftarrow Co(L_b)_3^{3+} + e \quad (4)$$

L_a und L_b sind dabei unterschiedliche Komplexbildner, jedoch sind beide vom Diamintyp.

Liegen die beiden Ionen des Redoxsystems mit unterschiedlichen Koordinationssphären in Lösung vor, so erhebt sich die Frage, wieweit sie kinetisch stabil sind, d.h. ob sie ihre Liganden nicht schon vor Ablauf der Durchtrittsreaktion austauschen.

Die Kobalt(III)-Verbindungen mit Diaminen als Komplexbildner sind als inerte Komplexe mit hohen Stabilitätskonstanten bekannt, die Werte sind in den vorangehenden Arbeiten[5-7] angegeben.

Anders ist dagegen das Verhalten der Kobalt(II)-Verbindungen, sie sind kinetisch instabil und tauschen die Liganden mit hoher Geschwindigkeit aus, wie es erst kürzlich an Kobalt(II)-hexamminionen nachgewiesen wurde[8]. Wegen der ausserdem vorhandenen geringeren thermodynamischen Stabilität der Kobalt(II)-Diaminkomplexe haben wir stets mit einem Überschuss an Komplexbildner (0.1 *M* Diamin) gearbeitet. Diese Arbeitsweise wurde auch bei den vorliegenden Untersuchungen übernommen, deshalb muss z.B. das Redoxsystem $Co\,en_2^{2+}/Co\,chn_3^{3+}$ in einem Überschuss an en als Komplexbildner untersucht werden. Die kinetische Instabilität der Co(II)-Komplexionen hat zur Folge, dass die während des Reduktionsvorganges an der Elektrode gebildeten Co(II)-Ionen mit dem in der Lösung vorhandenen Überschuss des Komplexbildners in folgender Weise weiterreagieren:

$$Co\,chn_3^{3+} + e \xrightarrow[\text{reaktion}]{\text{Elektroden-}} Co\,chn_3^{2+} \quad (5)$$

$$Co\,chn_3^{2+} + 3\,en \rightarrow Co\,en_3^{2+} + 3\,chn \quad (6)$$

Dabei bilden sich in geringer Konzentration $Co\,en_3^{2+}$-Ionen, die die Lage des Redoxpotentials um wenige mV verschieben. Bei diesen Untersuchungen erweist sich die Anwendung der rotierenden Scheibenelektrode als ein besonderer Vorteil, weil die nach Gl. (6) gebildeten Co(II)-Ionen infolge der Strömungsverhältnisse an der Elektrode sofort in das Innere der Lösung transportiert und dadurch stark verdünnt werden.

Die Anwendung der Gl. (2) auf elektrochemische Durchtrittsreaktionen ergibt:

$$k_{el12} = (k_{el11} \cdot k_{el22}/K_{12} \cdot f)^{\frac{1}{2}} \quad (7)$$

f kann nach

$$\ln f = \ln K_{12}/4 \ln (k_{11} \cdot k_{12}/Z^2) \quad (8)$$

berechnet werden[4]. Daraus ergibt sich jedoch, dass $f \rightarrow 1$ wenn $K_{12} \rightarrow 1$. Bei unseren Untersuchungen handelt es sich in jedem Fall um den Elektronenaustausch von Kobalt-Tris-Diaminkomplexionen, deren Gleichgewichtskonstante K_{12} nach

$$\Delta E\, n\, F = RT \ln K_{12} \quad (9)$$

aus der Differenz der Redoxpotentiale beider Redoxsysteme berechnet werden kann.

Für die Reaktion nach Gl. (3) und (4), bei einer maximalen Differenz der Redox-

potentiale von 20 mV erhält man einen Wert von

$$\log K_{12} = 0.338 \tag{10}$$

Bei allen übrigen Redoxsystemen ist log K_{12} noch geringer. Wir wollen daher für die Gleichgewichtskonstante $K_{12} = 1$ setzen, weil andere Störungen, wie z.B. die Reaktion nach Gl. (6) und die Auswertung der Versuchsergebnisse durch Extrapolation, grössere Fehler ergeben. Daher haben wir bei den folgenden Berechnungen die vereinfachte Gleichung

$$i_{012} = (i_{011} \times i_{022})^{\frac{1}{2}} \tag{11}$$

angewandt.

2. EXPERIMENTELLES

Die Verfahren zur Herstellung der Komplexverbindungen und Lösungen entsprechen den früheren Angaben[5-7]. Als Leitelektrolyt wurde 1 *N* KCl verwendet. Die Kobalt(II)-Komplexe wurden erst in der Lösung aus $CoCl_2 \cdot 6\,H_2O$ und einem der Komplexbildner hergestellt. Nach Potentialkonstanz wurde die Kobalt(III)-Komplexverbindung in Lösung aus einer Bürette zugesetzt und unmittelbar danach mit der Messung begonnen.

Die Gleichgewichtspotentiale zeigten im Gegensatz zu früheren Untersuchungen eine schwache Rührabhängigkeit, die bei einigen Konzentrationsverhältnissen bis 5 mV betrug. Diese Rührabhängigkeit des Potentials deuten wir durch den Ablauf der Reaktionen nach Gln. (5) und (6). Deshalb wurde nach jeder Änderung der Rührgeschwindigkeit das Gleichgewichtspotential erneut eingestellt.

Die Bestimmung der Austauschstromdichte erfolgte in der früher beschriebenen Weise[5]. Alle Messungen wurden bei $25 \pm 0.2°$ C durchgeführt.

3. ERGEBNISSE UND DISKUSSION

Die Konzentration der Co en_3^{3+}-, Co pn_3^{3+}- und Co bn_3^{3+}-Ionen wurde jeweils um eine Zehnerpotenz von 1×10^{-4}–1×10^{-3} *M*, bei Konstanthaltung der jeweiligen Co(II)-Konzentration (1 m*M*) variiert. (Abb. 1 und 2)

Die Messungen in 0.1 *M* chn erwiesen sich als schwierig. Es war schon bei der Untersuchung des Co chn_3^{2+}/Co chn_3^{3+}-Redoxsystems[7] beobachtet worden, dass hier in noch stärkerem Masse als bei den übrigen Redoxsystemen Bedeckungsvorgänge auf der Elektrodenoberfläche die Durchtrittsreaktionen beeinflussen, wobei angenommen wurde, dass neben den Co^{III}- auch die Co^{II}-Komplexionen bedeckend wirken.

Daher konnte in den Lösungen mit 1 m*M* Co chn_3^{2+} (0.1 *M* chn) die Austauschstromdichte in Abhängigkeit von der Co^{III}-Konzentration nur noch im Konzentrationsbereich von 2×10^{-5}–1×10^{-4} *M* bestimmt werden, oberhalb dieses Konzentrationsbereiches überwiegen die Bedeckungsvorgänge (Abb. 3).

Als Bezugspunkt für anzustellende Vergleiche wurde für jede Messreihe die Austauschstromdichte beim äquimolaren Konzentrationsverhältnis (1 m*M*) beider Redoxpartner gewählt.

Die Austauschstromdichten der einzelnen Redoxsysteme i_{011}, i_{022} sind vorangegangenen Arbeiten entnommen[5-7].

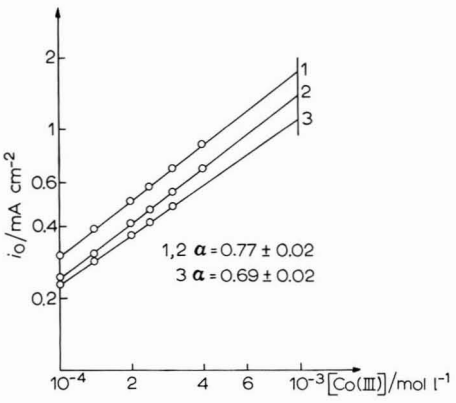

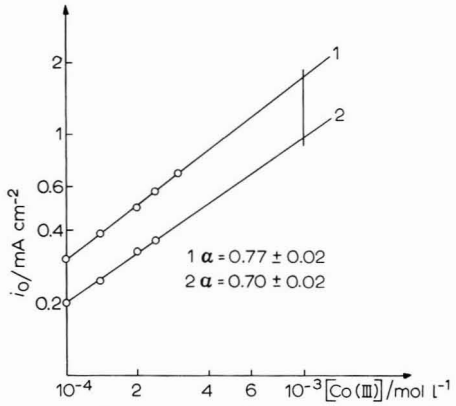

Abb. 1. Änderung der Konzentration der (1) Co pn_3^{3+}-, (2) Co bn_3^{3+}-, (3) Co chn_3^{3+}-Ionen von 1×10^{-4}–1×10^{-3} *M* bei Konstanz der Co en_3^{2+}-Konzentration ($c = 1$ m*M*).

Abb. 2. Änderung der Konzentration der (1) Co en_3^{3+}-, (2) Co chn_3^{3+}-Ionen von 1×10^{-4}–1×10^{-3} *M* bei Konstanz der Co pn_3^{2+}-Konzentration ($c = 1$ m*M*).

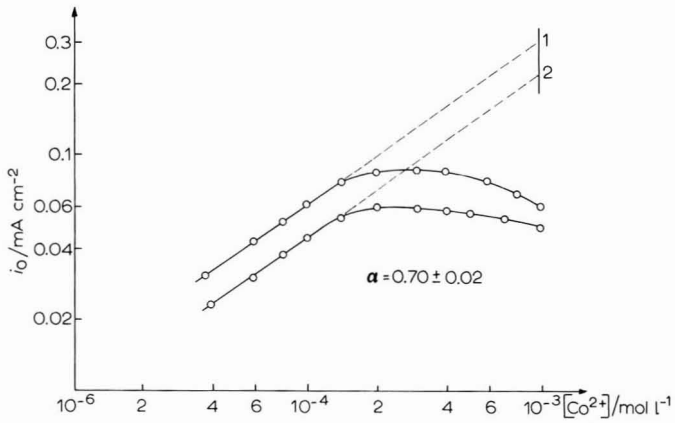

Abb. 3. Änderung der Konzentration der (1) Co en_3^{3+}-, (2) Co pn_3^{3+}-Ionen von 2×10^{-5}–1×10^{-3} *M* bei Konstanz der Co chn_3^{2+}-Konzentration ($c = 1$ m*M*).

TABELLE 1

Nr.	*Redoxsystem*	i_{011}/*mA cm*$^{-2}$	i_{022}/*mA cm*$^{-2}$	i_{012} (*beob.*)/ *mA cm*$^{-2}$	i_{012} (*ber.*)/ *mA cm*$^{-2}$
1	Co en_3^{2+}/Co pn_3^{3+}	2.4*	1.35	1.75	1.8
2	Co en_3^{2+}/Co bn_3^{3+}	2.4*	1.0	1.42	1.55
3	Co en_3^{2+}/Co chn_3^{3+}	2.4*	0.072	1.12	0.416
4	Co pn_3^{2+}/Co en_3^{3+}	1.35	2.4	1.75	1.8
5	Co pn_3^{2+}/Co chn_3^{3+}	1.35	0.072	1.0	0.312
6	Co chn_3^{2+}/Co en_3^{3+}	0.072	2.4	0.3	0.416
7	Co chn_3^{2+}/Co pn_3^{3+}	0.072	1.35	0.22	0.312

* Im Gegensatz zur vorangegangenen Arbeit[5] wurde hier mit 0.1 *M* en als Komplexbildner gearbeitet.

Die Ergebnisse der vorliegenden Untersuchungen sind in Tabelle 1 (Spalte 3) aufgeführt. Die Austauschstromdichten i_{012} der Redoxsysteme 1, 2 und 4 zeigen eine relativ gute Übereinstimmung mit den berechneten Werten nach Gl. (11) (Spalte 4). Auch die Austauschstromdichte für das Co bn_3^{2+}/Co bn_3^{3+}-Redoxsystem[6] ($i_0 = 1$ mA cm^{-2}) wird durch die vorliegenden Untersuchungen bestätigt.

Enorme Abweichungen ergeben sich aber für alle Redoxsysteme (3,5,6,7) die chn als Komplexbildner enthalten. Das trifft auch für die Durchtrittsfaktoren zu.

Für die Redoxsysteme 1,2 und 4 wurden folgende Werte bestimmt:

$$\left(\frac{\partial \log i_0}{\partial \log Co^{III}}\right)_{Co^{II}} = \alpha = 0.77 \pm 0.02; \quad \left(\frac{\partial \log i_0}{\partial \log Co^{II}}\right)_{Co^{III}} = 1 - \alpha = 0.23 \pm 0.02$$

Dagegen wurde für die Redoxsysteme 3 und 5 der Durchtrittsfaktor bei Änderung der Co chn_3^{3+}-Konzentration zu $\alpha = 0.70 \pm 0.03$ bestimmt. Diese Abweichung wird wahrscheinlich durch die Bedeckung der Elektrode mit chn hervorgerufen, wenn die Co chn_3^{3+}-Ionen nach dem Elektronenübergang weiter nach Gl. (6) reagieren. Die dadurch bedingte Verringerung der freien Oberfläche führt zu kleineren Austauschstromdichten.

Die Austauschstromdichten der Redoxsysteme 3 und 5 (Tabelle 1) deuten daraufhin, daśs der für das Redoxsystem Co chn_3^{2+}/Co chn_3^{3+} eingesetzte Wert von $i_0 = 0.072$ mA cm^{-2} viel zu niedrig und durch Bedeckungsvorgänge verfälscht ist. Berechnet man mit den Austauschstromdichten i_{011} und i_{012} nach Gl. (11) den Wert für i_{022}, dann ergibt sich für das Redoxsystem Co chn_3^{2+}/Co chn_3^{3+} eine Austauschstromdichte von

$$i_{022} = 0.630 \pm 0.11 \text{ mA cm}^{-2} \tag{13}$$

Der Einfluss der Elektrodenbedeckung ist bei diesem Wert gering und dürfte nur noch auf die Reaktion nach Gl. (6) zurückzuführen sein.

Die Anwendung der von Marcus für homogen-kinetische Redoxsysteme abgeleiteten Gl. (2) auf elektrochemische Redoxvorgänge findet sicher nur wenige Anwendungsbeispiele. Es zeigt sich jedoch, dass mit dieser Methode für das Co chn_3^{2+}/Co chn_3^{3+}-Redoxsystem eine höhere Geschwindigkeitskonstante

$$k_{el} = 6.5 \times 10^{-3} \text{ cm s}^{-1} \tag{14}$$

berechnet werden kann, die für einen Vergleich mit der entsprechenden homogenkinetischen Konstanten k_{hom} nach[4]

$$(k_{hom}/10^{11})^{\frac{1}{2}} \geqslant k_{el}/10^4 \tag{15}$$

geeignet ist. Leider ist uns der Wert für k_{hom} nicht bekannt. Schliesslich ergeben die Redoxsysteme 6,und 7 mit einen chn-Überschuss, dass die beobachteten Austauschstromdichten noch unter den mit $i_0 = 0.072$ mA cm^{-2} berechneten liegen, was offensichtlich durch eine Elektrodenbedeckung hervorgerufen wird, die sowohl durch chn als auch durch Co chn_3^{2+}-Ionen bedingt sein kann. Eingehendere Untersuchungen zur Aufklärung der Elektrodenbedeckung sind in Vorbereitung.

Trägt man die Austauschstromdichten gegen die entsprechenden Redoxpotentiale auf, so ergibt sich auch daraus für das Redoxsystem Co chn_3^{2+}/Co chn_3^{3+} eine Austauschstromdichte, die in den Fehlergrenzen des hier ermittelten Wertes (13) liegt (Abb. 4).

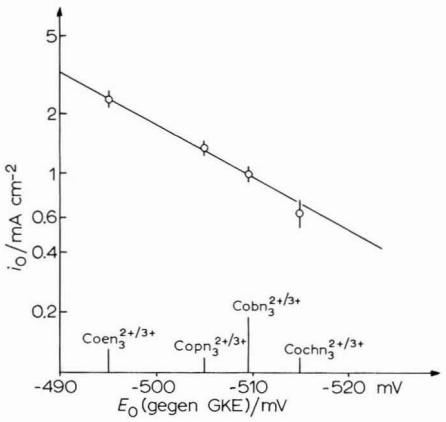

Abb. 4. Abhängigkeit der Austauschstromdichten vom Redoxpotential einiger Co^{II}/Co^{III}-Redoxsysteme.

Diese Abhängigkeit der Austauschstromdichte vom Redoxsystem führt zu der Annahme, dass die Ligandenfeldstärke der einzelnen Diamine ein wichtiger Faktor ist, der den angeregten Zustand für den Elektronenübergang beeinflusst.

In der gleichen Richtung wie die Geschwindigkeitskonstante der einzelnen Redoxsysteme abnimmt, fällt auch die Beständigkeit der Kobalt(III)-Tris-Diamine. Das findet seinen Ausdruck in der zunehmenden Hydrolyse[6,7], wenn man vom Co en_3^{3+}- zum Co chn_3^{3+}-Ion übergeht.

DANKSAGUNG

Herrn Prof. R. Landsberg gilt für Anregung und Diskussionen mein besonderer Dank.

5. ZUSAMMENFASSUNG

Eine von Marcus für homogenkinetische Austauschreaktionen abgeleitete Beziehung wird auf ihre Gültigkeit für elektrochemische Durchtrittsreaktionen geprüft. Die Übereinstimmung mit den berechneten Austauschstromdichten ist relativ gut.

Aus der Abweichung von den berechneten Werten kann auf eine starke Elektrodenbedeckung bei einem der früher untersuchten Systeme geschlossen werden.

Aus der Potentialabhängigkeit der Austauschstromdichten aller bisher von uns untersuchten Kobalt-Tris-Diamin-Redoxsysteme kann für ein Redoxsystem ein wesentlich höhere Austauschstromdichte bestimmt werden, die für einen Vergleich mit der entsprechenden homogenkinetischen Geschwindigkeitskonstanten nach der Theorie von Marcus geeignet ist.

SUMMARY

The validity of a relation derived by Marcus for homogeneous cross-reactions was tested using an electrochemical transfer reaction. The agreement between theory and experiment is good.

The investigation of the cross-reactions showed that electrode coverage is responsible for the discrepancy between theory and experiment which was found for a system previously examined.

The corrected exchange current is considerably higher and fits in well with the linear relationship between equilibrium potential and the log of the rate constant observed for four different cobalt-tris(diamin)redox systems.

LITERATUR

1 H. TAUBE, *Advan. Inorg. Chem. Radiochem.*, 1 (1959) 1.
2 A. G. SYKES, *Advan. Inorg. Chem. Radiochem.*, 10 (1967) 153.
3 N. SUTIN, *Ann. Rev. Phys. Chem.*, 17 (1966) 119.
4 (a) R. A. MARCUS, *Ann. Rev. Phys. Chem.*, 15 (1964) 155; (b) R. A. MARCUS, *Electrochim. Acta*, 13 (1968) 995.
5 H. BARTELT UND H. SKILANDAT, *J. Electroanal. Chem.*, 23 (1969) 407.
6 H. BARTELT UND H. SKILANDAT, *J. Electroanal. Chem.*, 24 (1970) 207.
7 H. BARTELT, *J. Electroanal. Chem.*, 25 (1970) 79.
8 R. MURRAY, S. T. LINCOLN, H. H. GLAESER, H. W. DODGEN UND I. P. HUNT, *Inorg. Chem.*, 8 (1969) 554.

Elsevier Sequoia S.A., Lausanne – Printed in The Netherlands

SHORT COMMUNICATIONS

On the estimation of the reversible halfwave potential

In many polarographic studies, especially those of complexation equilibria, precise values of the "reversible" halfwave potential are needed. Often the polarographic waves are not sufficiently reversible, and ingenious graphical extrapolation methods[1-4] have been used to estimate reversible halfwave potentials from so-called "quasi-reversible" waves. These methods[1-4] require only d.c. polarographic data. However, they become rather inaccurate when the waves deviate only slightly from reversible ones, and they become invalid when the redox processes do not follow Erdey-Grúz and Volmer kinetics[5]. In the latter cases, the method outlined below may be advantageous.

When the deviation from polarographic reversibility is minor, measurements of the faradaic admittance provide more accurate information on the rates of electrode reactions than one can obtain from d.c. polarography[6]. We have recently shown[7,8] that such faradaic admittance data, corrected for iR drop and phase-resolved, can be recorded automatically and with accuracy, speed and convenience comparable to those of d.c. polarography. We have also shown[9] that a dimensionless rate parameter, ζ, can easily be obtained from phase angle measurements, since

$$\frac{Y_F''}{Y_F'} = \frac{\zeta}{1+\zeta} \quad \text{or} \quad \zeta = \frac{Y_F''}{Y_F' - Y_F''} \tag{1}$$

where Y_F' and Y_F'' are the in-phase and quadrature components respectively of the faradaic admittance. Furthermore, this rate parameter is related to the Koutecký[10] rate parameter, χ, through a simple transformation of time scales:

$$\chi = \zeta(\tfrac{24}{7}\,\omega t)^{\frac{1}{2}} \tag{2}$$

where ω is the angular frequency used in the admittance measurements, and t is the drop age at which the d.c. polarographic current is measured. Provided that the measurement of the faradaic admittance is not interfered with by strong reactant adsorption[11], the value of χ can be obtained directly from the faradaic admittance, and the reversible polarogram can then be constructed according to[10]

$$i_{\text{reversible}} = i_{\text{measured}}/\mathrm{F}(\chi) \tag{3}$$

where $\mathrm{F}(\chi)$ is a tabulated function[12] of χ. This reconstruction of the reversible polarographic current, at any given potential, requires a.c. and d.c. data at that one potential only, and hence the procedure generates a set of independent data points. These can subsequently be used to verify, for example, whether the reconstructed d.c. polarographic wave yields a linear Tomeš plot[13] with the anticipated slope. Alternatively, the reversible halfwave potential can be calculated numerically from the Heyrovský–Ilkovič equation[14]

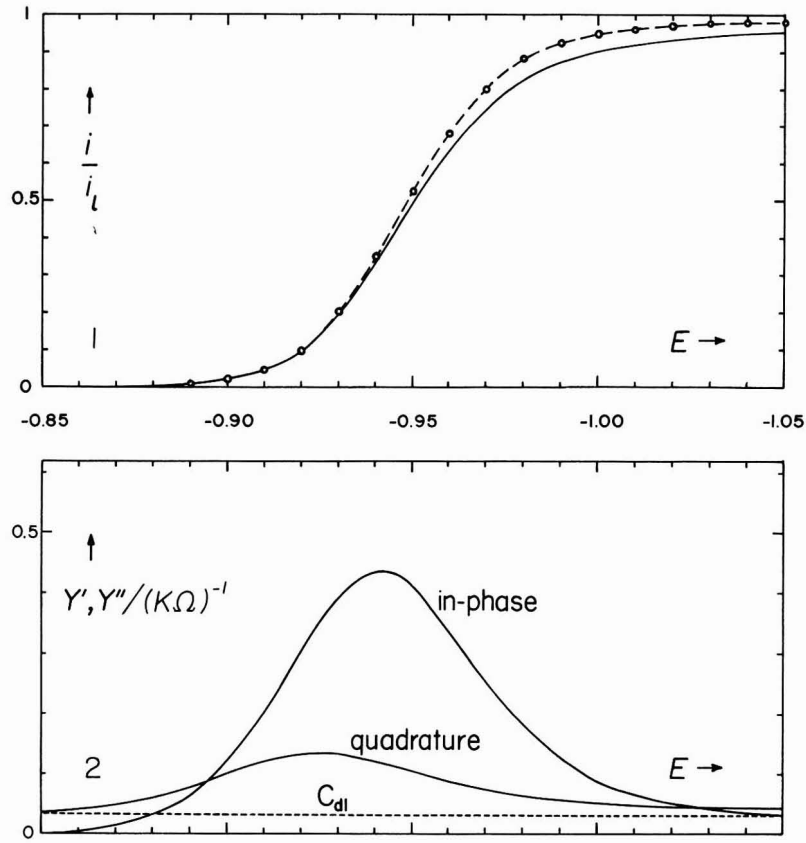

Fig. 1. D.c. polarogram of 1 m*M* $Zn(NO_3)_2$ in 1 *M* $NaClO_4$ at 25°C. Currents measured at 5.87 s drop age. Solid line: measured current, interrupted line: reconstituted "reversible" polarogram. Potentials are in volts *vs.* Ag/AgCl in satd. NaCl.

Fig. 2. Series-resistance-compensated, phase-resolved a.c. polarograms of 1 m*M* $Zn(NO_3)_2$ in 1 *M* $NaClO_4$ at 25°C, measured at 5.87 s drop age with 15.9 Hz signal of 10 mV amplitude. The interrupted line (C_{dl}) indicates the capacitive baseline for the quadrature component, as measured in the absence of Zn(II); the baseline for the in-phase component is at zero.

$$E_{\frac{1}{2}} = E + \frac{0.059}{n} \log \frac{i - \vec{i_l}}{\overleftarrow{i_l} - i}$$

where i is the reversible polarographic current calculated from eqn. (3) and where $\vec{i_l}$ and $\overleftarrow{i_l}$ are the limiting oxidation and reduction currents respectively. Note also that, in the above reconstruction method, no *a priori* dependence of the rate constants on potential need be presumed.

An example of the proposed method is shown in Figs. 1–4. The polarographic reduction of Zn(II) was chosen because it does not follow Erdey-Grúz and Volmer kinetics: the transfer coefficients $\vec{\alpha}$ and $\overleftarrow{\alpha}$ for the oxidation and reduction processes respectively do not add up to 1.00. This deviation from simple charge transfer kinetics is most probably connected with slow loss of coordinated water, as in the reduction of

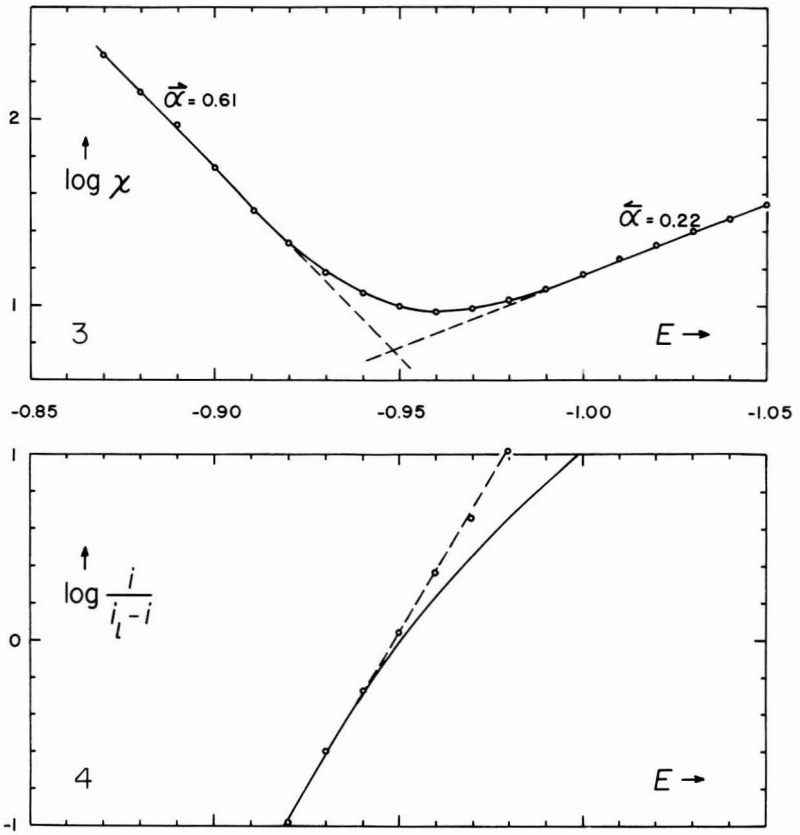

Fig. 3. Logarithmic plot of the Koutecký rate parameter χ *vs.* potential. Points: calcd. from a.c. polarogram, Fig. 2, using eqns. (1) and (2). Values of the charge transfer coefficients $\vec{\alpha}$ and $\overleftarrow{\alpha}$ are obtained from the slopes of the linear sections in the graph. Dashed lines show extrapolations of these linear sections to their intersection at the reversible halfwave potential.

Fig. 4. Logarithmic analysis of the actual wave (solid line) and of the reconstituted reversible polarogram (dashed). The dashed line is drawn under the theoretical slope, $(29.6\ \text{mV})^{-1}$.

Ni(II)[15] and In(III)[16], a process which in all these cases is catalyzed by adsorbed halide and thiocyanate ions. Figure 3 illustrates that, indeed, $\vec{\alpha} + \overleftarrow{\alpha} \neq 1$ for the reduction of Zn(II). It is therefore not surprising that the earlier polarographic methods for the estimation of the reversible halfwave potential of Zn(II) did not quite agree with each other[3,4] or with the results of our procedure. We believe our method to be more reliable because it does not depend on any implicit assumption regarding the current–voltage relationship.

From plots of log ζ or log χ *vs.* $-E$, see Fig. 3, one can obtain estimates of $\vec{\alpha}$ and $\overleftarrow{\alpha}$ at potentials positive and negative respectively of the reversible halfwave potential. One can subsequently make a linear extrapolation, assuming that the oxidation and reduction rate constants are exponential functions of potential over the small range of potentials covered by the extrapolation. If this assumption is justified, then the two extrapolated lines will intersect at the reversible halfwave potential, and

the measured values of χ at or near the reversible halfwave potential can be reconstructed from the two linear extrapolations. This procedure clearly illustrates how reaction rate constants change in the region of the polarographic wave, but it is not recommended for the determination of $E_{\frac{1}{2},\mathrm{rev}}$ since it is neither as accurate nor as general (because of the assumed exponential relationship) as the reconstruction of the reversible polarogram.

The proposed reconstruction method is believed to be the most accurate and general one available so far, although it is still limited. It applies only to slow, first-order surface reactions. It does not work when the d.c. polarographic wave is "totally irreversible", since then no experimental data (i, Y_F', Y_F'') can be obtained in the region of the reversible polarographic wave. Finally, the method does not work with "quasi-reversible" waves when there is appreciable reagent adsorption[11], as for example, with the reduction of Bi(III) from 0.1 M $HClO_4$ in the presence of small amounts of chloride or bromide[17].

Acknowledgement

The authors gladly acknowledge support of their work by the National Science Foundation (grant GP 8575), the Air Force Office of Scientific Research (OAR, USAF, grant 68-1344) and the Office of Naval Research.

Department of Chemistry,
Georgetown University,
Washington, D.C. 20007
(U.S.A.)

Robert de Levie
Lubomír Pospíšil

1 H. MATSUDA AND Y. AYABE, *Z. Elektrochem.*, 63 (1959) 1164; 66 (1962) 469.
2 J. KORYTA, *Electrochim. Acta*, 6 (1962) 67.
3 R. TAMAMUSHI, K. ISHIBASHI AND N. TANAKA, *Z. Physik. Chem. Frankfurt*, 35 (1962) 209.
4 R. TAMAMUSHI AND N. TANAKA, *Z. Physik. Chem. Frankfurt*, 39 (1963) 117.
5 T. ERDEY-GRÚZ AND M. VOLMER, *Z. Physik. Chem.*, 150A (1930) 203.
6 J. E. B. RANDLES, *Can. J. Chem.*, 37 (1959) 238.
7 R. DE LEVIE AND A. A. HUSOVSKY, *J. Electroanal. Chem.*, 20 (1969) 181.
8 R. DE LEVIE AND J. C. KREUSER, *J. Electroanal. Chem.*, 21 (1969) 221.
9 R. DE LEVIE AND A. A. HUSOVSKY, *J. Electroanal. Chem.*, 22 (1969) 29.
10 J. KOUTECKÝ, *Collection Czech. Chem. Commun.*, 18 (1953) 597.
11 P. DELAHAY, *J. Phys. Chem.*, 70 (1966) 2069, 2373.
12 J. WEBER AND J. KOUTECKÝ, *Collection Czech. Chem. Commun.*, 20 (1955) 980.
13 J. TOMEŠ, *Collection Czech. Chem. Commun.*, 9 (1937) 12.
14 J. HEYROVSKÝ AND D. ILKOVIČ, *Collection Czech. Chem. Commun.*, 7 (1935) 198.
15 A. A. VLČEK, *Chem. Listy*, 50 (1956) 828; J. DANDOY AND L. GIERST, *J. Electroanal. Chem.*, 2 (1961) 116.
16 L. POSPÍŠIL AND R. DE LEVIE, *J. Electroanal. Chem.*, 25 (1970) 245.
17 R. DE LEVIE AND L. POSPÍŠIL, in preparation.

Received April 13th, 1970

Elsevier Sequoia S.A., Lausanne – Printed in The Netherlands

Effect of solvent viscosity on boundary layer in electrode processes

Introduction

In connection with the use of electrochemical separation to determine reaction rates, limiting currents for the electrode reaction, $Ag + I^- \rightarrow AgI + e^-$, had to be established in a variety of solvents covering a broad viscosity range, *viz.* from 0.3 to 16 cP*. Since we think that the observed dependence of the limiting current density on the viscosity of the electrolyte may be of importance in polarography with solid microelectrodes, it is reported in the present communication.

Experimental

Limiting currents in sodium iodide solutions without any supporting electrolyte were determined by a radiochemical method previously described[1] using a cell of 50 ml volume. The electrolyte was agitated at 400 rev. min^{-1}. The circular silver anode, with an area of approx. 0.5 cm^2, was placed vertically in the cell.

Results

A summary of the data obtained is given in Table 1 in which t is the temperature,

TABLE 1

LIMITING CURRENT DENSITIES IN VARIOUS SOLVENTS FOR THE ELECTRODE REACTION, $Ag + I^- \rightarrow AgI + e^-$, AT A SODIUM IODIDE CONCENTRATION OF 1.0×10^{-4} M

Solvent	$t/°C$	η/cP	$i_l/\mu A\ cm^{-2}$	$D \times 10^5/cm^2\ s^{-1}$
Acetone	25	0.32[a]	>5700	2.5
Methanol	55	0.38[b]	1200	1.7
Methanol	25	0.55[a]	78	1.2
Ethanol	25	1.08[c]	51	0.51[e]
Propanol	25	2.00[d]	32	0.24[f]
Iso-propanol	25	2.1[b]	28	0.21[f]
Butanol	25	2.6[b]	22	0.18[f]
Ethylene glycol	55	5.7[b]	20	0.19
Ethylene glycol	25	16.3[b]	7.7	0.065[f]

[a] Ref. 2. [b] Figures obtained from semilog graphs of η (refs. 2–4) *vs.* $1/(t + 273.15)$. [c] Ref. 3. [d] Ref. 4. [e] Ref. 9. [f] Ref. 8.

η the viscosity of the solvent, i_l the limiting current density, and D the diffusion coefficient of the salt. All limiting current densities quoted, the uncertainties of which are estimated to be less than $\pm 10\%$, refer to a sodium iodide concentration of 1.0×10^{-4} M. The diffusion coefficient of sodium iodide in acetone was estimated from the equation[5],

$$D = \frac{RT}{F^2} \times \frac{\lambda_0^+ \lambda_0^-}{\lambda_0^+ + \lambda_0^-} \left(\frac{1}{z_+} + \frac{1}{z_-} \right) \qquad (1)$$

* 1 cP = 10^{-3} kg m^{-1} s^{-1}.

where the symbols have their usual meaning, using limiting equivalent conductances for Na^+ and I^- given in ref. 6. Diffusion coefficients in methanol at 25° and 55° were obtained from the value[7], $D = 1.0 \times 10^{-5}$ cm^2 s^{-1}, at 14° assuming $D\eta = \text{const.}$, which was also employed to estimate the 55° diffusion coefficient in ethylene glycol from the 25° value[8], $D = 0.065 \times 10^{-5}$ cm^2 s^{-1}, in this solvent. Calculations below involve transport numbers, t_-, of the iodide ion. For most of the alcohols studied this quantity is not available. Anion transport numbers in acetone, methanol, and ethanol, obtained from limiting equivalent conductances of Na^+ and I^- are $t_- = 0.58$[6], 0.58[10], and 0.57[10], respectively. The value, $t_- = 0.6$, was used for the other alcohols.

A graphic representation of the dependence of the limiting current density on the viscosity of the solvent is shown in Fig. 1. For convenience logarithmic scales have

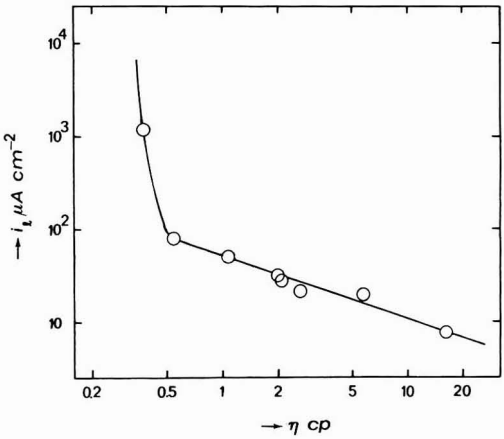

Fig. 1. Limiting current density as a function of viscosity of electrolyte.

been used. As can be seen there is an abrupt change in the curve at $\eta \simeq 0.5$ cP. For lower viscosities there is a very rapid increase in the limiting current density, and hence in the rate of transport of electroactive species to the anode surface, with decreasing viscosity of the electrolytic solution.

In unagitated solution, the transport of electroactive species to an electrode surface is generally purely diffusion controlled. In agitated solution, as in the present investigation, the transport is governed by convection and diffusion.

To give a correct picture of the boundary layer through which the rate determining transport of electroactive species to the electrode surface occurs is not a straightforward matter[11], especially for agitated solutions, and hardly possible at all under the non-ideal conditions in the present investigation. Nevertheless it might be of interest to have some kind of measure of the "thickness" of the boundary layer adjacent to the anode surface. To that end we shall adopt the highly idealized Nernst diffusion layer model[12], which assumes purely diffusion controlled mass transport through a layer of thickness, δ, in which the concentration of electroactive species increases linearly with the distance from the electrode surface. With this model, and with the actual experimental conditions, the limiting current density is given by the equation,

$$i_1 = FDc/(1-t_-)\delta \qquad (2)$$

where c is the concentration of sodium iodide (1×10^{-4} M). This equation has been used to calculate the thickness, δ, for the various solvents studied. A graphic representation of δ *vs.* the viscosity of the solvent is shown in Fig. 2. For $\eta \simeq 0.5$ cP, where

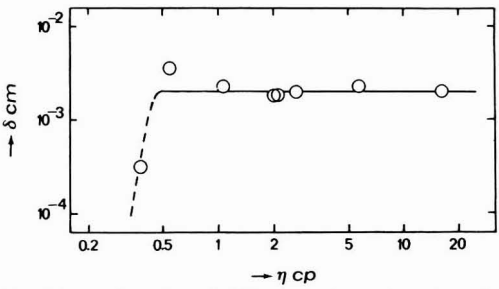

Fig. 2. Boundary layer "thickness", δ, as a function of solvent viscosity.

we observed a sudden change in the limiting current density *vs.* viscosity curve (Fig. 1), there is an abrupt change in the boundary layer thickness as defined by eqn. (2). For higher viscosities, δ is remarkably constant and approximately 2×10^{-3} cm. Below $\eta = 0.5$ cP there is a rapid decrease in δ. Thus, when going from methanol at 25° ($\eta = 0.55$ cP) to acetone ($\eta = 0.32$ cP) δ decreases to below 1×10^{-4} cm, *i.e.* by a factor of 20 or more.

Acknowledgements

The author thanks Dr. Michael Sharp for linguistic revision of the manuscript and the Swedish Natural Science Research Council for financial support.

Division of Physical Chemistry,
University of Umeå,
S-901 87 Umeå (Sweden)

P. Beronius

1 P. Beronius, *Acta Chem. Scand.*, 15 (1961) 1151.
2 R. C. Weast (Ed.), *Handbook of Chemistry and Physics*, The Chemical Rubber Co., Cleveland, Ohio, 49th ed., 1968–1969.
3 J. Timmermans, *Physico-Chemical Constants of Pure Organic Compounds*, Vol. I, Elsevier Publishing Co., Inc., New York, 1950.
4 A. Weissberger (Ed.), *Technique of Organic Chemistry*, Vol. VII, Interscience Publishers, Inc., New York, 2nd ed., 1955.
5 I. M. Kolthoff and J. J. Lingane, *Polarography*, Interscience Publishers, Inc., New York 1952, pp. 53–56.
6 C. W. Davies, *The Conductivity of Solutions*, Chapman and Hall, Ltd., London, 1933, p. 208.
7 *International Critical Tables V*, p. 72.
8 P. Beronius and R. Enberg, *Z. Physik. Chem. (Frankfurt)*, 46 (1965) 373.
9 S. Asunmaa, *Ann. Acad. Sci. Fennicae*, A 53 (1940) No. 11.
10 P. Beronius, G. Wikander and A.-M. Nilsson, *Z. Physik. Chem. (Frankfurt)*, 70 (1970) 52.
11 K. J. Vetter, *Electrochemical Kinetics*, Academic Press, New York, 1967, chap. 2B.
12 W. Nernst, *Z. Physik. Chem.*, 47 (1904) 52.

Received March 25th, 1970

Elsevier Sequoia S.A., Lausanne – Printed in The Netherlands

Radioelectrochemical microgram determination of bromide

Introduction

Determinations of microgram amounts of carrier bromide in dilute solutions, *ca.* 2×10^{-4} *M*, of ammonium radiobromide in anhydrous acetone were necessary. Because of the low concentrations, analyses could not be performed using standard methods with the accuracy required. Isotopic dilution analysis involving measurements of the radioactivities of electrodeposited silver bromide samples were therefore used. The method has been recently described[1] in connection with determinations of microgram amounts of chloride.

The purpose of the present paper is to show that about 60 μg of bromide can be determined by this means with an accuracy of ± 1 μg (99% confidence level).

Procedure

A 2 ml aliquot of aqueous ammonium radiobromide (The Radiochemical Centre, Amersham, England) of specific activity 100–200 mCi ^{82}Br/g Br was evaporated to dryness and dried at 110° for 1 h. A part of the solid residue was dissolved in 500 ml dry acetone and the solution (*ca.* 2×10^{-4} *M* as found below) transferred to a fresh bottle. This precaution was taken to prevent any change in the concentration due to further dissolution of undissolved ammonium bromide. (This salt is only sparingly soluble in acetone and dissolves slowly in this medium; according to our experience a saturated solution is about 5×10^{-4} *M* at room temperature.)

The concentration of carrier bromide in the radioactive stock solution thus prepared was determined by the following procedure. To a known volume, v (*ca.* 5 ml), of the radioactive stock was added a known quantity of inactive ammonium bromide (Δw μg Br) dissolved in acetone. A further quantity of this solvent was added to give a sample of 50 ml volume. The sample was transferred to an electrolytic cell[2,3] and small fractions, usually 0.5%, of its bromide content anodically deposited on silver microelectrodes, *cf.* ref. 4. The *beta* activities of the silver bromide electrodeposits were measured in a proportional flow counter. This procedure was repeated for several samples differing only with respect to their content of additional inactive bromide ions (Δw).

The conditions used in the electrolyses of the samples are given in Table 1, in which i is the current and t the time of deposition.

Results and discussion

The concentration of carrier bromide, w μg/ml, in the radioactive stock solution was calculated from the equation,

$$w = S\Delta w/(S_0 - S)v \qquad (1)$$

where S_0 is the specific activity of the stock solution and S the corresponding quantity

TABLE 1

EXPERIMENTAL CONDITIONS

Sample No.	*Approx. concn. NH_4Br/M*	*$i/\mu A$*	*t/s*	*Other conditions*
1	0.00002	50	24	Electrolytic cell: 50 ml vol.
2	0.0001	100	24	Anode: 0.126 cm^2 area, silver
3	0.0002	170	24	electrode
4	0.0003	240	24	Cathode: platinum wire
5	0.0003	240	24	Electrolyte: NH_4Br in acetone
6	0.0003	240	24	agitated at 100 rev/min
7	0.0003	310	24	Temp.: 25.0°C
8	0.0004	380	24	
9	0.0005	500	24	
10	0.0005	460	24	

TABLE 2

RESULTS

Sample No.	*v/ml*	*$\Delta w/\mu g$ Br*	*A/cpm*	*$S/cpm\ \mu Q^{-1}$*	*$w/\mu g\ Br\ ml^{-1}$*	*Dev. from av./%*
1	5.00	0	62773	52.311	—	—
2	5.02	411	16642	6.934	12.51	+2.5
3	5.00	670	17638	4.323	12.07	−1.2
4	5.02	938	18501	3.212	12.22	+0.1
5	4.98	947	18225	3.164	12.24	+0.2
6	5.02	953	17989	3.123	12.05	−1.3
7	4.98	1217	18518	2.489	12.21	±0.0
8	5.00	1505	18240	2.000	11.97	−2.0
9	5.00	1840	20424	1.702	12.38	+1.4
10	5.02	1844	18580	1.683	12.21	±0.0
					Av: 12.21	

for the isotopically diluted sample. The results of the calculations are shown in Table 2, in which A is the radioactivity of the electrodeposit corrected for dead-time losses, back-ground counts, and decay of ^{82}Br ($t_{\frac{1}{2}} = 35.87$ h according to ref. 5), and S the radioactivity per μQ of electric charge (equal to A/it). Each value of A is the average of 3 or 4 measurements. The quantity sought, w, in the penultimate column is independent of the degree of isotopic dilution. This fact illustrates the reliability of the procedure.

By rearranging eqn. (1), it can be shown that a graph of $1/S$ *vs.* $\Delta w/v$ should yield a straight line of intercept $1/S_0$ and slope $1/S_0 w$. A graph of this kind using the data in Table 2 is shown in Fig. 1. From the equation of the straight line, which has been fitted by means of a relative deviation least squares method[6] (the relative error in $1/S$ is independent of $\Delta w/v$) to give equal weights to all points, the value 12.19 ± 0.19 μg/ml (99% confidence level) is obtained for w. This figure differs slightly from the average, 12.21 μg/ml, of the point by point calculation (penultimate column in Table 2). This difference arises from the higher weight given to S_0 in the point by point calculation of w than that in the least squares treatment.

The quantity of carrier bromide determined is equal to $v \times w$ which amounts to 60 μg.

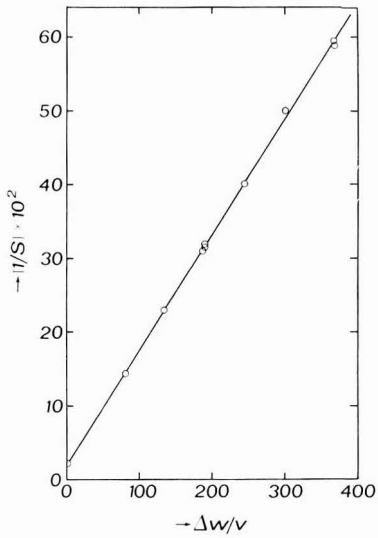

Fig. 1. Graph of $1/S$ *vs.* $\Delta w/v$ according to eqn. (1), ref. 1.

Acknowledgements

The authors thank Dr. Michael Sharp for linguistic revision of the manuscript and the Swedish Natural Science Research Council for financial support.

Division of Physical Chemistry,
University of Umeå,
S-901 87, Umeå (Sweden)

P. Beronius
A. Holmgren
A.-M. Nilsson
G. Wikander

1 P. BERONIUS, *J. Electroanal. Chem.*, 23 (1969) 324.
2 P. BERONIUS, U. ISACSSON AND A.-M. NILSSON, *Acta Chem. Scand.*, 24 (1970) 189.
3 P. BERONIUS, *Acta Chem. Scand.*, 15 (1961) 1151.
4 P. BERONIUS AND H. JOHANSSON, *J. Phys.-Chem.*, 72 (1968) 713.
5 B. S. DZHELEPOV AND L. K. PEKER, *Decay Schemes of Radioactive Nuclei*, Pergamon Press, Oxford, 1961, p. 200.
6 A. HALD, *Statistical Theory with Engineering Applications*, John Wiley and Sons, New York, 1965, pp. 551–557.

Received April 3rd, 1970

Elsevier Sequoia S.A., Lausanne Printed in The Netherlands

On the spectroelectrochemical evaluation of the "first order" hydrolysis of DPA cation radical in acetonitrile

In a study[1] of the hydrolysis of the cation radical of 9,10-diphenylanthracene (DPA), kinetic results obtained during potential step electrolysis at optically transparent electrodes (OTE) were not in agreement with those obtained during homogeneous relaxation. Reexamination of these results, particularly in view of recent thin-layer electrochemical results[2] which lend credence to the mechanism proposed by Sioda[3], namely

$$DPA \rightarrow DPA^{\cdot +} + e^{-} \tag{1}$$

$$DPA^{\cdot +} + H_2O \xrightarrow{k_1} DPA(OH)^{\cdot} + H^{+} \tag{2}$$

$$DPA(OH)^{\cdot} + DPA^{\cdot +} \xrightarrow{k_2} DPA(OH)^{+} + DPA \tag{3}$$

$$DPA(OH)^{+} + H_2O \xrightarrow{k_3} DPA(OH)_2 + H^{+} \tag{4}$$

where $DPA(OH)_2$ is *trans*-9,10-dihydro-9,10-diphenyl anthracene, indicates that the results of the two techniques should disagree. The participation of reaction (3) implies "regenerative" as well as "succeeding" kinetic character in the overall reaction scheme. Previous treatment[1] of results obtained during potential step electrolysis did not account for this regeneration.

Because the disappearance of $DPA^{\cdot +}$ is being measured, reactions (2) and (3) are of paramount interest. Taking $k_2 \gg k_1$, steady state kinetics* can be imposed on $DPA(OH)^{\cdot}$ yielding the diffusion–kinetic expressions describing the system:

$$\frac{\partial[DPA]}{\partial t} = D\frac{\partial^2[DPA]}{\partial x^2} + k_1'[DPA^{\cdot +}] \tag{5}$$

and

$$\frac{\partial[DPA^{\cdot +}]}{\partial t} = D\frac{\partial^2[DPA^{\cdot +}]}{\partial x^2} - 2\,k_1'[DPA^{\cdot +}] \tag{6}$$

where

$$k_1' = k_1[H_2O] \tag{7}$$

Solution of this diffusion–kinetic problem by the technique of digital simulation[4] predicts absorbance–time behavior during potential step electrolysis at optically transparent electrodes which is significantly different from that predicted on the basis of a simple first order succeeding reaction. The rate of disappearance of $DPA^{\cdot +}$ under homogeneous relaxation conditions (open circuit following electrode pulse) is given by

$$\frac{d[DPA^{\cdot +}]}{dt} = -2\,k_1'[DPA^{\cdot +}] \tag{8}$$

* The rate constant k_2 reflects an electron transfer reaction between two quite similar species, and such reactions are known to be quite fast. See, for example, refs. 5 and 6.

Assuming the validity of the steady state hypothesis, the observed rate constant for the homogeneous relaxation should be *twice* that obtained from the potential step case. Thus, recalculation of the rate constant from previous data (Fig. 6, ref. 1) gives rise to $k'_1 = 0.060\ (\pm 0.005)\ s^{-1}$ for that particular pulse experiment. The observed rate constant for the relaxation experiment at that same water concentration is $0.12\ s^{-1}$ (Fig. 7, ref. 1), a value *twice* k'_1 as now calculated from the pulse experiment.

Results of further pulse and relaxation spectroelectrochemical experiments, summarized in Table 1, are in accord with the predicted 1:2 ratio of rate constants

TABLE 1

KINETIC PARAMETERS FROM THE HYDROLYSIS OF 9,10-DIPHENYLANTHRACENE CATION RADICAL UNDER POTENTIAL STEP ELECTROLYSIS AND OPEN CIRCUIT RELAXATION CONDITIONS[a]

$[H_2O]/M$	k'_1/s^{-1} (*pulse*[b])	$k_{observed}/s^{-1}$ (*relaxation*[c])
2.50	0.16 (±0.01)	0.31 (±0.01)
3.00	0.19 (±0.01)	0.37 (±0.01)
4.00	0.23 (±0.02)	0.48 (±0.02)

[a] These results were obtained for 5.0×10^{-4} *M* DPA in acetonitrile containing 0.1 *M* TEAP at Pt-OTE, $T = 29 \pm 1°C$. The exptl. set-up and preparation has been described elsewhere[1]. Data were taken from 0.5 to 5.0 s.

[b] The rate constant k'_1 is defined in eqn. (7).

[c] As defined in eqn. (8), $k_{observed} = 2\,k'_1$.

evaluated by the two techniques. It is clear that the mechanism proposed by Sioda[3] is tenable. The steady state assumption regarding the concentration of DPA(OH)$^{\bullet}$ is apparently valid and can provide an avenue for the rapid, accurate evaluation of kinetic parameters of reaction schemes of this type.

Acknowledgement

This work was supported in part by Grant No. GM14036 from the Research Grant Branch of the National Institutes of Medical Science, National Institutes of Health, and by Grant No. GP9306 from the National Science Foundation.

Department of Chemistry,
Case Western Reserve University,
Cleveland, Ohio 44106 (U.S.A.)

Henry N. Blount
Theodore Kuwana

1 G. C. GRANT AND T. KUWANA, *J. Electroanal. Chem.*, 24 (1970) 11.
2 P. T. KISSINGER AND C. N. REILLEY, *Anal. Chem.*, 42 (1970) 12.
3 R. E. SIODA, *J. Phys. Chem.*, 72 (1968) 2322.
4 S. W. FELDBERG in A. J. BARD (Ed.), *Electroanalytical Chemistry, Volume III*, Marcel Dekker, Inc., New York, 1969.
5 N. WINOGRAD AND T. KUWANA, *J. Am. Chem. Soc.*, 92 (1970) 224.
6 S. ARAI AND L. M. DORFMAN in R. F. GOULD (Ed.), *Radiation Chemistry, Vol. II*, American Chemical Society, Washington D.C., 1968.

Received April 20th, 1970

The electrical double layer on PbO_2 in $HClO_4$

Previous communications[1,2] have reported impedance measurements on PbO_2 (α and β) electrodes in KNO_3 and SO_4^{2-} aqueous electrolytes. In this note we record complementary data for aqueous perchloric acid electrolytes.

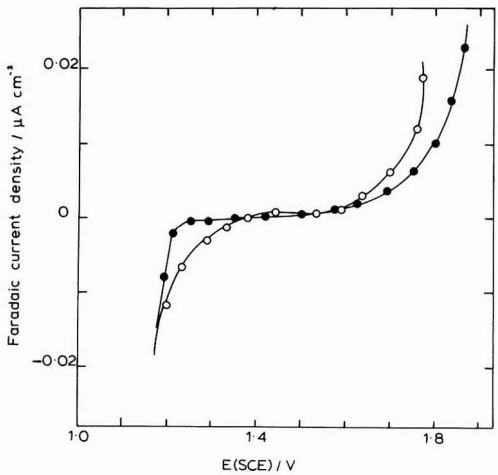

Fig. 1. Typical faradaic current–potential curves, electrodeposited PbO_2, 23°C, 0.135 mol l^{-1} $HClO_4$; (○) α-PbO_2; (●) β-PbO_2.

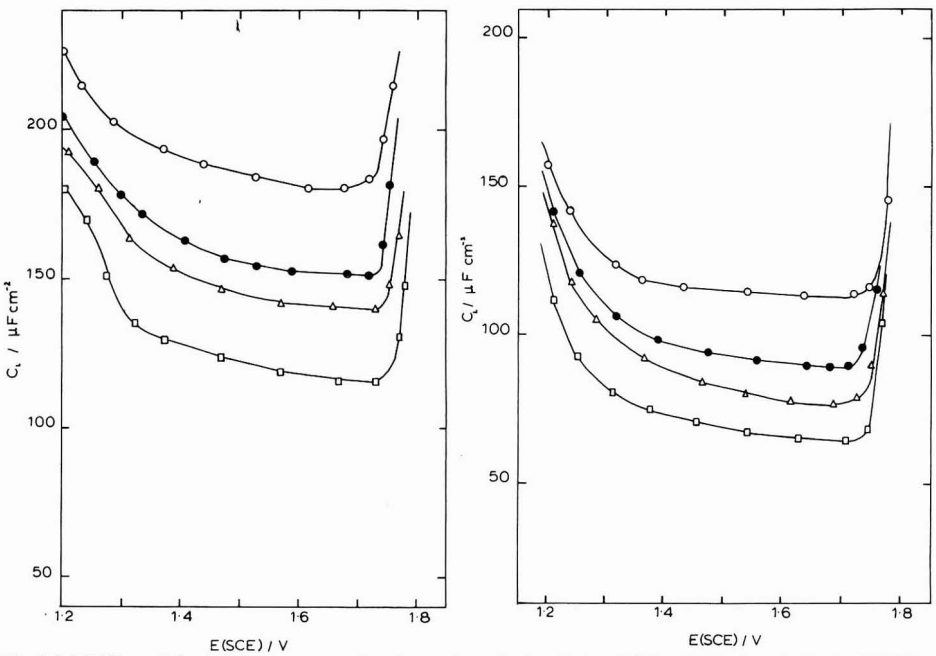

Fig. 2. (a) Differential capacitance curves for electrodeposited α-PbO_2, 23°C, 120 Hz; (○) 0.135, (●)0.0645, (△) 0.0095, (□) 0.003 mol l^{-1}. (b) As (a) for β-PbO_2.

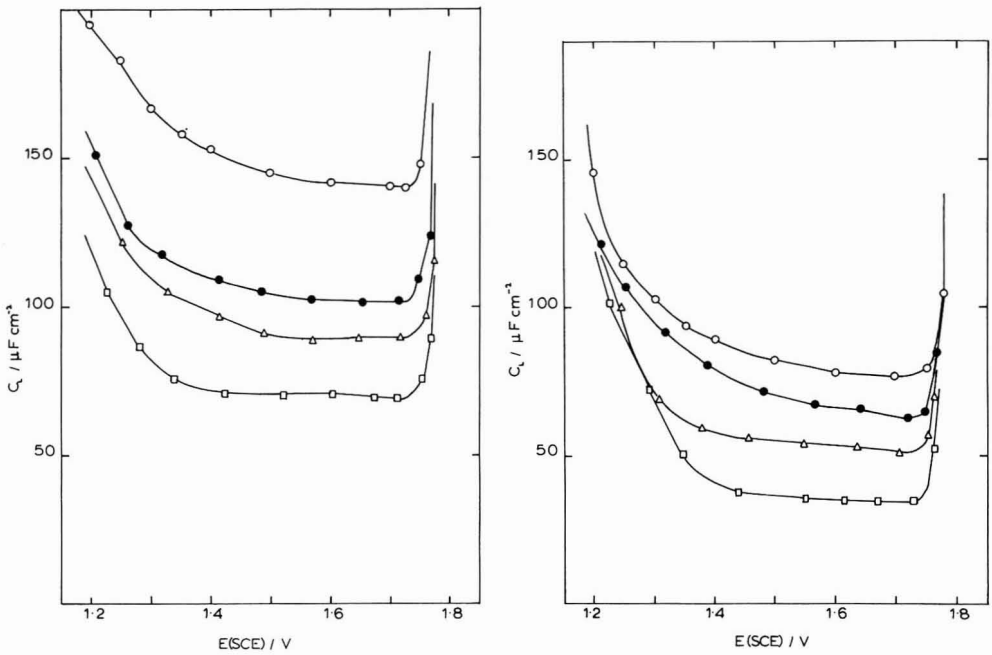

Fig. 3. (a) Typical dispersion of capacitance with frequency for electrodeposited α-PbO_2, 23°C, 0.0095 mol l^{-1}; (○) 120, (●) 300, (△) 500, (□) 1000 Hz. (b) As (a) for β-PbO_2.

Results and discussion

The faradaic current–potential curves (Fig. 1) indicate an experimentally polarizable region (α-PbO_2, 1.2–1.85 V SCE; β-PbO_2, 1.2–1.78 V SCE). Differential capacitance curves were obtained in this region for a series of electrolytes (Fig. 2). α-PbO_2 showed a more pronounced time dependence of capacitance ($\sim 50\%$ increase during 5 h, thereafter stable) than β-PbO_2 ($\sim 20\%$ increase during 2 h, thereafter stable). Frequency dispersion (Fig. 3) was somewhat similar for both polymorphs amounting to a 20% increase of C_L for a frequency change 1 kHz–500 Hz.

The differential capacitance curves (Fig. 2) are similar in shape, but capacitances are greater in magnitude than those reported by Kiseleva *et al.*[3]. However the present results are for stabilised electrodes, whereas these of Kiseleva *et al.* were taken after fairly short electrode-electrolyte contact times. The initial increase in capacitance with time has previously been noted by Kiseleva *et al.*[3] who considered it due to expansion of the PbO_2 lattice and adsorption of ClO_4^- ions. The shape of the capacitance curves (Fig. 2), particularly the absence of a pronounced minimum developing with dilution, strongly suggests that adsorption of the anion indeed occurs.

The greater time dependence of C_L observed in the case of α-PbO_2 than β-PbO_2 is apparently caused by the lower stability of the α-polymorph. A change to the β-form probably occurs as already discussed[2].

Chemistry Department,
Loughborough University of Technology,
Leicestershire (England)

J. P. Carr
N. A. Hampson
R. Taylor

1 J. P. CARR, N. A. HAMPSON AND R. TAYLOR, (KNO_3) *J. Electroanal. Chem.*, 27 (1970) 109.
2 J. P. CARR, N. A. HAMPSON AND R. TAYLOR, (SO_4^{2-}) *J. Electroanal. Chem.*, 27 (1970) 201.
3 I. G. KISELEVA, B. N. KABANOV AND D. J. LEIKIS, *Dokl. Akad. Nauk SSSR*, 49 (1954) 805.

Received May 12th, 1970

J. Electroanal. Chem., 27 (1970) 466–468

On the derivation and formulation of the electrocapillary equation of ideally polarizable electrodes

General derivations and formulations of the electrocapillary equation of ideally polarizable electrodes given so far in the literature[1-4] are unsatisfactory in three respects. The derivation and formulation for a general case is very complicated, the expression for the relative surface excess of ions in the literature is incorrect and the restrictions and classifications introduced in some papers[1,4] for the reference electrode for reasons of simplification seem to be an unnecessary limitation of the final equation.

An improved equation is attained if the derivation is made in the following way. As usual one has to start with the Gibbs adsorption-isotherm for the phase σ in a cell represented as

$$\begin{array}{ccccccc} \mathrm{Cu^{I}} & | & \text{phase M} & | & \sigma & | & \text{phase S} \\ & & \sum_m S_m^{z_m}, e^- & & & & \sum_k S_k^{z_k} \end{array} \quad \begin{array}{ccc} | & \text{reference electrode} & | & \mathrm{Cu^{II}} \\ & \text{(phase B)} & & \\ & \sum_b S_b^{z_b}, e & & \end{array}$$

The metal phase M consists of m metal ions $S_m^{z_m}$ and of a number of electrons e^- equivalent to ion charges z_m. The electrolyte phase S is composed of k molecules $S_k^{z_k}$. Equal numbers of anions and cations must be present in the electrolyte phase. Adjacent to phase S the reference electrode (phase B) is located. It consists of b molecules $S_b^{z_b}$ and of an equivalent number of electrons e^-. Finally, the electrical connections, $\mathrm{Cu^{I}}$ and $\mathrm{Cu^{II}}$, have to be considered.

The electrocapillary equation will be derived for the boundary phase (interface) σ between phase M and phase S. Gibbs' adsorption isotherm for this interphase is, when temperature and pressure are constant

$$-\mathrm{d}\gamma = \sum_m \Gamma_m \mathrm{d}\eta_{\sigma,m} + \Gamma_{e^-}\mathrm{d}\eta_{\sigma,e^-} + \sum_k \Gamma_k \mathrm{d}\eta_{\sigma,k} \qquad (1)$$

where γ is the surface tension, Γ are the amounts of substances in a 1-cm^2 column of the interphase σ, and η_σ are the electrochemical potentials in the interphase σ. For the metal ions and the electrons an equilibrium exists between the interphase and the metal phase so that $\eta_{\sigma,m}=\eta_{\mathrm{M},m}$ and $\eta_{\sigma,e^-}=\eta_{\mathrm{M},e^-}$. For the substances $S_k^{z_k}$ an equilibrium exists between the interphase and the electrolyte phase so that $\eta_{\sigma,k}=\eta_{\mathrm{S},k}$. The electrochemical potentials in the metal can now be substituted by $\eta_\mathrm{M}=\mu_\mathrm{M}+zF\varphi_\mathrm{M}$ whereas the electrochemical potentials in the electrolyte phase can be substituted by $\eta_\mathrm{S}=\mu_\mathrm{S}+zF\varphi_\mathrm{S}$ where μ_M and μ_S are the chemical potentials, and φ_M and φ_S are

the electrical potentials in phases M and S. The chemical potential of the metal ions in the metal can additionally be substituted by $\mu_{M,m} - z_m \mu_{M,e^-}$ where $\mu_{M,m}$ is the chemical potential of the neutral metal atoms. Furthermore, the charge $q_M = F(\Sigma z_m \Gamma_m - \Gamma_{e^-})$ on the metal side and the charge $q_S = F\Sigma z_k \Gamma_k$ on the electrolyte side of the interphase must be introduced. Overall the interphase must be neutral so that q_M equals q_S. Taking into account all the steps mentioned eqn. (1) results in

$$-d\gamma = \sum_m \Gamma_m d\mu_{M,m} + \sum_k \Gamma_k d\mu_{S,k} - (q_M/F) d\mu_{M,e^-} + q_M(d\varphi_M - d\varphi_S) \quad (2)$$

In this equation, the differential $d\varphi_M - d\varphi_S = d(\varphi_M - \varphi_S)$ of the potential difference between phases M and S occurs. It is characteristic of the ideally polarizable electrode that this potential difference is an independent variable. Experimentally only the cell voltage $E = \varphi_{Cu^I} - \varphi_{Cu^{II}}$ between the electrical connections Cu^I and Cu^{II} can be varied. For this reason the relations between $d\varphi_M$ and $d\varphi_{Cu^I}$, and $d\varphi_S$ and $d\varphi_{Cu^{II}}$ have to be set up. This will be possible if the potential determining reactions at the individual phase boundaries are used.

Between phase M and Cu^I the electron equilibrium is potential determining. In the state of equilibrium, $\eta_{Cu^I,e^-} = \eta_{M,e^-}$ holds for the electrochemical potentials of the electrons in phase M and in Cu^I; η is to be substituted by $\eta = \mu - F\varphi$. If one considers that the chemical potential of the electrons in Cu^I is constant and that $d\mu_{Cu^I,e^-}$ can be set equal to zero, the result is

$$d\varphi_M = d\varphi_{Cu^I} + (1/F) d\mu_{M,e^-} \quad (3)$$

Between phase S and the reference electrode (phase B) a potential determining reaction

$$\sum_b \nu_b S_b + \sum_j \nu_j S_j^{z_j} + ne^- = 0 \quad (4)$$

can be formulated. Equation (4) holds for a redox electrode as well as for a metal ion electrode. In the case of a redox process the stoichiometric coefficient ν_b equals 0 and the substances S_j are redox components in the electrolytic phase S. If however, the reference electrode is a metal ion electrode, eqn. (4) states that ν_b metal atoms change into metal ions in the electrolyte. During this process n electrons are released in the metal as excess charge. For these electrons a further equilibrium exists between the reference electrode (phase B) and Cu^{II}. In the state of equilibrium again the electrochemical potentials have to be set equal. After the substitution $\eta = \mu + zF\varphi$ differentiation can be carried out. If the constancy of the chemical potentials of the electrons in phase B and in Cu^{II} ($d\mu_{B,e^-} = 0$; $d\mu_{Cu^{II},e^-} = 0$), and the relation $\Sigma \nu_j z_j = n$ following from eqn. (4) are considered, the following equation is found

$$d\varphi_S = d\varphi_{Cu^{II}} - (1/nF) \sum_j \nu_j d\mu_j \quad (5)$$

Equations (3) and (5) have to be inserted in eqn. (2). The difference of differentials $d\varphi_{Cu^I} - d\varphi_{Cu^{II}}$ can be substituted for $d(\varphi_{Cu^I} - \varphi_{Cu^{II}}) = dE$ where E is the voltage applied to the cell. Moreover, one chemical potential μ_{m^*} out of μ_m and one chemical potential μ_{k^*} out of μ_k (whereby $k^* \neq j$) can be substituted by using the Gibbs–Duhem equation $\Sigma x_i d\mu_i = 0$. The following relation is obtained.

$$-\mathrm{d}\gamma = q_{\mathrm{M}}\mathrm{d}E + \sum_{m \neq m^*}\left(\Gamma_m - \frac{x_m}{x_{m^*}}\Gamma_{m^*}\right)\mathrm{d}\mu_{\mathrm{M},m} + \sum_{k \neq j,k^*}\left(\Gamma_k - \frac{x_k}{x_{k^*}}\Gamma_{k^*}\right)\mathrm{d}\mu_{\mathrm{S},k} + \\ + \sum_j\left(\Gamma_j - \frac{x_j}{x_{k^*}}\Gamma_{k^*} + \nu_j\frac{q_{\mathrm{M}}}{nF}\right)\mathrm{d}\mu_{\mathrm{S},j} \quad (6)$$

This is a complete formulation of the electrocapillary equation, when the electroneutrality relation in the electrolyte is considered as secondary condition. This means that if the chemical potential or the concentration of an ion is changed, the concentration of a counterion will have to be changed too.

The experimental aim is to determine a differential quotient $\partial\gamma/\partial\mu$ whereby E and the other μ values have to be kept constant. If S_i is an ion and the electroneutrality condition is considered, complete constancy of the other μ values in eqn. (6) cannot be reached. An approximate constancy can, however, be realised by choosing a type of ion as counterion for S_i whose concentration in the electrolyte is substantially higher than the concentration of S_i. Equation (6) therefore represents a relation which can be used approximately if one substance is available in excess. Equation (6) is very similar to an analogous relation for reversible electrodes given by Plieth and Vetter[5]. An electrocapillary equation including the electroneutrality condition can be obtained from eqn. (6) in the manner described in the paper cited, but should be necessary only for special experimental cases.

With eqn. (6) as general electrocapillary equation, an improvement to earlier formulations of the electrocapillary equation is attained. First, formulation is very much simplified. Secondly, the expression for the relative surface excess is now given in a correct manner. The relative surface excess for ions S_k in the literature is formulated by using the mole fraction of an undissociated neutral association product of the ion S_k with a counter ion S_l in the form $\Gamma_k - (x_{k,l}/x_{k^*})\Gamma_{k^*}$. But in a solution of several anions and cations it is usually impossible to state a mole fraction $x_{k,l}$. The correct expression for the relative surface excess must therefore be given with the mole fraction x_k of the ions S_k in the form $\Gamma_k - (x_k/x_{k^*})\Gamma_{k^*}$ as contained in eqn. (6). Thirdly, in some papers[1,4] separations of equations are carried out in two cases, one with a reference electrode reversible to the cation and one with a reference electrode reversible to the anion. It follows from eqn. (6) that for any reference electrode a simple equation can be formulated without using this separation (reference electrodes with complicating diffusion potentials will not be discussed; see ref. 1). From eqn. (6) the dependence of the surface tension on a potential determining substance in the electrolyte is evident. For substances S_j in the electrolyte which take part in the reference electrode reaction, an additional term $\nu_j q_{\mathrm{M}}/nF$ is added to the relative surface excess expression. But since q_{M} follows from the partial differential quotient $\partial\gamma/\partial E$ this does not restrict the determination of the relative surface excess for these substances.

Institute of Physical Chemistry W. J. Plieth
Free University Berlin,
Berlin-Dahlem (Germany)

1 F. O. KÖNIG, *Z. Physik. Chem.*, A154 (1931) 421, 455; *J. Phys. Chem.*, 38 (1934) 111, 339.
2 D. C. GRAHAME AND R. B. WHITNEY, *J. Am. Chem. Soc.*, 64 (1942) 1548.
3 R. PARSONS AND M. A. V. DEVANATHAN, *Trans. Faraday Soc.*, 49 (1953) 404.

4 D. M. MOHILNER, in A. J. BARD (Ed.), *Electroanalytical Chemistry, Vol. 1*, Dekker, New York, 1966, p. 241.
5 W. J. PLIETH AND K. J. VETTER, *Ber. Bunsenges. Physik. Chem.*, 72 (1968) 673; 73 (1969) 79.

Received February 16th, 1970; in revised form, May 26th, 1970

J. Electroanal. Chem., 27 (1970) 468–471

Polarographic studies on the copper–threonine complex in alkaline medium

Copper(II) forms a violet complex with proteins in alkaline medium. The reaction, known as the "biuret test", has been used for about a century for the qualitative and quantitative determination of proteins[1]. The reaction has been mostly studied by spectrophotometric methods but the polarographic method was found especially suitable for the study of the violet complexes formed by the interaction of copper(II) with certain amides, amino acids and related compounds[2–4]. The present communication deals with the polarographic studies on the copper(II)–threonine complex in alkaline medium.

Experimental

Stock solutions of copper nitrate (0.2 *M*) and potassium nitrate (1.0 *M*) were prepared by dissolving B.D.H.(A.R.) material in conductivity water. L-threonine (pure, L. Light and Co., Ltd.) was dissolved in conductivity water to prepare a 0.20 *M* stock solution. Polarograms were taken in a solution containing 0.6 *M* NaOH and also in phosphate buffer solution in the pH range 11 – 12.3[5].

Polarographic measurements were made using a Fisher Elecdropode. All polarograms (Fig. 1) were taken in a phosphate buffer solution of pH 11.8. Triply

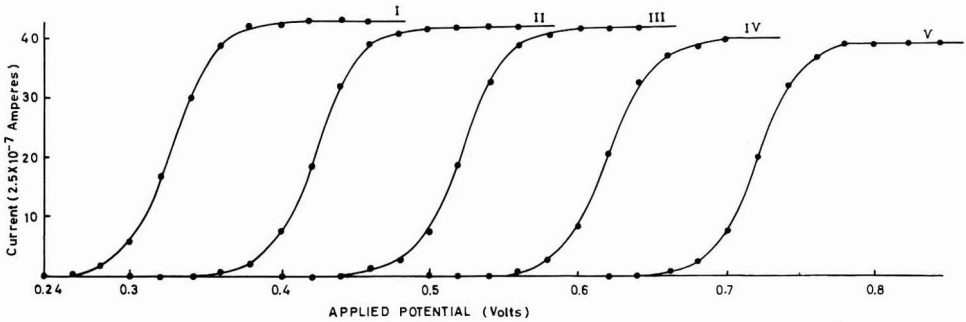

Fig. 1. Polarograms of 1 m*M* $Cu(NO_3)_2$ in L-threonine solution and buffer pH = 11.8. (I) 0.16 *M*, (II) 0.14 *M*, (III) 0.12 *M*, (IV) 0.10 *M*, (V) 0.08 *M*.

distilled mercury was used in the dropping mercury electrode and the saturated calomel electrode was used as a reference electrode. Purified nitrogen gas was bubbled through the solution to remove dissolved oxygen. The temperature was maintained at $30 \pm 0.1°C$ in a thermostat. No maximum suppressor was required as no maxima were observed in this case.

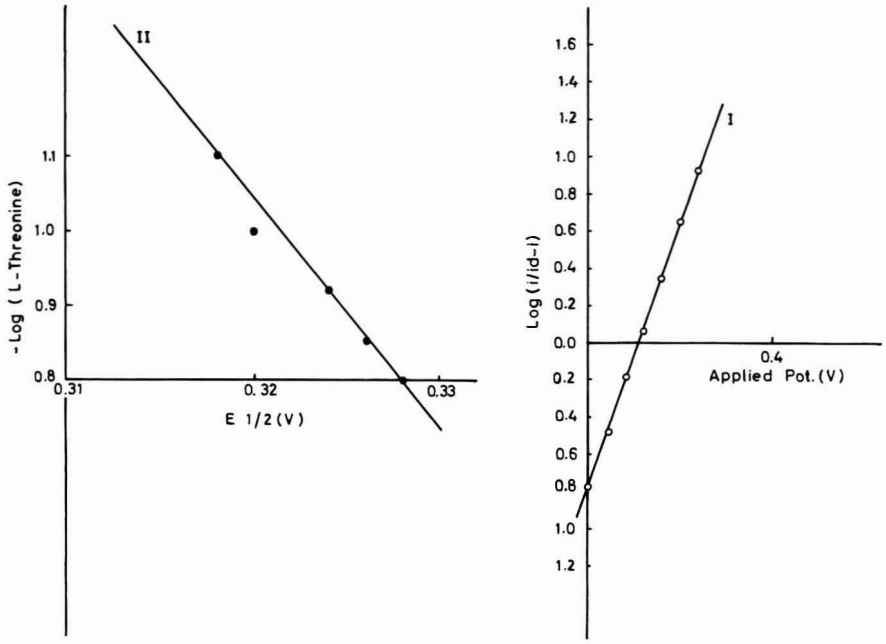

Fig. 2. (I) Logarithmic analysis of the reduction wave; $Cu(NO_3)_2 = 1$ mM, threonine = 0.16 M, buffer pH = 11.8. (II) Concn. function of half-wave potential. $Cu(NO_3)_2 = 1$ mM, buffer pH = 11.8.

Results and discussion

The polarograms are shown in Fig. 1. The reversibility of the reduction process was determined from the plot of Fig. 2 curve I. Straight lines were obtained with a slope of 0.035 V.

The dissociation of the copper–threonine complex may be represented by the general equation

$$Cu(Th)_p = Cu^{2+} + pTh^-$$

where Th^- represents the threonate, $CH_3-\underset{OH}{\underset{|}{CH}}-\underset{NH_2}{\underset{|}{CH}}-COO^-$ ion and p is the number of moles of threonine which combine with one mole of Cu(II). Following the treatment of Kolthoff and Lingane[6], a straight line of slope 0.032 V was obtained on plotting the half-wave potential *vs.* $-\log$ [threonine]. This slope corresponds to $p = 1$ *i.e.*, one mole of threonine is bound with one mole of copper(II) to form the complex. On this basis the formula of the complex may be represented as:

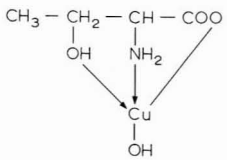

It may be noted that in a relatively low pH range only $-NH_2$ and $-COO^-$ groups are involved in the formation of the blue complex[7] but as the pH is raised the $-OH$ group also participates in complex formation and the colour of the solution changes to violet.

Department of Chemistry,
Aligarh Muslim University,
Aligarh (India)

Shahzad H. Khan
S. M. H. Rizvi
A. Aziz Khan
S. M. F. Rahman

1 F. KURZER, *Chem. Rev.*, 56 (1956) 95.
2 A. AZIZ KHAN AND W. U. MALIK, *Naturwiss.*, 46 (1959) 378.
3 A. AZIZ KHAN AND W. U. MALIK, *Z. Physik. Chem. Frankfurt*, 25 (1960) 130.
4 A. AZIZ KHAN AND W. U. MALIK, *J. Polarog. Soc.*, 2 (1959) 40.
5 H. T. S. BRITTON, *Hydrogen Ions*, Chapman and Hall Ltd., London, 1932, p. 220.
6 I. M. KOLTHOFF AND J. J. LINGANE, *Polarography*, Vol. 1, Interscience Publishers, New York, 1952, pp. 211–214.
7 N. C. LI AND E. DOODY, *J. Am. Chem. Soc.*, 74 (1952) 4184.

Received March 31st, 1969; in revised form April 6th, 1970.

Electrochemical oxidation of thiourea*

Kuz'mina and Songina[1] studied the oxidation of thiourea at a rotating platinum electrode in solutions of oxygen-containing acids and in hydrochloric acid solutions in order to develop a polarographic method for the determination of thiourea, and for the amperometric determination of small amounts of several oxidising agents. Preisler and Berger[2] found the oxidation–reduction potential of the thiourea–formamidine disulphide system to be 0.420 V in 0.05–1 *N* hydrochloric acid. Santhanam and Krishnan[3] studied the behaviour of thiourea during anodic oxidation using a stationary platinum gauze electrode with a view to establishing a satisfactory method for the estimation of this compound.

The present investigation deals with the elucidation of the mechanism of the oxidation of thiourea at a stationary platinum electrode in aqueous solutions of hydrochloric acid. The parameters utilised are anodic electrochemical reaction order, ionic exchange current densities, and transfer coefficients. The theoretical principles employed in their determination were those given by Vetter[4–7] and Parsons[8]. The anodic electrochemical reaction order is calculated using the equation:

$$\frac{\partial \log |i|}{\partial \log c_k} = \frac{\partial \log |i_+|}{\partial \log c_k} = z_{r,k}, \quad (\eta \gg RT/zF) \tag{1}$$

where η = charge transfer overvoltage, $z_{r,k}$ = anodic electrochemical reaction order, c_k = concentration of the species, i_+ = anodic current density. The ionic exchange

* Paper presented at the 10th Seminar on Electrochemistry held in Central Electrochemical Research Institute, Karaikudi.

current density values (i_0) and transfer coefficients ($\vec{\alpha}$ = anodic and $\overleftarrow{\alpha}$ = cathodic) are evaluated from Tafel plots.

Experimental

Reagents. Thiourea used was from E. Merck. The hydrochloric acid solution used was prepared using AnalaR grade material.

Apparatus. The standard type of apparatus with manual control of potential using a set of rheostats as recommended by Lingane was found satisfactory[9]. A platinum wire gauze was used as working electrode, a platinum spiral electrode as auxiliary electrode and a saturated calomel electrode as the reference electrode. A motor driven stirrer was used. A porous pot partition was used to separate the anode and the cathode in the cell.

Procedure. 100 ml of the supporting electrolyte, used for each run, were placed in a 400 ml beaker and an equal volume put in a porous vessel of convenient size placed in the beaker. A spiral platinum rod electrode was placed outside in the solution contained in the beaker and a platinum gauze electrode was placed in the solution in the porous vessel. For anodic runs, an initial electrolysis was carried out with the working electrode potential fixed at 0.7 V *vs.* SCE. When the current reached a negligibly low value, known concentrations of thiourea and the oxidised product were added to the solution in the porous vessel. With the rest potential at zero current noted, the potential of the working electrode was increased in steps of 25 mV and the current readings were taken. For the cathodic run, the gauze electrode was made the cathode and a similar procedure followed.

Results

As the current density values at different potentials were not reproducible, adsorption of the product on the electrode surface was suspected. Heating the elec-

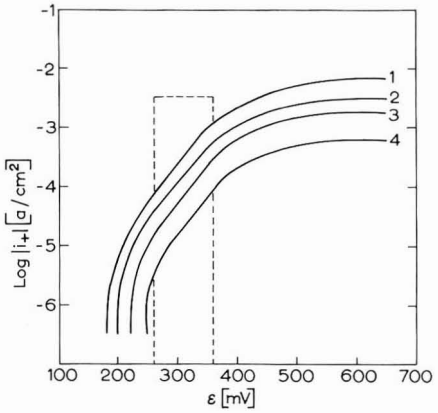

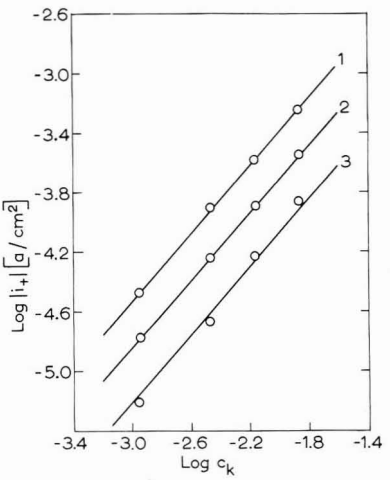

Fig. 1. Log $|i_+|$ *vs.* η plots for different concns. of thiourea in hydrochloric acid at 40° C. (1) 137.96×10^{-4}, (2) 67.98×10^{-4}, (3) 33.99×10^{-4}, (4) 11.33×10^{-4} *M*.

Fig. 2. Log $|i_+|$ *vs.* log c_k plots of thiourea in hydrochloric acid medium at the potentials: (1) 325, (2) 300, (3) 275 mV (*vs.* SCE).

trode in an alcoholic flame and then washing with distilled water, or keeping the electrode in stannous chloride in 6 *N* hydrochloric acid for about half an hour after each run and then washing with distilled water, was found essential for reproducibility. Pretreatment of the electrode seemed to play a very important role in these experiments.

The anodic potential *vs.* current density plots for several concentrations of thiourea at 40° C are given in Fig. 1. Exchange current density and transfer coefficient values evaluated are tabulated in Table 1. The anodic electrochemical reaction order is unity even when the oxidised product is pre-added to thiourea. Transfer coefficients are found to be independent of temperature. The anodic electrochemical reaction order is found to be 1.1 from Fig. 2.

The oxidation product of thiourea is confirmed to be formamidine disulphide as the infrared spectrum is the same as that of the compound prepared by a chemical method, as given by Preisler and Berger[2].

Under the conditions of electrolysis, formamidine disulphide hydrochloride is

TABLE 1

$\log (c_k/mol \cdot l^{-1})$	$\log (i_0/A\ cm^{-2})$	*Transfer coefficient* (α)
−2.95	−5.75	0.857
−2.47	−5.46	0.857
−2.17	−5.35	0.857
−1.87	−5.25	0.857

stable, for if thiourea were to be regenerated by decomposition of the former, there would be no correspondence between the theoretical and actual number of coulombs in the controlled potential coulometric runs[3].

In order to find the cathodic transfer coefficient, cathodic potential *vs.* current density plots were obtained with the oxidised product alone and also taken together with thiourea. The cathodic product was confirmed to be thiourea both from infrared spectra and thin-layer chromatography. The positive errors observed when thiourea was estimated by the controlled potential coulometric method without separating anode and cathode compartments also provides evidence for this.

Discussion

The electrochemical oxidation of thiourea at a platinum electrode may be characterised as an irreversible process since the anodic transfer coefficient differed markedly from the cathodic coefficient (about 0.8 and 0.2, respectively). As the anodic transfer coefficient is close to one, the process may be described as barrier free[10]. The activation energy of the reverse reaction would approach zero.

The overall reaction may be represented as:

$$2(NH_2)_2CS \rightarrow H_2N{\cdot}C(:NH)S{\cdot}S{\cdot}C(:NH)NH_2 + 2H^+ + 2e$$

As the anodic electrochemical reaction order is found to be one, the charge-transfer step should involve only one molecule of thiourea. The electrochemical oxidation is a one-electron process as shown by Santhanam and Krishnan[3] by controlled potential coulometry. The formation of formamidine disulphide suggests that

the tautomeric form of thiourea 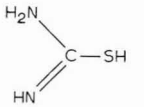 is converted into a free radical during the charge-transfer. The life of this free radical would necessarily be short and only the end product would be obtainable.

The possible steps involved are therefore:

1. formation of a free radical during the charge-transfer process:

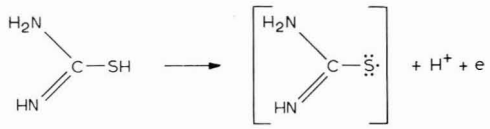

2. the combination of the free radicals to form formamidine disulphide

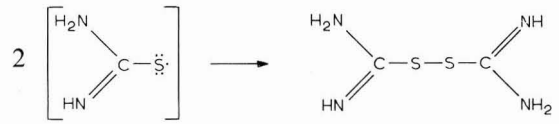

Obviously step (1) (the charge-transfer process) would be the rate-determining step.

The attainment of the limiting diffusion current, as indicated by the appearance of only short term fluctuations of current in the range, showed that no chemical reaction occurred after the charge-transfer process[11].

Acknowledgement

Thanks are due to the Council of Scientific and Industrial Research for the award of a scholarship to one of the authors (S.J.R.).

Chemical Laboratories,
Sri Venkateswara University Post-Graduate Centre,
Anantapur, A.P. (India)

S. Jayarama Reddy
V. R. Krishnan

1 N. N. KUZMINA AND O. A. SONGINA, *Chem. Abs.*, 57 (1962) 2857.
2 P. W. PREISLER AND L. BERGER, *J. Am. Chem. Soc.*, 69 (1947) 322.
3 K. S. V. SANTHANAM AND V. R. KRISHNAN, *Z. Physik. Chem. Frankfurt*, 34 (1962) 312.
4 K. J. VETTER, *Z. Physik. Chem. Leipzig*, 194 (1950) 199, 284.
5 K. J. VETTER, *Z. Elektrochem.*, 55 (1951) 121.
6 K. J. VETTER, *Z. Elektrochem.*, 59 (1955) 596.
7 K. J. VETTER, *Electrochemical Kinetics*, Academic Press, New York, 1967, p. 117.
8 R. PARSONS, *Trans. Faraday Soc.*, 47 (1951) 1332.
9 J. J. LINGANE, *Electroanalytical Chemistry*, Interscience Publishers, New York, 1953, p. 212.
10 L. I. KRISHTALIK, *Elektrochim. Acta*, 13 (1968) 1045.
11 K. J. VETTER, *Electrochemical Kinetics*, Academic Press, New York. 1967, p. 247.

Received January 19th, 1970; in revised form May 12th, 1970

Elsevier Sequoia S.A., Lausanne – Printed in The Netherlands

BOOK REVIEWS

Intermetallic Semiconducting Films by H. H. Wieder, Pergamon Press, Oxford, 1970, x+361 pp., £6.

Semiconductors in thin film form are likely to be used in the fabrication of important electronic components. The wide range of physical properties displayed by the binary compounds made from the elements in Groups IIIB and VB (the III–V compounds) makes them a particularly attractive subject for study. This most useful and timely book is a review of the methods of preparation, electrical transport properties and device applications of some of the III–V compounds. It might be sub-titled "What's what in III–V thin films"; but it never pretends to ask "why is what what?". Anybody working with semiconductor thin films ought to have this book.

There are six chapters: 1. Preparation of III–V compound layers. 2. Structure and Morphology of Films. 3. Electrical and Galvanomagnetic Properties. 4. Optical Properties. 5. Device and Applications. 6. Measurement Techniques.

The author's method of giving the facts, which are numerous, and blending in the appropriate semiconductor physics is pleasing. The coverage of evaporation and chemical deposition techniques in chapter one is good. The treatment of the deviation from phase equilibria, what one might term the physical chemistry of films, is poor. The section on cathodic sputtering is not good, but then this is a rapidly developing field.

Chapter two is adequate. Chapter three is an extension of chapter one plus a detailed discussion of the interpretation of such properties as the Hall and Seebeck coefficient. There is also an excellent section on high-frequency charge carrier transport phenomena.

The chapter on optical properties is a useful source of facts, but is perhaps the least good in the matter of interpretative discussion.

Chapter five is concerned with various devices and applications of films of the III–V compounds. Hall generators are particularly well dealt with, but the field effect thin film transistor is poorly covered.

The final chapter on techniques is a workman-like effort which will prove useful to the research worker. It is a pity that the important subject of field effect measurements is left out.

Since this book's strength lies in the large amount of information it contains, it is sad to note that the information will have to be dug out because the subject index is utterly inadequate and there is no author index. It would be advisable for the reader to make up a resumé table of the bulk properties of the III–V compounds as an aid to reading this book. American scientific slang obtrudes in an occasionally abrasive way. There are singularly few misprints and the diagrams and photographs are well done. The title is obviously incorrect.

M. Green, Zenith Radio Research Corp. (UK) Ltd.

Molecular Spectroscopy IX, Butterworth and Co. Ltd., London, 1969, 129 pages, £2.18.0.

This book contains the General lectures presented at the Ninth European Congress on Molecular Spectroscopy, held in Madrid in September 1967, and is reprinted from *Pure and Applied Chemistry*, Vol. 18, No. 3 (1969). This Congress was devoted mainly to infrared and Raman spectroscopy, and this restriction is reflected in the scope of the eight general lectures. Even so, these differ greatly in content, and much of the discussion has wider applications.

G. C. Pimentel (*Infrared study of transient molecules in chemical lasers*) shows how the successful generation of chemical laser action brings together the spectroscopists' art and the kineticists' insight, to the benefit of both disciplines. I. M. Mills (*Band contour calculations and* l-*doubling effects in symmetric top vibration–rotation spectra*) illustrates the power of modern computing techniques in the simulation of complex spectra, and shows how this can lead to the derivation of the signs and magnitudes of small term in the molecular Hamiltonian, even in spectra which are only partially resolved. R. N. Jones (*The measurement of infrared spectra with digitally recording spectrophotometers*) discusses the various ways of interfacing digital computers and experimental equipment. While nostalgic for the early days of a small dedicated computer, he recognises the power of a fast large core computer in such matters as the deconvolution of finite slit distortions and correction for calibration errors. He favours the use of an "intelligent" terminal, in which a large fast computer converses with many pieces of equipment *via* small dedicated computers. Y. Morino (*Intramolecular potential function of polyatomic molecules by vibration rotation interactions*) stresses the advantages of internal valence coordinates in the representation of the anharmonicity of potential functions, and draws together infrared and microwave methods for their derivation. L. A. Gribov (*The theory of intensities in the infrared spectra of polyatomic molecules*) starts with a warning against drawing detailed conclusions on the form of vibrations from band intensities, but is able to give a satisfying account of relative band intensities in a number of hydrocarbons using a model of interacting oscillators which are localised in bonds or groups. S. Califano (*Force field of large molecules*) stresses the difficulty of determining a unique force field for a large molecule, and tests several models which involve a limited transfer of force constants between chemically related molecules. B. Crawford and his coworkers (*Infrared intensities in condensed phases*) show how measurements of attenuated total reflectance lead to both the dispersion and the absorption of a liquid. It is found that the Lorentz–Lorentz model for the dielectric effect, and the Lorentz collision model of an oscillator, as modified by Van Vleck and Weisskopf, gives a good account of the absorption by a number of simple liquids. Finally G. Amat (*Recent progress in the study of vibrational resonance*; article in French) describes the application of perturbation theory to the vibrational resonances in CO_2, H_2O and HCN, including the re-assignment of ν_1 for CO_2.

These articles, though now inevitably somewhat dated, are valuable reviews of current fields of interest, but will appeal most to spectroscopic specialists.

R. N. Dixon, University of Bristol

Acids and Bases: *Their Quantitative Behaviour*, by R. P. Bell, F. R. S., Methuen's Monographs on Chemical Subjects, 2nd edn., 1969, 107 pages, 26/-.

The appearance of a second edition of this little monograph will be greatly welcomed by those who require an up-to-date summary suitable for recommendation to undergraduate students. The style is clear and eminently readable, and the text contains just sufficient on each topic to give a good grasp of the general outline of the field and is not so cluttered with examples and technical details as to obscure the thread of the argument. This is surely a notable achievement in a topic which has always figured so prominently in the development of physical chemistry and has continued to expand in scope particularly with the development of new techniques in the last decade or two. At the same time, the older, well-established quantitative knowledge has been in no sense superseded and still retains its fundamental importance wherever solution chemistry is relevant.

Practically the whole book is devoted to proton acids, for which the quantitative study has been highly developed, largely because of the possibility of putting all the acids on a common scale in a well-defined way. This emphasis accords with the author's well-known view that, despite the obvious stimulus to investigation provided by the Lewis nomenclature, it would be better to retain the word "acid" for proton acids alone and to speak of Lewis acids and bases rather in terms of electron acceptors and donors. The student will find a clear statement of this opinion in the last chapter, where the matter is rightly reduced to the level of semantics, but he will also find there a short appreciation of the fertility of the Lewis concept as applied to "hard and soft acids and bases", together with some suggestions for further reading.

In this new edition the chapters on isotope effects and on fast proton exchange reactions and their relation to acid–base catalysis will serve particularly well as readable, introductory summaries of two modern developments.

P. A. H. Wyatt, University of St. Andrews

JOURNAL OF ELECTROANALYTICAL CHEMISTRY AND INTERFACIAL ELECTROCHEMISTRY, VOLUME 27, 1970

AUTHOR INDEX

AL ATTAR, A. A. A. 59
ANDREOLI, R. 177
APPLEBY, A. J. 325, 335, 347
ARMSTRONG, R. D. 21, 158
AZIZ KHAN, A. 471

BAGOTZKY, V. S. 31
BARAK, H. 167
BARTELT, H. 447
BECK, W. H. 59
BEJERANO, T. 69
BELLOMO, A. 267
BELLUGI, L. 431
BERONIUS, P. 458, 461
BIEGLER, T. 314
BIGHI, C. 385
BIONDI, C. 431
BLOCH, O. 101
BLOUNT, H. N. 464
BORGHESANI, G. 385
BRABEC, V. 145

CARPENTER, A. K. 1
CARR, J. P. 109, 201, 466
CAUQUIS, G. App. 3
COMBES, R. 174
CREASON, S. C. 189

DAMASKIN, B. B. 81
DAVOLIO, G. 135
DESMARQUEST, J. P. 101
DICKINSON, T. 158
DRYHURST, G. 375

ELUARD, A. 117

FAWCETT, W. R. 219
FLEISCHMANN, M. 207
FLORENCE, T. M. 273
FORGACS, CH. 69
FRANKLIN, T. C. 303
FRIED, I. 167
FRUMKIN, A. 81

GAVIOLI, G. B. 135, 177
GILEADI, E. 69
GILES, R. D. 11, 161
GRANDI, G. 177
GUIDETTI, E. S. 135

HAMPSON, N. A. 109, 201, 466
HANSEN, B. H. 375
HARKINS, E. B. 375
HARRISON, J. A. 161
HELMY, A. K. 257
HOLLECK, L. 355
HOLMGREN, A. 461

IKEDA, S. 243
ITABASHI, E. 243
ITOH, T. 303

JHAMB, O. P. 151
JOVIĆ, F. 397

KASTENING, B. 355
KAZARINOV, V. E. App. 1
KHAN, S. H. 471
KOLLAR, R. 233
KÖNIG, G. 421
KRISHNAN, V. R. 473
KUHN, A. T. 319
KUWANA, T. 464

LAKOMOV, V. I. 403
LAKSHMANAN, S. 127, 170
LANDSBERG, R. App. 11
DE LEVIE, R. 454
LINDEMANN, J. App. 11
LOHS, K. 421

MACKEY, M. D. 219
MALATESTA, F. 283, 295
MALIK, W. U. 151
MCCLELLAND, D. H. 303

NAITO, M. 303
NELSON, R. F. 1, 189
NILSSON, A.-M. 461

OLDFIELD, J. W. 207
OLIVIERI, G. App. 7

PALEČEK, E. 145
PARSONS, R. 314
PEDRIALI, R. 385
PERRAULT, G. G. 47
PETERSON, P. 1
PETRY, O. A. 81, App. 1
PHILP JR, R. H. 369
PIRTSKHALAVA, J. N. 31
PLESKOV, YU. V. 403
PLICHON, V. 233
PLIETH, W. J. 468
POSPÍŠIL, L. 454
PULIDORI, E. 385

RABUZIN, T. 397
RACE, W. P. 21, 158
RAHMAN, S. M. F. 471
RANGARAJAN, S. K. 127, 170
RASPI, G. 283, 295
REDDY, S. J. 473
RIZVI, S. M. H. 471
ROTENBERG, Z. A. 403

SABET, V. M. 257
SADEK, H. 257
SAULNIER, J. 233
SERVE, D. App. 3
SMILJANIĆ, G. 397
SOHR, H. 421

TADROS, T. F. 257
TAYLOR, R. 109, 201, 466
THIRSK, H. R. 21
TRASATTI, S. App. 7
TRÉMILLON, B. 117, 174
TRINH-DINH, C. 101

VASSILYEV, YU. B. 31
VEDEL, J. 174

WEBER, J. 31
WHITFIELD, R. 158
WIKANDER, G. 461
WOLF, H. App. 11
WRIGHT, P. M. 319

ZATKA, A. 164

JOURNAL OF ELECTROANALYTICAL CHEMISTRY AND INTERFACIAL ELECTROCHEMISTRY, VOLUME 27, 1970

SUBJECT INDEX

Activity coefficients,
— in mixed electrolytes (Lakshmanan, Rangarajan) 170
Adenosine-5′-triphosphate,
polarographic study of — (Sohr *et al.*) 421
Adsorption,
— of anions on platinum electrodes (Bagotzky *et al.*) 31
— of cesium and potassium cations on platinum electrode (Kazarinov, Petry) App. 1
— of potential determining ions at aluminium oxide–aq. interface (Sadek *et al.*) 257
— of sulphide ions at mercury electrode (Armstrong *et al.*) 21
mixed — at mercury–soln interfaces (Lakshmanan, Rangarajan) 127
Adsorption isotherm,
congruence of — and double layer model for ethyl bromide (Trasatti, Olivieri) App. 7
Adsorption, specific,
effect of — of anions on polarographic reduction (Grandi *et al.*) 177
Alkali chloride mixture,
detn of standard potential in — (Combes *et al.*) 174
Alkaline earth salts,
solubility products of — of fatty acids in water (Al Attar, Beck) 59
Alkaline hydroxides, molten,
properties of mercury in — (Trémillon, Eluard) 117
Aluminium oxide–aq. interface,
adsorption of potential determining ions at — (Sadek *et al.*) 257
Anodic oxidation,
potentiodynamic sweep measurement of — of silver in alkaline solns (Giles, Harrison) 161
Anodic stripping voltammetry,
— with all glassy carbon electrode mercury-plated *in situ* (Florence) 273

Bromide,
detn of — by radioelectrochemical microgram (Beronius *et al.*) 461

Cathodic reduction
— of haloaromatics (Peterson *et al.*) 1
Cesium ions,
adsorption of — on platinum electrode (Kazarinov, Petry) App. 1
Chronopotentiometry, cyclic,
electronic instrument for — (Rabuzin *et al.*) 397
Cobalt redox systems,
detn of exchange current densities of — with various ligands (Bartelt) 447
Copper–threonine complex,
polarographic studies on the — in alkaline medium (Khan *et al.*) 471
Cu^{+}/Cu^{0} couple,
e.c. detn of reverse standard potential of — in water and methanol (Desmarquest *et al.*) 101
Cu^{2+}/Cu^{+} couple,
e.c. detn of reverse standard potential of — in water and methanol (Desmarquest *et al.*) 101

1,2-Dichloroethane,
e.c. reduction of molybdosilicic acid in — (Kollar *et al.*) 233
Diffusion coefficient,
microcoulometric detn of — with modified DME (Biondi, Bellugi) 431
Di-n-propyl-N-nitrosoamine,
reduction mechanism of — at DME (Pulidori *et al.*) 385
9,10-Diphenylanthracene cation radical,
spectrochemical evaluation of first order hydrolysis of — in acetonitrile (Blount, Kuwana) 464
Double-layer capacity,
— at metal–solid electrolyte interphase (Armstrong *et al.*) 158
Double-layer structure,
study of — by electron photoemission (Rotenberg *et al.*) 403
Dyes,
interaction of surface active agents with — (Malik, Jhamb) 151

Electrocapillary equation,
derivation and formulation of — for ideally polarizable electrodes (Plieth) 468
Electrochemical oxidation,
nature of the radical observed during — of perchlorate solns in organic media (Cauquis, Serve) App. 3

Electrode,
adsorption of anions on smooter platinum — (Bagotzky *et al.*) 31
adsorption on platinum — (Kazarinov, Petry) App. 1
adsorption of sulphide ions at a mercury — (Armstrong *et al.*) 21
alkaline earth ion — of third kind (Al Attar, Beck) 59
calomel reference — in propylene carbonate (Fried, Barak) 167
controlled drop time mercury — in a.c. polarography (Zatka) 164
electrocapillary eqn of ideally polarizable — (Plieth) 468
glassy carbon — mercury-plated *in situ* (Florence) 273
lanthanum ion — of third kind (Al Attar, Beck) 59
modified dropping mercury — for microcoulometric detn of diffusion coefficient (Biondi, Bellugi) 431
osmium — for evolution of hydrogen (Kuhn, Wright) 319
paraffinated graphite — in hypochlorite reduction (Landsberg *et al.*) App. 11
platinum–ruthenium alloy — for oxygen reduction in orthophosphoric acid (Appleby) 347
potentiostatic study of magnesium — in aq. soln (Perrault) 47
reduction mechanisn of di-n-propyl-nitrosoamine at dropping mercury — (Pulidor *et al.*) 385
relationship between adsorbed hydrogen and potential of hydrogen — (Franklin *et al.*) 303
rotating disk — for oxidation of N,N,N′,N′-tetramethyl-*p*-phenylenediamine (Philp Jr.) 369
ruthenium — for evolution of hydrogen (Kuhn, Wright) 319
silver single crystal — in concd. chloride solns (Giles) 11
smooth pre-reduced gold — for oxygen reduction in orthophosphoric acid (Appleby) 325
smooth pre-reduced iridium — for oxygen reduction in orthophosphoric acid (Appleby) 325
smooth pre-reduced rhodium — for oxygen reduction in orthophosphoric acid (Appleby) 335
smooth pre-reduced ruthenium — for oxygen reduction in orthophosphoric acid (Appleby) 335
Electrode charge,
notion of — and Lippmann equation (Frumkin *et al.*) 81
Electrode processes,
effect of solvent viscosity on boundary layer in — (Beronius) 458
Electrode reactions,
selective inhibition of — by organic compounds (Bejerano *et al.*) 69
Electrode photoemission
— as new method for study of double layer structure and kinetics of e.c. reactions (Rotenberg *et al.*) 403
Electrons, number of,
microcoulometric detn of — involved in diffusion controlled processes (Biondi, Bellugi) 431
Electron transfer rate,
dependence of — on inhibitor concentration (Kastening, Holleck) 355
Electroreduction
— of peroxydisulphate anion in formamide (Fawcett, Mackey) 219
Ethyl bromide,
new results regarding — with congruence of adsorption isotherm and double layer model (Trasatti, Olivieri) App. 7
Exchange current densities,
detn of — in redox systems of cobalt in various ligands (Bartelt) 447

Fatty acids, long-chain normal,
thermodynamic solubility products of salts of — in water (Al Attar, Beck) 59
Formamide,
electroreduction of eroxydisulphate anion in — (Fawcett, Mackey) 219

Guggenheim's relation
— for various salts (Lakshmanan, Rangarajan) 170

Half-wave potential,
estimation of reversible — (De Levie, Pospíšil) 454
Haloaromatics,
cathodic reduction of — (Peterson *et al.*) 1
Hydrogen
cathodic evolution of — on ruthenium and osmium electrodes (Kuhn, Wright) 319
relationship between adsorbed — and potential of the — electrode (Franklin *et al.*) 303
Hydrolysis, "first order",
spectrochemical evaluation of — of 9,10-diphenylanthracene cation radical in acetonitrile (Blount, Kuwana) 464
Hydroxonium ions,
evaluation of number of — involved in polarographic processes (Biondi, Bellugi) 431

Hypochlorite,
reduction of — at paraffinated graphite electrode (Landsberg *et al.*) App. 11

Impedance,
— of lead dioxide–aq. electrolyte interphase (Carr *et al.*) 201
Impedance, anomalous faradaic,
— of the nickelocene–nickelocinium system in acetonitrile (Biegler, Parsons) 314

Kinetics of e.c. reactions,
study of — by electron photoemission (Rotenberg *et al.*) 403

Lanthanum salts,
solubility products of — of fatty acids in water (Al Attar, Beck) 59
Lead dioxide,
electrical double layer of — in aq. KNO_3 (Carr *et al.*) 109
electrical double layer on — in perchloric acid (Carr *et al.*) 466
impedance of —/aq. electrolyte interphase (Carr *et al.*) 201
Lippmann equation,
electrode charge and — (Frumkin *et al.*) 81

Mercury,
potential–acidity equilibrium diagram of properties of — in eutectic alkaline hydroxide melt (Trémillon, Eluard) 117
Mercury/solution interfaces,
thermodynamic analysis of adsorption at — (Lakshmanan, Rangarajan) 127
Metal–solid electrolyte interphase,
double-layer capacity at — (Armstrong *et al.*) 158
Molybdosilicic acid
e.c. reduction of — in 1,2,-dichloroethane (Kollar *et al.*) 233

Nickel(II),
catalytic polarographic wave of — in aq. thiocyanate solns containing tetraethylammonium ions (Itabiashi, Ikeda) 243
Nickelocene–nickelocinium system
anomalous faradaic impedance of — in acetonitrile (Biegler, Parsons) 314
Nitrobenzyl halides,
cathodic reduction of — (Peterson *et al.*) 1
Noise,
generation–recombination — in weak electrolytes (Fleischmann, Oldfield) 207

Orthophosphoric acid,
— as solvent for various electrodes for oxygen reduction (Appleby) 325, 335, 347
Oscillometry, inductive,
— (Bellomo) 267
Oxygen reduction,
— on various electrodes in 85% orthophosphoric acid (Appleby) 325, 335, 347

Parabanic acid,
e.c. reduction of —: products and mechanism (Dryhurst *et al.*) 375
Perchlorate solns in organic media,
nature of the radical observed during e.c. oxidation of — (Cauquis, Serve) App. 3
Perchloric acid,
— as aq. electrolyte for measurements on double layer on lead dioxide (Carr *et al.*) 466
Peroxydisulphate anion,
electroreduction of — in formamide (Fawcett, Mackey) 219
Phenol,
inhibition of bromium and iodine evolution on platinum (Bejerano *et al.*) 69
Phenylmethyl sulphoxide,
polarography of — (Gavioli *et al.*) 137
Platinum,
anomalies in the yield of stripping of silver on — (Raspi, Malatesta) 283, 295
Polarographic reduction,
effect of adsorption of anions on — (Grandi *et al.*) 177
Polarographic wave, catalytic
— of Ni(II) in aq. thiocyanate solns containing tetraethylammonium ions (Itabashi, Ikeda) 243
Polarography,
catalytic currents in aq. solns of phenylmethyl sulphoxide in — (Gavioli *et al.*) 137
study of adenosine-5′-triphosphate by — (Sohr *et al.*) 421
Polarography, a.c.,
behaviour of polynucleotides in — (Brabec, Paleček) 145
controlled drop time mercury electrode in — (Zatka) 164
Polynucleotides,
a.c. polarographic behaviour and reducibility of — (Brabec, Paleček) 145
Potassium nitrate,
— as electrolyte for study of double layer at lead dioxide (Carr *et al.*) 109
Potentiodynamic sweep measurement,
— of anodic oxidation of silver in alkaline solns (Giles, Harrison) 161
Propylene carbonate,
calomel reference electrode in — (Fried, Barak) 167
Proton transfer rate,
dependence of — on inhibitor concentration

(Kastening, Holleck) 355

Radioelectrochemical microgram,
— for detn of bromide (Beronius *et al.*) 461
Reduction, e.c.,
— of molybdosilicic acid in 1,2-dichloroethane (Kollar *et al.*) 233
Reduction mechanism,
— of di-n-propyl-N-nitrosoamine at DME (Pulidori *et al.*) 385
— of parabanic acid and its products (Dryhurst *et al.*) 375

Silver,
anomalies in the yield of stripping of — on platinum (Raspi, Malatesta) 283, 295
potentiodynamic sweep measurement of anodic oxidation of — in alkaline solns (Giles, Harrison) 163
Silver single crystal,
anodic behaviour of — electrodes in concentrated chloride solns (Giles) 11
Sodium ions,
adsorption of — on platinum electrode (Kazarinov, Petry) App. 1
Solubility products,
thermodynamic — of alkaline earth and lanthanum salts of fatty acids in water (Al Attar, Beck) 59
Spectrophotometry,
— of dye–surfactant interaction (Malik, Jhamb) 151
Standard potential
detn of — in molten alkali chloride mixture (Combes *et al.*) 174
Standard potentials, reverse,
e.c. detn of — for non-complexed Cu^{2+}/Cu^{+} and Cu^{+}/Cu^{0} couples in water and methanol (Desmarquest *et al.*) 101
Sulphates,
— as electrolytes for lead dioxide impedance studies (Carr *et al.*) 201
Sulphide ions,
kinetics of adsorption of — at mercury electrode (Armstrong *et al.*) 21

Tetraethylammonium ions,
effect of — on catalytic wave of nickel(II)–thiocyanate systems (Itabashi, Ikeda) 243
N,N,N′,N′-Tetramethyl-*p*-phenylenediamine,
half-wave potential shifts in oxidation of — at rotating disk electrode (Philp Jr.) 369
Thiocyanate aq. solution,
polarography of nickel(II) in — containing tetraethylammonium ions (Itabashi, Ikeda) 243
Thiourea,
e.c. oxidation of — (Reddy, Krishnan) 473
Threonine complex,
polarographic studies of — with copper in alkaline medium (Khan *et al.*) 471

Viscosity,
effect of solvent — on boundary layer in electrode processes (Beronius) 458
Voltammetry, anodic stripping,
— with mercury–carbon electrode (Florence) 273
Voltammetry, rotating disk,
rapid data acquisition in — (Creason, Nelson) 189

Preliminary note

Zur Bestimmung des Blockierungsgrades von paraffinierten Graphitelektroden bei der Reduktion von Hypochlorit mit potentiostatischen Einschaltmessungen

R. LANDSBERG, H. WOLF und J. LINDEMANN

Sektion Chemie der Humboldt-Universität zu Berlin, 108 Berlin, Bunsenstr. 1 (D.D.R.)

(Eingegangen am 11. August 1970)

Im folgenden werden die für teilweise blockierte Elektrodenoberflächen abgeleiteten Beziehungen bei potentiostatischen Einschaltmessungen[1] auf die Reduktion von Hypochlorit an paraffinierten Graphitelektroden angewendet. Die Blockierungsparameter teilweise blockierter Graphitelektroden wurden schon mit Hilfe der Methode der nichtlinearen Diffusion aus stationären Messungen an der rotierenden Scheibenelektrode bestimmt[2-4].

Die vorliegenden Messungen wurden nach der in Ref. 1 beschriebenen Methode durchgeführt. Wir verwendeten für unsere Untersuchungen eine 10^{-3}-molare KOCl-Lösung in 1 *M* KOH bei 20°C. Als Messelektrode diente eine paraffinierte Graphitelektrode aus spektralreinem Graphit (Hersteller: VEB Elektrokohle Berlin-Lichtenberg). Die geometrische Elektrodenoberfläche betrug 0.196 cm^2. Die Elektrodenvorbehandlung erfolgte elektrochemisch in 1 *M* KOH nach der bereits beschriebenen Methode[3,4].

In Abb. 1 sind Strom–Zeit-Kurven aus potentiostatischen Einschaltmessungen an der "unblockierten" (Kurve c) und an teilweise blockierten Elektroden (Kurven a und b) dargestellt. Die Kurve ohne Messpunkte (Kurve d) ist für reine Diffusionsüberspannung theoretisch berechnet worden.

Als Diffusionskoeffizient wurde der Wert von 1.0×10^{-5} cm^2 s^{-1} bei 20°C aus den stationären Messungen[3] verwendet, der sich auch bei der potentiostatischen Einschaltmessung an der "unblockierten" Graphitelektrode (Kurve c) ergab.

Der Ordinatenabschnitt bei Kurve c ist auf Durchtrittsüberspannung (Messpotential: −1000 mV gegen ges. Kalomelelektrode (GKE)) zurückzuführen.

Man erhält für den Durchtrittsstrom einen Wert von $I_D = 1.0 \times 10^{-3}$ A cm^{-2}, der auch bei stationären Messungen bei gleicher Überspannung (−1000 mV GKE) in der gleichen Grössenordnung gefunden wurde.

Die Kurven a und b zeigen den für eine teilweise Elektrodenblockierung typischen Verlauf. Diese Kurven ergaben sich nach einer 10-minütigen anodischen Elektrodenvorbehandlung bei +200 mV (Kurve a) und ±0 mV (Kurve b) einer unblockierten Elektrode. Die Blockierungsparameter wurden aus den Messkurven nach der früher beschriebenen Methode[1] bestimmt. Danach ist der Anstieg des ersten Teiles der Messkurve (kurze Zeiten) eine Funktion des Blockierungsgrades. Ausserdem lässt sich der Blockierungsgrad aus dem

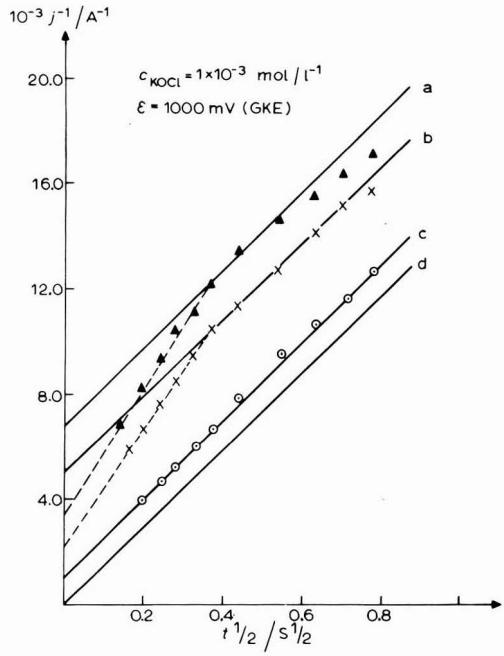

Abb.1. Potentiostatische Einschaltkurven für die Hypochlorit-Reduktion an paraffinierten Graphitelektroden in 1 *M* KOH bei 20°C; $c_{KOCl} = 1.0 \times 10^{-3}$ mol l^{-1}; Messpotential: −1000 mV GKE. (a) Teilweise blockierte Elektrode, 10 min bei +200 mV GKE vorbehandelt; (b) teilweise blockierte Elektrode, 10 min bei ±0 mV GKE vorbehandelt; (c) unblockierte Elektrode, 3 min bei −1700 mV GKE vorbehandelt; (d) für reine Diffusionsüberspannung berechnete Kurve.

Verhältnis der Durchtrittsströme an der unblockierten und teilweise blockierten Elektrode bei konstantem Potential und konstanter Konzentration nach Gl. (1) bestimmen:

$$\psi = 1 - I_{DB}/I_D \qquad (1)$$

ψ = Blockierungsgrad, I_{DB} = Durchtrittsstrom an einer teilweise blockierten Elektrode, I_D = Durchtrittsstrom an einer unblockierten Elektrode.

In der folgenden Tabelle sind die Blockierungsgrade in Abhängigkeit vom Elektrodenvorbehandlungspotential zusammengestellt, die nach der stationären Messmethode (Methode der nichtlinearen Diffusion) und der potentiostatischen Einschaltmethode bestimmt wurden.

Die nach der potentiostatischen Einschaltmethode aus Durchtritt und Anstieg bestimmten Blockierungsgrade stimmen gut überein. Die bei gleicher Elektrodenvorbehandlung aus stationären Messungen berechneten Werte liegen immer tiefer. Diese Differenzen dürften auf die zwangsläufig unterschiedlichen Messtechniken zurückzuführen sein★.

★So wird bei den stationären Messungen nach der Elektrodenvorbehandlung die Strom–Spannungskurve von der beginnenden Wasserstoffentwicklung zu positiveren Potentialen durchfahren, so dass unter Umständen schon ein Teil der Elektrodenblockierung reduziert sein kann. Es gibt auch aus anderen Messungen Hinweise dafür, dass ein Teil der Elektrodenblockierung auf der Kohleoberfläche sehr schnell reduziert wird.

TABELLE 1

ABHÄNGIGKEIT DES BLOCKIERUNGSGRADES VOM ELEKTRODENVORBEHANDLUNGS-POTENTIAL AN TEILWEISE BLOCKIERTEN GRAPHITELEKTRODEN
Vergleich der Bestimmungsmethoden

Elektrodenvorbehandlungspotential E/mV (GKE)	*Potentiostatische Einschaltmessungen*		*Stationäre Messmethode*
	Durchtritt (Gl. 1)	*Anstieg*	*(Grenzstrom)*
± 0	43%	42%	39%
+200	65%	67%	42%
+400	66%	68%	50%

Die mittleren Radien der aktiven Stellen liegen bei den stationären Messungen und bei den Einschaltmessungen in der Grössenordnung von 10^{-3} cm.

Zusammenfassend kann gesagt werden, dass auch mit Hilfe potentiostatischen Einschaltmessungen unter Verwendung der bereits beschriebenen Modellvorstellungen[1] Blockierungserscheinungen an Graphitelektroden nachgewiesen und quantitativ bestimmt werden können.

LITERATUR

1 J. Lindemann und R. Landsberg, *J. Electroanal. Chem.*, im Druck.
2 F. Scheller, R. Landsberg und H. Wolf, *Electrochim. Acta*, 15 (1970) 525.
3 H. Wolf und R. Landsberg, *Electrochim. Acta*, im Druck.
4 H. Wolf und R. Landsberg, *J. Electroanal. Chem.*, im Druck.

Vol. 27 No. 3 JOURNAL OF ELECTROANALYTICAL CHEMISTRY AND INTERFACIAL ELECTROCHEMISTRY OCTOBER 1970

CONTENTS

Oxygen reduction at smooth pre-reduced gold and iridium electrodes in 85% orthophosphoric acid
A. J. APPLEBY (Chicago, Ill., U.S.A.) 325

Oxygen reduction studies at smooth pre-reduced ruthenium and rhodium electrodes in 85% orthophosphoric acid
A. J. APPLEBY (Chicago, Ill., U.S.A.) 335

Oxygen reduction on platinum–ruthenium alloy electrodes in 85% orthophosphoric acid
A. J. APPLEBY (Chicago, Ill., U.S.A.) 347

Protonen- und Elektronentransfer an inhibitorbedeckten Elektroden
B. KASTENING UND L. HOLLECK (Jülich und Bamberg, Deutschland) 355

Half-wave potential shifts at rotating disk electrodes. Oxidation of N,N,N′,N′-tetramethyl-*p*-phenylenediamine
R. H. PHILP JR. (Columbia, S.C., U.S.A.). 369

Electrochemical reduction of parabanic acid: products and mechanism
G. DRYHURST, B. H. HANSEN AND E. B. HARKINS (Norman, Okla, U.S.A.) 375

Reduction mechanism of nitrogen compounds at the DME.I. Di-n-propyl-N-nitrosoamine
E. PULIDORI, G. BORGHESANI, C. BIGHI AND R. PEDRIALI (Ferrara, Italy) 385

An electronic instrument for cyclic chronopotentiometry
T. RABUZIN, G. SMILJANIĆ AND F. JOVIĆ (Zagreb, Yugoslavia). 397

Electron photoemission as a new method for studying the electric double layer structure and the kinetics of electrochemical reactions
Z. A. ROTENBERG, V. I. LAKOMOV AND YU. V. PLESKOV (Moscow, U.S.S.R.) 403

Polarographische Untersuchungen am Adenosin-5′-triphosphat (ATP)
H. SOHR, K. LOHS UND G. KÖNIG (Berlin, D.D.R.). 421

Millicoulometric determination of n and D with modified DME and evaluation of the number of H_3O^+ ions involved in a polarographic process
C. BIONDI AND L. BELLUGI (Roma, Italy) 431

Untersuchungen mit Bestimmung von Austauschstromdichten an Redoxsystemen des Kobalts mit unterschiedlichen Liganden
H. BARTELT (Berlin, D.D.R.). 447

Short Communications

On the estimation of the reversible halfwave potential
R. DE LEVIE AND L. POSPÍŠIL (Washington, D.C., U.S.A.). 454

Effect of solvent viscosity on boundary layer in electrode processes
P. BERONIUS (Umeå, Sweden) 458

Radioelectrochemical microgram determination of bromide
P. BERONIUS, A. HOLMGREN, A.-M. NILSSON AND G. WIKANDER (Umeå, Sweden). . . 461

On the spectroelectrochemical evaluation of the "first order" hydrolysis of DPA cation radical in acetonitrile
H. N. BLOUNT AND T. KUWANA (Cleveland, Ohio, U.S.A.) 464

Continued on page 4 of cover

Continued from inside page of cover

The electrical double layer on PbO_2 in $HClO_4$
J. P. CARR, N. A. HAMPSON AND R. TAYLOR (Loughborough, England) 466

On the derivation and formulation of the electrocapillary equation of ideally polarizable electrodes
W. J. PLIETH (Berlin, Germany) 468

Polarographic studies on the copper–threonine complex in alkine medium
S. H. KHAN, S. M. H. RIZVI, A. AZIZ KHAN AND S. M. F. RAHMAN (Aligarh, India) . . 471

Electrochemical oxidation of thiourea
S. J. REDDY AND V. R. KRISHNAN (Anantapur, A. P., India) 473

Book Reviews 477

Author Index 480

Subject Index 481

Preliminary Note

Zur Bestimmung des Blockierungsgrades von paraffinierten Graphitelektroden bei der Reduktion von Hypochlorit mit potentiostatischen Einschaltmessungen.
R. LANDSBERG H. WOLF UND J. LINDEMANN (Berlin, D.D.R.) . . . . . App. 7

JOURNAL OF ELECTROANALYTICAL CHEMISTRY AND INTERFACIAL ELECTROCHEMISTRY

Provisional publication schedule 1970/1971

Vol. **28**, No. **1** November 1970
No. **2** December 1970 **(Complete in two issues)**

Vol. **29**, No. **1** January 1971
No. **2** February 1971 **(Complete in two issues)**

Vol. **30**, No. **1** March 1971
No. **2** April 1971
No. **3** May 1971 **(Complete in three issues)**

Vol. **31**, No. **1** June 1971
No. **2** July 1971 **(Complete in two issues)**

Vol. **32**, No. **1** August 1971
No. **2** September 1971
No. **3** October 1971 **(Complete in three issues)**

Vol. **33**, No. **1** November 1971
No. **2** December 1971 **(Complete in two issues)**

Subscription information will be found inside the front cover